

**Mechanochemistry: analytical and mechanistic insight into the early phase of the Maillard reaction using high-resolution mass spectrometry**

Haoran Xing

Department of Food Science and Agricultural Chemistry

McGill University, Montreal

June 2021

A thesis submitted to McGill University in partial fulfilment of the requirements of the degree of  
Doctor in Philosophy

© Haoran Xing, 2021

Suggested short title:

Mechanochemical applications in food science

## Abstract

Understanding and controlling the complex network of the Maillard reaction cascade still poses great challenges to the researchers even after a century of its discovery. In this thesis, mechanochemistry, in combination with high-resolution mass spectrometry (HRMS) is proposed to address these challenges. Mechanochemistry was utilized as a tool for the controlled generation of Maillard reaction intermediates whether from amino acids or proteins in a solvent-free environment, on the other hand, high-resolution mass spectrometry, ESI-qTOF-MS, in conjunction with tandem mass spectrometry (MS/MS) and isotope labeling technique was employed as an efficient analytical platform in addition to FTIR and NMR spectroscopy to solve fundamental problems in mechanistic understanding of the Maillard reaction and in the analysis of complex reaction mixtures; particularly in discriminating between isomeric structures formed in these mixtures using mass spectrometry. The two most important isomeric structures generated from the initial stage of the Maillard reaction are the Schiff bases and their Amadori rearrangement products. Diagnostic ions obtained from MS/MS fragmentations were used for the discrimination between glucose derived Schiff bases and their corresponding Amadori compounds. In these studies, the ESI-qTOF-MS/MS system was operated under both positive and negative ionization modes to obtain three types of molecular ions: protonated, sodiated, and deprotonated. Each of the three molecular ions was subsequently fragmented at three different collision-induced disassociation energies (10, 15, and 20 eV) to generate unique MS/MS fragmentation patterns for each analyte. Analysis of the MS/MS data has indicated that protonated and deprotonated molecular ions generated unique diagnostic ions able to discriminate between Schiff bases and their corresponding Amadori compounds. Whereas sodiated ions generated identical diagnostic ions but vastly differing in their relative intensities. Furthermore, it was demonstrated that relative intensities of the diagnostic ions originating from Amadori and Schiff bases can be used to predict their ratio in the analytical sample. The application of this technique showed that ball milling of glucose with different amino acids almost exclusively results in the formation of a mixture of Schiff bases and Amadori compounds with minimal degradation, and that amino acids with basic side chains generated more Schiff bases and those with acidic side chains generated more Amadori products.

The thermochemical properties of ball-milled reaction mixtures were also investigated through heating, melting, and pyrolysis due to their potential application as Maillard flavor precursors. Direct video recordings of their melting behavior showed that the browning of the ball-milled

mixtures starts at lower temperatures and proceed more slowly compared to the non-milled mixtures. Furthermore, pyrolysis of ball-milled mixtures generated more pyrazines and fewer furan derivatives compared to the non-milled mixtures. The chemical composition of the ball-milled glucose-histidine was also investigated by high-resolution mass spectrometry. The decarboxylation and C2-C3 sugar chain cleavage reactions were identified as the most important transformations during ball milling. These findings further support the utility of mechanochemically generated mixtures as potential Maillard flavor and browning precursors. The model systems containing glycolaldehyde and histidine or phenylalanine as well as their corresponding amines (histamine and phenethylamine) were also investigated and lead to important mechanistic insights regarding the enhanced reactivity of the Maillard reaction under ball-milling conditions, where the Maillard reaction proceed through the formation and degradation of 5-oxazolidinone intermediates. The conversion of Schiff bases into reactive 5-oxazolidinone in these model systems was proposed as the basis for the observed enhanced reactivity. In addition to the potential applications of mechanochemistry using small molecular weight reactants, this study further explored mechanochemical reactions using large molecular weight reactants such as mechanochemical glycation of lysozyme and depolymerization of inulin. The results showed that mechanochemical induced glycation of lysozyme leads to selective formation of mono-glycated adducts. Moreover, the mono-glycated lysozyme was found to maintain its tertiary structure and therefore preserve the enzymatic activity despite undergoing the harsh milling conditions. Finally, it was observed that depolymerization of inulin under ball milling conditions resulted in the selective formation of fructo-oligosaccharides with a degree of polymerization ranging between 4 and 7. The addition of Lewis acid catalysts, such as  $\text{AlCl}_3$ , significantly improved the yield but shifting the composition of the reaction mixture to difructose dianhydride-rich mixtures. Both mixtures are considered as having prebiotic properties which can be used as functional food ingredients.

Despite the resurgence of mechanochemistry in different disciplines as a fast, solvent-free, and non-thermal synthetic methodology, its application in the field of food science is still in its infancy and needs further exploration.

## Résumé

Comprendre et contrôler le réseau complexe de la cascade de réaction de Maillard pose encore de grands défis aux chercheurs, même un siècle après sa découverte. Dans cette thèse, la mécano-chimie combinée à la spectrométrie de masse à haute résolution (HRMS) est proposée pour relever ces défis. D'une part, la mécano-chimie a été utilisée comme outil pour la génération contrôlée d'intermédiaires de la réaction de Maillard, que ce soit à partir d'acides aminés ou de protéines, dans un environnement sans solvant. D'autre part, la spectrométrie de masse à haute résolution, ESI-qTOF-MS, en conjonction avec la spectrométrie de masse en tandem (MS/MS) et la technique de marquage isotopique, a été utilisée comme plateforme analytique efficace en plus de la spectroscopie infrarouge à transformée de Fourier (FTIR) et de la spectroscopie de résonance magnétique nucléaire (NMR). Ces méthodes ont permis de résoudre des problèmes fondamentaux dans la compréhension mécanistique de la réaction de Maillard et dans l'analyse de mélanges réactionnels complexes, en particulier pour différencier les structures isomères formées dans ces mélanges en utilisant la spectrométrie de masse. Les deux structures isomériques les plus importantes générées à partir de l'étape initiale de la réaction de Maillard sont les bases de Schiff et de leurs produits de réarrangement d'Amadori. Les ions diagnostiques obtenus à partir de la fragmentation MS/MS ont été utilisés pour distinguer les bases de Schiff dérivées du glucose de leurs composés Amadori correspondants. Dans ces études, le système ESI-qTOF-MS/MS a été utilisé dans les modes d'ionisation positive et négative pour obtenir trois types d'ions moléculaires: protoné, sodé et déprotoné. Chacun des trois ions moléculaires a ensuite été fragmenté à trois différentes énergies de dissociation induite par collision (10, 15, et 20 eV) pour générer des modèles de fragmentation MS/MS uniques pour chaque analyte. L'analyse des données MS/MS a indiqué que les ions moléculaires protonés et déprotonés ont généré des ions de diagnostic uniques capables de faire la distinction entre les bases de Schiff et leurs composés Amadori correspondants, alors que les ions sodés généraient des ions diagnostiques identiques mais différant considérablement dans leurs intensités relatives. De plus, il a été démontré que les intensités relatives des ions diagnostiques provenant des bases d'Amadori et Schiff peuvent être utilisées pour prédire leur proportion dans l'échantillon d'analyse. L'application de cette technique a démontré que le broyage à billes du glucose avec différents acides aminés aboutit presque exclusivement à la formation d'un mélange de bases de Schiff et de composés Amadori avec une dégradation minimale. Les acides aminés avec des chaînes latérales basiques généraient plus de

bases de Schiff et les acides aminés avec des chaînes latérales acides généraient plus de produits Amadori.

Les propriétés thermochimiques des mélanges réactionnels broyés à billes ont été étudiées par chauffage, fusion et pyrolyse en raison de leur application potentielle comme précurseurs d'arômes de Maillard. Les enregistrements vidéo de leur comportement de fusion ont montré que le brunissement des mélanges broyés à billes débute à des températures plus basses et se déroule plus lentement que les mélanges non broyés. De plus, la pyrolyse des mélanges broyés à billes a généré plus de pyrazines et moins de dérivés furaniques par rapport aux mélanges non broyés. La composition chimique du mélange broyé à billes a été étudiée par spectrométrie de masse à haute résolution. Les réactions de décarboxylation et de clivage de la chaîne de sucre en C2-C3 ont été identifiées comme les transformations les plus importantes pendant le broyage à billes. Ces découvertes soutiennent en outre l'utilité des mélanges générés mécanochemiquement en tant que précurseurs potentiels d'arômes de Maillard. Les systèmes modèles contenant du glycolaldéhyde et de l'histidine ou de la phénylalanine ainsi que leurs amines correspondantes (histamine et phénéthylamine) ont également été étudiés et conduisent à des informations mécanistiques importantes concernant la réactivité accrue de la réaction de Maillard sous broyage à billes. Nous avons découvert que la réaction de Maillard se déroule par la formation et la dégradation d'intermédiaires de 5-oxazolidinone. La conversion des bases de Schiff en 5-oxazolidinone réactive dans ces systèmes modèles a été proposée comme base de la réactivité améliorée observée. En plus des applications potentielles de la mécanochemie en utilisant des réactifs de faible poids moléculaire, cette étude a exploré plus en détail les réactions mécanochemiques utilisant des réactifs de grande masse moléculaire tels que la glycation mécanochemique du lysozyme et la dépolymérisation de l'inuline. Les résultats ont montré que la glycation induite mécanochemiquement du lysozyme conduit à la formation sélective d'adduits monoglycés. De plus, le lysozyme monoglycé s'est avéré maintenir sa structure tertiaire et donc a pu préserver son activité enzymatique malgré les conditions de broyage difficiles. Enfin, il a été observé que la dépolymérisation de l'inuline dans des conditions de broyage à billes entraîne la formation sélective de fructo-oligosaccharides avec un degré de polymérisation compris entre 4 et 7. L'addition d'acides de Lewis en guise de catalyseurs, tels que  $AlCl_3$ , améliorerait significativement le rendement mais favorise la production de mélanges riches en difructose dianhydride. Les deux

mélanges sont considérés comme ayant des propriétés prébiotiques qui peuvent être utilisés comme ingrédients alimentaires fonctionnels.

Malgré la résurgence de la mécano-chimie dans différentes disciplines en tant que méthodologie synthétique rapide, sans solvant et non thermique, son application dans le domaine de la science alimentaire en est encore à ses balbutiements et doit être explorée plus profondément à l'avenir.

## Statement from the Thesis Office

In accordance with the regulations of Graduate and Postdoctoral Studies of McGill University, the following statement from the Guidelines for Thesis Preparation is included:

*Candidates have the option of including, as part of the thesis, the text of one or more papers submitted, or to be submitted, for publication, or the clearly-duplicated text of one or more published papers. These texts must conform to the “Guidelines for Thesis Preparation” and must be bound together as an integral part of the thesis.*

*The thesis must be more than a collection of manuscripts. All components must be integrated into a cohesive unit with a logical progression from one chapter to the next. In order to ensure that the thesis has continuity, connecting texts that provide logical bridges between the different papers are mandatory.*

*The thesis must conform to all other requirements of the “Guidelines for Thesis Preparation” in addition to the manuscripts.*

*As manuscripts for publication are frequently very concise documents, where appropriate, additional material must be provided in sufficient detail to allow a clear and precise judgement to be made of the importance and originality of the research reported in the thesis.*

*In general, when co-authored papers are included in a thesis, the candidate must have made a substantial contribution to all papers included in the thesis. In addition, the candidate is required to make an explicit statement in the thesis as to who contributed to such work and to what extent. This statement should appear in a single section entitled “Contribution of Authors” as a preface of the thesis.*

*When previously published copyright material is presented in a thesis, the candidate must obtain, if necessary, signed waivers from the co-authors and publishers and submit these to the Thesis Office with the final deposition.*

## **Acknowledgements**

I am grateful to everyone who has helped me during my Ph.D. study. First and foremost, I would like to express my deepest gratitude and appreciation to my advisor, Dr. Varoujan Yaylayan, who has given me this opportunity, guided me, and inspired me throughout my Ph.D. study. I am especially grateful for his time, patience, and support.

I would like to thank the members of my thesis evaluation committee and reviewers. I would also like to thank Dr. Alexander Wahba and Dr. Lan Liu for their assistance in obtaining mass spectroscopy data, Dr. Tara Sprules and Dr. Robin Stein for their expertise in nuclear magnetic resonance spectroscopy experiments, and the support from Mr. Yvan Gariepy for scanning electron microscopy experiment. I am grateful to my colleagues, friends, and lab mates (Raheleh, EunSil, and Carlyne) who have kept me company during my study.

Finally, I would like to thank my parents and my family for their unconditional love and support.

## Contribution of authors

This thesis is presented in a manuscript format and consists of nine chapters. Chapter 1 presents the rationale for conducting this study, research hypothesis, experimental methodology, objectives, and the significance of the study. In Chapter 2, a current and in-depth literature review is presented on mechanochemistry and the Maillard reaction. Specifically, the challenges of control and analysis of the Maillard reaction have been identified, and how high-resolution mass spectrometry and mechanochemistry can be used to address those challenges. Chapters 3 through 8 are based on published manuscripts and are bridged logically and sequentially through connecting paragraphs. Chapter 9 presents a brief conclusion and the contributions of this investigation to knowledge. This dissertation is in accordance with guidelines for thesis preparation as published by the Faculty of Graduate Studies and Research of McGill University

The present author was responsible for the concepts, design of experiments, experimental work, and manuscript preparation in all the published and submitted papers. Dr. Varoujan Yaylayan, the thesis supervisor, had direct advisory input into the work as it progressed, and as manuscript co-author critically edited the dissertation prior to its submission. Dr. Valeri V. Mossine also co-authored Chapter 3 “Diagnostic MS/MS fragmentation patterns for the discrimination between Schiff bases and their Amadori or Heyns rearrangement products” who provided synthetic standards to the study and edited and reviewed the manuscript.

## Publications

Xing, H., & Yaylayan, V. (2021). Insight into the mechanochemistry of the Maillard reaction: Degradation of Schiff bases via 5-oxazolidinone intermediate. *European Food Research and Technology*, **247**, 1095-1106. [doi.org/10.1007/s00217-021-03690-5](https://doi.org/10.1007/s00217-021-03690-5)

Xing, H., & Yaylayan, V. (2021). Investigation of thermo-chemical properties of mechanochemically generated glucose–histidine Maillard reaction mixtures. *European Food Research and Technology*, **247**(1), 111-120. [doi.org/10.1007/s00217-020-03611-y](https://doi.org/10.1007/s00217-020-03611-y)

Xing, H., & Yaylayan, V. (2020). Mechanochemical generation of Schiff bases and Amadori products and utilization of diagnostic MS/MS fragmentation patterns in negative ionization mode for their analysis. *Carbohydrate Research*, **495**, 108091. [doi.org/10.1016/j.carres.2020.108091](https://doi.org/10.1016/j.carres.2020.108091)

Xing, H., Mossine, V. V., & Yaylayan, V. (2020). Diagnostic MS/MS fragmentation patterns for the discrimination between Schiff bases and their Amadori or Heyns rearrangement products. *Carbohydrate Research*, **491**, 107985. [doi.org/10.1016/j.carres.2020.107985](https://doi.org/10.1016/j.carres.2020.107985)

Xing, H., & Yaylayan, V. (2019). Mechanochemically Induced Controlled Glycation of Lysozyme and Its Effect on Enzymatic Activity and Conformational Changes. *Journal of Agricultural and Food Chemistry*, **67**(11), 3249-3255. [doi.org/10.1021/acs.jafc.9b00070](https://doi.org/10.1021/acs.jafc.9b00070)

Xing, H., & Yaylayan, V. A. (2018). Mechanochemical depolymerization of inulin. *Carbohydrate Research*, **460**, 14-18. [doi.org/10.1016/j.carres.2018.02.009](https://doi.org/10.1016/j.carres.2018.02.009)

## Conference presentations

Xing, H., “The applications of mechanochemical method in food science” Presentation, *23rd Annual Green Chemistry & Engineering Conference/ 9th International Conference on Green & Sustainable Chemistry*, (2019) Reston, VA, USA.

# Table of Contents

<b>Abstract</b> .....	<b>ii</b>
<b>Résumé</b> .....	<b>iv</b>
<b>Statement from the Thesis Office</b> .....	<b>vii</b>
<b>Acknowledgements</b> .....	<b>viii</b>
<b>Contribution of authors</b> .....	<b>ix</b>
<b>Publications</b> .....	<b>x</b>
<b>Conference presentations</b> .....	<b>xi</b>
<b>Table of Contents</b> .....	<b>xii</b>
<b>List of Tables</b> .....	<b>xvii</b>
<b>List of Figures</b> .....	<b>xix</b>
<b>List of Schemes</b> .....	<b>xxiv</b>
<b>List of Abbreviations</b> .....	<b>xxv</b>
<b>Chapter 1 Introduction</b> .....	<b>1</b>
1.1 General introduction.....	2
1.2 Rationale and Objectives of the Proposed Research.....	4
1.3 The Experimental Approach .....	7
1.4 Significance of the Proposed Research .....	8
1.5 References .....	9
<b>Chapter 2 Literature review</b> .....	<b>11</b>
2.1 Mechanochemistry .....	12
2.1.1 General introduction on mechanochemistry .....	12
2.1.2 Renaissance of mechanochemistry .....	14
2.1.3 Experimental set-up and the control of the mechanochemical reactions.....	15
2.1.4 Understanding mechanochemistry.....	20
2.2 The Maillard Reaction.....	25
2.2.1 The complexity of the Maillard reaction .....	26
2.2.2 Challenges to the analysis of the Maillard reaction .....	35
2.2.3 Challenges facing the control of the Maillard reaction.....	38
2.2.4 The Maillard reaction under different stimuli.....	43
2.3 References .....	49

<b>Connecting paragraph.....</b>	<b>66</b>
<b>Chapter 3 Diagnostic MS/MS fragmentation patterns for the discrimination between Schiff bases and their Amadori or Heyns rearrangement products .....</b>	<b>67</b>
3.1 Abstract .....	68
3.2 Introduction .....	69
3.3 Material and Methods.....	70
3.3.1 Materials .....	70
3.3.2 ESI/MS/MS under formic acid condition .....	70
3.3.3 ESI/MS/MS under sodium formate condition .....	71
3.4 Results and Discussion.....	71
3.4.1 Diagnostic MS/MS fragmentations under acidic conditions .....	77
3.4.2 Diagnostic MS/MS fragmentations under neutral condition .....	81
3.5 Conclusion.....	83
3.6 References .....	83
3.7 Supplementary information.....	86
<b>Connecting paragraph.....</b>	<b>97</b>
<b>Chapter 4 Mechanochemical generation of Schiff bases and Amadori products and utilization of diagnostic MS/MS fragmentation patterns in negative ionization mode for their analysis.....</b>	<b>98</b>
4.1 Abstract .....	99
4.2 Introduction .....	100
4.3 Material and Methods.....	101
4.3.1 Materials and Reagents .....	101
4.3.2 Sample Preparation .....	102
4.3.3 ESI-qToF-MS/MS under sodium formate condition .....	102
4.3.4 LC-ESI-qToF-MS/MS under formic acid condition.....	102
4.4 Results and Discussion.....	103
4.4.1 Diagnostic MS/MS fragmentations of Schiff bases and ARPs under negative ionization mode.....	104
4.4.2 The utility of the MS/MS diagnostic ions generated under ESI negative mode in qualitatively estimating the ratio of glycine Schiff bases and ARPs in prepared mixtures of synthetic standards.....	107

4.4.3 Application of the MS/MS diagnostic ions generated under ESI negative mode in predicting the formation of Schiff bases and their ARPs in mechanochemically generated reaction mixture from glucose and glycine.....	108
4.4.4 The effect of the side chain of the amino acid on the formation of the Schiff base/ARP and the analysis through MS/MS fragmentation .....	112
4.5 Conclusion.....	115
4.6 References .....	115
4.7 Supplementary information.....	117
4.7.1 Material and Method.....	117
4.7.2 Tables and figures .....	120
<b>Connecting paragraph.....</b>	<b>136</b>
<b>Chapter 5 Investigation of thermo-chemical properties of mechanochemically generated glucose–histidine Maillard reaction mixtures .....</b>	<b>137</b>
5.1 Abstract .....	138
5.2 Introduction .....	139
5.3 Material and Methods.....	140
5.3.1 Material .....	140
5.3.2 Sample preparation .....	141
5.3.3 Melting studies.....	141
5.3.4 Scanning electron microscope (SEM) .....	142
5.3.5 ESI-qToF-MS study.....	142
5.3.6 NMR .....	143
5.3.7 FTIR.....	143
5.3.8 Pyrolysis-GC/MS.....	143
5.4 Results and Discussion.....	144
5.4.1 Histidine/ glucose milled separately .....	144
5.4.2 Histidine and glucose milled together.....	148
5.4.3 Comparison of the volatiles formed in milled and not-milled glucose/histidine mixtures.....	152
5.5 References .....	156
5.6 Supplementary information.....	158
<b>Connecting paragraph.....</b>	<b>181</b>
<b>Chapter 6 Insight into the mechanochemistry of the Maillard reaction: Degradation of Schiff bases via 5-oxazolidinone intermediate.....</b>	<b>182</b>

6.1 Abstract .....	183
6.2 Introduction .....	184
6.3 Material and methods .....	185
6.3.1 Materials .....	185
6.3.2 Sample preparation .....	185
6.3.3 FTIR.....	186
6.3.4 Electrospray ionization/quadrupole time of flight/mass spectrometry (ESI/qTOF/MS) .....	186
6.4 Results and Discussion.....	186
6.4.1 Data mining: Comparing the specific masses generated by equivalent chemical transformations from the amino acid side chains in L-histidine and L-phenylalanine.....	187
6.4.2 Exploratory analysis.....	189
6.4.3 Glycolaldehyde-amino acid model systems.....	190
6.4.4 Glycolaldehyde-histamine and glycolaldehyde-phenethylamine model systems.....	195
6.4.5 FTIR spectroscopic evidence for the formation 5-oxazolidinone during ball milling of paraformaldehyde with 20 common amino acids .....	201
6.5 References .....	203
6.6 Supplementary information.....	206
<b>Connecting paragraph.....</b>	<b>212</b>
<b>Chapter 7 Mechanochemically Induced Controlled Glycation of Lysozyme and Its Effect on Enzymatic Activity and Conformational Changes .....</b>	<b>213</b>
7.1 Abstract .....	214
7.2 Introduction .....	215
7.3 Materials and Methods .....	216
7.3.1 Materials .....	216
7.3.2 Sample Preparation .....	216
7.3.3 Quadruple-time-of-flight-ESI mass spectrometry (Q-TOF-ESI-MS). .....	217
7.3.4 FTIR.....	217
7.3.5 Residual Lysozyme Activity.....	218
7.3.6 Intrinsic Fluorescence Spectroscopy.....	218
7.3.7 Statistical analyses .....	218
7.4 Results and Discussion.....	219
7.4.1 Analysis of the distribution of glycoconjugate profile .....	219

7.4.2 Investigation of the factors influencing the efficiency of mechanochemical glycation .....	220
7.4.3 Effect of milling on conformational changes and the residual enzymatic activity ....	223
7.5 References .....	228
<b>Connecting paragraph.....</b>	<b>233</b>
<b>Chapter 8 Mechanochemical depolymerization of inulin .....</b>	<b>234</b>
8.1 Abstract .....	235
8.2 Introduction .....	236
8.3 Materials and Methods .....	237
8.3.1 Materials and reagents .....	237
8.3.2 Ball-Milling.....	237
8.3.3 Electrospray ionization/quadrupole time of flight/tandem mass spectrometry (ESI/qTOF/MS/MS) analysis .....	237
8.3.4 ESI-MS data processing.....	238
8.3.5 Identification of mono- and oligosaccharides.....	238
8.3.6 Dialysis .....	239
8.4 Results and Discussion.....	239
8.4.1 ESI/qTOF/MS analysis of inulin .....	240
8.4.2 The effect of milling time, frequency, and catalyst on the observed oligosaccharide profile.....	242
8.4.3 Milling efficiency.....	244
8.5 Conclusion.....	245
8.6 References .....	246
<b>Chapter 9 General conclusions, contributions to knowledge, and suggestions for future research.....</b>	<b>249</b>
9.1 General conclusions .....	250
9.2 Contributions to the knowledge .....	251
9.3 Suggestions for future research.....	252

## List of Tables

<b>Table 2.1</b> Comparison of the behavior of the Maillard reaction under different stimuli (mechanical force, sound waves, electricity or electric field, and simulated sunlight).....	48
<b>Table 3.1</b> MS and MS/MS spectral data of Schiff base, Amadori and Heyns compounds and their significant and diagnostic fragment ions. ....	73
<b>Table 3.2</b> Elemental composition of important product ions generated for glycine/glucose Schiff base, Amadori and Heyns compounds during MS/MS under acidic and neutral conditions. ....	74
<b>Table 4.1</b> ESI-qToF-MS and MS/MS (CID at 10eV) fragmentations under negative ionization mode of standard Schiff bases, and ARPs. ....	105
<b>Table 4.2</b> ESI-qToF-MS and MS/MS (CID at 10eV) fragmentations of selected ions in the ball-milled sugar-amino acid model systems under negative ionization mode .....	111
<b>Table 5.1</b> Video demonstrations of the melting behavior of glucose histidine models .....	142
<b>Table 5.2</b> Comparison of volatiles <sup>a</sup> generated from milled (30 mins, 30 Hz) and non-milled glucose-histidine (1:1) mixtures when pyrolyzed at 120 °C for 20 s. ....	154
<b>Table 6.1</b> The number of incidences observed of selected transformations in both histidine- and phenylalanine- glycolaldehyde (GA) model systems. ....	188
<b>Table 6.2</b> Observed masses from HRMS data from histidine-glycolaldehyde and phenylalanine-glycolaldehyde (GA) model systems corresponding to the structures shown in Figure 6.4. ....	194
<b>Table 6.3</b> Masses observed in ball-milled <sup>15</sup> N-phenylalanine-glycolaldehyde (GA). ....	195
<b>Table 6.4</b> Observed masses from HRMS data from histamine-glycolaldehyde and phenethylamine-glycolaldehyde (GA) model systems corresponding to the structures shown in Figure 6.5. ....	200
<b>Table 6.5</b> Amino acids that exhibit stable 5-oxazolidinone absorption bands in the FTIR spectrum when ball milled with paraformaldehyde (30 min, 30 Hz). ....	202
<b>Table 7.1</b> ESI/MS based calculated values of glycoform distribution in mechanochemically-induced glycated lysozyme a .....	222
<b>Table 8.1</b> Elemental compositional of all the ions observed.....	241
<b>Table 8.2</b> Details of group dp 1-3 (see Figure 8.1), the relative content is expressed as percent of the all identified ions.....	243
<b>Table 8.3</b> MS/MS data for ions at [M+X] <sup>+</sup> 365, 527, 689, 851, 1004 and 1013 (dp 2-7).....	244
<b>Table 8.4</b> Total amount of mono-, di-, and tri- saccharides detected in 20µg inulin using AEC-PAD.....	245

## Supplementary tables

<b>Table S 3.1</b> Tentative assignments of chemical shifts (ppm) in $^{13}\text{C}$ NMR spectra and relative populations of the anomeric forms of the compounds in $\text{D}_2\text{O}$ solutions at $25^\circ\text{C}$ .....	88
<b>Table S 3.2</b> Summary and comparison of all the product ions from MS/MS of Schiff base, Amadori, and Heyn's compound at different collision energy under acid condition. Numbers reported in the table is the relative abundance. ....	90
<b>Table S 3.3</b> Summary and comparison of all the product ions from MS/MS of Schiff base, Amadori, and Heyn's compound at different collision voltage of 10 eV under neutral condition. Numbers reported in the table is the relative abundance. ....	92
<b>Table S 4.1</b> Tentative assignments of chemical shifts (ppm) in $^{13}\text{C}$ NMR spectra and relative populations of the anomeric forms of the compounds in $\text{D}_2\text{O}$ solutions at $25^\circ\text{C}$ .....	119
<b>Table S 4.2</b> Comparing different ions from different systems on predicting the prepared mixtures. ....	120
<b>Table S 4.3</b> ESI-qToF-MS in positive mode and MS/MS (CID 10 eV) study on the ball milled sugar-amino acid model systems. ....	121
<b>Table S 4.4</b> Elemental composition of reported $m/z$ . ....	122
<b>Table S 5.1</b> Elemental composition of selected $m/z$ s from ball-milled histidine (60 min, 30Hz). ....	169
<b>Table S 5.2</b> Ions related to molecular species observed in milled histidine/glucose under ESI(+ve/-ve)/ionization modes. (see Figures S5.7-S5.8) .....	170
<b>Table S 5.3</b> Estimation of the yields <sup>a</sup> of Schiff base and ARP formed in milled glucose/histidine model system using $^1\text{H}$ NMR (in $\text{D}_2\text{O}$ and MeOD).....	172
<b>Table S 5.4</b> Elemental composition of all the ions observed in ball-milled glucose-histidine sample under ESI positive ionization mode. ....	173
<b>Table S 5.5</b> Elemental composition of all the ions observed in ball-milled glucose-histidine sample under ESI negative ionization mode. ....	176
<b>Table S 5.6</b> HRMS study of the milled and aged samples. The average relative intensities ( $n=2$ ) of selected ions are compared at different aging time. (n.d. indicates not detected). ....	178
<b>Table S 5.7</b> $^{13}\text{C}$ NMR (quantitative) peak assignment and integration. ....	180
<b>Table S 6.1</b> Extracted equivalent masses ( $m/z$ ) from histidine and phenylalanine model systems. ....	209

## List of Figures

<b>Figure 1.1</b> Rationale for using high-resolution mass spectrometry and mechanochemistry to study and control the Maillard reaction. (MR = Maillard reaction) .....	4
<b>Figure 1.2</b> General scheme of the proposed research. ....	5
<b>Figure 1.3</b> General experimental approach for the proposed research. ....	7
<b>Figure 2.1</b> The four distinct but related areas of mechanochemistry research. (TC = critical temperature, LAG = liquid-assisted grinding, MOFs = metal-organic frameworks, AFM = atomic force microscopy; Adapted from Suslick (2014) [5]).....	13
<b>Figure 2.2</b> Comparison of the molar energy for (a) the KMnO <sub>4</sub> -mediated oxidation of <i>p</i> -toluidine; [6] and (b) Suzuki–Miyaura reaction of aryl bromides with phenylboronic acid [13] carried out with different methods of energy entry. (PBM = planetary ball mill, VBM = vibrational ball mill; Adapted from Stolle group [6, 13]).....	14
<b>Figure 2.3</b> Comparison of vibratory ball mill, planetary ball mill, and twin-screw extrusion for conducting mechanochemical reactions. (Figures of instrumental appearance and accessories of vibratory ball mill and planetary ball mill are adapted from Retsch® company website; Figures of instrumental appearance and accessories of twin-screw extrusion are adapted from Crawford <i>et al.</i> (2017) [29]; Figures of Schematic illustration are adapted from Tan <i>et al.</i> (2019) [8]).....	17
<b>Figure 2.4</b> Parameters that control the mechanochemical reactions in ball mills. (LAG = Liquid-assisted grinding; Reproduced from Stolle (2015) [6]). ....	18
<b>Figure 2.5</b> Schematic illustration of the fundamental understanding of the mechanochemical transformations in organic chemistry.....	21
<b>Figure 2.6</b> Schematic illustration of the relationship between control and understanding of the Maillard reaction.....	25
<b>Figure 2.7</b> Hodge’s diagram. (Reproduced from Hodge (1953) [75] and Nursten (2005) [82]).	27
<b>Figure 2.8</b> Yaylayan’s classification of the Maillard reaction as an interaction of the components in different chemical pools. (Reproduced from Yaylayan (1997) [76]) .....	29
<b>Figure 2.9</b> Post-Schiff base transformations. ....	31
<b>Figure 2.10</b> Schematic illustration of the elementary transformations of the Maillard reaction. ....	33
<b>Figure 2.11</b> The initial stage of the Maillard reaction and subsequent breakdown of Amadori rearrangement product under different pH values. ....	34
<b>Figure 2.12</b> Schematic diagram illustrating the control of the Maillard reaction through the participating reactants, process variables, and use of novel technologies. ....	38
<b>Figure 2.13</b> Comparison of mechanochemical, sonochemical, electrochemical, and photochemical induced Maillard reaction .....	43
<b>Figure 3.1</b> MS and MS/MS spectra acquired at 0, 10, 15, 20 eV of glycine Schiff base under acidic condition. ....	75

<b>Figure 3.2</b> MS and MS/MS spectra acquired at 0, 10, 15, 20 eV of glycine Amadori compound under acidic condition.....	75
<b>Figure 3.3</b> MS and MS/MS spectra acquired at 0, 10, 15, 20 eV of glycine Heyns compound under acidic condition; the diagnostic ions are indicated in the graph. ....	76
<b>Figure 3.4</b> MS and MS/MS spectra at 0 and 10eV of glycine Schiff base, Amadori, and Heyns compound under neutral condition; the diagnostic ions are indicated in the graph.....	76
<b>Figure 4.1</b> MS/MS fragmentation in negative mode of standard glycine Schiff base and ARP and their mixture at 1:2 and 2:1 molar ratio. The diagnostic ions are indicated with arrows. ..	110
<b>Figure 4.2</b> MS/MS fragmentation in negative mode of ball-milled amino acid and glucose adducts. All the mechanochemical mixtures were prepared by ball mill glucose with the amino acid at 1:1 molar ratio for 30 mins at 30 Hz. The diagnostic ions are indicated with arrows. ....	114
<b>Figure 5.1</b> SEM micrographs of native histidine, native glucose, milled histidine, and milled glucose .....	145
<b>Figure 5.2</b> Evaluation of thermal reactivity of glucose/histidine model systems based on browning measurement at 420 nm under various conditions.....	147
<b>Figure 5.3</b> Changing of the relative intensities of selected ions during storage at 1 day and 3 days at room temperature. Results obtained from HRMS are from two independent trial (n=2). .....	151
<b>Figure 5.4</b> Maillard reaction products generated from ball milling of glucose and histidine (30 mins, 30 Hz) under positive ionization mode showing sodiated ions. The glycosidic linkage of the disaccharide-histidine condensation adduct at <i>m/z</i> 502 is unknown. (see also Table S5.4) .....	155
<b>Figure 6.1</b> MS spectra of ball-milled (30 min, 30 Hz) (a) histidine-glycolaldehyde and (b) phenylalanine-glycolaldehyde. ....	188
<b>Figure 6.2</b> Proposed histidine-glycolaldehyde and phenylalanine-glycolaldehyde reaction pathways and the proposed dimerization mechanism of Schiff base and Amadori compounds (see box with solid lines; n.d.: Not detected).....	193
<b>Figure 6.3</b> (a) MS spectrum of ball-milled histamine and glycolaldehyde; (b) MS/MS spectrum of the ion at <i>m/z</i> 271. ....	197
<b>Figure 6.4</b> (a) MS spectrum of ball-milled (30 min, 30Hz) phenethylamine and glycolaldehyde shown between <i>m/z</i> 290 and 300; (b) MS/MS spectrum of the ion at <i>m/z</i> 291.....	198
<b>Figure 6.5</b> Proposed histamine-glycolaldehyde and phenethylamine-glycolaldehyde reaction pathways and the MS/MS fragmentations of the dihydropyrazine derivatives. (n.d.: not detected).....	199
<b>Figure 6.6</b> Superimposed FTIR spectra of ball-milled (30 min, 30Hz) phenylalanine alone (red), paraformaldehyde (PFA)/phenylalanine (green) and PFA/[ <sup>13</sup> C-1]-phenylalanine (purple). .....	202
<b>Figure 7.1</b> Superimposed second derivative FTIR spectra of amide I region of native lysozyme (Native, red solid line), 30 minutes milled lysozyme (M30, magenta dashed line), and 60 minutes milled lysozyme (M60, blue dashed line) with/without 9% glucose. ....	225

<b>Figure 7.2</b> (a) Residual lysozyme activity and (b) intrinsic fluorescence ( $\lambda_{\text{ex}}=290$ nm) before and after milling at 30 minutes (M30) and 60 minutes (M60) with and without glucose (Glu); the values are reported as the mean $\pm$ standard deviation of triplicates; * indicates significant difference at $p < 0.05$ .....	226
<b>Figure 7.3</b> Time-dependent superimposed FTIR spectra of amide I, amide II and amide II' which appear upon H/D exchange of amide II, a series of 4 spectra were recorded for lysozyme (Native, red lines) and 60 minutes milled lysozyme (M60, green lines) with/without 9% glucose (M60+Glu, blue lines) during the H/D exchange process over 1-hour period with 20 minutes interval at room temperature. ....	227
<b>Figure 8.1</b> Oligosaccharide profile after milling treatments. Expressed as percentage of total intensity of all identified peaks. Results are average of triplicate analysis, with error bars indicating standard deviation. ....	242

## Supplementary figures

<b>Figure S 3.1</b> Extracted ion chromatogram of Schiff base, Amadori, and Heyn's compound under acidic condition.....	89
<b>Figure S 3.2</b> MS and MS/MS spectra acquired at 0, 10, 15, 20 eV of proline Schiff base under acidic conditions. ....	93
<b>Figure S 3.3</b> MS and MS/MS spectra acquired at 0, 10, 15, 20 eV of proline ARP under acidic condition. ....	94
<b>Figure S 3.4</b> CID of various mixtures of glycine Schiff base and its ARP at different molar ratios acquired under protonation .....	96
<b>Figure S 4.1</b> MS/MS (neutral condition) of the deprotonated ion of the standard pure proline Schiff base, proline ARP, and alanine ARP. ....	124
<b>Figure S 4.2</b> MS/MS (acidic condition) of the deprotonated ion of the standard pure proline Schiff base, proline ARP, and alanine ARP .....	125
<b>Figure S 4.3</b> MS/MS spectra of a mixture of standard glycine Schiff base (S) and its ARP (A) at molar ratio of (a) 2:1, (b) 1:1, and (c) 1:2. The spectra were recorded under MS acidic condition at CID 10 eV on the deprotonated ion $[M-H]^-$ at $m/z$ 236. The $m/z$ at 116 is the diagnostic ion for Schiff base, and the $m/z$ at 146 is the diagnostic ion for ARP. ....	126
<b>Figure S 4.4</b> MS/MS of prepared mixture of glycine Schiff base and ARP at molar ratio of 1:2 and 2:1. (a) Relative intensities of the diagnostic ions. (b) Comparison of diagnostic ions from the ball-milled glucose-glycine-( $AlCl_3/Na_2CO_3$ ) sample to the prepared mixtures. ....	127

<b>Figure S 4.5</b> MS/MS CID fragmentation at 20 eV of the mixture of glycine Schiff base and ARP at 5 different molar ratios. All models have m/z 97 as the most abundant product ion. The ion at m/z 88 is diagnostic for ARP, the ion at m/z 118 is diagnostic for Schiff base.....	128
<b>Figure S 4.6</b> MS (top, ESI +ve) and MS/MS (bottom, sodiated adduct peak, 10eV) spectra of ball milled glucose and glycine model system. ....	129
<b>Figure S 4.7</b> MS (top, ESI -ve) and MS/MS (bottom, deprotonated adduct peak, 10eV) spectra of ball milled glucose and glycine model system. ....	130
<b>Figure S 4.8</b> ssNMR spectra of standard mixtures of milled glucose and milled glycine to verify CP-MAS NMR response to the mixture of glucose and glycine at different ratio (from top to bottom (Gly-Glc %): 100%-0%; 80%-20%; 60%-40%; 40%-60%; 20%-80%; 0%-100%). ....	131
<b>Figure S 4.9</b> Superimposed ssNMR spectra. Green: ball milled glucose-glycine (30 mins/ 30Hz); Red: Standard mixture of glucose and glycine (Glc:Gly 4:1). The total conversion was estimated by curve fitting.....	132
<b>Figure S 4.10</b> ESI(-ve)/MS spectra of ball milled glucose with various amino acids. The condensation adduct ion is highlighted in red. The ion at m/z 255.2326 is a common contaminate ion with elemental composition C <sub>16</sub> H <sub>31</sub> O <sub>2</sub> (ppm 0.76), the cluster was proposed belong to lipid variety based on the elemental composition and mass defect. The “neutral losses” were annotated as grey dashed line. The spectra are annotated using R package ‘ <i>InterpretMSSpectrum</i> ’ (Rapid Communications in Mass Spectrometry, 2017. 31(15): p. 1261-1266.).....	133
<b>Figure S 4.11</b> ESI(-ve)/MS (top) and MS/MS (bottom, [M-H]- @ m/z 236, 10eV) spectra of ball milled glucose and glycine model system and AlCl <sub>3</sub> (1% w/w).....	134
<b>Figure S 4.12</b> ESI(-ve)/MS (top) and MS/MS (bottom, [M-H]- @ m/z 236, 10eV) spectra of ball milled glucose and glycine model system and Na <sub>2</sub> CO <sub>3</sub> (1% w/w).....	135
<b>Figure S 5.1</b> ESI (+ve)/MS spectra of ball-milled glucose for 60 min, 30Hz. ....	158
<b>Figure S 5.2</b> ESI (+ve)/MS spectra of ball-milled histidine for 60 min, 30Hz.....	158
<b>Figure S 5.3</b> Superimposed FTIR spectra of glucose (blue) and ball-milled glucose (red, 60 min, 30Hz).....	159
<b>Figure S 5.4</b> Superimposed FTIR spectra of histidine (blue) and ball-milled histidine (red, 60 min, 30Hz).....	159
<b>Figure S 5.5</b> The aromatic proton region of <sup>1</sup> H NMR Spectrum of ball-milled glucose-histidine in D <sub>2</sub> O. The tentative assignments are annotated on the structures shown.....	160
<b>Figure S 5.6</b> The aromatic proton region of <sup>1</sup> H NMR Spectrum of ball-milled glucose-histidine in MeOD. The tentative assignments are annotated on the structures shown.....	161
<b>Figure S 5.7</b> ESI (+ve)/MS/MS spectra of the ball-milled glucose-histidine mixture (30 min, 30Hz).....	162
<b>Figure S 5.8</b> ESI(-ve)/MS/MS spectra of the ball-milled glucose-histidine mixture (30 min, 30Hz). ....	163
<b>Figure S 5.9</b> ESI(+ve)/MS spectra of the heated sample (80 mins at 90 °C).....	164

<b>Figure S 5.10</b> ESI(+ve)/MS spectra of (1) 1 day aging of milled sample (30 min, 30Hz), and (b) 3 days aging of milled sample (30 min, 30Hz).....	164
<b>Figure S 5.11</b> <sup>13</sup> C NMR spectra of ball milled U- <sup>13</sup> C <sub>6</sub> -glucose and histidine in quantitative mode. Blue spectrum: standard mixture of - <sup>13</sup> C <sub>6</sub> -glucose and histidine. Green spectrum: milled 30 mins/ 30Hz. Red spectrum: milled 30 mins/ 30Hz and aged 3 days at room temperature. 165	165
<b>Figure S 5.12</b> Maillard reaction products generated from ball milled glucose and histidine (30 min, 30 Hz) under positive ionization mode showing protonated ions. (see also Table S5.4)...	166
<b>Figure S 5.13</b> Maillard reaction products generated from ball milled glucose and histidine (30 min, 30 Hz) under negative ionization mode showing deprotonated ions. (see also Table S5.5). .....	167
<b>Figure S 5.14</b> Summary highlighting the decarboxylation and C2-C3 fragmentations of the proposed Schiff base adduct. All structures shown (except histidine ) incorporated C3 and/or C2 from glucose (positive ionization mode, see Table S5.4) and ions detected in negative ionization mode incorporated the predicted number of carbon atoms from <sup>13</sup> U6-glucose (see Table S5.5).....	168
<b>Figure S 6.1</b> Data analysis pipeline: extraction of amino acid side chain specific reaction products. VK=Van Krevelen. (Note: For the <i>m/z</i> correction rules, (b)&(e) assuming all the ions from histidine model are sodiated, and all the ions from phenylalanine model are protonated; (c)&(f) assuming all the ions from histidine model are protonated, and all the ions from phenylalanine model are sodiated.).....	206
<b>Figure S 6.2</b> Mass difference network constructed using the seven transformations listed in Table 6.1 from the masses generated by equivalent chemical transformations in the histidine-glycolaldehyde model system. (The network is generated by R language (version 3.6.3) package <i>igraph</i> (version 1.2.5)).....	207
<b>Figure S 6.3</b> MS data visualization using (a) Kendrick mass defect plot (scaled by water) and (b) Van Krevelen diagrams. Masses involved in glycolaldehyde addition are highlighted in green in (a), and as circles in (b). Masses involved in histidine addition are highlighted in squares in (b). (The graphs are generated by R language (version 3.6.3) package <i>ggplot2</i> (version 3.2.3)).....	208

## List of Schemes

- Scheme 3.1** Proposed diagnostic collision-induced fragmentations of the glycine Schiff base and Amadori or Heyns rearrangement products under acidic conditions. The characteristic loss of water molecules from ARP is not shown..... 80
- Scheme 3.2** Proposed diagnostic collision-induced fragmentations of the glycine Schiff base and Amadori or Heyns rearrangement products under neutral sodiation conditions. .... 82
- Scheme 4.1** Proposed MS/MS fragmentation patterns under positive and negative ionization modes for the discrimination between Schiff bases and their Amadori rearrangement products modelled after glycine and proline Schiff bases and their Amadori rearrangement products. The fragmentation pattern was tested in mechanochemically generated mixtures of Schiff bases and Amadori products from glucose and various amino acids (including glycine, isoleucine, phenylalanine, aspartic acid, and histidine). .... 106

## Supplementary schemes

- Scheme S 3.1** Comparison of the proposed diagnostic collision-induced fragmentations of the proline and glycine Schiff base and Amadori rearrangement products under acidic conditions. The characteristic loss of water molecules from ARP is not shown..... 95

## List of Abbreviations

AA	Amino Acid
AEC	Anion Exchange Chromatography
AFM	Atomic Force Microscopy
AGEs	Advanced Glycation End products
ARP	Amadori Rearrangement Product
CE	Capillary Electrophoresis
CID	Collision-Induced Dissociations
CP-MAS NMR	Cross-Polarization Magic Angle Spinning Nuclear Magnetic Resonance
DFDAs	D-fructose dianhydrides
DP	Degree of polymerization
ESI-qTOF-MS	Electrospray ionization - quadrupole time-of-flight - mass spectrometry
FOS	Fructooligosaccharide
FT-ICR	Fourier-transform ion cyclotron resonance
ATR-FTIR	Attenuated total reflectance - Fourier-transform infrared spectroscopy
GC/MS	Gas chromatography - mass spectrometry
HILIC	Hydrophilic interaction liquid chromatography
HPP	Hydrostatic Pressure Processing
HRMS	High-resolution mass spectrometry
HRP	Heyns Rearrangement Product
IC-PAD	Ion exchange chromatography - Pulsed Amperometric Detection
ILAG	Ion- and liquid- assisted grinding
IUPAC	International Union of Pure and Applied Chemistry
LAG	Liquid-assisted grinding
LC/MS	Liquid chromatography - mass spectrometry
LZM	Lysozyme
m/z	mass-to-charge ratio
MOFs	Metal-organic frameworks
MR	Maillard reaction
MRPs	Maillard reaction products
MS/MS	Tandem mass spectrometry
MWCO	Molecular-weight cutoff
NMR	Nuclear magnetic resonance spectroscopy
PBM	Planetary ball mill
PEF	Pulsed electric field
PMMA	Polymethyl methacrylate
POLAG	Polymer-assisted grinding
PXRD	X-ray powder diffraction
RP	Reversed phase
SEM	Scanning electron microscope
ssNMR	Solid-state nuclear magnetic resonance spectroscopy
TC	Critical temperature
VBM	Vibrational ball mill

# Chapter 1 Introduction

## 1.1 General introduction

The interest in the study of the Maillard reaction has been continuing ever since its first discovery by the French chemists Louis-Camille Maillard in 1912. [1] The Maillard reaction is not only one of the most intensely researched reactions in food chemistry but also has significant implications in the pathophysiology of diabetes and aging. [2, 3] In food systems, the Maillard reaction is closely related to the quality and safety of thermally processed foods. It is responsible for the generation of so called Maillard flavors and colors [4] and at the same time, it is associated with the generation of thermally generated toxicants and with diminished nutritional value of processed foods through glycation of proteins and loss of essential amino acids. [5] When performed outside of the food environment, the Maillard reaction can be used to generate processed flavors [6, 7] from well-formulated mixtures of precursors and carefully controlled reaction conditions. However, understanding and directing the Maillard reaction to the desired end are challenging tasks since it is considered as a complex reaction cascade rather than a single chemical transformation. [8] Therefore, understanding and controlling the reaction are at the center of the Maillard reaction research today.

Various analytical protocols have been developed for an in-depth understanding of the Maillard reaction, of which GC/MS and LC/MS are the most frequently used methods for unraveling the molecular information on the Maillard reaction products. [9-13] The former technique is suited for the analysis of volatile and semi-volatile reaction products and the latter is suited for the analysis of non-volatile residues. However, compared to GC/MS where reproducible electron impact fragmentations can be compared to commercially available comprehensive databases which allows direct structural elucidation, LC/MS on the other hand, normally requires subsequent tandem mass spectrometry (MS/MS) for unequivocal structural assignments even when using high-resolution mass spectrometry. Considering the molecular complexity of the Maillard reaction, it can be compared to a metabolome, [14] and subsequently, the common metabolomic protocols and tools using high-resolution mass spectrometry have been applied to the study of the Maillard reaction. [13, 15] However, the much-needed information on using MS/MS for distinguishing various isomeric intermediates formed in the Maillard reaction is still not available. [12, 16, 17]

Mechanochemistry has recently emerged as a popular method for conducting various organic transformations in the solid-state without bulk solvation and much thermal energy input. [18] This

technique not only has been recognized as “greener” and more energy-efficient compared to solution-based thermochemistry but also has created unique synthetic opportunities for obtaining compounds that are not accessible otherwise. [19] Recent advances in mechanochemistry have broadened its applications in various fields, except in Food Science where it remains unexplored.[20] In this thesis, as a non-thermal and solvent-free method, mechanochemistry is proposed as a controlled method of conducting Maillard reaction outside of the food environment with potential applications in the generating processed flavors or functionally modified proteins.

## 1.2 Rationale and Objectives of the Proposed Research

The rationale for using high-resolution mass spectrometry as a high throughput analytical platform to study the Maillard reaction is illustrated in Figure 1.1. The high-resolution mass spectrometry allows accurate assignment of elemental composition and MS/MS fragmentations can provide further structural information that can be verified through isotope labelling technique. Unlike, the thermally catalyzed Maillard reaction in the solvent phase - where the important intermediates generated are usually degraded or polymerized at the end of the reaction with little or no opportunity to be isolated or even identified - reactions performed under ball milling conditions are more likely to retain many of the reactive intermediates due to shorter time scale of the reaction and the almost room temperature conditions. Furthermore, the reaction generates higher yields due to solvent-free conditions and lack of solvent interferences. Mechanochemistry by ball milling is therefore proposed as a promising tool to conduct and control the Maillard reaction for the above-mentioned advantages.

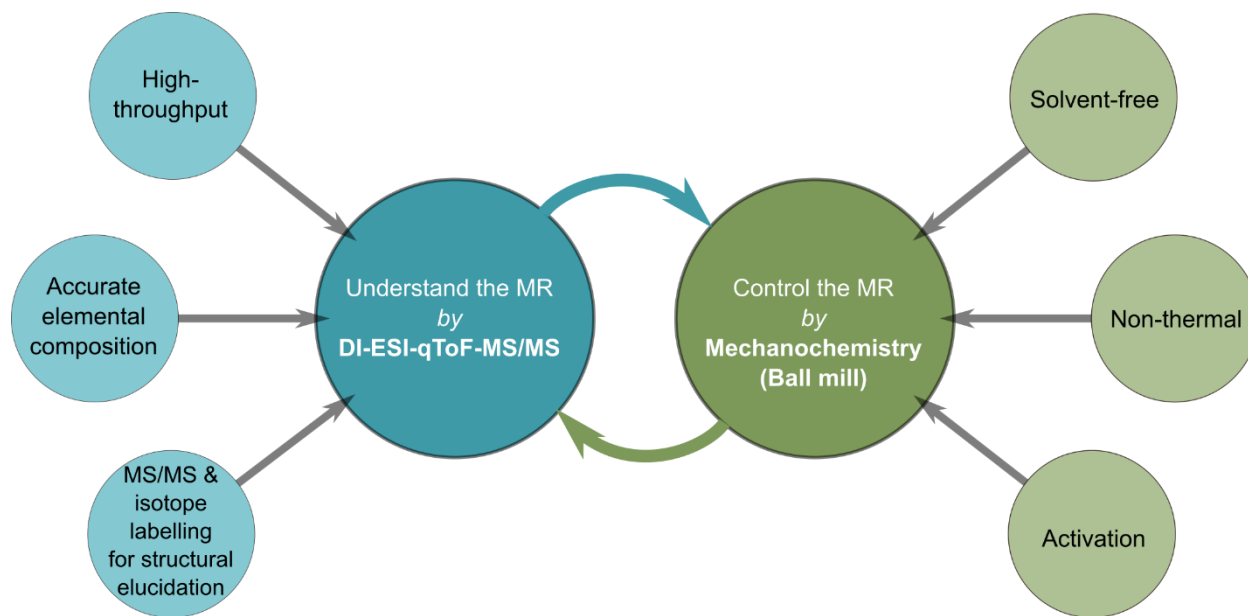


**Figure 1.1** Rationale for using high-resolution mass spectrometry and mechanochemistry to study and control the Maillard reaction. (MR = Maillard reaction)

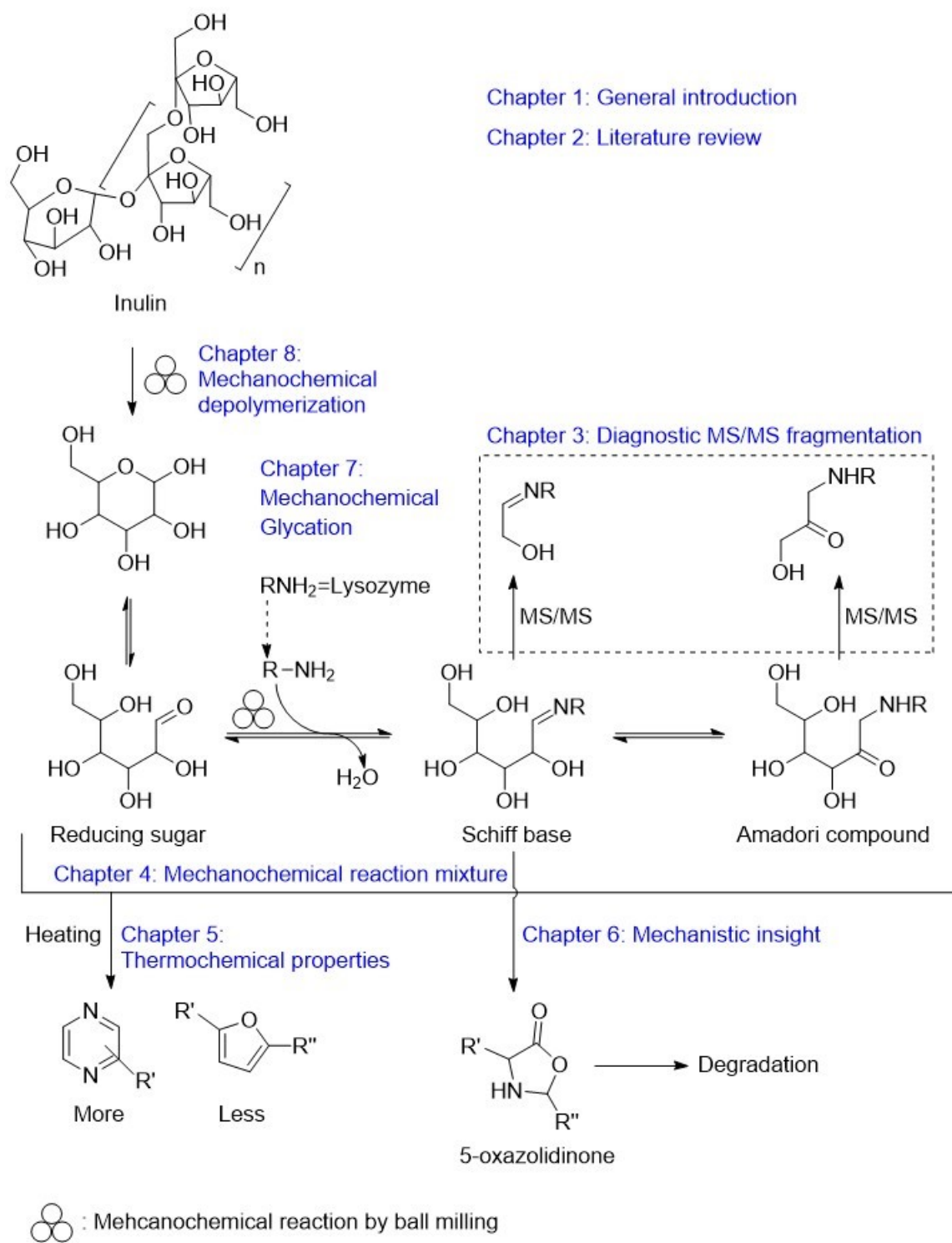


**Figure 1.2** General scheme of the proposed research.

As illustrated in Figure 1.2, the proposed research consists of six specific objectives:

1. To distinguish the isomeric pair of Schiff bases and Amadori rearrangement products through identification of their diagnostic MS/MS fragmentations.
2. To apply the MS/MS diagnostic ions identified above to investigate the formation of Schiff bases and Amadori rearrangement products in the ball milled Maillard reaction mixtures of glucose and various amino acids.
3. To investigate the thermochemical properties of the Maillard reaction mixtures generated through ball milling for the purpose of estimating their potential as flavor precursors.
4. To provide mechanistic insight into the mechanochemically induced Maillard reactions through isotope labelling technique.
5. To investigate the mechanochemical glycation of proteins using lysozyme as an example.
6. To investigate mechanochemically induced depolymerization of polysaccharides using inulin as an example

### 1.3 The Experimental Approach

A general experimental approach of this study is summarised in Figure 1.3. Details on the materials and methods can be found in each chapter.

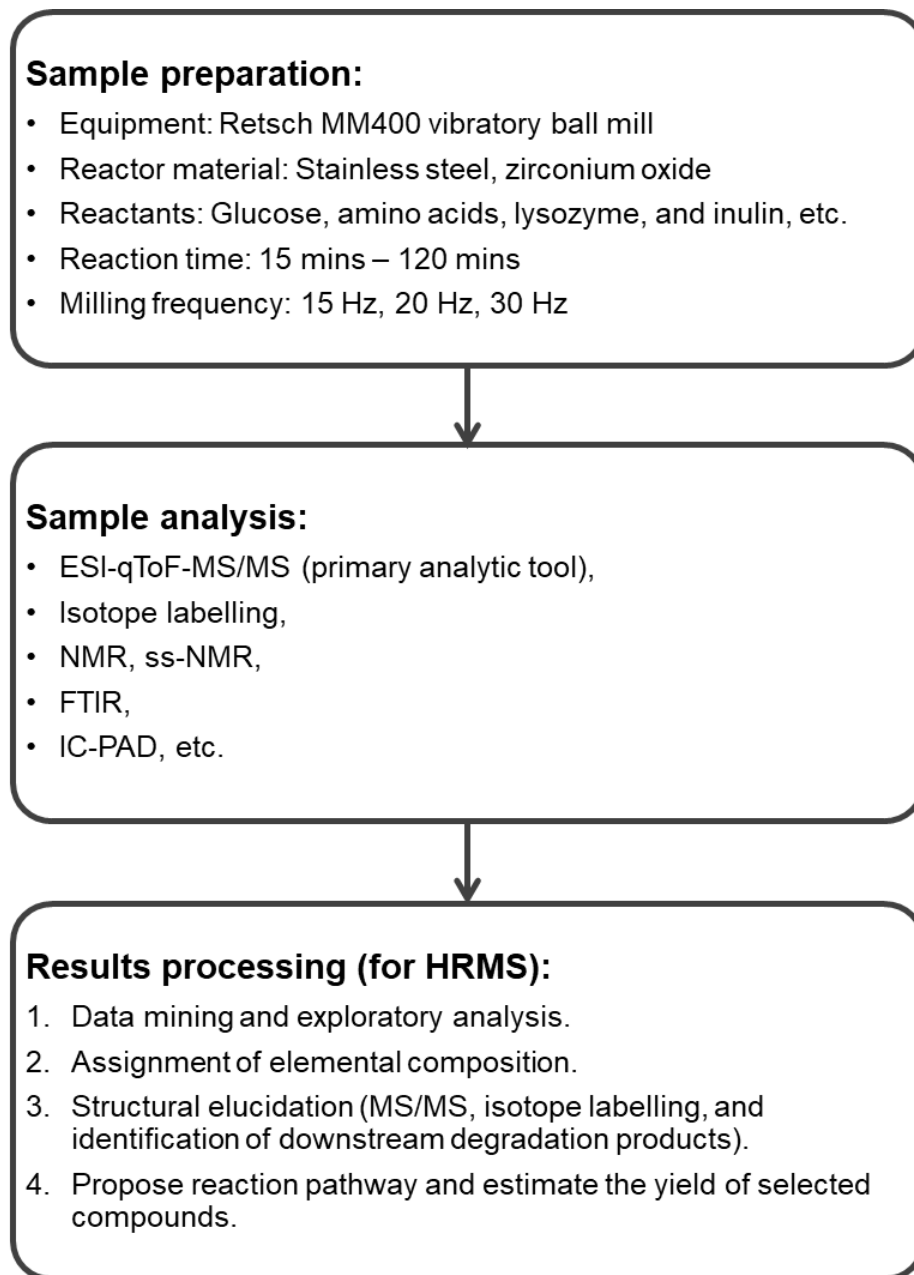


**Figure 1.3** General experimental approach for the proposed research.

## 1.4 Significance of the Proposed Research

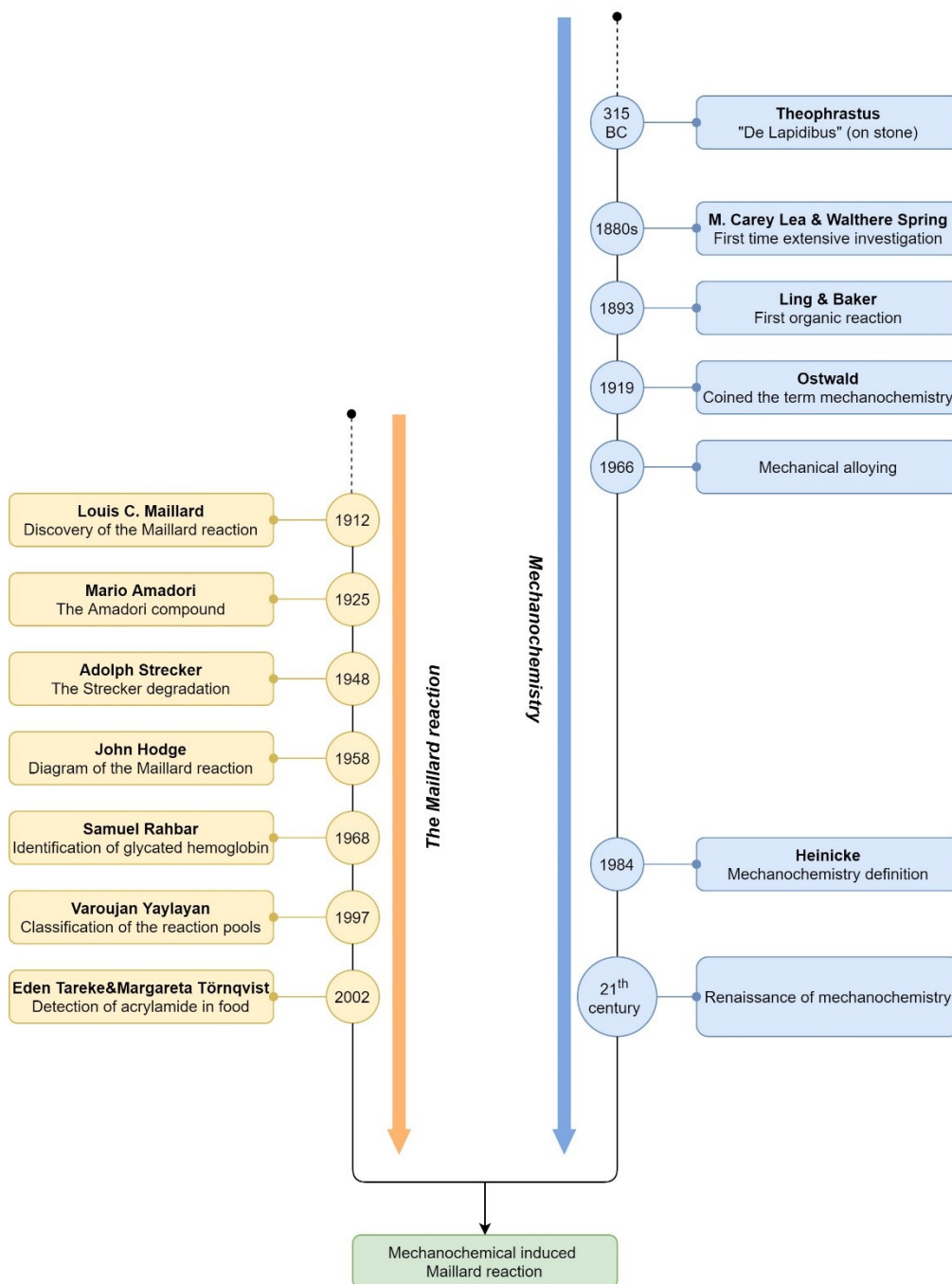
Despite the resurgence of mechanochemistry in different disciplines as a fast, solvent-free, and non-thermal synthetic methodology, its application in the field of food science is still in its infancy. The properties of mechanochemistry are particularly well-suited to control the Maillard reaction and to generate reaction intermediates that would be otherwise difficult or impossible to obtain by conventional thermal chemistry. The Maillard reaction intermediates generated by ball milling in this work can be considered as important and viable flavor precursors that meet the increasing demand of the ready-to-eat food industry to enhance the flavors of plant-based meat products. Furthermore, altering functional properties of proteins and polysaccharides through mechanochemistry was demonstrated in the present study to be a better alternative to conventional thermal chemistry for the controlled generation of functional food ingredients in a “greener” way with improved selectivity and efficiency. Such examples include the controlled glycation of lysozyme for modification of protein functionality and controlled depolymerization of inulin for biomass valorization and development of prebiotic mixtures. The findings of this thesis not only have implications to the food industry, but also to the theoretical understanding of one of the most important reactions in Food Chemistry the Maillard reaction. The studies reported here, provides mechanistic insight for an in-depth understanding of the solid-state Maillard reaction under ball milling conditions. The structural elucidation was achieved by the combined use of chromatography, high-resolution mass spectrometry, tandem mass spectrometry, FTIR, NMR and isotope labeling techniques. For the first time, diagnostic MS/MS fragmentations were identified to distinguish the two most important isomeric intermediates formed in the initial phase of the Maillard reaction – Schiff bases and Amadori compounds. This analytical advantage can provide an important tool for the workers in the field of “omics” research on the Maillard reaction to extract more detailed structural information from their databases and estimate the relative amounts of the two most important precursors in the Maillard reaction.

## 1.5 References

1. Maillard, L., *Action of amino acids on sugars. Formation of melanoidins in a methodical way*. *Compte-Rendu de l'Academie des Sciences*, 1912. **154**: p. 66-68.
2. Somoza, V., *Five years of research on health risks and benefits of Maillard reaction products: An update*. *Molecular Nutrition & Food Research*, 2005. **49**(7): p. 663-672.
3. Hellwig, M. and T. Henle, *Baking, Ageing, Diabetes: A Short History of the Maillard Reaction*. *Angewandte Chemie International Edition*, 2014. **53**(39): p. 10316-10329.
4. Parker, J.K., 8 - *Thermal generation of aroma*, in *Flavour Development, Analysis and Perception in Food and Beverages*. 2015, Woodhead Publishing. p. 151-185.
5. Stadler, R.H. and D.R. Lineback, *Process-induced food toxicants: occurrence, formation, mitigation, and health risks*. 2008: John Wiley & Sons.
6. Sucan, M.K. and D.K. Weerasinghe, *Process and reaction flavors: An overview*. 2005, ACS Publications.
7. Wang, Z., et al., *Advanced glycation end-product N $\epsilon$ -carboxymethyl-Lysine accelerates progression of atherosclerotic calcification in diabetes*. *Atherosclerosis*, 2012. **221**(2): p. 387-396.
8. Hodge, J.E., *Dehydrated foods, chemistry of browning reactions in model systems*. *Journal of agricultural and food chemistry*, 1953. **1**(15): p. 928-943.
9. Huyghues-Despointes, A., V.A. Yaylayan, and A. Keyhani, *Pyrolysis/GC/MS Analysis of 1-[(2'-carboxyl)pyrrolidinyl]-1-deoxy-D-fructose (Proline Amadori Compound)*. *Journal of Agricultural and Food Chemistry*, 1994. **42**(11): p. 2519-2524.
10. Keyhani, A. and V.A. Yaylayan, *Pyrolysis/GC/MS Analysis of N-(1-Deoxy-d-fructos-1-yl)-l-phenylalanine: Identification of Novel Pyridine and Naphthalene Derivatives*. *Journal of Agricultural and Food Chemistry*, 1996. **44**(1): p. 223-229.
11. Stadler, R.H., et al., *In-depth mechanistic study on the formation of acrylamide and other vinylogous compounds by the Maillard reaction*. *Journal of Agricultural and Food Chemistry*, 2004. **52**(17): p. 5550-5558.
12. Davidek, T., et al., *Analysis of Amadori compounds by high-performance cation exchange chromatography coupled to tandem mass spectrometry*. *Analytical chemistry*, 2005. **77**(1): p. 140-147.

13. Hemmler, D., et al., *Evolution of complex maillard chemical reactions, resolved in time*. Scientific reports, 2017. **7**(1): p. 1-6.
14. Moritz, F., et al., *Chapter 12 - Mass differences in metabolome analyses of untargeted direct infusion ultra-high resolution MS data*, in *Fundamentals and Applications of Fourier Transform Mass Spectrometry*, B. Kanawati and P. Schmitt-Kopplin, Editors. 2019, Elsevier. p. 357-405.
15. Hemmler, D., et al., *Insights into the Chemistry of Non-Enzymatic Browning Reactions in Different Ribose-Amino Acid Model Systems*. Scientific Reports, 2018. **8**(1): p. 16879.
16. Hau, J., S. Devaud, and I. Blank, *Detection of Amadori compounds by capillary electrophoresis coupled to tandem mass spectrometry*. Electrophoresis, 2004. **25**(13): p. 2077-2083.
17. Wang, J., et al., *Electrospray positive ionization tandem mass spectrometry of Amadori compounds*. Journal of Mass Spectrometry, 2008. **43**(2): p. 262-264.
18. James, S.L., et al., *Mechanochemistry: opportunities for new and cleaner synthesis*. Chemical Society Reviews, 2012. **41**(1): p. 413-447.
19. Friščić, T., C. Mottillo, and H.M. Titi, *Mechanochemistry for Synthesis*. Angewandte Chemie International Edition, 2020. **59**(3): p. 1018-1029.
20. Viton, F., H.R. Oertling, and R. Fumeaux, *Mechanical generation of flavour compositions*. 2017, U.S. Patent US20170079316A1.

## Chapter 2 Literature review



## 2.1 Mechanochemistry

### 2.1.1 General introduction on mechanochemistry

In performing chemical reactions, energy input is often required to overcome the activation energy barriers and initiate the intended chemical transformations. Depending on the nature of the energy input, the type of chemistry under study can be subdivided into several areas including thermochemistry (thermal energy), photochemistry (UV or visible light), electrochemistry (electricity or electric field), sonochemistry (ultrasound), and mechanochemistry (mechanical energy). Due to increasing awareness and necessity of environmental protection and sustainability issues together with the need for more efficient chemical synthetic methodologies, there has been a growing emphasis on the development of novel methods such as photochemistry, electrochemistry, and mechanochemistry as the alternate synthetic routes to traditional thermochemistry. [1]

According to the International Union of Pure and Applied Chemistry (IUPAC), a mechanochemical transformation is defined as a “*chemical reaction that is induced by the direct absorption of mechanical energy*”. [2] The mechanical energy may be supplied in both liquid and solid phase reaction systems and is manifested in many forms such as shearing, stretching, grinding, friction, impact, and compression, etc. [3, 4] Hence, the term mechanochemistry covers a wide range of subjects in various research fields. [5] (Figure 2.1) However, today, the term mechanochemistry most frequently refers to a solid-state reaction where the mechanical energy is supplied by ball milling or with the use of the twin-screw extruders as newly emerging alternative. Therefore, grinding or milling often used as synonyms in a mechanochemical context. In a solid-state system, the mechanical energy from ball milling results in a series of events before the initiation of a chemical transformation which includes size reduction, phase transformation, and creation of active sites or surfaces for efficient contact (see Section 2.1.4 for details). [3, 6]

Mechanochemistry enjoys a rich and storied history where the first description of a mechanochemical transformation dates back to as early as 315 BC where elemental Hg was obtained by grinding mercury (II) sulfide (HgS) with a copper mortar and pestle. [7] However, the method remained almost dormant till the 20<sup>th</sup> century. There are only a handful of research activities that can be found in this period. [7] Solution-based thermochemistry, on the other hand, has dominated synthetic research laboratories and industrial manufacturing since modern

chemistry was formulated in the 17<sup>th</sup> century. [8] Interest in mechanochemistry has grown exponentially over the preceding 20 years. Since then, a wide range of applications has been identified in various fields including organic synthesis, [3, 9, 10] organometallic synthesis, [11, 12] coordination compounds, [12] main group, [8] and supramolecular synthesis. [12]

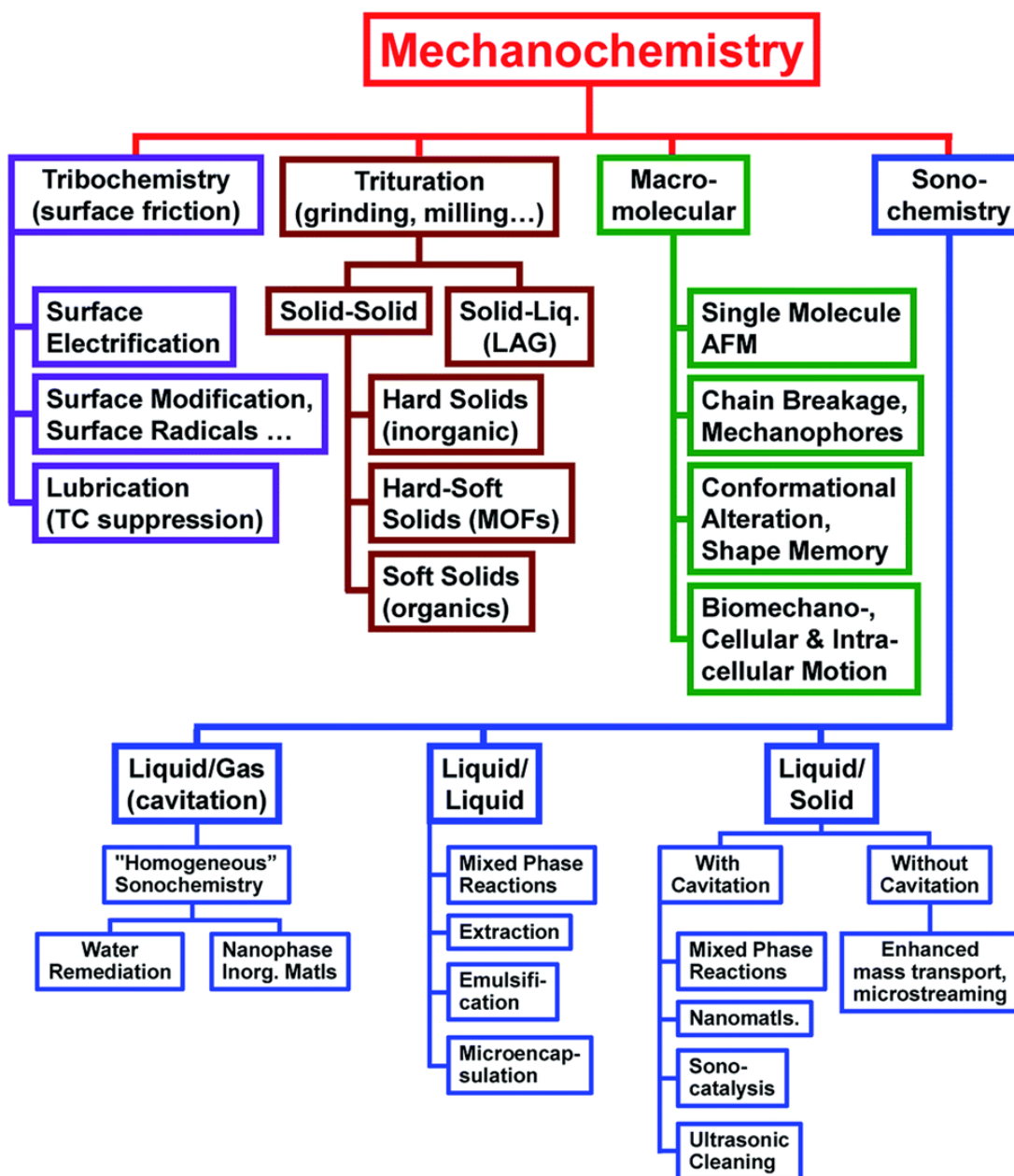


**Figure 2.1** The four distinct but related areas of mechanochemistry research. (TC = critical temperature, LAG = liquid-assisted grinding, MOFs = metal-organic frameworks, AFM = atomic force microscopy; Adapted from Suslick (2014) [5])

### 2.1.2 Renaissance of mechanochemistry

The reason for mechanochemistry regaining its popularity are twofold. Firstly, mechanochemistry is considered as a suitable methodology for Green Chemistry applications due to the fact that reactions can be conducted without bulk solvation and can be completed in the absence of solvents within a short period of time. [3] This implies elimination of hazardous organic solvents and the energy-consuming work-up procedures. Furthermore, the absence of solvents also makes the mechanochemistry an energy efficient technology. Stolle group has shown that the energy consumption of a mechanochemical reaction is only a fraction of that used under classical thermal and microwave heating conditions. (Figure 2.2) [6, 13] The reason for this energy efficiency can be attributed to the fact that the mechanical energy supplied during ball milling is directly imparted onto the solid-state reactants, while in the solution-based reaction systems, a substantial amount of thermal energy is likely dissipated by the solvent. [6] Kaupp group also provided mechanistic insight into the energy efficiency of the mechanochemical reactions by pointing out that the mechanochemical reactivity is largely due to surface activation that normally requires lower energy input (ca. 0.05-0.5 kJ/mol). [14-16]

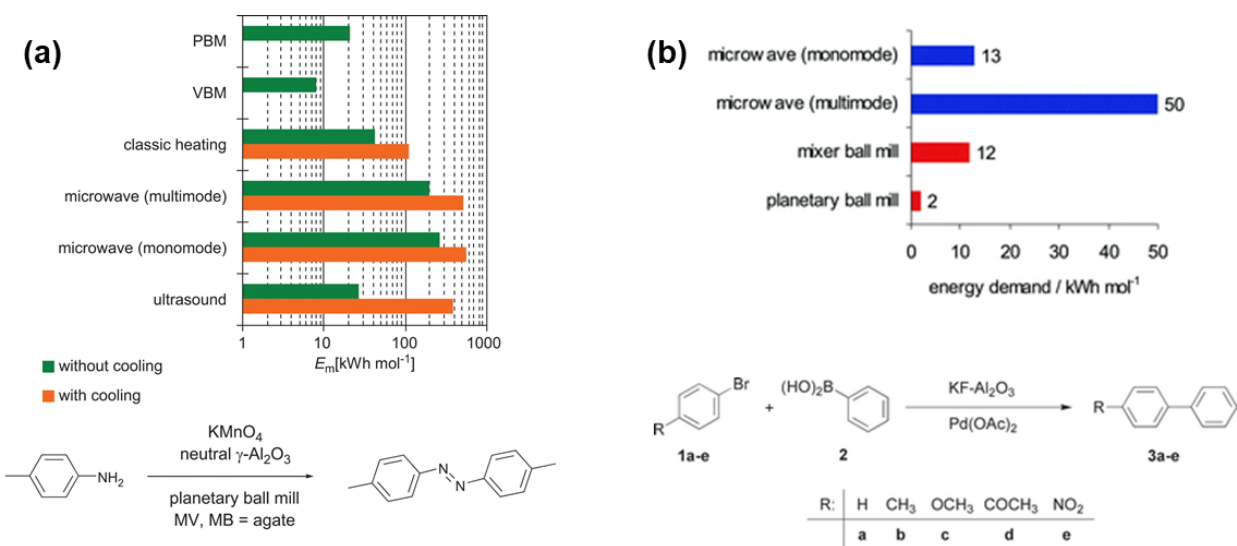


**Figure 2.2** Comparison of the molar energy for (a) the  $KMnO_4$ -mediated oxidation of *p*-toluidine; [6] and (b) Suzuki–Miyaura reaction of aryl bromides with phenylboronic acid [13] carried out with different methods of energy entry. (PBM = planetary ball mill, VBM = vibrational ball mill; Adapted from Stolle group [6, 13])

In addition to being energy-efficient green technology, the unique reaction conditions of mechanochemistry during ball milling also offer improved selectivity, [17] fast reaction rates with quantitative yields, [18-20] opportunities for new compound discovery, [21] and a way of obtaining compounds that are inaccessible otherwise or too unstable under solution-based thermochemistry. [1] Another interesting property of solid-state reactions is the anisotropy of organic crystals, this implies that the reactions performed in solid state such as ball milling may favor a specific orientation of the solid crystals depending on the inherent nature of the reactants, which is not applicable in solution-based chemistry. [22] Moreover, due to the absence of solvents, the mechanochemical method can circumvent the solubility issues and is particularly suited for non-soluble reactants, such as carbonates, [23] oxides, [24] and biopolymers like cellulose, etc. [25-27] Overall, mechanochemistry by ball milling offers tremendous potential for sustainable preparation of unique molecules, which has fueled the renaissance of this solvent-free and non-thermal methodology.

### **2.1.3 Experimental set-up and the control of the mechanochemical reactions**

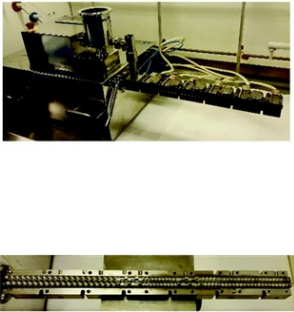
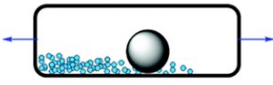
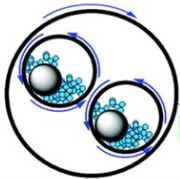
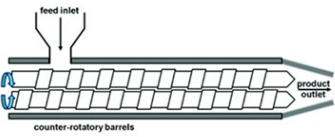
#### **2.1.3.1 Apparatus for conducting the mechanochemical reactions**

The traditional mortar and pestle represents the simplest setup for conducting mechanochemical reactions. However, in manual operations due to reproducibility issues and the overall limited mechanical energy input, the mechanochemical reactions are commonly conducted in automated high-intensity ball mills. [6] A basic setup of a ball mill consists of a reactor (the milling vial) and the milling media (the milling balls). Depending on how the ball mills are operated, they can be commonly classified as vibratory ball mills or planetary ball mills. (Figure 2.3)

**In the case of the vibratory ball mills**, the reactor performs radial oscillations in a horizontal plane causing the balls to attain very high velocities (in the order of several m/s) and colliding with the inside wall of the reactor or with each other if there are more than one milling ball. The resulting impact is considered the main source of the mechanical energy. When operated at a lower frequency, the milling balls are more likely to roll against the inside wall of the reactor creating more frictional forces. (Figure 2.3) **In the planetary ball mills**, the reactors are fixed on a rotating disc while spinning in the opposite direction about their own axes at the same time. The milling balls are accelerated by centrifugal forces and slide along the inside wall of the reactor creating

frictional energy. Moreover, during the alternation of the centrifugal forces as a result of counter-rotation between the reactor and rotating disc, the milling balls are lifted off the reactor and collide with the opposite wall of the reactor creating impact forces. (Figure 2.3) [6, 28]

Furthermore, **twin-screw extrusion** was recently developed as a tool for conducting continuous mechanochemical reactions to overcome the scalability challenges of ball milling. [10, 29, 30] It has recently been identified by IUPAC as one of the ten chemical innovations that will change the world. [31] In this setup, solid reagents are ground together by a pair of counter-rotatory screws as the mixture is transported along the extrusion path through a barrel and collected at the end. Reactive extrusion is more versatile compared to ball milling. For example, different sections of the screws can be selected to perform different functions for the purpose of mixing, conveying, or grinding. (Figure 2.3) Moreover, it can be easily integrated into flow chemistry, where reactions are run in a continuous flow stream rather than in a batch. This makes the mechanochemistry even more sustainable and attractive methodology. Although the twin-screw extrusion has been thoroughly investigated and applied in different fields such as polymer, materials and food sciences, however, it is only recently that started attracting the attention of chemists for its potential use in the preparation of synthetic compounds. [10, 29] Therefore, it is likely that in the coming years, we may see more applications of extrusion in synthetic chemistry. Furthermore, the mechanical forces created during the **ultrasound** treatments are also substantial, especially the tensile forces created on polymeric surfaces during the collapse of the cavitation bubbles. (Figure 2.1) [4, 32, 33] Therefore, a sonochemical experimental setup can also be used to conduct mechanochemical reactions. Finally, single molecular mechanochemistry using **atomic force microscopy (AFM)** can also be considered as an additional setup for carrying out mechanochemical studies. (Figure 2.1) [4, 34] Nevertheless, the ball mills are still the mainstream set-up for conducting mechanochemical research. The parameters for the control of the mechanochemical reactions in ball milling have been comprehensively reviewed by several groups. [6, 28]

	Vibratory ball mill	Planetary ball mill	Twin screw extrusion
Instrumental appearance & accessories			
Schematic illustration			
Motion description	Milling vial vibrating from side to side	Milling vial that sitting on a rotating disc spinning at a opposite direction	Solid reactants are grounded and compressed by a pair of counter-rotatory screws as the it is transported along the extrusion path through a barrel
Scale	Batch (mg to g)	Batch (mg to kg)	Continuous (kg/ hr)

**Figure 2.3** Comparison of vibratory ball mill, planetary ball mill, and twin-screw extrusion for conducting mechanochemical reactions. (Figures of instrumental appearance and accessories of vibratory ball mill and planetary ball mill are adapted from Retsch® company website; Figures of instrumental appearance and accessories of twin-screw extrusion are adapted from Crawford *et al.* (2017) [29]; Figures of Schematic illustration are adapted from Tan *et al.* (2019) [8])

### 2.1.3.2 Control of mechanochemical reactions in ball mills

Stolle (2015) classified the reaction variables in mechanochemistry into three categories including chemical parameters, technological parameters, and process parameters. (Figure 2.4) [6]

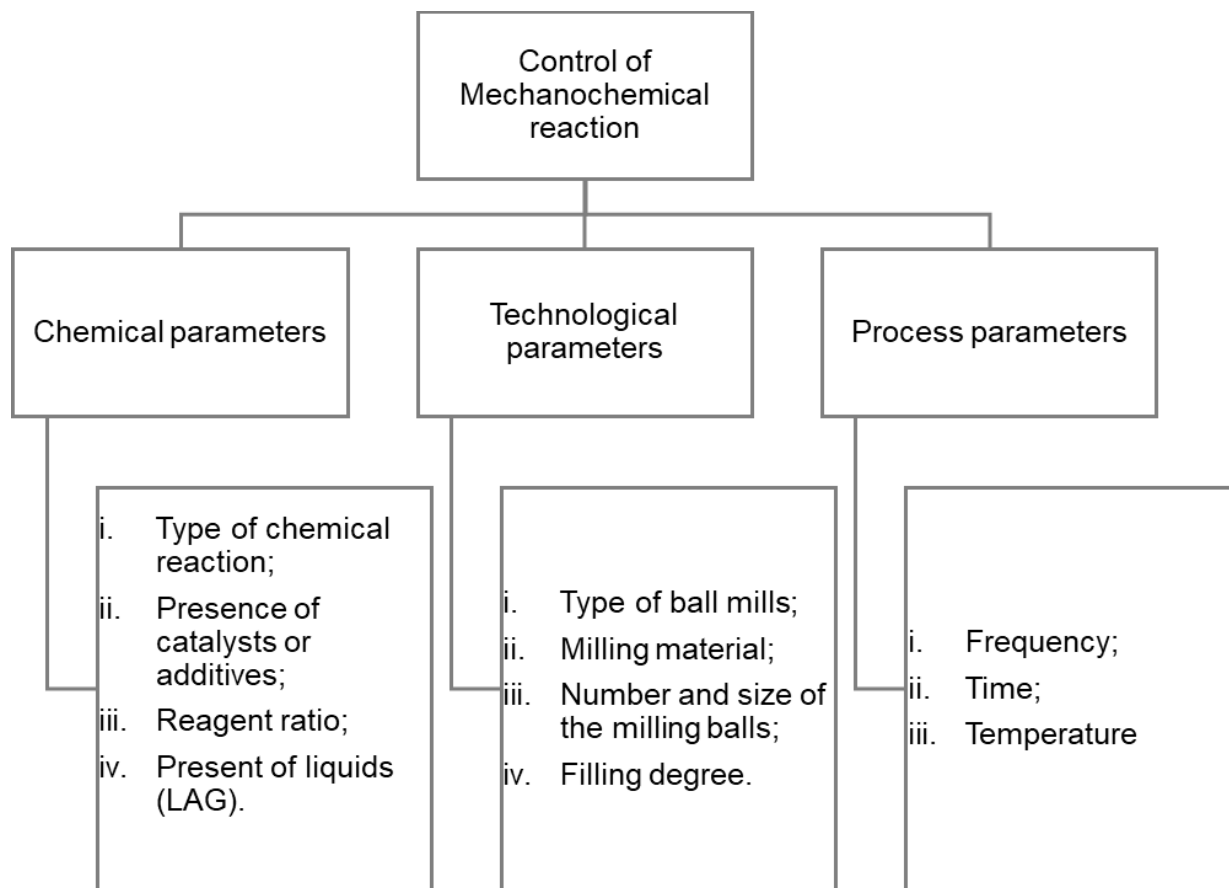


**Figure 2.4** Parameters that control the mechanochemical reactions in ball mills. (LAG = Liquid-assisted grinding; Reproduced from Stolle (2015) [6]).

**The technological and process parameters** together determine the total amount of mechanical energy input into a particular reaction. For example, *the vibrational frequency* of a mixer mill or rotational speed of a planetary mill are considered one of the most important parameters for controlling the outcome of a mechanochemical reaction since it directly determines the amount of mechanical energy input. [6, 10] Frequency affects the motion of the milling balls, which in turn influences the reaction kinetics and reaction outcome. (see Section 2.1.3.1 for details) Mack *et al.* (2017) suggested that the energetics in a ball mill are linked to Arrhenius' equation similar to solution-based chemistry. [35]

*The material* of the milling vial and milling balls also affect the mechanochemical reaction. [6] The density of the material determines the energy input. For example, tungsten carbide mill balls ( $\rho = 15.6 \text{ g/cm}^3$ ) provide higher kinetic energy than Teflon ( $\rho = 2.3 \text{ g/cm}^3$ ). [6] The chemical stability of the material of the milling vials should also be considered. For example, the corrosion of stainless-steel vials and leaching of the metal ions into the reaction medium have been reported to influence the outcome of the reaction. [28] Milling balls made of copper, on the other hand, have been reported to catalyze certain reactions. [36] Finally, transparent milling vials made from polymethyl methacrylate (PMMA) have been developed for *in-situ* reaction monitoring which significantly contributed to the unraveling of the mechanisms underlying the mechanochemical transformations. [37]

*The size and number of milling balls, the ratio of weight of the milling balls to the sample, and the ratio of volume of the milling balls to the volume of the reactor* all can influence the kinetics of the reaction and the mechanical energy supplied to the system. [6] Novel developments in the design of the reaction vials have also been made, such as modification of the reactor to include temperature and pressure sensors, [38, 39] specially designed reactors for gaseous reactants, [40] combining ball milling process with photochemistry and photocatalytic chemistry, [41] and aging. [26, 42]

**The chemical parameters**, on the other hand, have been the major factor contributing to the increase in the number of applications using mechanochemistry. For example, at the beginning of the 21<sup>st</sup> century, most research was focused on expanding the type of chemical reactions that can be conducted under ball milling conditions, [3] while in the last 10 years, majority of the advances made in the field of mechanochemistry were mainly focused on improving the reaction yields

using various additives and catalysts. [43] Both homogeneous and heterogeneous catalysts have been used in mechanochemical reactions for improving the yield, promoting selectivity, and lowering the activation energy (termed mechano-catalytic reactions). [44] Recently, biocatalysts (e.g. enzymes) have also been successfully employed in mechanochemical processes and they have exhibited remarkable performance compared to traditional solution-based reaction conditions (termed mechano-enzymatic reactions). [45]

The mechanochemical reactivity and selectivity can also be controlled by the addition of sub-stoichiometric amounts of solvents to the grinding process, this was termed liquid-assisted grinding (LAG). [46] The amount of the liquid added is measured by the ratio ( $\eta$ ) of the liquid ( $\mu\text{L}$ ) to the total solids (mg), where the LAG reaction lies in the range of  $0 < \eta \leq 1$ , and neat grinding at  $\eta = 0$ . [21, 43] The liquid in LAG processes may act as lubricant, enhancing overall mixing and reaction kinetics, as well as improving the amorphization of the reactants. [6] Similarly, processes that explore the addition of a sub-stoichiometric amounts of other additives to control the mechanochemical reactions are termed similarly, such as ion- and liquid-assisted grinding (ILAG), [47] vapor-assisted aging, [42] and polymer-assisted grinding (POLAG). [48] All of the above-mentioned additives have enhanced the potential of mechanochemistry and broadened the range of its applications allowing more controlled reaction outcomes. Milling auxiliaries are also frequently used in mechanochemical reactions. Compared to additives or catalysts, the milling auxiliaries are inert fillers and act as a solid “diluting” agent (e.g. NaCl salt). [49] It is often added in stoichiometric amounts (1-5 equivalents) to assist the breakdown of aggregated clumps of solids and results in a more powder-like homogeneous mixture. Therefore, it is particularly useful in preventing the formation of sticky or viscous reaction mixtures which may hinder the adequate movement of the milling balls. [49]

#### **2.1.4 Understanding mechanochemistry**

The diverse reactivities observed under ball milling relative to the conventional thermal approaches necessitates a fundamental understanding of the transformations induced by mechanical forces. Along with the expansion of mechanochemistry to various domains, our understanding of its fundamental principles continues to evolve. (Figure 2.5) [3, 7, 22, 50, 51] Mechanochemical reactions can be studied by a variety of solid-state characterization techniques

(*ex-situ*), such as X-ray powder diffraction (PXRD), FTIR, Raman spectroscopy, and solid-state NMR. [3, 21, 28] The *in-situ* measurements using PXRD or Raman spectroscopy has also been developed for real-time monitoring and characterization without interrupting the milling process. [21, 37, 52]

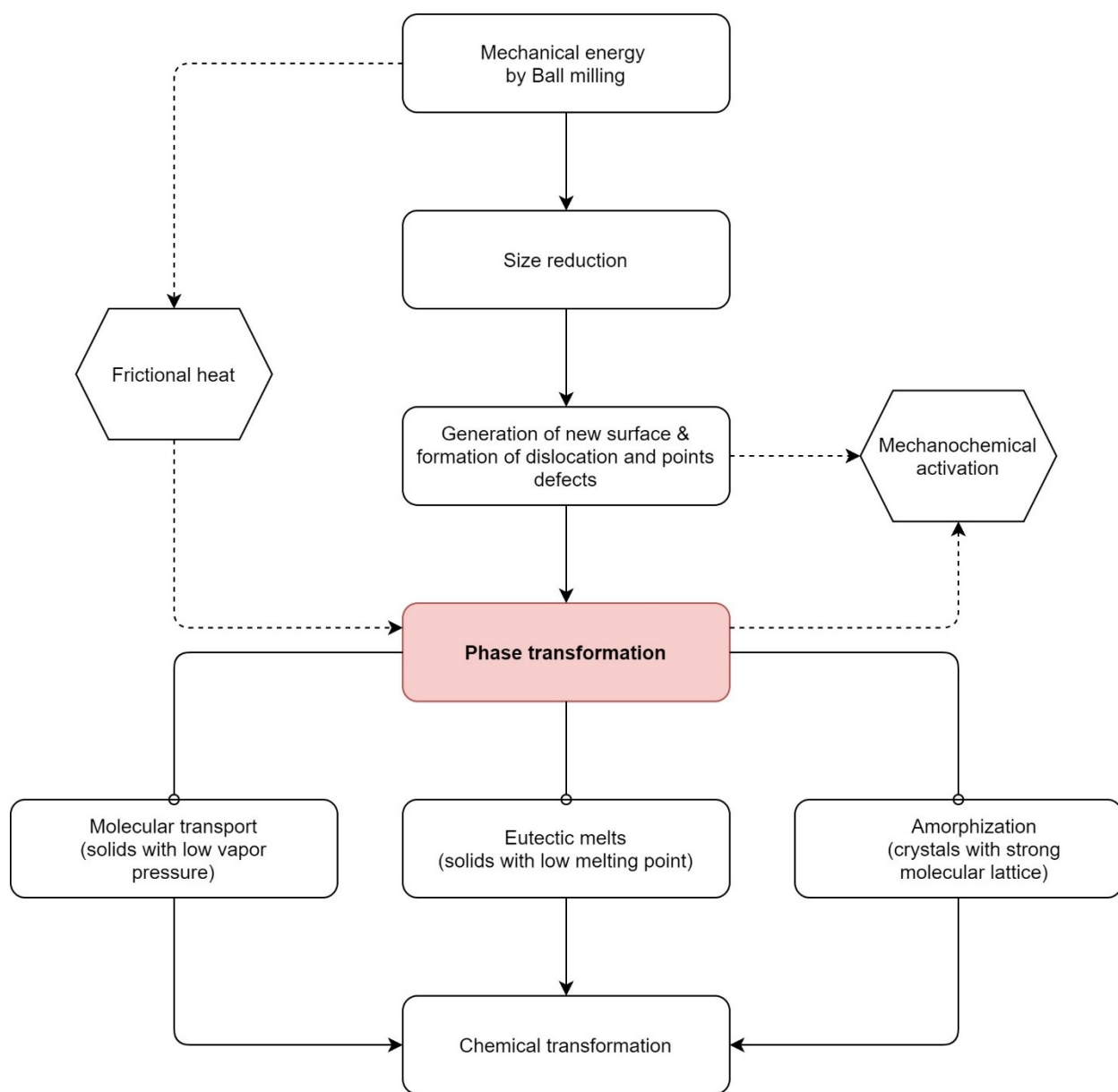


**Figure 2.5** Schematic illustration of the fundamental understanding of the mechanochemical transformations in organic chemistry

Organic and inorganic solids undergo various processes during ball milling in addition to particle size reduction; such as generation of new surfaces, the formation of dislocations and point defects, and phase transformations. These changes are considered to be important steps before any chemical transformation can actually take place. (Figure 2.5) [3, 10, 22, 53] These steps do not necessarily occur in the above-mentioned sequence, but the final result is essentially the same which is the intimate mixing of the reactants, a prerequisite for any type of chemical reaction. [22]

However, the diversity of the conditions under which mechanochemical reactions can occur, and the variations in the nature of the reactants employed makes it quite difficult to establish general rules for predicting the outcome of each reaction. For example, inorganic solids behave differently compared to organic solids during ball milling. The frictional heat plays a more important role in inorganic systems compared to organic reactants. The two most widely cited theoretical models for describing an inorganic mechanochemical reaction (metals or metal oxide) are “hot spot” and “magma-plasma” theories. Both models consider generation of localized heating in the order of several hundred or thousands of degrees Celsius for a very brief periods of time ( $10^{-3}$ – $10^{-4}$  s). [54] However, the two theories can hardly be applied to explain organic mechanochemical reaction systems since no reaction product can survive the extensive thermal decompositions at these temperatures. Despite frictional heat, which is inevitable in standard ball milling processes (except cryo-mills), in an organic reaction system, the type of reaction conducted plays a more important role in heat generation than the ball mill itself. [39] Boldyreva (2013) compared the similarities and differences between organic and inorganic mechanochemical reactions and summarized the particularities of the organic solids in mechanochemical transformations compared to the inorganic solids. This included the mechanical behavior of deformations, the lower vapor pressures, and the anisotropy of the organic crystals. [22]

During the investigation of mechanochemical co-crystal formation, Frišćić and Jones (2009) proposed three pathways leading to the formation of various non-covalent interactions (such as hydrogen bonds, van der Waal’s and  $\pi$ - $\pi$  stacking); including (i) molecular transport across surfaces for low vapor pressure solids, (ii) formation of eutectic melts, or (iii) formation of an amorphous phase. [55] (Figure 2.5) Similarly, the three pathways can be applied to covalent interactions as well. Depending on the nature of the reactants, an organic mechanochemical

reaction involving covalent bonding can be explained by all or several of the above mentioned three pathways.

#### **2.1.4.1 Eutectic intermediates**

It has been reported that the majority of organic mechanochemical reactions involving covalent bond formation proceed through a eutectic melt formation. [56] Rothenberg et al. (2001) observed the formation of a liquid phase at a temperature well below the melting point of the individual reactants during the investigation of a wide range of organic transformations in solid-state in mortar and pestle, including aldol condensation, ketone oxidation, phenol bromination, benzhydrol etherification and oligomerization of benzylic alcohols, etc. [56] Eutectic melt mechanism is relevant to product formation, especially from organic solids with low melting points, that are mediated by an intermediate liquid phase that subsequently disappears as the reaction approaches to completion.

#### **2.1.4.2 Molecular transport**

In the case of reactants with lower vapor pressure, molecular diffusion was proposed as a possible mechanism, in which product formation is expected to occur readily upon contact between solid reactants. The supplied mechanical energy can then assist such processes by accelerating the release and transport of loosely attached molecules in the lattice. [55] For example, the Kaupp group (1998) reported the synthesis of azomethine from solid anilines and solid benzaldehydes by grinding. By using atomic force microscopy and scanning near-field optical microscopy, the authors reported that the reaction proceeds without forming a liquid phase, instead the long-distance migration of the aldehydes into the lattice of aniline derivatives was observed. This result indicates that the reaction can take place not only at the points of contact of the two solids but also at the proximity where sublimation was enabling the reaction to occur in non-contacting interfaces. [57]

#### **2.1.4.3 Amorphization**

Mechanical energy can also induce amorphization in the organic solids whose molecules are strongly held in their crystal lattice (e.g. sugar crystals by substantial hydrogen bonding). The amorphous state produced during ball milling is expected to be more flexible which facilitates solid-state diffusion, hence increased reactivity. The impeccable evidence from the *in-situ* monitoring using PXRD also supports the formation of amorphous intermediate states. [55]

Amorphization of organic molecules using ball milling is a well-explored area in the pharmaceutical industry. The active pharmaceutical ingredients and the excipients in the amorphous phase are expected to have increased solubility and bioavailability. Descamps group have thoroughly investigated the amorphization of ball-milled sugars. [58-64] Caron *et al.* (2011) reported that milling-induced amorphization of  $\alpha$ -lactose, cannot be defined as a simple biphasic system consisting only of crystals and amorphous solids, instead, the process creates a state of continuum ranging from highly ordered crystalline structures to less ordered amorphous structures. [63] Furthermore, structural water plays an important role in determining the amorphization process due to its plasticizing effect, which can depress the effective glass transition temperature [64]. This underlines the importance of having hydrated reactants or *in-situ* generated water in a non-thermal milling environment. Descamps *et al.* (2007) also reported that milling crystalline compounds at below their glass transition temperatures directly induces solid-state vitrification, whereas milling crystalline compounds at above their glass transition temperatures induces polymorphic transformations, which results in the formation of metastable states. [62] Those results obtained outside of the study of organic mechanochemical transformations are important to our understanding of the mechanochemical reactivity that proceeds through intermediate amorphous phase.

There is no doubt that mechanochemistry is emerging as a powerful and environmentally benign synthetic methodology, however, its applications in the food science field are currently not explored, despite advances in related disciplines providing a solid theoretical background. For example, specific functional group transformations that play an important role in the various Maillard reaction steps, have been already studied, i.e. imine formation, [19, 57] aldol condensation, [65] and various quantitative multistep and sequential reactions. [18, 66] Examining those reactions from the perspective of Food Chemistry would be desirable.

## 2.2 The Maillard Reaction

The interest in the study of the Maillard reaction has been continuing ever since its discovery by the French chemists Louis-Camille Maillard in 1912. [67] The Maillard reaction is not only one of the most intensively researched reactions in food chemistry, but also it plays an important role in pathophysiology of diabetes and aging. [68, 69] In the food system, the Maillard reaction is closely related to the quality and safety of thermally processed foods. It is responsible not only for the generation of Maillard flavors, [70] but also for the generation of toxicants [71] and for the diminished nutritional value of proteins. [72] When performed outside of the food matrix, the Maillard reaction can be used to generate processed flavors [73] from a well-formulated mixture of precursors and carefully controlled reaction conditions and can modify the functionality of food related proteins. [74] However, understanding and directing the Maillard reaction to the desired end are challenging tasks since it is considered as a complex reaction cascade instead of a single chemical transformation. Therefore, understanding and controlling the reaction have been the focus of the Maillard reaction research today. (Figure 2.6)

The following sections critically reviews the Maillard reaction from these two perspectives – understanding and control. (Figure 2.6) Furthermore, to address the importance of the ever-expanding novel food processing technologies, the Maillard reaction under different stimuli (mechanical energy, sound wave, electricity, and light) is also discussed.

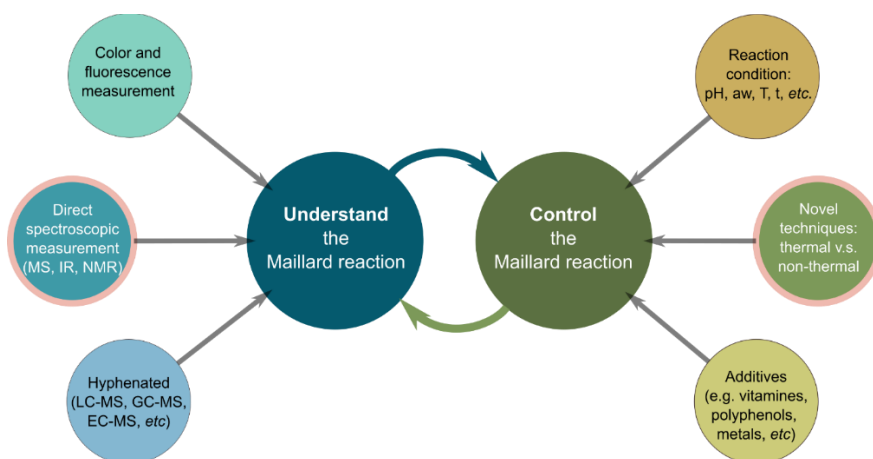


**Figure 2.6** Schematic illustration of the relationship between control and understanding of the Maillard reaction.

### 2.2.1 The complexity of the Maillard reaction

The two most accepted conceptual approaches for the understanding of the complexity of the Maillard reaction were proposed by Hodge (1953) [75] and Yaylayan (1997) [76] and are discussed here. Moreover, the importance of post-Schiff base transformations is highlighted [77] with a focus on the formation of 5-oxazolidinone [77, 78] and post-Schiff base sugar fragmentations. [79] Elementary transformations that built up the reaction cascade are also reviewed.

#### 2.2.1.1 Hodge's diagram

The first systematic understanding of the complexity of the Maillard reaction was proposed by Hodge (1953), [75] where the reaction was divided into three distinct stages consisting of initial, intermediate, and final phases. (Figure 2.7) According to this scheme, the reaction is initiated by the condensation between an  $\alpha$ -hydroxy carbonyl group of reducing sugars and an amino group from an amino acid, peptide, or protein leading to the formation of a Schiff base (a sub-class of imines). Due to its instability, the initially formed Schiff bases subsequently rearrange into its more stable isomer the Amadori compound (starting from an aldose) or Heyn's compound (starting from a ketose) under slightly acidic conditions and at intermediate water activity values. [75, 80] The subsequent degradation of the Amadori (or Heyn's) compound kick-starts the reaction cascade following repetitive and consecutive enolizations, dehydrations, fragmentations, redox, and condensation reactions leading to a broad array of reactive intermediates that will either polymerize to the characteristic yellow-brown colors or form stable volatile and aroma-active compounds in the final stages. [75, 80] Although the complexity of the Maillard reaction cannot be fully described by this simplified diagram, [81] however, it provided a solid background that led to more comprehensive studies. Amendments based on Hodge's diagram have also been proposed over the years. For example, the comprehensive summary by Nursten (1981, 2005), [80, 82] Tressl *et al.* (1995) that detailed the sugar fragmentations under different pH values, [83] and Weenen (1998) reviewed the contribution of ARPs together with sugar fragmentations on the formation of flavors. [84]

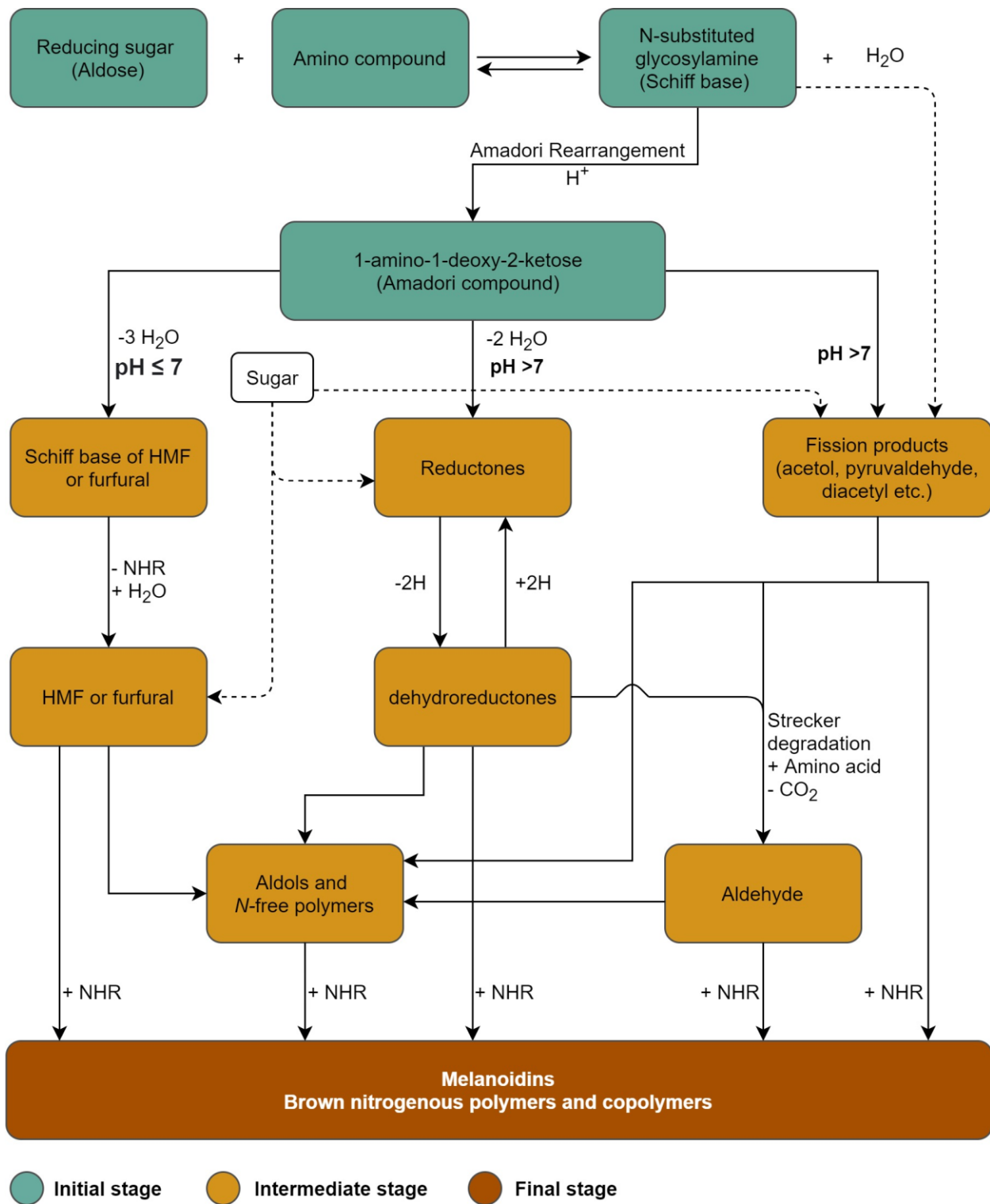
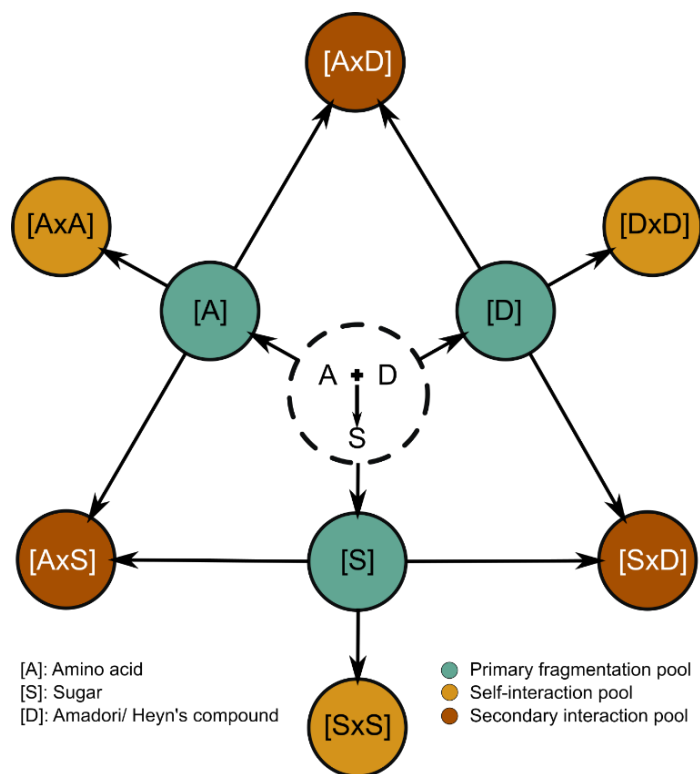


Figure 2.7 Hodge's diagram. (Reproduced from Hodge (1953) [75] and Nursten (2005) [82])

### **2.2.1.2 Yaylayan's classification of reaction pools**

A different concept to understand the Maillard reaction was proposed by Yaylayan (1997) where the Maillard reaction products were proposed to originate from three hypothetical “chemical pools” derived from sugars, amino acids, and the Amadori (or Heyn's) compounds. Subsequently, Arnoldi (2002) proposed to include a lipid-derived chemical pool to accommodate the contribution from lipids in the food matrix. [85] The reaction cascade was then considered to proceed through self-interactions of the proposed chemical pools (random reactions within the components of the same chemical pools) and through secondary interaction of the chemical pools (random reactions between components of different chemical pools) following a defined number of basic organic transformations that occur consecutively and in parallel. [76] (Figure 2.8) Compared to Hodge's diagram where the degradation of the Amadori compound was the primary consideration, Yaylayan's classification also takes into account the independent degradations of the sugars and amino acids. Moreover, the “origin” of different intermediates produced in the reaction cascade is also addressed. [76] This conceptual classification in conjunction with isotope labeling technique and high-throughput spectroscopic analytical protocols can be considered as a powerful predictive tool in searching for reaction intermediates and their pathways of generation in the Maillard reaction, [76, 86-89] hence, it provides a more holistic understanding of the molecular complexity of the Maillard reaction.



**Figure 2.8** Yaylayan's classification of the Maillard reaction as an interaction of the components in different chemical pools. (Reproduced from Yaylayan (1997) [76])

### 2.2.1.3 Post-Schiff base transformations: 5-oxazolidinone formation and Namiki's pathway

Both Hodge's diagram and Yaylayan's classification seem to overlook the critical role of Schiff bases in initiating and propagating the Maillard reaction. Indeed, the Amadori rearrangement preferentially occurs under conditions commonly encountered in food systems, i.e. intermediate moisture content and slightly acidic pH (5-7). [75, 77] However, various post-Schiff base transformations also contribute to the diversity of the Maillard reaction products. [77] Before their transformation into Amadori compounds, the initially formed Schiff bases can also undergo several reactions depending on the conditions. For example, the base-catalyzed transamination, [90-92] the intramolecular cyclization with either the side chain or the carboxylic acid group of the amino acids leading to 5-oxazolidinone moiety, [77, 78, 93, 94] and to the Namiki pathway. [79, 95, 96] (Figure 2.9) Those post-Schiff base transformations can be critical in determining the profile of the Maillard reaction products generated, especially under dry and basic conditions where Schiff bases tend to prevail. [77, 78, 92] For example, the formation of 5-oxazolidinones promotes subsequent decarboxylation reactions leading to the formation of *N*-protonated

azomethine ylides which are known to undergo a 1,2-prototropic shifts leading to two decarboxylated and isomeric Schiff bases. Their subsequent hydrolysis can lead to the formation of unique reaction products different from the degradation of Amadori compounds. (Figure 2.9) [77, 78] The 5-oxazolidinone has also been identified as an important intermediate in the formation of acrylamide, a thermally generated carcinogen. [97-100] A second example of post-Schiff base transformation is the Namiki pathway that was proposed by the Namiki group, which involves sugar fragmentation at C2-C3 position and the subsequent formation of 1,4-disubstituted pyrazinium cation radicals before the Amadori rearrangement. (Figure 2.9) [79, 95, 96, 101, 102] The glycolaldehyde generated from the retro-aldolization together with the free radicals opens a new route towards the color formation in the Maillard reaction. [79, 103]

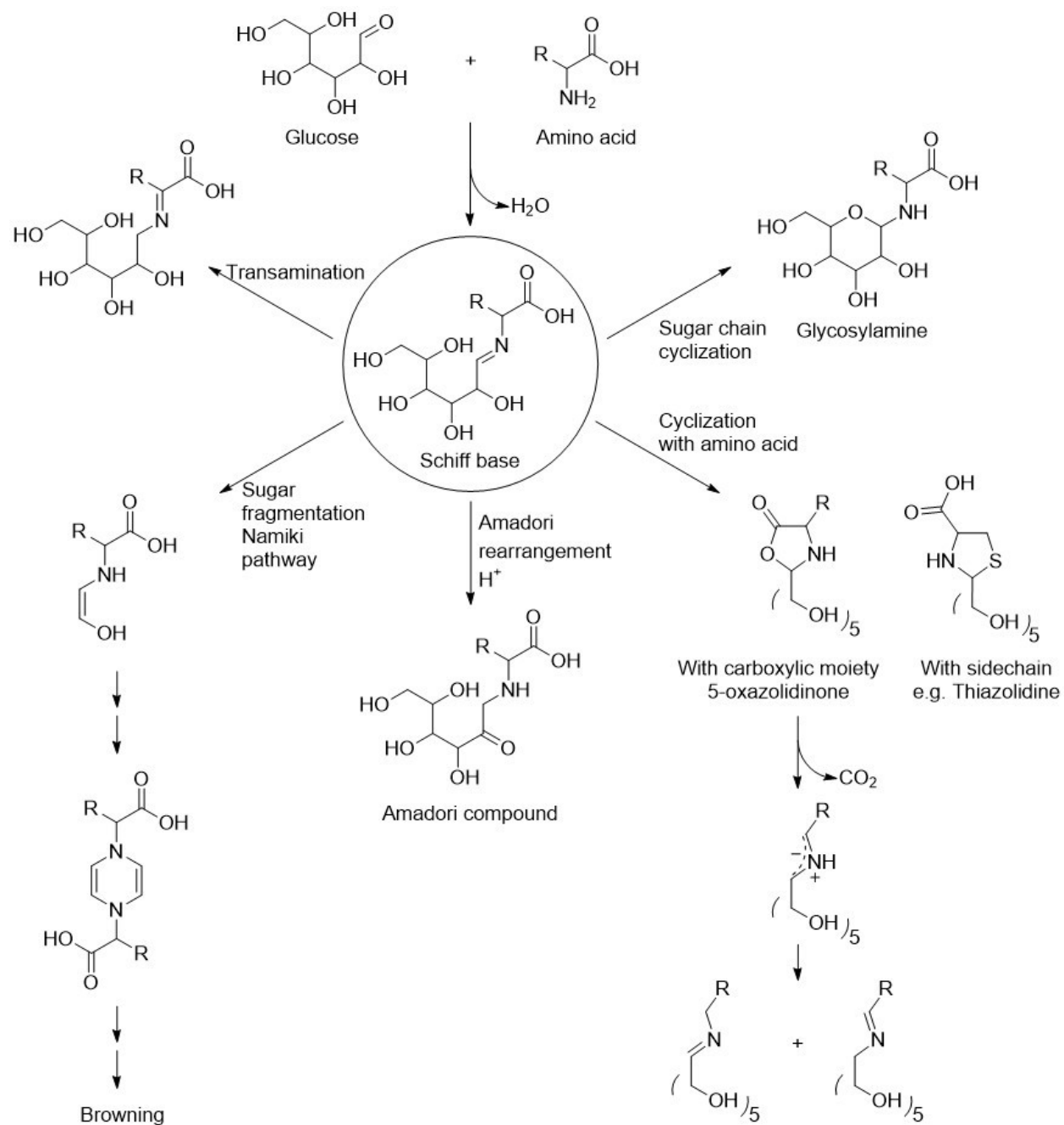


**Figure 2.9** Post-Schiff base transformations.

#### 2.2.1.4 Building blocks and the elementary transformations of the Maillard reaction

Despite its complexity, the Maillard reaction cascade can be simplified if assumed it consists of a set of simpler chemical transformations such as isomerization, fragmentation, condensation, and redox reactions, etc. This has been comprehensively reviewed by Yaylayan (1997) [76] and Parker (2015). [70] Due to the practical applications of using this type of classification of the Maillard reaction for the purpose of interpretation of complex HRMS data, in this section, the above mentioned basic transformations were further broken down into three categories, namely, reactions that lead to bond-formation which results in increased molecular weight, reactions that lead to bond-breaking which results in decreased molecular weights, and isomerization, which do not affect the molecular weight of the products. (Figure 2.10)

**Isomerization reactions** include mutarotation, enolization, tautomerization, and cyclization that normally do not result in changes in molecular weight, but they are considered vital for determining the fate of the subsequent reactions. For example, mutarotation of reducing sugars exposes the carbonyl groups and allows the condensation with amines; keto-enol tautomerization of ARP under different conditions results in different precursors to different fragmentation products; (Figure 2.11) cyclization of the imine with a carboxylic moiety of the amino acids leading to eventual decarboxylation; and cyclization of the sugar chain promoting dehydration, etc. (Figure 2.11) Those isomers can not be identified by their  $m/z$  (the mass to charge ratio) values, however, their elemental composition, MS/MS fragmentations or identification of their unique downstream fragmentation products can be considered as possible means for elucidating their presence during HRMS analysis.

**Bond-breaking:** Breaking of the carbon backbone of the sugar moiety fuels the progression of the Maillard reaction. They can undergo several types of cleavage reactions, such as retro-aldolization [104], hydrolytic  $\alpha$ -dicarbonyl cleavage [105], oxidative  $\alpha$ -dicarbonyl cleavage, [106] and hydrolytic  $\beta$ -dicarbonyl cleavages to produce reactive aldehydes and carboxylic acids (Figure 2.11) [84] Moreover, the amino acid can also undergo Strecker degradation and generate side chain specific aldehydes through decarboxylation and hydrolysis. [107]

**Bond-formation:** Carbonyl-amine condensation and aldol condensations are the two most frequently encountered reactions that are responsible for molecular weight increases. The carbonyl-amine condensation is not only the starting point for the Maillard reaction, but also

initiates the Strecker degradation, resulting in the formation of Strecker aldehydes and pyrazines, and plays an important role in the final stages of polymerization. Similarly, aldol condensation is one of the key reactions in both intermediate and final stages responsible for the polymerization of aldehydes. [108]

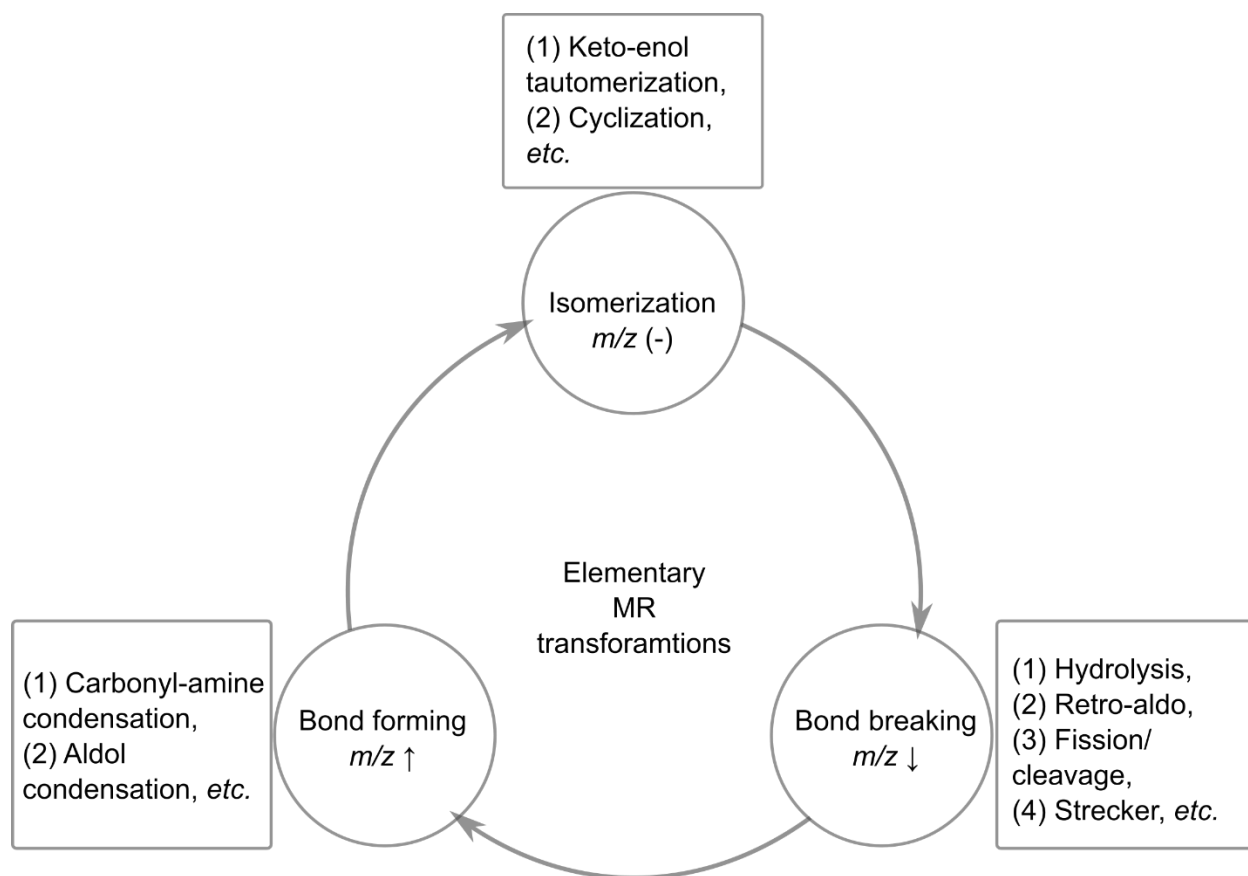


**Figure 2.10** Schematic illustration of the elementary transformations of the Maillard reaction.

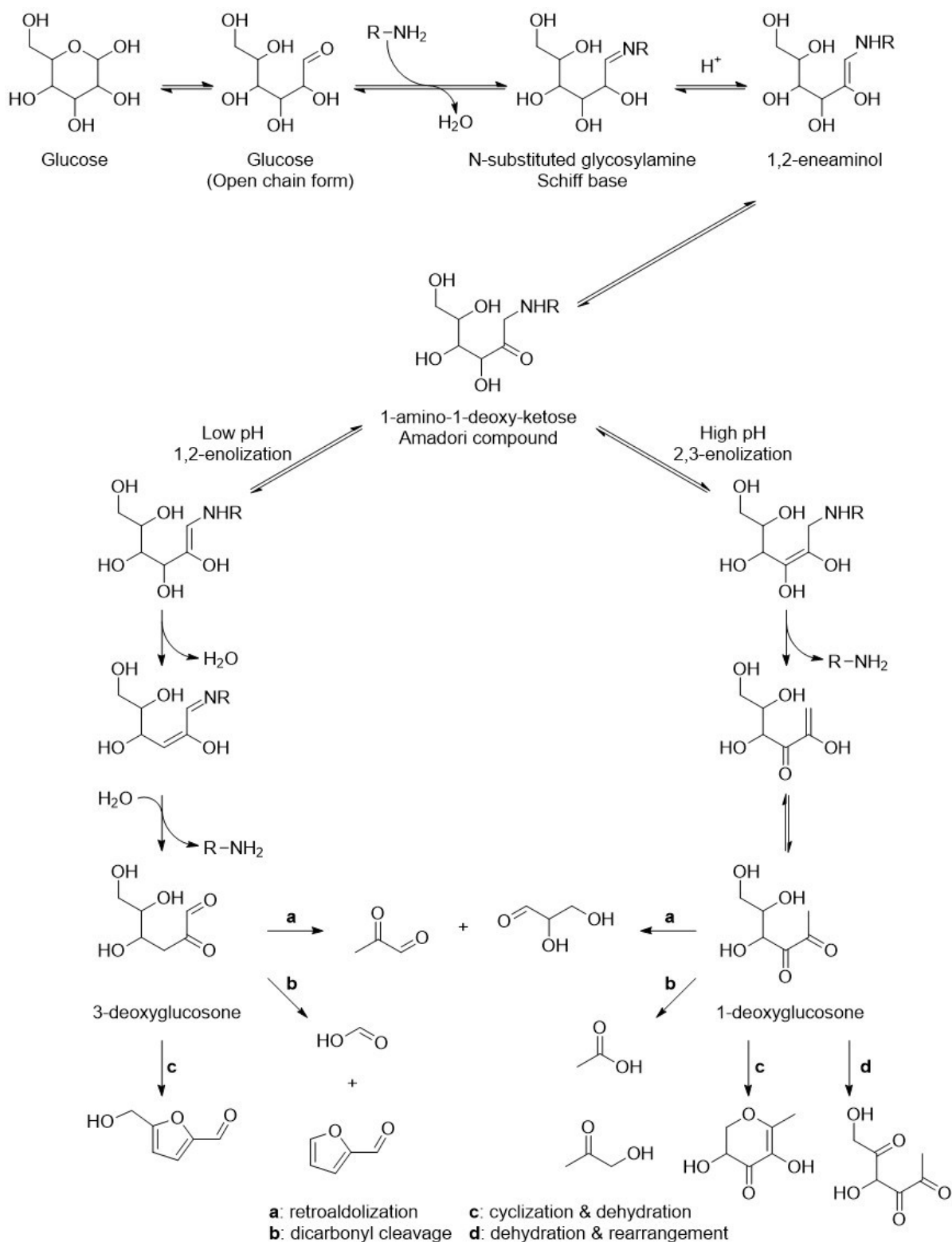


**Figure 2.11** The initial stage of the Maillard reaction and subsequent breakdown of Amadori rearrangement product under different pH values.

## 2.2.2 Challenges to the analysis of the Maillard reaction

In the previous section, we have demonstrated the complexity of the Maillard reaction. The four initial precursors (sugar, amino acid, Schiff base, and ARP) can each generate unique reaction products that can participate in the subsequent reaction cascade, resulting in the generation of an extremely complex reaction mixtures. Such mixtures exhibit a wide range of molecular weights, isomeric and stereochemical diversity with a complex dynamic range of concentrations and chemical stability. Moreover, an additional layer of complexity is added with the interaction of other components from outside of the framework of the Maillard reaction in real food or biological system, such as lipids, vitamins, metals, and polyphenols, etc. (see Section 2.2.3.1 for details) Therefore, a model system containing thoughtfully formulated reactants is normally considered for the study the Maillard reaction.

### 2.2.2.1 Analytical strategies

Despite the formation of a multitude of reaction products from simple Maillard reaction model systems containing only sugars and amino acids; color measurements and other direct optical spectroscopic methods, such as UV-Vis and fluorescence, [109, 110] still constitute the simplest yet effective way to assess the progression of the Maillard reaction due to the intensity of chromophores generated in the final stages of the reaction. However, down to the molecular level, the chemical diversity of the reaction products can vary from polar to non-polar products, [111] with a molecular weight ranging from as small as 30 Da (formaldehyde) up to polymers in the kDa ranges. [112] Another challenge in the analysis of the Maillard reaction is that both volatile and non-volatile residues are generated in wide concentration ranges. This places additional stringent requirement on the detectors used. What makes these complicated systems analytically even more challenging, is the formation of various isomers with differing chemical stabilities. For example, due to its reactivity, the Schiff bases, formed in the initial stage, are less studied compared to their more stable isomer the Amadori or Heyn's compounds and they still remain notoriously difficult to analyze in the Maillard reaction research. As a result, there are no comprehensive analytical strategies available to study the reaction as a whole in a single run. Common methods for studying the Maillard reaction are summarized in Figure 2.6.

**Direct spectroscopic measurements** examine the Maillard reaction mixtures collectively or chromatographically separated and purified fractions. Infrared spectroscopy (IR) collects

information on the presence of different functional groups; nuclear magnetic resonance spectroscopy (NMR) collects information on the type of nuclei present and their connectivity; and mass spectroscopy (MS) collects information on the distribution of molecular masses (the  $m/z$ : mass to charge ratio). However, due to the previously mentioned challenges regarding the molecular diversity and a dynamic concentration range of the Maillard reaction products, the separation and purification of reaction intermediates is not an easy task. The IR and NMR approaches fall short compared to MS analysis in terms of the clarity of the information obtained since IR and NMR spectra of complex mixtures normally require further mathematical treatments and statistical operations to generate useful structural information. On the other hand, the high-resolution MS can separate thousands of compounds based on their molecular weights in a single run and allows assignment of accurate elemental composition. Moreover, the proposed structures can be further elucidated during subsequent tandem mass spectrometry (MS/MS) and isotope labelling technique.

**Chromatographic separations** can be hyphenated with a spectroscopic detector for improved separation efficiency. The gas chromatography (GC) coupled with MS represents the most powerful technique in this category owing to its separation efficiency and the reproducible electron impact fragmentations. Moreover, the Yaylayan group advanced the GC/MS methodology for the Maillard reaction analysis by coupling in-line pyrolysis and isotope labeling techniques, which extended the usefulness of the technique in terms of experimental flexibility, reproducibility, as well as its ability for structural elucidation. [104, 113, 114] For these reasons, GC/MS type of analysis significantly contributed to our understanding of the Maillard reaction. [97, 98, 115, 116]

However, GC/MS is limited to the analysis of volatile or semi-volatile compounds of the Maillard reaction. For the analysis of the non-volatile residues, derivatization is needed. This process might interfere with the Maillard reaction and result in artifact formation and over-complicated spectra that are difficult to interpret. In this case, liquid chromatography (LC) or capillary electrophoresis (CE) can be used to separate the non-volatile residues of the Maillard reaction products. Hydrophilic interaction columns of LC (HILIC) and ion exchange columns (IC) have been developed for the separation of polar carbohydrate derivatives. [117, 118] Reversed-phase columns (RP) have been used to separate less polar reaction products such as furosine [119] and quinoxaline derivatives (derived from trapping  $\alpha$ -dicarbonyl with *o*-phenylenediamine). [120]

Capillary electrophoresis (CE) has also been developed as an alternative to LC for its better separation efficiency. [121-123] Various detectors can be coupled with LC or CE for optimized targeted analysis of selected Maillard reaction products, such as MS, [124] electrochemical detector, [117] and optical detectors, [125], etc. The tandem mass spectrometry (MS/MS) can also be used as a powerful tool for structural elucidation, however, the currently available information is limited only to few stable Maillard reaction products, such as the Amadori compound, [126-129], furosine, [130] acrylamide, [131] and 5-hydroxymethylfurfural (HMF). [131, 132]

#### **2.2.2.2 “Maillardomics” – study of the Maillard reaction using “-omics” tools and protocols.**

Considering the complexity of the Maillard reaction, targeted analysis cannot thoroughly assess the Maillard reaction in detail. Alternatively, due to the similarities of the Maillard reaction system to a metabolic system, [133] comprehensive understanding of the Maillard reaction is likely to be achieved by omics-type analysis, where all the molecules in a system are studied and characterized collectively. Despite widely available omics-tools and protocols from related fields such as metabolomics, genomics, and proteomics, etc., its application to the Maillard reaction system is still a challenging task considering the diversity of the molecules and isomers generated from the Maillard reaction cascade for several reasons. Firstly, there is a lack of standard databases for rapid annotation and screening of the Maillard reaction products for the high-throughput type of analysis using MS or NMR. Secondly, there is a need for integration of results from several analytical platforms, for which the required software and hardware is currently lacking. Finally, when dealing with real food systems or biological systems, it is difficult to identify the origin of targeted compounds, e.g. distinguishing the specific precursors of the various products, whether originating from the Maillard reaction or from lipid oxidation, or distinguishing the Maillard reaction products from enzymatic reactions. Nevertheless, recent studies by Hemmler *et al.* elegantly brought the Maillard reaction into the omics world. [88, 89, 134] By using direct injection Fourier-transform ion cyclotron resonance (FT-ICR) mass spectrometry together with metabolomic visualization tools such as utilization of mass difference network, Van Krevelen diagrams, and Kendrick mass defect analysis, etc., the author holistically and collectively streamlined the previous breakthroughs in Maillard reaction research with the current omics technologies. [88, 89]

### 2.2.3 Challenges facing the control of the Maillard reaction

Given the complexity of the Maillard reaction pathways and the diversity of the compounds formed, it is a difficult task to direct the Maillard reaction towards a desirable end such as the formation of taste and aroma compounds instead of toxicants and carcinogens or controlling the extent of glycation of proteins in food. Strategies to achieve this goal are numerous and constitute a major area of Maillard reaction research. These are broken down briefly into three categories. (Figure 2.12)

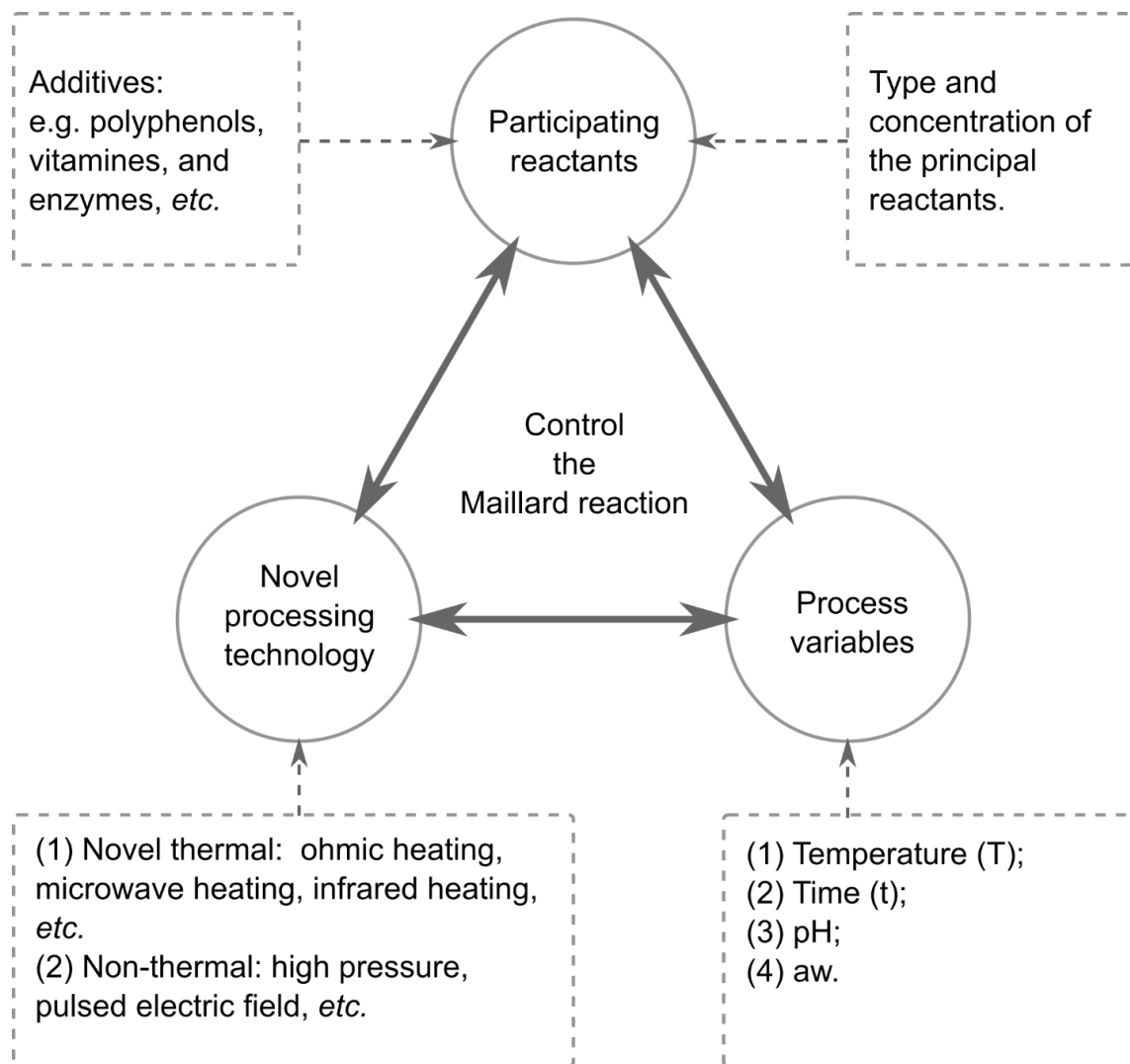


**Figure 2.12** Schematic diagram illustrating the control of the Maillard reaction through the participating reactants, process variables, and use of novel technologies.

### 2.2.3.1 Participating reactants

The choice of the main reactants, i.e. the sugars and the amino acids, plays an important role in determining the Maillard reaction rates and the product distribution. Generally, pentoses (e.g. ribose) are more reactive than hexoses (e.g. glucose), aldoses (e.g. glucose) are more reactive than ketoses (e.g. fructose), monosaccharides (e.g. glucose) are more reactive than disaccharides (e.g. maltose). [135, 136] Several factors determine the reactivity of the reducing sugars in the Maillard reaction such as stability of the acyclic forms, conformation of the rings, steric hindrance, the gauche effect, as well as the positioning of the C3 and C4 hydroxyl groups. [135] In the case of amino acids, lysine and arginine were shown to be the most reactive amino acids for the initial condensation and color formation, while glutamic acid and asparagine are the least reactive. [137] Different amino acids generate different side chain-specific Strecker aldehydes through Strecker reaction, [107] sulfur-containing amino acids are responsible for meaty flavor related compounds, [70] rhamnose is the most suitable precursor for the formation of furaneol, [70] and maltol formation is reserved to maltose or lactose instead of glucose. [138]

In a real food system, the Maillard reaction precursors or intermediates often interact with other food components (proteins, lipids, vitamins, and minerals) or are woven into other reaction cascades (e.g. lipid oxidation [139]). This fact increases its complexity and makes the analysis even more difficult, however, it provides opportunities for formulating and adding active compounds inspired from these interactions to guide the reaction flow in a controlled manner. A recent comprehensive review [140] offered a mechanistic view on how various functional ingredients interact with the Maillard reaction intermediates. Briefly, three categories of such functional ingredients are currently being actively researched, namely plant polyphenols (e.g. epicatechin [141, 142]), vitamins (e.g. pyridoxamine [143]), and enzymes (fructosamine oxidase, [144] and asparaginase [145]). Metals have also been used for the control of the Maillard reaction. [146-149] There is an expanding list of components that can be used to manipulate the Maillard reaction, an in-depth understanding of their mechanism of action will help to direct the Maillard reaction to the desired end.

### 2.2.3.2 Process variables

Process variables affecting thermally catalyzed Maillard reaction include reaction temperature (T), reaction time (t), pH, and water activity ( $a_w$ ), the kinetics aspect of the Maillard reaction has been critically reviewed by several groups. [81, 108, 150]

**Temperature & pH:** There are several steps in the Maillard reaction cascade that are sensitive to reaction temperature and pH at differing extents. Changing those variables might result in drastic changes in the kinetics and product distribution. For example, degradation of the ARPs is pH dependent. (Figure 2.11) Furthermore, the process variables also affect the reactivity of the initial reactants, i.e. the reducing sugars and the amino acids. The reducing sugars are only reactive when they are in an open-chain form whose concentration increases with increasing temperature and decreasing pH values. However, the active form of the amino-containing reactants is the un-protonated free forms which predominate when the pH is higher than the pKa value of the amino group. It has been reported that the first step in the Maillard reaction sequence has an optimum pH that is weakly acidic, maximizing the concentration of the open-chain forms of the sugars and simultaneously protonating the carbonyl groups making them better electrophiles, at the same time ensuring that the amino groups remain un-protonated. [70, 102] However, it is generally believed that the reaction and browning rates increase with increasing pH values. [81] The dynamic nature of the Maillard reaction itself also affects the pH, i.e. the pH of the reaction system decreases over the reaction time due to the generation of stable organic acids (such as acetic acid and formic acid) from the oxidative cleavage of the sugar chains. [151] As a result, the reaction may eventually become auto-inhibiting.

**Water activity** is also frequently recognized as an important factor. It has been reported that the optimum water activity lies at relatively low ranges (0.4-0.8) which promotes condensation and dehydration reactions. [81] However, below the optimum values, the solubility and mobility of the reactants gradually become limiting creating difficulty in diffusion and finally inhibiting contact between reactants. Water does not only act as a reaction medium for sugar and amino acids but also participates in hydrolytic reactions. The dual role of water in the Maillard reaction has been recognized by Van Boekel (2001). [81]

### 2.2.3.3 Novel technologies

The goal of food processing is to ensure food safety and at the same time to maintain food quality to which the Maillard reaction is closely linked (e.g. food color and organoleptic properties; thermally generated toxicants). It is therefore important to understand how the Maillard reaction behaves under different processing conditions, especially for technologies using different type of energy input other than thermal energy.

**Novel thermal processing techniques:** Various novel food processing technologies can be divided into thermal and non-thermal methods. (Figure 2.12) The concern of novel thermal processing technologies is generally to achieve more efficient heat transfer in a shorter period of time compared to conventional methods. Novel thermal processing technologies mainly influence the two most important process variables that are important for the control of the Maillard reaction: time and temperature. For example, the use of steam injection [152] or ohmic heating [153] tend to achieve instantaneous and uniform temperature increases and to avoid temperature gradients and heat transfer limitations. Electromagnetic irradiation represents another class of novel heating technology, which includes infrared heating, [154] microwave heating, [155] and radiofrequency heating. [156] All the novel heating methods mentioned are characterized by reduction in the heating times, to achieve minimal quality losses, and significant increases in energy savings over conventional heating methods such as baking and roasting. However, some of those technologies may pose challenges in terms of generation of Maillard reaction flavors, e.g. microwave heating. [157, 158] Furthermore, sound waves have also been increasingly explored as an efficient novel thermal processing method, such as ultrasound processing. (see Section 2.2.4 for details) [159, 160]

**Non-thermal processing techniques:** Although heat is the most commonly used energy input to reduce microbial load and enzymatic activity in food, other non-thermal technologies have also been developed to achieve the same goals. The most iconic and successful example in this class is the high hydrostatic pressure processing (HPP), where food items are immersed in liquids and placed under a high-pressure environment ranging from 300 to 600 MPa at ambient or refrigerated temperatures for 2 to 30 min. [161] It has been used for preserving fresh fruit, vegetables, or seafood as an alternative process to sterilization, pasteurization, and blanching for minimizing deterioration of natural flavors. Despite being a non-thermal process, HPP also affects the course of the Maillard reaction. In theory, high pressure favors bimolecular interactions rather than

unimolecular fragmentations, thus promoting carbonyl-amine condensations, and inhibition of subsequent sugar and amino acid breakdown. [162] This has been confirmed in a model system study with tryptophan and glucose or xylose, where the acceleration of the early-stage Maillard reaction with pressure was observed as well as the slowdown of subsequent steps. [163] However, during the storage of HP processed foods, the initiated Maillard reaction might continue and cause off-flavors and discoloration. High-pressure processing also affects the Maillard reaction through pressure-induced changes in pH values. The formation and subsequent degradation of glucose-lysine Amadori products were accelerated by high pressure treatments (400 MPa, 60 °C) and resulted in increased levels of intermediates and advanced reaction products. [164, 165]

Pulsed electric field (PEF) processing is another non-thermal technique that is gaining increased interest. PEF processing explores the permeability of biological membranes with the application of short pulses (in the range of  $\mu\text{s}$  to  $\text{ms}$ ) of high electric fields (over 10 kV/cm). The result of PEF treatment is the disintegration of the phospholipid bilayer of cell membranes (especially under acidic conditions), known as electroporation, which leads to cell death and can be used for microbial inactivation. [166] PEF processing is a promising technique that can be used in controlling the Maillard reaction. Two major findings have been reported so far: reduction of 5-(hydroxymethyl)-2-furfural (HMF) content in fruit juices [167] and acrylamide in potato products [166, 168] as a result of PEF processing. The reason for the first observation was attributed to the reduction in the reductone content as a result of redox reactions and the reason for the second finding has been attributed to the release of asparaginase as a result of PEF induced cell disintegration. Overall, the understanding of the Maillard reaction under PEF treatment is still incomplete, and more studies are needed in response to this emerging non-thermal technology. [169, 170]

### 2.2.4 The Maillard reaction under different stimuli

The emergence of diverse novel food processing techniques using a variety of energy sources, such as electromagnetic and sound waves, electricity, and pressure, has been driving the need for more in-depth understanding of the Maillard reaction. This aspect of the Maillard reaction has not been reviewed yet. Currently, light, electricity, and mechanical forces are emerging as alternative energy sources to facilitate chemical transformations during the Maillard reaction. Those technologies (namely, photochemistry, electrochemistry, and mechanochemistry) are currently enjoying a resurgence for their ability to enable a large variety of chemical transformations in a “green” manner which was inaccessible using thermal energy. [1] The following comparative discussion of the mechanochemical, sonochemical, electrochemical, and photochemical induced Maillard reaction is based on the most relevant literature. (Figure 2.13 & Table 2.1)

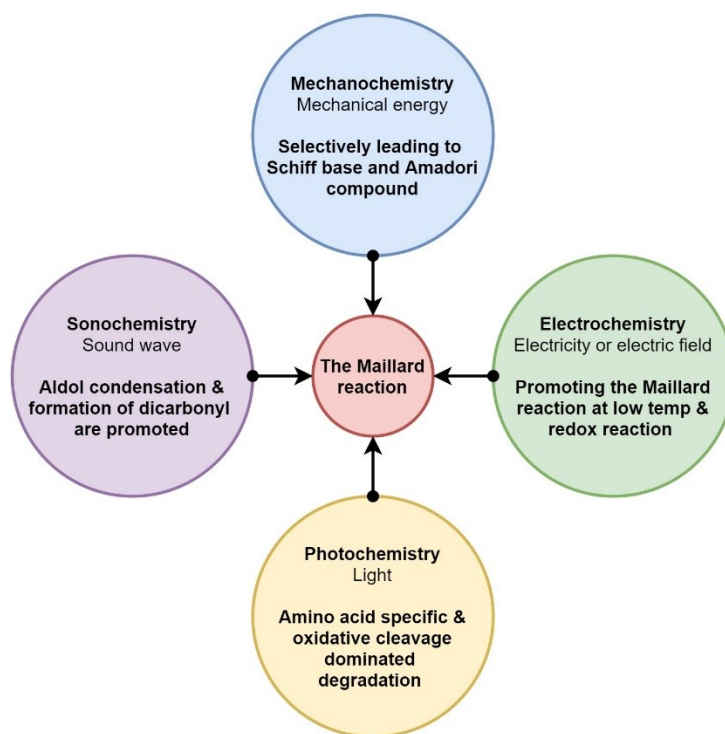


**Figure 2.13** Comparison of mechanochemical, sonochemical, electrochemical, and photochemical induced Maillard reaction

#### 2.2.4.1 Mechanochemistry

The details of the background of mechanochemistry have been provided earlier in Section 2.1. In short, mechanochemistry concerns chemical transformations resulting from direct absorption of mechanical energy commonly supplied by ball milling. Mechanochemical reactions can be conducted without bulk solvation and without supply of thermal energy. It is often applauded for its short reaction times and quantitative yields with minimum energy consumption. Although there are numerous mechanochemistry-based synthetic strategies with almost quantitative yields for the formation of imines [19, 57] (the first step of the Maillard reaction), however, there are no examples of its application to perform the Maillard reaction through ball milling, except in the patent literature reported by Nestlé (2017). [171] In this patent, they described a process to obtain Maillard flavor precursors by ball-milling of sugars and amino acids in the solid-state (20 minutes reaction time at 15 Hz). After solid-phase microextraction-GC/MS analysis of these mixtures, they reported the formation of various volatiles, such as 2-acetyl-1-pyrroline, 2,5-dimethylfuran and 2,5-dimethyl-4-(1-pyrrolidinyl)-3(2H)-furanone, etc. Moreover, according to the sensory panel, a significant improvement in the aroma intensity was noted when the ball-milled mixtures were added as flavor precursors before baking of experimental wafers compared to adding non-milled mixtures. [171] However, in this patent, the non-volatile residues formed from ball milling were not identified or disclosed nor the thermochemical properties of the mechanochemical reaction mixture during baking were reported. It seems the mechanochemical method is particularly well-suited for the generation of process flavors from the Maillard reaction. Conventionally, the manufacture of the Maillard reaction flavors is usually carried out under hydrothermal conditions where the reactants (sugar and amino acids) are dissolved in a buffer under controlled pH conditions. The solvent, normally water, needs to be removed after the reaction which is considered an energy-consuming step and may lead to considerable losses in the aroma-active volatiles. [73] The mechanochemical method, on the other hand, can eliminate the use of solvents. Moreover, the mechanochemical reaction can be considered as non-thermal process - the generally observed average reaction temperatures do not exceed 40 to 60 °C (depends on the reaction time and material of reactors) thus minimizing degradation of the target compounds and the loss of volatiles. [39, 172]

Although milling is commonly practiced in food processing, e.g. milling grains, however, the energy input in such processes allows only size reduction instead of chemical transformations and

are not considered as part of mechanochemistry. On the other hand, extrusion is emerging as the next-generation technology for conducting continuous mechanochemical reactions (see Section 2.1.3.1 for details). [31] The extrusion has already been extensively explored in the food industry for its ability to combine mixing, cooking, and texturizing in a single run. [173] However, the mechanochemical aspects of the extrusion has not been addressed yet. There are examples available in the literature concerning the application of extrusion in carrying out the Maillard reaction, for example, Yaylayan *et al.* (1992) investigated the generation of Maillard reaction flavors from glucose and tryptophan by extrusion, where they reported similar yields compared to aqueous reflux, but the rates of formation were around 8 times faster. [174] The mechanochemical effect can also be created in the liquid phase manifested as tensile forces (as compared to impact, kneading, and grinding in solid-state). These forces can be commonly encountered in processes such as homogenization, but the intensities are too weak to induce significant mechanochemical consequences. However, in a recent emerging processing technique using ultrasound it has been shown that mechanochemical effect can be created at the surface of the cavitation bubbles. [4]

#### **2.2.4.2 Sonochemistry**

When passing through a liquid media, ultrasound (frequency range between 20 kHz to 100 kHz) generates a continuous wave-type motion which creates alternate cycles of compression and expansion. During these alternating cycles, cavities are produced in the liquid medium and are promoted to grow to a critical size until they collapse. Upon collapsing, various radicals and a substantial amount of tensile forces are generated on the surface together with the release of acoustic energy in the form of heat to the surrounding molecules. [175]

Ultrasound alone, or in combination with pressure or heat, is becoming a promising alternative to conventional thermal food processing technique due to its ability to generate a substantial amount of heat in a short period of time, therefore, resulting in the rapid inactivation of microorganisms and enzymes in an energy-efficient manner. [176] Additionally, ultrasound has also been used for assisting various food processing steps for achieving optimum results, such as cutting, sterilization, extraction, drying, freezing, etc. [177] Furthermore, ultrasound has been recently identified as a promising tool for reducing allergenicity of proteins owing to the mechanical forces generated that results in the modification of the allergenic protein structure. [178]

The ultrasound-induced Maillard reaction has been recently reviewed by Yu *et al.* (2020). [159] Not surprisingly, and probably due to the high temperatures generated, the Maillard reaction can be initiated and promoted by ultrasound and results in the formation of colors and flavors. [159, 179] Aldol condensation is similarly promoted by ultrasound due to the high-pressure environment created from collapsing cavitation bubbles, which results in the generation of a variety of longer carbon chain substituted pyrazines that would be difficult or impossible to obtain from conventional thermal chemical methods. [180] Formation of 1,2-dicarbonyls is significantly promoted by ultrasound as well, hence, more Maillard reaction products are expected to form under ultrasound processing. [181] Furthermore, due to the high temperature and free radicals produced, lipid oxidation is also accelerated, which results in the formation of more carbonyl compounds able to participate in the Maillard reaction cascade. [182] The ultrasound has also been explored as a tool for post-translational modification of proteins owing to its ability to produce tensile forces that can modify the structure of the proteins, as well as its ability to promote the Maillard reaction. [159, 183]

#### **2.2.4.3 Electrochemistry**

Maillard reaction induced by electrochemistry is less explored, despite recent advances in pulsed electric field (PEF) and ohmic heating. The electrochemical properties of the Maillard reaction products have been extensively reviewed by Rizzi (2013). [184] The application of electrical energy in a chemical reaction system essentially concerns the selective addition or removal of electrons from one entity to another, such a process is considered as part of redox chemistry. [185] Furthermore, the electrochemical method creates new synthetic opportunities by reversing the polarity of known functional groups (e.g. electrophile and nucleophile interconversion), which cannot be achieved by other means. [186] In addition to the electric current that are commonly used for conducting electrochemical reactions (using electrodes), static electric fields are also increasingly being recognized as a tool for controlling chemical synthesis in the context of electrochemistry. [187] The PEF used for food processing is an example that falls in this category. The effect of PEF processing on Maillard reaction has been studied by Wang *et al.* [169, 170] They reported that PEF significantly promotes the Maillard reaction in a glucose-glycine model system at low temperatures (40 °C), especially at higher intensities (over 30 kV/cm). [169] The kinetic

study of Maillard reaction under PEF processing was also carried out by the same group, where they observed an enhanced browning accompanied by a reduction in pH with increased PEF intensity (i.e. higher field intensity and longer processing time). [170] The reason for this observation was attributed to the formation of organic acids such as formic acid and acetic acid. [170] Moreover, other studies have also observed a lower 5-(hydroxymethyl)-2-furfural (HMF) content for PEF processed juices as a result of the decreased formation of reductones. [167] Nevertheless, a detailed understanding is still needed.

In the field of electro-organic synthesis, it has been recently reported that carefully aligned external electric fields (direction, intensity, and multi-dimension, etc.) affect the chemical bonds, chemical structures, and reactions since most molecules and transition states have some degree of polarity. [187, 188] Most effects of an external electric field can be rationalized as field-induced stabilization of ionic structures, for example, orienting the electrical field along the “bond axis” will facilitate bond-breaking; orienting along the “reaction axis” will catalyze the reaction; flipping the field's orientation along the reaction-axis will cause inhibition; orienting the field off-reaction-axis will control stereo-selectivity and remove forbidden-orbital mixing. [187] Detailed understanding of the electrochemical behavior of the Maillard reaction will likely make PEF processing an even more powerful non-thermal technique and possibly an elegant synthetic tool for obtaining the desired Maillard reaction intermediates.

#### **2.2.4.4 Photochemistry**

Photochemical induced Maillard reaction is similarly less explored, [134, 189] despite its significance in food systems and its importance under physiological conditions. Photochemical reactions are normally induced by irradiation of UV light (100-400 nm) or visible light (400-700 nm). These conditions are commonly encountered in food processing or storage, as well as in eye lenses and on the skin during solar exposure. [190] As mentioned above UV light has also been employed as a novel non-thermal food processing tool. [191]

Photochemical reactions compared to other types of chemistries proceed in a completely different direction, in which molecules upon absorption of photons reach an electronically excited state. This results in a completely different electronic distribution compared to the ground state, hence, imparting different chemical properties and reactivity. Photochemical reactions are also highly

selective, and the photochemical reactivity is reserved only to certain families of compounds that can harvest light energy. [192] Photon-induced Maillard reaction was investigated by Hemmler *et al.* (2019) using simulated sunlight. [134] The Maillard reaction in model systems containing ribose and lysine or arginine or histidine was initiated by heating, followed by exposure to simulated sunlight. The results showed that the light irradiation promoted the flow of reaction cascade to a different set of transformations (dominated by oxidative cleavage) compared to thermal conditions. Moreover, photochemical degradations have been shown to have increased amino acid specificity, and the reactions were highly selective towards the formation of electron-rich aromatic heterocycles, such as pyrroles and pyrimidines. [134]

**Table 2.1** Comparison of the behavior of the Maillard reaction under different stimuli (mechanical force, sound waves, electricity or electric field, and simulated sunlight).

	Mechanochemistry	Sonochemistry	Electrochemistry	Photochemistry
Energy source	Mechanical energy by high-intensity ball mills	Sound wave with a frequency range from 20 kHz to 100 kHz.	Electricity or static electric field (over 30 kV/cm)	An electromagnetic wave with a frequency range of 100 nm to 700 nm
Mechanism of action	Size reduction, phase transformation, and intensive mixing	Formation of the cavitation bubble and subsequent collapse	Flow of electrons	Reach an electronically excited state
Solvents (as reaction media)	No	Yes	Yes	Optional
Maillard reaction behavior	Selectively leading to Schiff base and Amadori compound	Promoting aldol condensation and 1,2-dicarbonyl formation	Promoting low-temperature Maillard reaction, and redox reactions	Amino acid-specific and promoting oxidative cleavage

In conclusion, understanding and hence directing the complex Maillard reaction cascade to a desired end are challenging tasks. Addressing these two challenges through the application of high-resolution mass spectrometry and non-thermal solvent-free mechanochemistry is the topic of the remaining chapters of this thesis.

## 2.3 References

1. Robertson, J.C., M.L. Coote, and A.C. Bissember, *Synthetic applications of light, electricity, mechanical force and flow*. Nature Reviews Chemistry, 2019. **3**(5): p. 290-304.
2. IUPAC, *Compendium of Chemical Terminology, 2nd ed. (the "Gold Book")*. Compiled by A. D. McNaught and A. Wilkinson. Blackwell Scientific Publications, Oxford (1997). Online version (2019-) created by S. J. Chalk. ISBN 0-9678550-9-8. 1997.
3. James, S.L., et al., *Mechanochemistry: opportunities for new and cleaner synthesis*. Chemical Society Reviews, 2012. **41**(1): p. 413-447.
4. Beyer, M.K. and H. Clausen-Schaumann, *Mechanochemistry: The Mechanical Activation of Covalent Bonds*. Chemical Reviews, 2005. **105**(8): p. 2921-2948.
5. Suslick, K.S., *Mechanochemistry and sonochemistry: concluding remarks*. Faraday Discussions, 2014. **170**(0): p. 411-422.
6. Stolle, A., *CHAPTER 10 Technical Implications of Organic Syntheses in Ball Mills, in Ball Milling Towards Green Synthesis: Applications, Projects, Challenges*. 2015, The Royal Society of Chemistry. p. 241-276.
7. Takacs, L., *The historical development of mechanochemistry*. Chemical Society Reviews, 2013. **42**(18): p. 7649-7659.
8. Tan, D. and F. García, *Main group mechanochemistry: from curiosity to established protocols*. Chemical Society Reviews, 2019. **48**(8): p. 2274-2292.
9. Howard, Joseph L., Q. Cao, and D.L. Browne, *Mechanochemistry as an emerging tool for molecular synthesis: what can it offer?* Chemical Science, 2018. **9**(12): p. 3080-3094.
10. Andersen, J. and J. Mack, *Mechanochemistry and organic synthesis: from mystical to practical*. Green Chemistry, 2018. **20**(7): p. 1435-1443.
11. Rightmire, N.R. and T.P. Hanusa, *Advances in organometallic synthesis with mechanochemical methods*. Dalton Transactions, 2016. **45**(6): p. 2352-2362.
12. Braga, D., et al., *Mechanochemical preparation of molecular and supramolecular organometallic materials and coordination networks*. Dalton Transactions, 2006(10): p. 1249-1263.

13. Schneider, F., et al., *Energetic assessment of the Suzuki–Miyaura reaction: a curtate life cycle assessment as an easily understandable and applicable tool for reaction optimization*. Green Chemistry, 2009. **11**(11): p. 1894-1899.
14. Kaupp, G., *Solid-state molecular syntheses: complete reactions without auxiliaries based on the new solid-state mechanism*. CrystEngComm, 2003. **5**(23): p. 117-133.
15. Kaupp, G., J. Schmeyers, and U.D. Hangen, *Anisotropic molecular movements in organic crystals by mechanical stress*. Journal of Physical Organic Chemistry, 2002. **15**(6): p. 307-313.
16. Kaupp, G., *Waste-free large-scale syntheses without auxiliaries for sustainable production omitting purifying workup*. CrystEngComm, 2006. **8**(11): p. 794-804.
17. Hernández, J.G. and C. Bolm, *Altering Product Selectivity by Mechanochemistry*. The Journal of Organic Chemistry, 2017. **82**(8): p. 4007-4019.
18. Kaupp, G., J. Schmeyers, and J. Boy, *Iminium Salts in Solid-State Syntheses Giving 100% Yield*. Journal für praktische Chemie, 2000. **342**(3): p. 269-280.
19. Kaupp, G., J. Schmeyers, and J. Boy, *Quantitative Solid-State Reactions of Amines with Carbonyl Compounds and Isothiocyanates*. Tetrahedron, 2000. **56**(36): p. 6899-6911.
20. Kaupp, G., M. Reza Naimi-Jamal, and J. Schmeyers, *Solvent-free Knoevenagel condensations and Michael additions in the solid state and in the melt with quantitative yield*. Tetrahedron, 2003. **59**(21): p. 3753-3760.
21. Do, J.-L. and T. Friščić, *Mechanochemistry: A Force of Synthesis*. ACS Central Science, 2017. **3**(1): p. 13-19.
22. Boldyreva, E., *Mechanochemistry of inorganic and organic systems: what is similar, what is different?* Chemical Society Reviews, 2013. **42**(18): p. 7719-7738.
23. Li, Y.X., et al., *Preparation of nano-sized CeO<sub>2</sub> by mechanochemical reaction of cerium carbonate with sodium hydroxide*. Materials Letters, 2004. **58**(1): p. 245-249.
24. Xiao, W., et al., *Facile Synthesis of Highly Porous Metal Oxides by Mechanochemical Nanocasting*. Chemistry of Materials, 2018. **30**(9): p. 2924-2929.
25. Meine, N., R. Rinaldi, and F. Schüth, *Solvent-Free Catalytic Depolymerization of Cellulose to Water-Soluble Oligosaccharides*. ChemSusChem, 2012. **5**(8): p. 1449-1454.

26. Hammerer, F., et al., *Solvent-free enzyme activity: quick, high-yielding mechano-enzymatic hydrolysis of cellulose into glucose*. *Angewandte Chemie International Edition*, 2018.
27. Furusato, S., et al., *Mechanochemical Decomposition of Crystalline Cellulose in the Presence of Protonated Layered Niobium Molybdate Solid Acid Catalyst*. *ChemSusChem*, 2018. **11**(5): p. 888-896.
28. Margetić, D. and V. Štrukil, *Chapter 1 - Practical Considerations in Mechanochemical Organic Synthesis*, in *Mechanochemical Organic Synthesis*, D. Margetić and V. Štrukil, Editors. 2016, Elsevier: Boston. p. 1-54.
29. Crawford, D.E., et al., *Organic synthesis by Twin Screw Extrusion (TSE): continuous, scalable and solvent-free*. *Green Chemistry*, 2017. **19**(6): p. 1507-1518.
30. Egleston, B.D., et al., *Continuous and scalable synthesis of a porous organic cage by twin screw extrusion (TSE)*. *Chemical Science*, 2020. **11**(25): p. 6582-6589.
31. Gomollón-Bel, F., *Ten Chemical Innovations That Will Change Our World: IUPAC identifies emerging technologies in Chemistry with potential to make our planet more sustainable*. *Chemistry International*, 2019. **41**(2): p. 12.
32. Nguyen, T.Q. and H.-H. Kausch, *Mechanochemical degradation in transient elongational flow*, in *Macromolecules: Synthesis, Order and Advanced Properties*. 1992, Springer Berlin Heidelberg: Berlin, Heidelberg. p. 73-182.
33. Nguyen, T.Q., Q.Z. Liang, and H.-H. Kausch, *Kinetics of ultrasonic and transient elongational flow degradation: a comparative study*. *Polymer*, 1997. **38**(15): p. 3783-3793.
34. Ribas-Arino, J. and D. Marx, *Covalent mechanochemistry: theoretical concepts and computational tools with applications to molecular nanomechanics*. *Chemical reviews*, 2012. **112**(10): p. 5412-5487.
35. Andersen, J.M. and J. Mack, *Decoupling the Arrhenius equation via mechanochemistry*. *Chemical Science*, 2017. **8**(8): p. 5447-5453.
36. Su, W., et al., *Solvent-Free Cross-Dehydrogenative Coupling Reactions under High Speed Ball-Milling Conditions Applied to the Synthesis of Functionalized Tetrahydroisoquinolines*. *The Journal of Organic Chemistry*, 2011. **76**(21): p. 9144-9150.

37. Friščić, T., et al., *Real-time and in situ monitoring of mechanochemical milling reactions*. Nature Chemistry, 2013. **5**(1): p. 66-73.
38. Doppiu, S., L. Schultz, and O. Gutfleisch, *In situ pressure and temperature monitoring during the conversion of Mg into MgH<sub>2</sub> by high-pressure reactive ball milling*. Journal of Alloys and Compounds, 2007. **427**(1): p. 204-208.
39. Kulla, H., et al., *Warming up for mechanochemistry – temperature development in ball mills during synthesis*. Chemical Communications, 2017. **53**(10): p. 1664-1667.
40. Bolm, C. and J.G. Hernández, *Mechanochemistry of Gaseous Reactants*. Angewandte Chemie International Edition, 2019. **58**(11): p. 3285-3299.
41. Stojaković, J., B.S. Farris, and L.R. MacGillivray, *Liquid-assisted vortex grinding supports the single-step solid-state construction of a [2.2]paracyclophane*. Faraday Discussions, 2014. **170**(0): p. 35-40.
42. Jia, C., et al., *Efficient vapour-assisted aging and liquid-assisted grinding synthesis of a microporous copper-adeninate framework*. CrystEngComm, 2014. **16**(29): p. 6552-6555.
43. Friščić, T., C. Mottillo, and H.M. Titi, *Mechanochemistry for Synthesis*. Angewandte Chemie International Edition, 2020. **59**(3): p. 1018-1029.
44. Hick, S.M., et al., *Mechanocatalysis for biomass-derived chemicals and fuels*. Green Chemistry, 2010. **12**(3): p. 468-474.
45. Kaabel, S., T. Friščić, and K. Auclair, *Mechanoenzymatic Transformations in the Absence of Bulk Water: A More Natural Way of Using Enzymes*. ChemBioChem, 2020. **21**(6): p. 742-758.
46. Friščić, T., et al., *Screening for Inclusion Compounds and Systematic Construction of Three-Component Solids by Liquid-Assisted Grinding*. Angewandte Chemie International Edition, 2006. **45**(45): p. 7546-7550.
47. Friščić, T., et al., *Ion - and Liquid -Assisted Grinding: Improved Mechanochemical Synthesis of Metal–Organic Frameworks Reveals Salt Inclusion and Anion Templating*. Angewandte Chemie International Edition, 2010. **49**(4): p. 712-715.
48. Hasa, D., et al., *Cocrystal Formation through Mechanochemistry: from Neat and Liquid - Assisted Grinding to Polymer -Assisted Grinding*. Angewandte Chemie International Edition, 2015. **54**(25): p. 7371-7375.

49. Stolle, A., et al., *Ball milling in organic synthesis: solutions and challenges*. Chemical Society Reviews, 2011. **40**(5): p. 2317-2329.
50. Ardila-Fierro, K.J., et al., *Direct Visualization of a Mechanochemically Induced Molecular Rearrangement*. Angewandte Chemie International Edition, 2020. **59**(32): p. 13458-13462.
51. Friščić, T. and W. Jones, *Recent advances in understanding the mechanism of cocrystal formation via grinding*. Crystal Growth and Design, 2009. **9**(3): p. 1621-1637.
52. Užarević, K., I. Halasz, and T. Friščić, *Real-Time and In Situ Monitoring of Mechanochemical Reactions: A New Playground for All Chemists*. The Journal of Physical Chemistry Letters, 2015. **6**(20): p. 4129-4140.
53. Fernández-Bertran, J.F., *Mechanochemistry: an overview*. Pure and Applied Chemistry, 1999. **71**(4): p. 581.
54. Baláž, P., *Mechanochemistry in nanoscience and minerals engineering*. 2008, Springer, Berlin Heidelberg.
55. Friščić, T. and W. Jones, *Recent Advances in Understanding the Mechanism of Cocrystal Formation via Grinding*. Crystal Growth & Design, 2009. **9**(3): p. 1621-1637.
56. Rothenberg, G., et al., *Understanding solid/solid organic reactions*. Journal of the American Chemical Society, 2001. **123**(36): p. 8701-8708.
57. Schmeyers, J., et al., *Quantitative solid–solid synthesis of azomethines*. Journal of the Chemical Society, Perkin Transactions 2, 1998(4): p. 989-994.
58. Dujardin, N., et al., *Solid state vitrification of crystalline  $\alpha$  and  $\beta$ -D-glucose by mechanical milling*. Solid State Communications, 2008. **148**(1-2): p. 78-82.
59. Dujardin, N., et al., *First obtaining of glass solutions and phase diagram of glucose with fully tunable anomeric concentration*. Journal of pharmaceutical sciences, 2010. **99**(3): p. 1476-1483.
60. Dujardin, N., et al., *Solid State Mutarotation of Glucose*. The Journal of Physical Chemistry B, 2011. **115**(7): p. 1698-1705.
61. Descamps, M., et al., *The amorphous state of pharmaceuticals obtained or transformed by milling: Sub-Tg features and rejuvenation*. Journal of Non-Crystalline Solids, 2015. **407**: p. 72-80.

62. Descamps, M., et al., *Transformation of Pharmaceutical Compounds upon Milling and Comilling: The Role of Tg*. Journal of Pharmaceutical Sciences, 2007. **96**(5): p. 1398-1407.
63. Caron, V., et al., *Solid state amorphization kinetic of alpha lactose upon mechanical milling*. Carbohydrate Research, 2011. **346**(16): p. 2622-2628.
64. Willart, J.F., et al., *Amorphization of sugar hydrates upon milling*. Carbohydrate Research, 2010. **345**(11): p. 1613-1616.
65. Raston, C.L. and J.L. Scott, *Chemoselective, solvent-free aldol condensation reaction*. Green Chemistry, 2000. **2**(2): p. 49-52.
66. Kaupp, G., et al., *Cascade Reactions in Quantitative Solid-State Syntheses*. Angewandte Chemie International Edition, 1999. **38**(19): p. 2896-2899.
67. Maillard, L., *Action of amino acids on sugars. Formation of melanoidins in a methodical way*. Comptes-Rendus de l'Academie des Sciences, 1912. **154**: p. 66-68.
68. Somoza, V., *Five years of research on health risks and benefits of Maillard reaction products: An update*. Molecular Nutrition & Food Research, 2005. **49**(7): p. 663-672.
69. Hellwig, M. and T. Henle, *Baking, Ageing, Diabetes: A Short History of the Maillard Reaction*. Angewandte Chemie International Edition, 2014. **53**(39): p. 10316-10329.
70. Parker, J.K., *8 - Thermal generation of aroma*, in *Flavour Development, Analysis and Perception in Food and Beverages*. 2015, Woodhead Publishing. p. 151-185.
71. Stadler, R.H. and D.R. Lineback, *Process-induced food toxicants: occurrence, formation, mitigation, and health risks*. 2008: John Wiley & Sons.
72. de Vrese, M., et al., *Protein-bound D-amino acids, and to a lesser extent lysinoalanine, decrease true ileal protein digestibility in minipigs as determined with <sup>15</sup>N-labeling*. The Journal of nutrition, 2000. **130**(8): p. 2026-2031.
73. Sukan, M.K. and D.K. Weerasinghe, *Process and reaction flavors: An overview*. 2005, ACS Publications.
74. Wang, Z., et al., *Advanced glycation end-product N ε-carboxymethyl-Lysine accelerates progression of atherosclerotic calcification in diabetes*. Atherosclerosis, 2012. **221**(2): p. 387-396.
75. Hodge, J.E., *Dehydrated foods, chemistry of browning reactions in model systems*. Journal of agricultural and food chemistry, 1953. **1**(15): p. 928-943.

76. Yaylayan, V.A., *Classification of the Maillard reaction: A conceptual approach*. Trends in Food Science & Technology, 1997. **8**(1): p. 13-18.
77. Chu, F.L. and V.A. Yaylayan, *Post-Schiff Base Chemistry of the Maillard Reaction: Mechanism of Imine Isomerization*. Annals of the New York Academy of Sciences, 2008. **1126**(1): p. 30-37.
78. Chu, F.L. and V.A. Yaylayan, *FTIR monitoring of oxazolidin-5-one formation and decomposition in a glycolaldehyde-phenylalanine model system by isotope labeling techniques*. Carbohydrate research, 2009. **344**(2): p. 229-236.
79. Namiki, M. and T. Hayashi, *A new mechanism of the Maillard reaction involving sugar fragmentation and free radical formation*. 1983, ACS Publications.
80. Nursten, H., *Recent developments in studies of the Maillard reaction*. Food Chemistry, 1981. **6**(3): p. 263-277.
81. van Boekel, M.A.J.S., *Kinetic aspects of the Maillard reaction: a critical review*. Food / Nahrung, 2001. **45**(3): p. 150-159.
82. Nursten, H.E., *The Maillard reaction: chemistry, biochemistry, and implications*. 2005: Royal Society of Chemistry.
83. Tressl, R., et al., *Formation of Isoleucine-Specific Maillard Products from [1-13C]-D-Glucose and [1-13C]-D-Fructose*. Journal of Agricultural and Food Chemistry, 1995. **43**(5): p. 1163-1169.
84. Weenen, H., *Reactive intermediates and carbohydrate fragmentation in Maillard chemistry*. Food Chemistry, 1998. **62**(4): p. 393-401.
85. Arnoldi, A., *11 - Thermal processing and nutritional quality*, in *The Nutrition Handbook for Food Processors*, C.J.K. Henry and C. Chapman, Editors. 2002, Woodhead Publishing. p. 265-292.
86. Yaylayan, V.A., et al., *The Role of Creatine in the Generation of N-Methylacrylamide: A New Toxicant in Cooked Meat*. Journal of Agricultural and Food Chemistry, 2004. **52**(17): p. 5559-5565.
87. Yaylayan, V.A. and A. Keyhani, *Elucidation of the mechanism of pyrrole formation during thermal degradation of 13C-labeled l-serines*. Food Chemistry, 2001. **74**(1): p. 1-9.

88. Hemmler, D., et al., *Evolution of complex maillard chemical reactions, resolved in time*. Scientific reports, 2017. **7**(1): p. 1-6.
89. Hemmler, D., et al., *Insights into the Chemistry of Non-Enzymatic Browning Reactions in Different Ribose-Amino Acid Model Systems*. Scientific Reports, 2018. **8**(1): p. 16879.
90. Hølteland, A., *The browning reaction*. Starch-Stärke, 1966. **18**(10): p. 319-328.
91. Herbst, R. and L. Engel, *A reaction between  $\alpha$ -ketonic acids and  $\alpha$ -amino acids*. Journal of Biological Chemistry, 1934. **107**(2): p. 505-512.
92. Wnorowski, A. and V.A. Yaylayan, *Monitoring carbonyl-amine reaction between pyruvic acid and  $\alpha$ -amino alcohols by FTIR spectroscopy a possible route to Amadori products*. Journal of agricultural and food chemistry, 2003. **51**(22): p. 6537-6543.
93. Manini, P., M. d'Ischi, and G. Prota, *An Unusual Decarboxylative Maillard Reaction between l-DOPA and d-Glucose under Biomimetic Conditions: Factors Governing Competition with Pictet–Spengler Condensation*. The Journal of Organic Chemistry, 2001. **66**(15): p. 5048-5053.
94. Manini, P., A. Napolitano, and M. d'Ischia, *Reactions of d-glucose with phenolic amino acids: further insights into the competition between Maillard and Pictet–Spengler condensation pathways*. Carbohydrate Research, 2005. **340**(18): p. 2719-2727.
95. Hayashi, T., S. Mase, and M. Namiki, *Formation of the N, N'-Dialkylpyrazine Cation Radical from Glyoxal Dialkylimine Produced on Reaction of a Sugar with an Amine or Amino Acid*. Agricultural and Biological Chemistry, 1985. **49**(11): p. 3131-3137.
96. Glomb, M.A. and V.M. Monnier, *Mechanism of protein modification by glyoxal and glycolaldehyde, reactive intermediates of the Maillard reaction*. Journal of Biological Chemistry, 1995. **270**(17): p. 10017-10026.
97. Yaylayan, V.A., A. Wnorowski, and C. Perez Locas, *Why Asparagine Needs Carbohydrates To Generate Acrylamide*. Journal of Agricultural and Food Chemistry, 2003. **51**(6): p. 1753-1757.
98. Stadler, R.H., et al., *In-depth mechanistic study on the formation of acrylamide and other vinylogous compounds by the Maillard reaction*. Journal of Agricultural and Food Chemistry, 2004. **52**(17): p. 5550-5558.
99. Yaylayan, V.A. and R.H. Stadler, *Acrylamide formation in food: a mechanistic perspective*. Journal of AOAC International, 2005. **88**(1): p. 262-267.

100. Yaylayan, V.A., *Acrylamide formation and its impact on the mechanism of the early Maillard reaction*. Journal of Food & Nutrition Research, 2009. **48**(1).
101. Hayashi, T., Y. Ohta, and M. Namiki, *Electron spin resonance spectral study on the structure of the novel free radical products formed by the reactions of sugars with amino acids or amines*. Journal of agricultural and food chemistry, 1977. **25**(6): p. 1282-1287.
102. Namiki, M., *Chemistry of Maillard Reactions: Recent Studies on the Browning Reaction Mechanism and the Development of Antioxidants and Mutagens*, in *Advances in Food Research*, C.O. Chichester and B.S. Schweigert, Editors. 1988, Academic Press. p. 115-184.
103. Hofmann, T., W. Bors, and K. Stettmaier, *Studies on Radical Intermediates in the Early Stage of the Nonenzymatic Browning Reaction of Carbohydrates and Amino Acids*. Journal of Agricultural and Food Chemistry, 1999. **47**(2): p. 379-390.
104. Yaylayan, V.A. and A. Keyhani, *Origin of Carbohydrate Degradation Products in L-Alanine/d-[13C]Glucose Model Systems*. Journal of Agricultural and Food Chemistry, 2000. **48**(6): p. 2415-2419.
105. Brands, C.M.J. and M.A.J.S. van Boekel, *Reactions of Monosaccharides during Heating of Sugar–Casein Systems: Building of a Reaction Network Model*. Journal of Agricultural and Food Chemistry, 2001. **49**(10): p. 4667-4675.
106. Smuda, M. and M.A. Glomb, *Fragmentation Pathways during Maillard-Induced Carbohydrate Degradation*. Journal of Agricultural and Food Chemistry, 2013. **61**(43): p. 10198-10208.
107. Yaylayan, V.A., *Recent advances in the chemistry of Strecker degradation and Amadori rearrangement: Implications to aroma and color formation*. Food Science and Technology Research, 2003. **9**(1): p. 1-6.
108. Balagiannis, D.P., *10 - Predicting aroma formation with kinetic models*, in *Flavour Development, Analysis and Perception in Food and Beverages*, J.K. Parker, J.S. Elmore, and L. Methven, Editors. 2015, Woodhead Publishing. p. 211-233.
109. Ajandouz, E.H., et al., *Effects of pH on Caramelization and Maillard Reaction Kinetics in Fructose-Lysine Model Systems*. Journal of Food Science, 2001. **66**(7): p. 926-931.
110. Morales, F.J., C. Romero, and S. Jiménez-Pérez, *Fluorescence associated with Maillard reaction in milk and milk-resembling systems*. Food Chemistry, 1996. **57**(3): p. 423-428.

111. Coleman, W.M., III, *A Study of the Behavior of Polar and Nonpolar Solid-Phase Microextraction Fibers for the Extraction of Maillard Reaction Products*. Journal of Chromatographic Science, 1997. **35**(6): p. 245-258.
112. Morales, F.J., V. Somoza, and V. Fogliano, *Physiological relevance of dietary melanoidins*. Amino Acids, 2012. **42**(4): p. 1097-1109.
113. Huyghues-Despointes, A., V.A. Yaylayan, and A. Keyhani, *Pyrolysis/GC/MS Analysis of 1-[(2'-carboxyl)pyrrolidinyl]-1-deoxy-D-fructose (Proline Amadori Compound)*. Journal of Agricultural and Food Chemistry, 1994. **42**(11): p. 2519-2524.
114. Keyhani, A. and V.A. Yaylayan, *Pyrolysis/GC/MS Analysis of N-(1-Deoxy-d-fructos-1-yl)-l-phenylalanine: Identification of Novel Pyridine and Naphthalene Derivatives*. Journal of Agricultural and Food Chemistry, 1996. **44**(1): p. 223-229.
115. Perez Locas, C. and V.A. Yaylayan, *Further Insight into Thermally and pH-Induced Generation of Acrylamide from Glucose/Asparagine Model Systems*. Journal of Agricultural and Food Chemistry, 2008. **56**(15): p. 6069-6074.
116. Perez Locas, C. and V.A. Yaylayan, *Isotope Labeling Studies on the Formation of 5-(Hydroxymethyl)-2-furaldehyde (HMF) from Sucrose by Pyrolysis-GC/MS*. Journal of Agricultural and Food Chemistry, 2008. **56**(15): p. 6717-6723.
117. Blank, I., et al., *Analysis of Amadori compounds by high performance anion exchange chromatography–pulse amperometric detection*. International Congress Series, 2002. **1245**: p. 263-267.
118. Antonio, C., et al., *Hydrophilic interaction chromatography/electrospray mass spectrometry analysis of carbohydrate-related metabolites from Arabidopsis thaliana leaf tissue*. Rapid Communications in Mass Spectrometry, 2008. **22**(9): p. 1399-1407.
119. Mayer, H.K., et al., *RP-HPLC analysis of furosine and acid-soluble  $\beta$ -lactoglobulin to assess the heat load of extended shelf life milk samples in Austria*. Dairy Science & Technology, 2010. **90**(4): p. 413-428.
120. Degen, J., M. Hellwig, and T. Henle, *1,2-Dicarbonyl Compounds in Commonly Consumed Foods*. Journal of Agricultural and Food Chemistry, 2012. **60**(28): p. 7071-7079.

121. Tomlinson, A.J., J.A. Mlotkiewicz, and I.A.S. Lewis, *Application of capillary electrophoresis to the separation of coloured products of Maillard reactions*. Food Chemistry, 1994. **49**(3): p. 219-223.
122. Vallejo-Cordoba, B., M.A. Mazorra-Manzano, and A.F. González-Córdova, *New Capillary Electrophoresis Method for the Determination of Furosine in Dairy Products*. Journal of Agricultural and Food Chemistry, 2004. **52**(19): p. 5787-5790.
123. Bermudo, E., et al., *Field amplified sample injection–capillary electrophoresis–tandem mass spectrometry for the analysis of acrylamide in foodstuffs*. Journal of Chromatography A, 2007. **1159**(1): p. 225-232.
124. Scheijen, J.L.J.M., et al., *Analysis of advanced glycation endproducts in selected food items by ultra-performance liquid chromatography tandem mass spectrometry: Presentation of a dietary AGE database*. Food Chemistry, 2016. **190**: p. 1145-1150.
125. Yuan, J.-P. and F. Chen, *Separation and Identification of Furanic Compounds in Fruit Juices and Drinks by High-Performance Liquid Chromatography Photodiode Array Detection*. Journal of Agricultural and Food Chemistry, 1998. **46**(4): p. 1286-1291.
126. Mennella, C., et al., *Glycation of lysine-containing dipeptides*. Journal of Peptide Science, 2006. **12**(4): p. 291-296.
127. Wang, J., et al., *Electrospray positive ionization tandem mass spectrometry of Amadori compounds*. Journal of Mass Spectrometry, 2008. **43**(2): p. 262-264.
128. Hau, J., S. Devaud, and I. Blank, *Detection of Amadori compounds by capillary electrophoresis coupled to tandem mass spectrometry*. Electrophoresis, 2004. **25**(13): p. 2077-2083.
129. Davidek, T., et al., *Analysis of Amadori compounds by high-performance cation exchange chromatography coupled to tandem mass spectrometry*. Analytical chemistry, 2005. **77**(1): p. 140-147.
130. Troise, A.D., et al., *Quantification of Nε-(2-Furoylmethyl)-l-lysine (furosine), Nε-(Carboxymethyl)-l-lysine (CML), Nε-(Carboxyethyl)-l-lysine (CEL) and total lysine through stable isotope dilution assay and tandem mass spectrometry*. Food Chemistry, 2015. **188**: p. 357-364.

131. Qin, L., et al., *Isotope dilution HPLC-MS/MS for simultaneous quantification of acrylamide and 5-hydroxymethylfurfural (HMF) in thermally processed seafood*. Food Chemistry, 2017. **232**: p. 633-638.
132. Serra-Cayuela, A., et al., *Identification of 5-hydroxymethyl-2-furfural (5-HMF) in Cava sparkling wines by LC-DAD-MS/MS and NMR spectrometry*. Food Chemistry, 2013. **141**(4): p. 3373-3380.
133. Moritz, F., et al., *Chapter 12 - Mass differences in metabolome analyses of untargeted direct infusion ultra-high resolution MS data*, in *Fundamentals and Applications of Fourier Transform Mass Spectrometry*, B. Kanawati and P. Schmitt-Kopplin, Editors. 2019, Elsevier. p. 357-405.
134. Hemmler, D., et al., *Simulated Sunlight Selectively Modifies Maillard Reaction Products in a Wide Array of Chemical Reactions*. Chemistry – A European Journal, 2019. **25**(57): p. 13208-13217.
135. Laroque, D., et al., *Kinetic study on the Maillard reaction. Consideration of sugar reactivity*. Food Chemistry, 2008. **111**(4): p. 1032-1042.
136. Wedzicha, B.L. and C. Kedward, *Kinetics of the oligosaccharide-glycine-sulphite reaction: relationship to the browning of oligosaccharide mixtures*. Food Chemistry, 1995. **54**(4): p. 397-402.
137. Wedzicha, B. and L.P. Leong, *Modelling and control of Maillard browning*. European food and drink review, 1998(SPRING): p. 37-42.
138. Yaylayan, V.A. and S. Mandeville, *Stereochemical Control of Maltol Formation in Maillard Reaction*. Journal of Agricultural and Food Chemistry, 1994. **42**(3): p. 771-775.
139. Zamora, R. and F.J. Hidalgo, *Coordinate Contribution of Lipid Oxidation and Maillard Reaction to the Nonenzymatic Food Browning*. Critical Reviews in Food Science and Nutrition, 2005. **45**(1): p. 49-59.
140. Lund, M.N. and C.A. Ray, *Control of Maillard Reactions in Foods: Strategies and Chemical Mechanisms*. Journal of Agricultural and Food Chemistry, 2017. **65**(23): p. 4537-4552.
141. Yin, J., et al., *Epicatechin and epigallocatechin gallate inhibit formation of intermediary radicals during heating of lysine and glucose*. Food Chemistry, 2014. **146**: p. 48-55.

142. Totlani, V.M. and D.G. Peterson, *Epicatechin Carbonyl-Trapping Reactions in Aqueous Maillard Systems: Identification and Structural Elucidation*. Journal of Agricultural and Food Chemistry, 2006. **54**(19): p. 7311-7318.
143. Nagaraj, R.H., et al., *Effect of pyridoxamine on chemical modification of proteins by carbonyls in diabetic rats: characterization of a major product from the reaction of pyridoxamine and methylglyoxal*. Archives of Biochemistry and Biophysics, 2002. **402**(1): p. 110-119.
144. Troise, A.D., et al., *Faox enzymes inhibited Maillard reaction development during storage both in protein glucose model system and low lactose UHT milk*. Amino Acids, 2014. **46**(2): p. 279-288.
145. Xu, F., M.-J. Oruna-Concha, and J.S. Elmore, *The use of asparaginase to reduce acrylamide levels in cooked food*. Food Chemistry, 2016. **210**: p. 163-171.
146. Troise, A.D. and V. Fogliano, *Reactants encapsulation and Maillard Reaction*. Trends in Food Science & Technology, 2013. **33**(1): p. 63-74.
147. Nashalian, O. and V.A. Yaylayan, *Sugar-Conjugated Bis(glycinato)copper(II) Complexes and Their Modulating Influence on the Maillard Reaction*. Journal of Agricultural and Food Chemistry, 2015. **63**(17): p. 4353-4360.
148. Harohally, N.V., S.M. Srinivas, and S. Umesh, *ZnCl<sub>2</sub>-mediated practical protocol for the synthesis of Amadori ketoses*. Food chemistry, 2014. **158**: p. 340-344.
149. Cerny, C., F. Fitzpatrick, and J. Ferreira, *Effect of salt and sucrose addition on the formation of the Amadori compound from methionine and glucose at 40 C*. Food chemistry, 2011. **125**(3): p. 973-977.
150. Yaylayan, V.A., A. Huyghues-Despointes, and M.S. Feather, *Chemistry of Amadori rearrangement products: Analysis, synthesis, kinetics, reactions, and spectroscopic properties*. Critical Reviews in Food Science and Nutrition, 1994. **34**(4): p. 321-369.
151. Pellegrino, L., et al., *Maillard Compounds as Crosslinks in Heated  $\beta$ -Casein-Glucose Systems*, in *The Maillard Reaction in Foods and Medicine*, J. O'Brien, et al., Editors. 2005, Woodhead Publishing. p. 100-106.
152. BURTON, H., *THE PROCESS: ITS BASIC PRINCIPLES AND DEVELOPMENTS*. International Journal of Dairy Technology, 1965. **18**(2): p. 58-65.

153. Knirsch, M.C., et al., *Ohmic heating – a review*. Trends in Food Science & Technology, 2010. **21**(9): p. 436-441.
154. Krishnamurthy, K., et al., *Infrared Heating in Food Processing: An Overview*. Comprehensive Reviews in Food Science and Food Safety, 2008. **7**(1): p. 2-13.
155. Chandrasekaran, S., S. Ramanathan, and T. Basak, *Microwave food processing—A review*. Food Research International, 2013. **52**(1): p. 243-261.
156. Piyasena, P., et al., *Radio Frequency Heating of Foods: Principles, Applications and Related Properties—A Review*. Critical Reviews in Food Science and Nutrition, 2003. **43**(6): p. 587-606.
157. Yaylayan, V.A., N.G. Forage, and S. Mandeville, *Microwave and Thermally Induced Maillard Reactions*, in *Thermally Generated Flavors*. 1993, American Chemical Society. p. 449-456.
158. Yaylayan, V.A., et al., *Microwave-assisted synthesis and extraction of selected Maillard reaction products*. Journal of agricultural and food chemistry, 1997. **45**(1): p. 149-152.
159. Yu, H., et al., *Recent advances of ultrasound-assisted Maillard reaction*. Ultrasonics Sonochemistry, 2020. **64**: p. 104844.
160. Majid, I., G.A. Nayik, and V. Nanda, *Ultrasonication and food technology: A review*. Cogent Food & Agriculture, 2015. **1**(1): p. 1071022.
161. Farkes, D.F. and D.G. Hoover, *High Pressure Processing*. Journal of Food Science, 2000. **65**(s8): p. 47-64.
162. Tamaoka, T., N. Itoh, and R. Hayashi, *High Pressure Effect on Maillard Reaction*. Agricultural and Biological Chemistry, 1991. **55**(8): p. 2071-2074.
163. Isaacs, N.S. and M. Coulson, *Effect of pressure on processes modelling the Maillard reaction*. Journal of Physical Organic Chemistry, 1996. **9**(9): p. 639-644.
164. Moreno, F.J., et al., *High-Pressure Effects on Maillard Reaction between Glucose and Lysine*. Journal of Agricultural and Food Chemistry, 2003. **51**(2): p. 394-400.
165. Hill, V.M., D.A. Ledward, and J.M. Ames, *Influence of High Hydrostatic Pressure and pH on the Rate of Maillard Browning in a Glucose–Lysine System*. Journal of Agricultural and Food Chemistry, 1996. **44**(2): p. 594-598.

166. Jaeger, H., A. Janositz, and D. Knorr, *The Maillard reaction and its control during food processing. The potential of emerging technologies*. Pathologie Biologie, 2010. **58**(3): p. 207-213.
167. Aguiló-Aguayo, I., et al., *Changes in quality attributes throughout storage of strawberry juice processed by high-intensity pulsed electric fields or heat treatments*. LWT - Food Science and Technology, 2009. **42**(4): p. 813-818.
168. Genovese, J., et al., *Important factors to consider for acrylamide mitigation in potato crisps using pulsed electric fields*. Innovative Food Science & Emerging Technologies, 2019. **55**: p. 18-26.
169. Wang, J., et al., *Study on the Maillard Reaction Enhanced by Pulsed Electric Field in a Glycin–Glucose Model System*. Food and Bioprocess Technology, 2011. **4**(3): p. 469-474.
170. Wang, Z., et al., *Kinetic modeling of Maillard reaction system subjected to pulsed electric field*. Innovative Food Science & Emerging Technologies, 2013. **20**: p. 121-125.
171. Viton, F., H.R. Oertling, and R. Fumeaux, *Mechanical generation of flavour compositions*. 2017, U.S. Patent US20170079316A1.
172. Schmidt, R., H. Martin Scholze, and A. Stolle, *Temperature progression in a mixer ball mill*. International Journal of Industrial Chemistry, 2016. **7**(2): p. 181-186.
173. Fellows, P.J., *15 - Extrusion*, in *Food Processing Technology (Third Edition)*, P.J. Fellows, Editor. 2009, Woodhead Publishing. p. 456-477.
174. Yaylayan, V., J. Fichtali, and F. Van de Voort, *Production of Maillard reaction flavour precursors by extrusion processing*. Food Research International, 1992. **25**(3): p. 175-180.
175. Pokhrel, N., P.K. Vabbina, and N. Pala, *Sonochemistry: Science and Engineering*. Ultrasonics Sonochemistry, 2016. **29**: p. 104-128.
176. Rastogi, N.K., *Opportunities and Challenges in Application of Ultrasound in Food Processing*. Critical Reviews in Food Science and Nutrition, 2011. **51**(8): p. 705-722.
177. Chemat, F., H. Zill e, and M.K. Khan, *Applications of ultrasound in food technology: Processing, preservation and extraction*. Ultrasonics Sonochemistry, 2011. **18**(4): p. 813-835.

178. Stanic-Vucinic, D., et al., *Structural changes and allergenic properties of  $\beta$ -lactoglobulin upon exposure to high-intensity ultrasound*. *Molecular Nutrition & Food Research*, 2012. **56**(12): p. 1894-1905.
179. Guan, Y.-G., et al., *Effects of Ultrasound on a Glycin–Glucose Model System—A Means of Promoting Maillard Reaction*. *Food and Bioprocess Technology*, 2011. **4**(8): p. 1391-1398.
180. Yu, H., et al., *Effects of high-intensity ultrasound on Maillard reaction in a model system of d-xylose and l-lysine*. *Ultrasonics Sonochemistry*, 2017. **34**: p. 154-163.
181. Yu, H., et al., *Kinetic study of high-intensity ultrasound-assisted Maillard reaction in a model system of d-glucose and glycine*. *Food Chemistry*, 2018. **269**: p. 628-637.
182. Yu, H., et al., *Effects of high-intensity ultrasound and oil type on the Maillard reaction of d-glucose and glycine in oil-in-water systems*. *npj Science of Food*, 2018. **2**(1): p. 2.
183. Zhu, D., S. Damodaran, and J.A. Lucey, *Formation of Whey Protein Isolate (WPI)–Dextran Conjugates in Aqueous Solutions*. *Journal of Agricultural and Food Chemistry*, 2008. **56**(16): p. 7113-7118.
184. Rizzi, G.P., *Electrochemical Aspects of the Maillard Reaction and Related Reactions*. *Food Reviews International*, 2013. **29**(2): p. 178-191.
185. Yan, M., Y. Kawamata, and P.S. Baran, *Synthetic Organic Electrochemical Methods Since 2000: On the Verge of a Renaissance*. *Chemical Reviews*, 2017. **117**(21): p. 13230-13319.
186. Little, R.D. and K.D. Moeller, *Organic electrochemistry as a tool for synthesis*. *Electrochem. Soc. Interface*, 2002. **11**: p. 36-42.
187. Shaik, S., et al., *Structure and reactivity/selectivity control by oriented-external electric fields*. *Chemical Society Reviews*, 2018. **47**(14): p. 5125-5145.
188. Ciampi, S., et al., *Harnessing electrostatic catalysis in single molecule, electrochemical and chemical systems: a rapidly growing experimental tool box*. *Chemical Society Reviews*, 2018. **47**(14): p. 5146-5164.
189. Bohart, G.S. and J.F. Carson, *Effects of Trace Metals, Oxygen and Light on the Glucose–Glycine Browning Reaction*. *Nature*, 1955. **175**(4454): p. 470-471.
190. Henning, C. and M.A. Glomb, *Pathways of the Maillard reaction under physiological conditions*. *Glycoconjugate Journal*, 2016. **33**(4): p. 499-512.

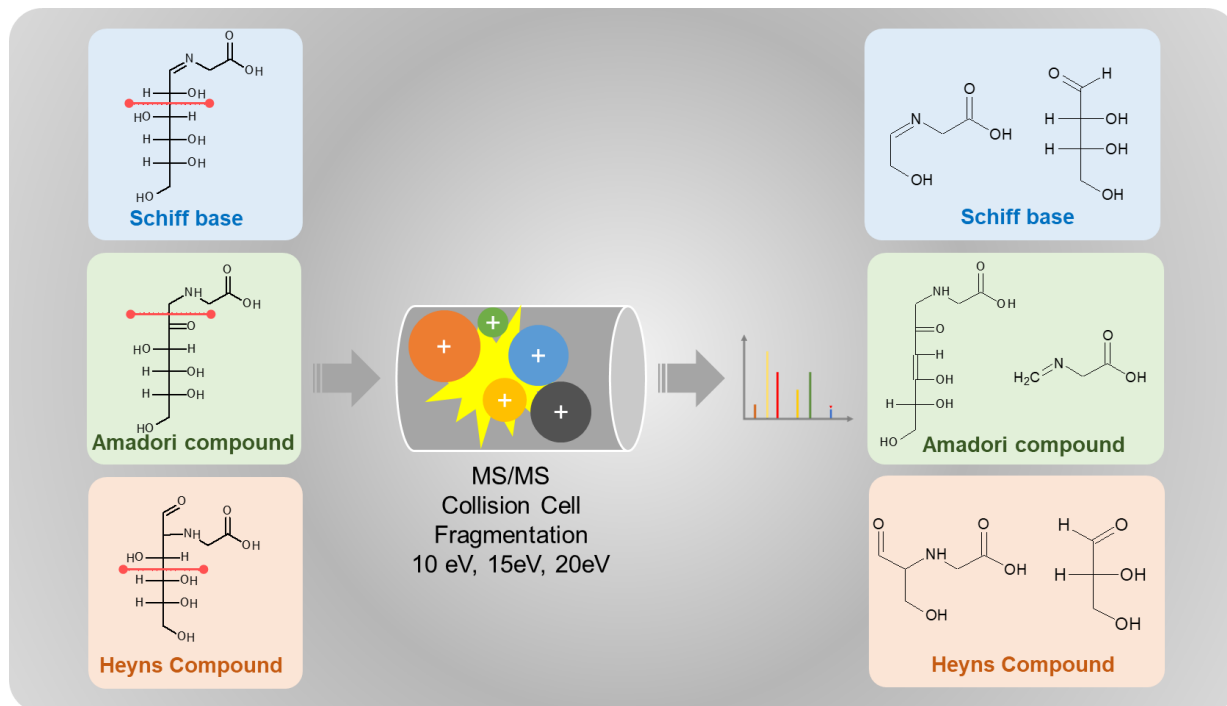
191. Koutchma, T., *UV Light for Processing Foods*. Ozone: Science & Engineering, 2008. **30**(1): p. 93-98.
192. Hoffmann, N., *Photochemical Reactions as Key Steps in Organic Synthesis*. Chemical Reviews, 2008. **108**(3): p. 1052-1103.

## Connecting paragraph

Chapter 2 provides the background on mechanochemistry and the Maillard reaction. The application of high-resolution mass spectrometry and mechanochemistry to understand and control the Maillard reaction has been rationalized. In Chapter 3, the potential of using MS/MS fragmentations to solve one of the challenges of the Maillard reaction which is distinguishing isomeric Maillard reaction intermediates was investigated. Three isomeric sugar-amino acid adducts known as Schiff base, Amadori compound, and Heyn's compound were synthesized and fragmented using different collision energies under ESI positive ionization mode.

Chapter 3 was published in the *Carbohydrate Research*: Xing, H., Mossine, V. V., & Yaylayan, V. (2020). Diagnostic MS/MS fragmentation patterns for the discrimination between Schiff bases and their Amadori or Heyns rearrangement products. *Carbohydrate Research*, **491**, 107985.

## Chapter 3 Diagnostic MS/MS fragmentation patterns for the discrimination between Schiff bases and their Amadori or Heyns rearrangement products



### 3.1 Abstract

Schiff bases, the Amadori and Heyns rearrangement products are the most important isomeric intermediates involved in the early Maillard reaction; distinguishing between them by analytical spectroscopic techniques remains a challenge. Here we demonstrate that MS/MS fragmentation patterns can be used for the discrimination between glucose derived Schiff bases, Amadori, and Heyns compounds with glycine. An ESI-qTOF-MS system operated in the positive mode under both acidic and neutral conditions was employed to generate unique MS/MS fragmentation patterns of the molecules. Analysis of the MS data has indicated that acidic medium is suitable for generating characteristic and diagnostic ions. At high collision energy (20 eV), the spectrum of Schiff base was largely uninformative, whereas both Amadori and Heyns compounds undergo characteristic fragmentations with high diagnostic value. At low collision energy values (10eV), we observed formation of prominent diagnostic ions from the Schiff base precursor, as well as extensive dehydration reactions of all three molecules. Under acidic conditions, the diagnostic fragmentation pattern of the Amadori compound featured consecutive dehydration reactions. At higher values (20 eV) it underwent the  $\alpha$ -fission at the carbonyl group and produced a prominent diagnostic ion  $[AA+H+CH_2]^+$  at  $m/z$  88. The Schiff base was found to preferentially undergo the retro-aldol degradation and produce diagnostic ions at  $m/z$  118  $[AA+H+diose]^+$  and  $m/z$  140  $[AA+Na+diose]^+$ , together with their sugar complements at  $m/z$  85  $[tetrose+H-2H_2O]^+$  and  $m/z$  143  $[tetrose+Na]^+$ . In the case of Heyns compound, several diagnostic ions were also detected, including the ions at  $m/z$  154  $[M+H-2H_2O-C_2H_4O_2]^+$ ,  $m/z$  170  $[AA+Na+triose]^+$  and  $m/z$  142  $[AA+H+Furan]^+$ .

**Keywords:** Diagnostic ions, Schiff base, Amadori compound, Heyns compound, tandem mass spectrometry (MS/MS), Collision induced fragmentations, Maillard reaction

## 3.2 Introduction

The Maillard reaction is a common term for a broad array of reactions that typically involve reducing sugars, such as glucose, and aliphatic amino groups of biological molecules. It has been the focus of great interest for researchers in areas as diverse as human pathology and food chemistry for more than 100 years.[1, 2] The complex reaction cascade is initiated by the formation of a Schiff base (or glycosylamine) between a reducing sugar and an amino acid. In presence of a nucleophilic catalyst, glycosylamine derived from an aldose can rearrange into a more stable 1-amino-1-deoxy-2-ketose; such reaction is termed the Amadori rearrangement. When glycosylamine is derived from a ketose sugar, it can rearrange into a 2-amino-2-deoxyaldose, or Heyns rearrangement product (HRP).[2] The breakdown of the Amadori or the Heyns rearrangement products ultimately yields a complex mixture of volatile carbocyclic and heterocyclic compounds, as well as characteristic yellow-brown oligomers and polymers.[3]

Although the initial stage of the Maillard reaction is well-documented, the analytical discrimination of the early intermediates, i.e. isomeric Schiff base and ARP (or HRP), remains a challenge. As a result, the critical role played by Schiff bases for initiating and propagating the Maillard reaction perhaps may have been undervalued. Besides rearranging into ARP and HRP, Schiff bases can undergo various transformations, such as the base-catalyzed transamination,[4-6] the intramolecular cyclization leading to decarboxylated isomeric imines via oxazolidin-5-one intermediate,[7, 8] the decarboxylative transamination,[9] the Namiki oxidative fragmentation pathway,[10, 11] and the acid-catalyzed Pictet-Spengler condensation pathway.[12, 13]

Structural identification of small organic molecules have been one of the cornerstone applications of mass spectrometry over the last decades, especially with the development of the electrospray ionization in combination with a collision cell (ESI-MS/MS).[14] It can also be considered as one of the key analytical techniques that is capable of generating large datasets in the emerging “omics” fields. Recently, the Maillard reaction has also been investigated in this regard. [15, 16] As a complex reaction cascade, hundreds and thousands of ions were detected in various Maillard reaction mixtures represented simply by their  $m/z$  values where the same molecular weight or a given elemental composition could represent different isomeric structures. The main goal of this study was to develop MS/MS based tools to distinguish the isomeric intermediates from the Maillard reaction such as Amadori compounds and Schiff bases without lengthy separation and

purification steps. The MS/MS fragmentation of Amadori compounds under protonated positive ion mode have been studied extensively and systematically by LC-ESI-MS/MS.[17-19] The potential of distinguishing between proline derived Amadori and Heyn's compounds,[20] or distinguishing between hexose versus pentose-derived Amadori compounds by their MS/MS fragmentation patterns have been already reported. [17] However, to the best of our knowledge, there are no published studies on the MS/MS behaviour of the Schiff bases, nor on their chemical behaviour under different collision energies. To fill this knowledge gap, we ventured to identify specific and diagnostic collision-induced dissociations (CID) of glucose/glycine derived Schiff base and ARP and of fructose derived HRP by LC-ESI-MS/MS under acidic (formic acid) and ESI-MS/MS under neutral (sodium formate) conditions using variable collision energies.

### **3.3 Material and Methods**

#### **3.3.1 Materials**

All reagents and chemicals were purchased from Sigma-Aldrich Chemical Co. (Oakville, ON, Canada) and used without further purification. Synthesis and characterization of *N*-carboxymethyl-D-glucosylamine (Schiff base), 1-carboxymethylamino-1-deoxy-D-fructose (Amadori compound), 2-carboxymethylamino-2-deoxy-D-glucose (Heyns compound), 1-[(2'-carboxy)pyrrolidinyl]-1-deoxy-D-fructose (proline Amadori compound), and *N*-[(2'-carboxy)pyrrolidinyl]-D-glucosylamine (proline Schiff base) were performed according to published procedures. [21-23] See Table S1 for <sup>13</sup>C-NMR chemical shifts and the supplementary material for more details on their preparation.

#### **3.3.2 ESI/MS/MS under formic acid condition**

Samples were analyzed using an Agilent 1290 Infinity II LC system coupled to the 6545 qToF - MS (Agilent Technologies, Santa Clara, USA). The LC separation was conducted on a Poroshell120 EC-C18 analytical column (Agilent Technologies; 2.7 μm × 3 mm × 100 mm) connected with a Poroshell120 EC-C18 guard column (Agilent Technologies; 2.7 μm × 3 mm × 5 mm). The elution condition was at a flow rate of 0.4 ml/min with the mobile phase as the mixture of 0.1% (V/V) aqueous formic acid (40%) with methanol (60%). The injection volume was 1 μL, and the column temperature was set to 20 °C. The samples were analyzed in positive electrospray ionization mode using product ion (MS/MS) experiment. The drying gas temperature was at

275 °C with a flow of 10 mL/min, the sheath gas temperature was at 300 °C with a flow of 12 mL/min, the pressure on the nebulizer at 45 psi, the capillary voltage at 4500 V, the fragmentor voltage at 1000 V, the skimmer voltage at 50 V, and the nozzle voltage at 2000 V. The Tandem mass spectrometry (MS/MS) data was collected by scans between  $m/z$  50 and 1000 at a scan rate of 3 spectra/s for four different collision energies (0 V, 10 V, 15 V, and 20 V) for the ions at  $[M+H]^+$  238. The data sets were processed with MassHunter Profinder B.08.00 software (Agilent Technologies).

### 3.3.3 ESI/MS/MS under sodium formate condition

The diluted sample solutions (1  $\mu$ L) in methanol/ water (10%/ 90%) were supplied to the source directly via a syringe. The analysis was on a Bruker Maxis Impact quadrupole time of flight mass spectrometer (Bruker Daltonics, Bremen, Germany) operated in positive ion mode. Instrument calibration was performed using sodium formate clusters. The electrospray interphase settings were as follows: nebulizer pressure, 0.6 bar; drying gas, 4 L/min; temperature, 180 °C; and capillary voltage, 4500 V. The scan range was from  $m/z$  50 to 800. Tandem mass spectrometry (MS/MS) was carried out in MRM mode using 10.0 eV collision energy for the ions at  $[M+Na]^+$  260. The data were analyzed using Bruker Compass Data Analysis software, version 4.2.

## 3.4 Results and Discussion

In-source fragmentations are usually observed under ESI conditions depending on the structural features of the analytes (e.g. presence of basic or acidic functional groups) and on the environmental conditions (e.g. solvents or calibration compound used for a specific MS system); all the three analytes exhibited minor in-source fragmentations mainly under acidic conditions (Figures 3.1-3.3). Under acidic analytical conditions, samples were introduced as they were eluted from a reverse-phase LC column. To facilitate protonation of the samples, water/methanol mixture containing 0.1% formic acid was used as the mobile phase. Schiff base, ARP, and HRP showed similar retention times (1.101, 1.070 and 1.080 min respectively) as shown in Figure S3.1. The MS spectra of these peaks indicated the occurrence of acid catalyzed hydrolysis especially for the Schiff base (see Table 3.1 Entry 1 & Figure 3.1) which was identified as the most labile molecule compared to the ARP and HRP generating free glycine and free sugar, the latter being the most abundant peak, while the intact protonated Schiff base represented only 11.2% of the total ion

intensity. Furthermore, dehydrations were also observed for ARP and HRP, especially for the former. (Table 3.1 Entries 5, 9 & Figures 3.2 & 3.3) The environmental conditions could play a critical role in distinguishing the Schiff base from the ARP, since the former, as indicated, can undergo hydrolysis and/or rearrange under acidic conditions to ARP and consequently undergo acid catalyzed dehydrations as shown in Table 3.1 (Entries 2 & 3) and Figure 3.1. Because of this concern, the Schiff base, ARP and HRP were also analyzed under neutral conditions in sodium formate cluster calibrated system. In this setup, samples were introduced as dilute solutions in water/methanol to the source directly via a syringe, resulting in the formation of sodiated ions (Figure 3.4). The extra stability gained by the analytes under neutral conditions was reflected in the intensities of molecular ions generated at  $[M+Na]^+ = 260$  as shown in Figure 3.4 (100% relative peak intensity in all cases). Some in-source fragmentation still observed for the Schiff base. (Table 3.1 Entry 17 & Figure 3.4) However, the overall stability was greatly enhanced relative to the acidic condition, which is the most adopted MS/MS analytical conditions from literature. In this study, MS/MS under both acidic and neutral condition were investigated, and the product ions were screened elementally and reported in Table 3.2, the relative abundances of the product ions and their proposed structure can be found in supplementary material (Tables S3.2 & S3.3).

**Table 3.1** MS and MS/MS spectral data of Schiff base, Amadori and Heyns compounds and their significant and diagnostic fragment ions.

#	Compound	Precursor ion [M+X] <sup>+</sup> (m/z)	CID voltage (eV) <sup>a</sup>	Significant fragment ions in MS and MS/MS spectra [M+X] <sup>+</sup> (m/z) <sup>c</sup>
Acidic conditions (ESI +ve)				
1	Glycine Schiff base	[M+H] <sup>+</sup> 238	0	238, 203
2			10	238, 220, 202, <b>118</b> <sup>b</sup> , 85, 76
3			15	220, 202, 127, <b>118</b> , 85, 97, 76
4			20	n/a
5	Glycine Amadori	[M+H] <sup>+</sup> 238	0	238, 220
6			10	<b>220, 202</b>
7			15	220, 202, <b>97, 88</b> , 76
8			20	202, <b>97, 88</b> , 76
9	Glycine Heyns	[M+H] <sup>+</sup> 238	0	238, 220, 202
10			10	220, 202, <b>154, 130</b>
11			15 and 20	202, 156, <b>154, 142, 130</b> , 126, 118, 117, 101, 99, 97, 84, 76
12	Proline Schiff base	[M+H] <sup>+</sup> 278	0	278, 116
13			10 and 15	278, 260, 242, 232, 214, <b>158</b> , 116, <b>85</b> , 70
14			20	116, 70
15	Proline Amadori	[M+H] <sup>+</sup> 278	0	278, 260
16			10, 15 and 20	278, 260, 242, 232, 214, <b>128</b> , 116, 100, 70
Neutral conditions (ESI +ve)				
17	Glycine Schiff base	[M+Na] <sup>+</sup> 260	0	260, 203, 143, 140
18			10	<b>143, 140</b>
19	Glycine Amadori	[M+Na] <sup>+</sup> 260	0	260
20			10	260, <b>242, 224</b>
21	Glycine Heyns	[M+Na] <sup>+</sup> 260	0	260
22			10	260, <b>170, 164</b> , 143, 140, <b>113, 108</b>

<sup>a</sup>: CID voltage at 0 represents ions found in the MS spectra without collision (fragmentation occurs during ionization).

<sup>b</sup>: The characteristic ions are in bold, where they are either uniquely present in a sample or significantly differ in their relative abundances.

<sup>c</sup>: Proposed structural assignments and relative abundances are reported in the supplementary material (see Tables S3.1 and S3.2)

**Table 3.2** Elemental composition of important product ions generated for glycine/glucose Schiff base, Amadori and Heyns compounds during MS/MS under acidic and neutral conditions.

Acidic Condition				Neutral Condition			
#	m/z	MF	Error (ppm)	#	m/z	MF	Error (ppm)
<i>Fragments derived from the adduct</i>				<i>Fragments derived from the adduct</i>			
1	238.0914	C <sub>8</sub> H <sub>16</sub> NO <sub>7</sub>	5.783	1	260.0735	C <sub>8</sub> H <sub>15</sub> NNaO <sub>7</sub>	4.312
2	220.0812	C <sub>8</sub> H <sub>14</sub> NO <sub>6</sub>	0.964	2	242.0631	C <sub>8</sub> H <sub>13</sub> NNaO <sub>6</sub>	3.953
3	202.0710	C <sub>8</sub> H <sub>12</sub> NO <sub>5</sub>	1.225	3	224.0522	C <sub>8</sub> H <sub>11</sub> NNaO <sub>5</sub>	5.767
4	184.0605	C <sub>8</sub> H <sub>10</sub> NO <sub>4</sub>	5.883	4	216.0842	C <sub>7</sub> H <sub>15</sub> NNaO <sub>5</sub>	2.741
5	174.0757	C <sub>7</sub> H <sub>12</sub> NO <sub>4</sub>	3.636	5	198.0729	C <sub>7</sub> H <sub>13</sub> NNaO <sub>4</sub>	6.702
6	126.0546	C <sub>6</sub> H <sub>8</sub> NO <sub>2</sub>	6.374	6	180.0628	C <sub>7</sub> H <sub>11</sub> NNaO <sub>3</sub>	4.792
7	156.0652	C <sub>7</sub> H <sub>10</sub> NO <sub>3</sub>	6.204	7	162.0516	C <sub>7</sub> H <sub>9</sub> NNaO <sub>2</sub>	9.245
8	154.0491	C <sub>7</sub> H <sub>8</sub> NO <sub>3</sub>	4.662				
<i>Fragments containing glycine</i>				<i>Fragments containing glycine</i>			
9	76.0388	C <sub>2</sub> H <sub>6</sub> NO <sub>2</sub>	11.224	8	98.0206	C <sub>2</sub> H <sub>5</sub> NNaO <sub>2</sub>	12.223
10	88.0389	C <sub>3</sub> H <sub>6</sub> NO <sub>2</sub>	8.558	9	110.0209	C <sub>3</sub> H <sub>5</sub> NNaO <sub>2</sub>	8.163
11	118.0495	C <sub>4</sub> H <sub>8</sub> NO <sub>3</sub>	6.93	10	140.0310	C <sub>4</sub> H <sub>7</sub> NNaO <sub>3</sub>	9.732
12	72.0443	C <sub>3</sub> H <sub>6</sub> NO	8.867	11	170.0417	C <sub>5</sub> H <sub>9</sub> NNaO <sub>4</sub>	7.219
13	130.0501	C <sub>5</sub> H <sub>8</sub> NO <sub>3</sub>	6.291	12	108.0426	C <sub>4</sub> H <sub>7</sub> NNaO	0.615
14	102.0546	C <sub>4</sub> H <sub>8</sub> NO <sub>2</sub>	8.853	13	164.0310	C <sub>6</sub> H <sub>7</sub> NNaO <sub>3</sub>	8.308
15	84.0421	C <sub>4</sub> H <sub>6</sub> NO	9.981				
16	142.0495	C <sub>6</sub> H <sub>8</sub> NO <sub>3</sub>	5.759				
<i>Sugar fragments</i>				<i>Sugar fragments</i>			
17	163.0598	C <sub>6</sub> H <sub>11</sub> O <sub>5</sub>	5.203	14	185.0424	C <sub>6</sub> H <sub>10</sub> NaO <sub>5</sub>	1.044
18	145.0498	C <sub>6</sub> H <sub>9</sub> O <sub>4</sub>	1.956	15	167.0309	C <sub>6</sub> H <sub>8</sub> NaO <sub>4</sub>	6.756
19	127.0384	C <sub>6</sub> H <sub>7</sub> O <sub>3</sub>	7.235	16	173.0415	C <sub>5</sub> H <sub>10</sub> NaO <sub>5</sub>	6.317
20	109.0279	C <sub>6</sub> H <sub>5</sub> O <sub>2</sub>	6.919	17	155.0320	C <sub>5</sub> H <sub>8</sub> NaO <sub>4</sub>	0.183
21	97.0279	C <sub>5</sub> H <sub>5</sub> O <sub>2</sub>	9.836	18	143.0308	C <sub>4</sub> H <sub>8</sub> NaO <sub>4</sub>	8.588
22	99.0438	C <sub>5</sub> H <sub>7</sub> O <sub>2</sub>	9.132	19	113.0202	C <sub>3</sub> H <sub>6</sub> NaO <sub>3</sub>	11.181
23	117.0551	C <sub>5</sub> H <sub>9</sub> O <sub>3</sub>	4.862				
24	101.0209	C <sub>4</sub> H <sub>5</sub> O <sub>3</sub>	11.572				
25	85.0283	C <sub>4</sub> H <sub>5</sub> O <sub>2</sub>	11.224				
26	69.0326	C <sub>4</sub> H <sub>5</sub> O	6.371				
27	61.0288	C <sub>2</sub> H <sub>5</sub> O <sub>2</sub>	2.53				

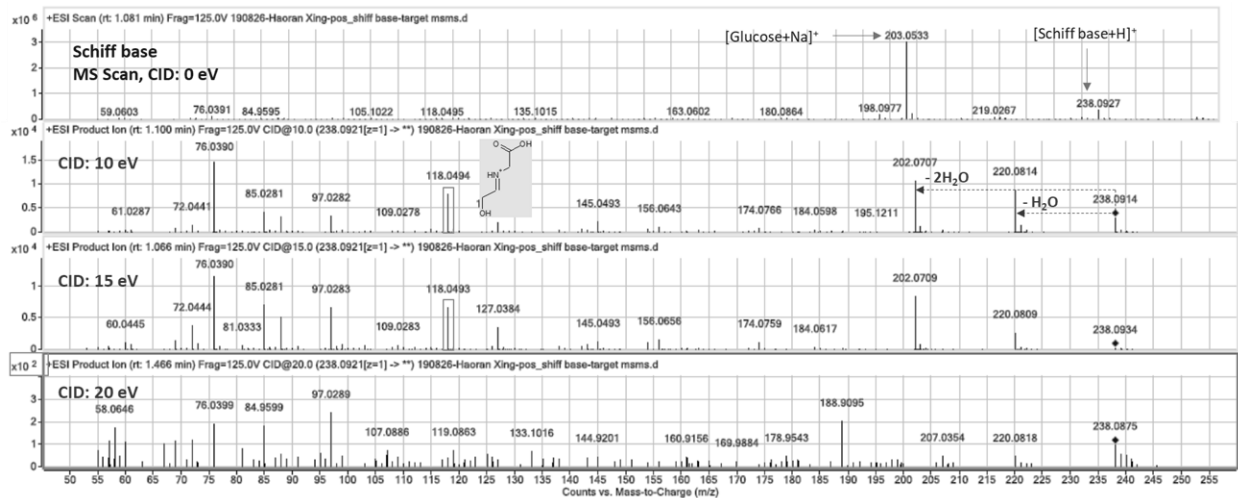


**Figure 3.1** MS and MS/MS spectra acquired at 0, 10, 15, 20 eV of glycine Schiff base under acidic condition.

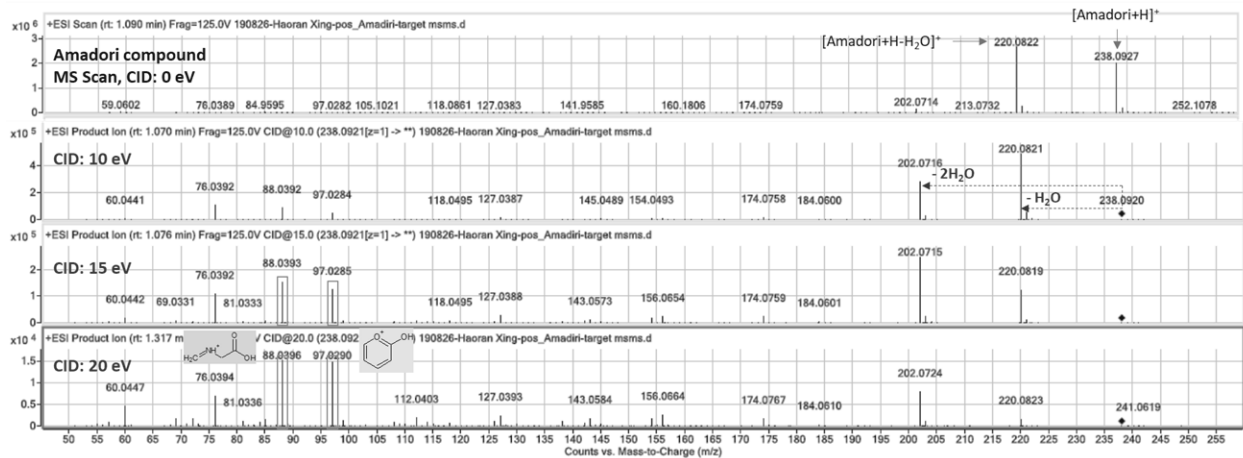


**Figure 3.2** MS and MS/MS spectra acquired at 0, 10, 15, 20 eV of glycine Amadori compound under acidic condition.

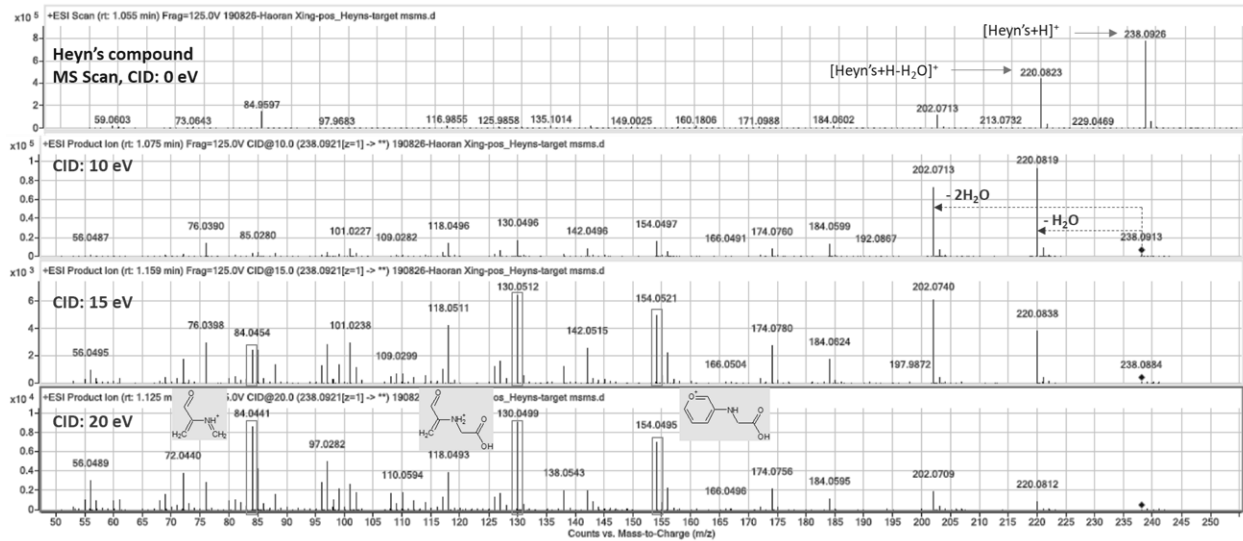


**Figure 3.3** MS and MS/MS spectra acquired at 0, 10, 15, 20 eV of glycine Heyns compound under acidic condition; the diagnostic ions are indicated in the graph.

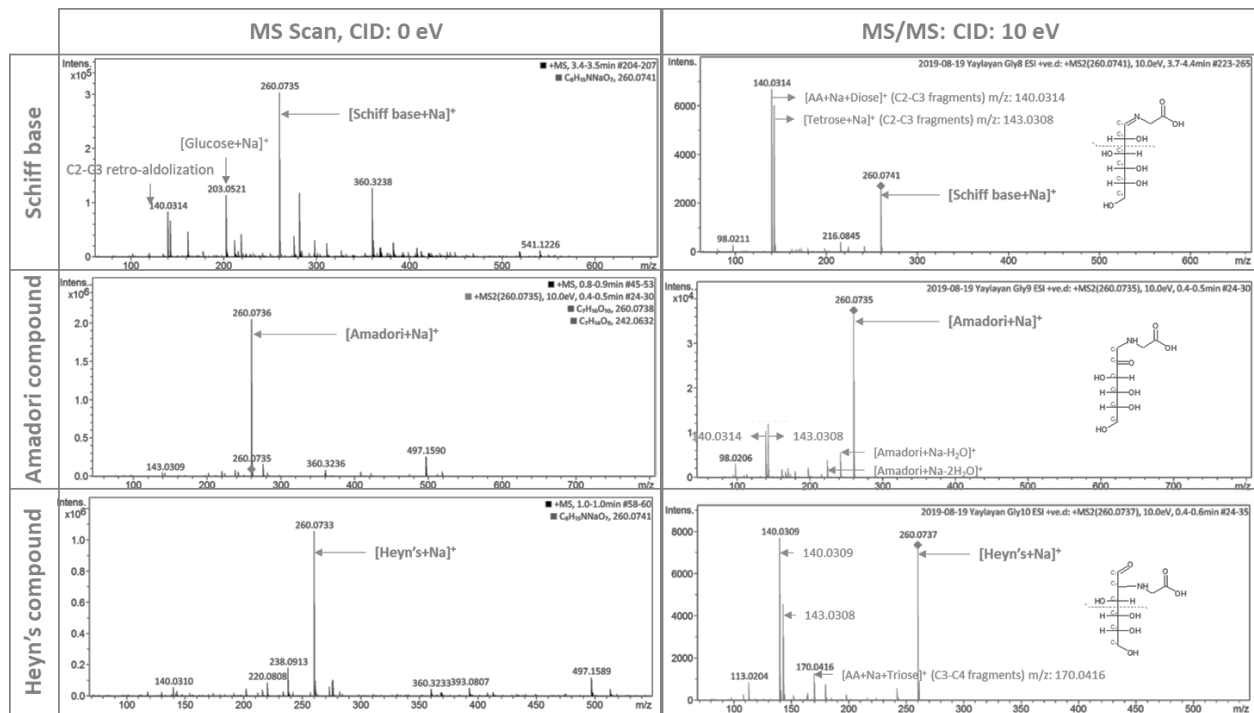


**Figure 3.4** MS and MS/MS spectra at 0 and 10eV of glycine Schiff base, Amadori, and Heyns compound under neutral condition; the diagnostic ions are indicated in the graph.

### 3.4.1 Diagnostic MS/MS fragmentations under acidic conditions

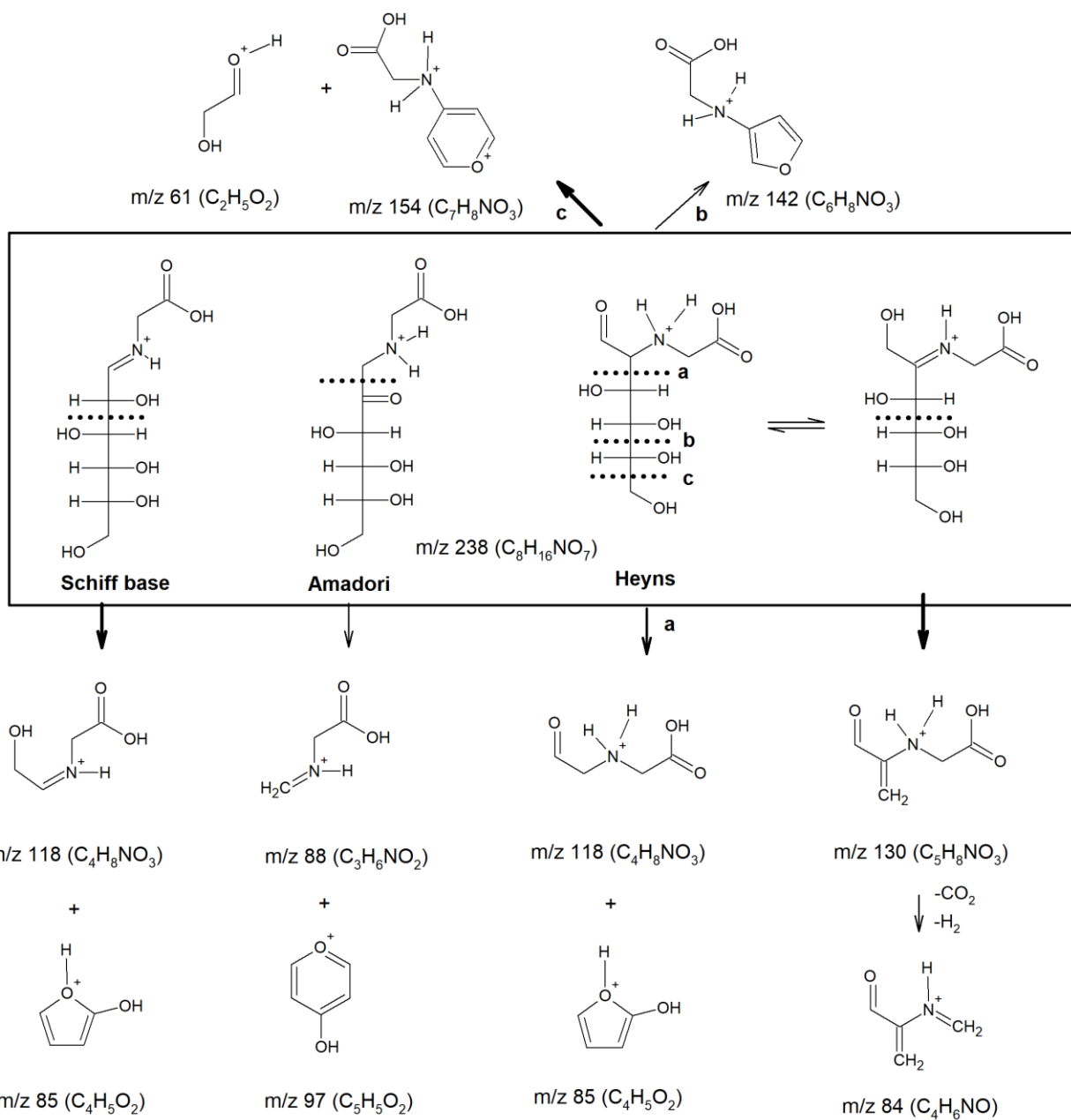
Under acidic conditions, the MS/MS fragmentation pattern of ARP was in accordance with those reported in the literature,[17, 19] where series of dehydration reactions lead to the formation of characteristic  $[M+H-n(18)]^+$  peaks in the MS/MS spectrum under low CID voltage (10eV), whereas high CID voltage (20eV) resulted in  $\alpha$ -fission between the C-1 and C-2 of sugar backbone carbon atoms.[18, 20] This fragmentation pattern, where dehydrated ion series has been observed as the most abundant peaks in the spectrum, is typical of most of the Amadori compounds of eighteen amino acids with glucose studied in the literature.[19] Under all investigated conditions reported in the literature, the cleavage of the sugar moiety during MS/MS fragmentations of Amadori compounds was only observed between C1-C2 or C5-C6 of the sugar, leaving a  $-CH_2$  unit attached to an amino acid or leading to a loss of formaldehyde  $[-H_2CO]$  from the terminal carbon of the hexose, consistent with data reported in Table 3.1 (Entries 6-8 & Figure 3.2). Briefly, under conditions of low collision energy, dehydrated products were the most abundant peaks with 100% relative intensity for  $[M+H-H_2O]^+$  (m/z 220) or  $[M+H-2H_2O]^+$  (m/z 202) at 10eV or 15eV respectively. At higher collision energy values (20 eV), the glycine ARP generated  $[AA+H+CH_2]^+$  (m/z 88) through  $\alpha$ -fission as the most abundant peak, as well as the complementary sugar portion at m/z 97 (proposed as a 5-carbon pyrylium ion). (Scheme 3.1)

Contrary to the ARP, the Schiff base showed a different behaviour under MS/MS fragmentation, especially under lower energy conditions (10 and 15eV) generating through C2-C3 retro-aldol cleavage a diagnostic ion at (m/z 118) incorporating intact amino acid and two carbon moiety from the sugar in addition to its complementary 4-carbon sugar fragment at m/z 85 (see Table 3.1 Entries 2, 3 & Scheme 3.1). Overall, the Schiff base of glycine and glucose appears to be less stable during MS/MS fragmentation compared to its Amadori counterpart. Even when submitted to low collision voltage (10 eV), the Schiff base generated the most abundant peak  $[AA+H]^+$  at m/z 76 representing the free glycine released during the fragmentation process. It appears that the free glycine was released from doubly dehydrated Schiff base precursor at m/z 202 leaving behind the sugar residue at m/z 145 (see Table 3.2). At 15 eV, the spectrum does not differ much from the one operated at 10 eV. However, at 20 eV the ion count intensity was too low ( $\times 10^2$ ) to provide useful information, and most of the ions could not be identified elementally. (Figure 3.1) This property of Schiff bases can be exploited to detect their presence in mixtures containing various amounts of Amadori products. When the ion at m/z 238  $[M+H]^+$  in five different mixtures of glycine Schiff base and

its ARP (molar ratios of 1:0, 1:2, 1:1, 2:1, 0:1) was fragmented using collision energy of 20 eV where Schiff bases no longer generate any fragments, the intensity of ions generated from the ARP predominates the spectrum and its diagnostic ion at  $m/z$  88 increased proportionately to the increased content of ARP. On the other hand, the intensity of the diagnostic ion originating from the Schiff base at  $m/z$  118 was only detected in trace abundances as expected (see Figure S3.4).

Although Heyn's rearrangement product is structurally different from ARP, its MS/MS fragmentation pattern was partially similar to that of ARP and partially to that of the Schiff base (see Scheme 3.1). Its resemblance to the behaviour of ARP was manifested through the presence of dehydration peaks and its similarity to the behaviour of the Schiff base was indicated through detection of the ion at  $m/z$  130 (Scheme 3.1). From the elemental composition of the ion at  $m/z$  130 ( $C_5H_8NO_3$ ) it can be concluded that it incorporates intact glycine with three carbon unit originating from the sugar. Such a structure can only be generated through retro-aldol cleavage of the Schiff base of fructose with glycine at C3-C4 as shown in Scheme 3.1. This implies that open form of Heyn's product is prone to isomerization to produce fructose/glycine Schiff base adduct as shown in Scheme 3.1. This diagnostic ion is generated only under acidic conditions, although its precursor ions  $m/z$  170 was also detected under neutral conditions. Furthermore, detection of the high intensity protonated ion at  $m/z$  118 and the same ion at  $m/z$  140 under sodiation with common molecular formula of  $C_4H_8NO_3$  indicates the predominance of the open form of the Heyn's product under MS/MS analytical conditions, since this ion can be generated only through C2-C3 retro-aldolization of the open form of the Heyn's product. This is equivalent to the process observed in the case of Schiff base shown in Scheme 3.1. The diagnostic ion at  $m/z$  130 was absent from both Schiff base and the ARP and it is the most abundant ion at higher collision voltages of the HRP indicating its stability and therefore the tendency of accumulating relative to the other fragments. Its three-carbon sugar complement was detected only under sodiation condition at  $m/z$  113. (Table 3.1 Entry 22; Scheme 3.2) Interestingly, Yuan *et al.* (2016) [20] reported a characteristic fragment ion from MS/MS of proline Heyn's compound at  $m/z$  182 formed by the loss of two water molecules and a two-carbon sugar moiety  $[M+H-2H_2O-C_2H_4O_2]^+$ , this fragment ion was absent from the MS/MS of its Amadori compound and can be considered as a diagnostic ion for Heyn's products. The glycine equivalent of this ion was also identified in its Heyn's product at  $m/z$  142 ( $C_6H_8NO_3$ ) (Scheme 3.1) along with its two-carbon split moiety at  $m/z$  61 ( $C_2H_5O_2$ ). The ion at  $m/z$  142 was nearly absent from MS/MS fragmentation of glycine Schiff base and Amadori

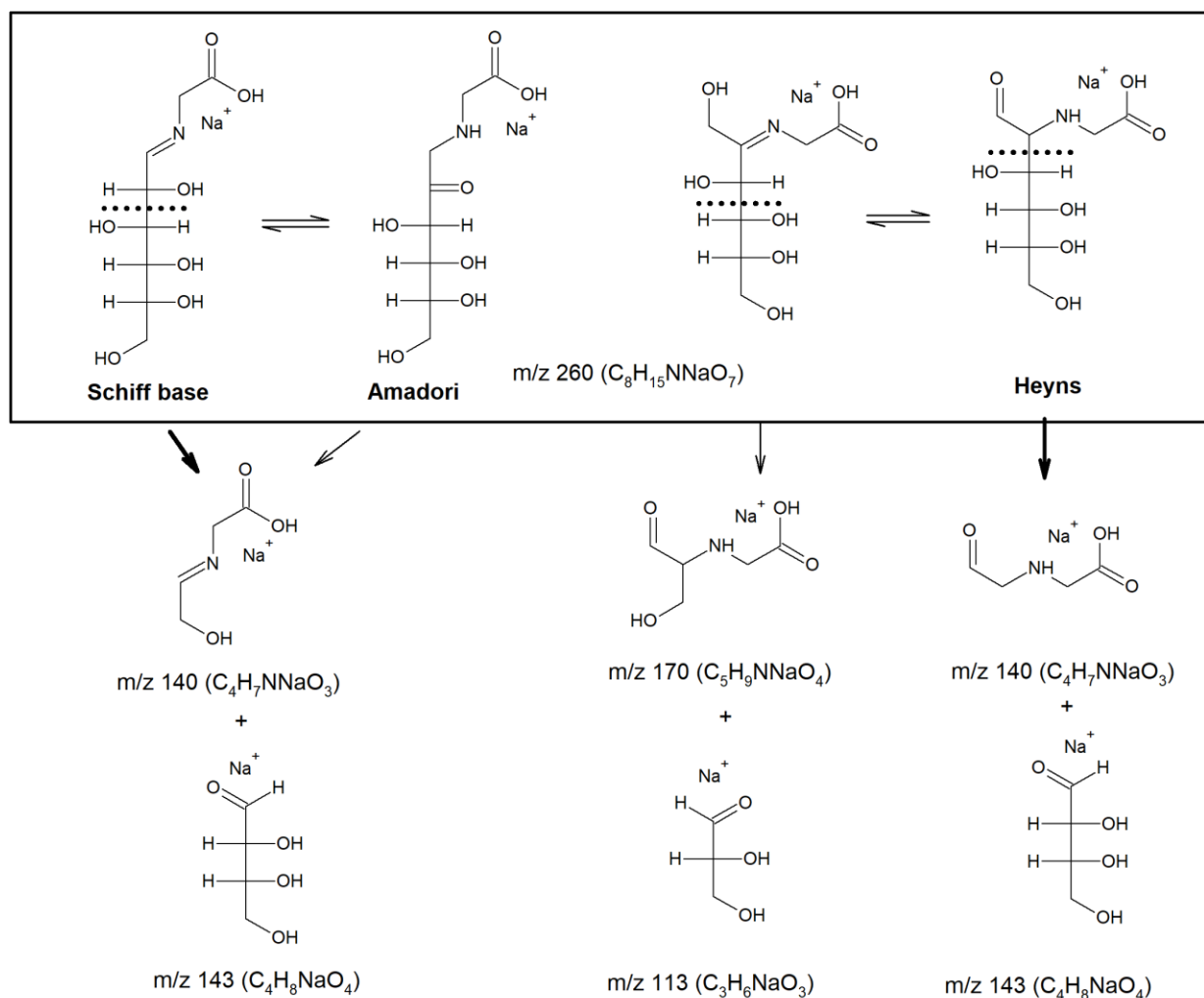
compound making it a good candidate as diagnostic ion for HRP. Furthermore, we have identified another fragment ion at  $m/z$  154  $[M+H-3H_2O-H_2CO]^+$  that also preferentially formed only in Heyns compound, that can also be considered as a diagnostic ion. (Figure 3.3) To illustrate the generality of the diagnostic fragmentation patterns proposed above, another set of Amadori and Schiff base of glucose this time using proline was studied under the same conditions (see Table 3.1, Figures S3.3 and S3.4). The product ion from the Amadori compound at  $m/z$  128 was identified as the diagnostic fragments  $([AA+H+CH_2]^+)$  which is the equivalent to  $m/z$  88 of glycine ARP. Proline Schiff base, on the other hand, produced the diagnostic fragment at  $m/z$  158 equivalent to  $m/z$  118 of glycine Schiff base (see Scheme S3.1). Furthermore, both proline Schiff base and ARP behaved the same way compared to glycine Schiff base and ARP in response to increased CID energy at 10, 15, and 20 eV. Both ARPs showed dehydration as the major product ions at low CID energy values and tended to undergo  $\alpha$ -fission and results in accumulation of the diagnostic ion at  $m/z$  88 (glycine ARP) and  $m/z$  128 (proline ARP) at higher energies.



**Scheme 3.1** Proposed diagnostic collision-induced fragmentations of the glycine Schiff base and Amadori or Heyns rearrangement products under acidic conditions. The characteristic loss of water molecules from ARP is not shown.

### 3.4.2 Diagnostic MS/MS fragmentations under neutral condition

When the mass spectrometric run was performed in presence of sodium formate, both molecular ions and their major fragments were detected exclusively as sodium adducts. (Figure 3.4) There was no evidence that the Schiff base underwent the Amadori rearrangement under such conditions. Additionally, direct infusion of the analytes compared to prior LC separation also reduced the time that Schiff base spent in aqueous environment and minimized its hydrolysis. Under neutral conditions, dehydration of the sugar moiety and the dehydration of its subsequent retro-aldolization products were also not significant, thus allowing for the detection of intact triose and tetrose species at  $m/z$  113 and 143 respectively (Scheme 3.2). Under acidic conditions, these molecules underwent dehydration and cyclization into furan and pyran derivatives, as shown in Scheme 1. Under neutral conditions, in the MS/MS spectrum of the Heyns compound, a peak at  $m/z$  170 (see Scheme 3.2) was detected which was not observed under acidic conditions. This ion can be considered as diagnostic ion for Heyns product under sodiation condition. Taking together all the data, it seems that the retro-aldolization of C2-C3 sugar chain was the main pathway of fragmentation for all the three intermediates studied under neutral conditions; in the spectra of the Schiff base and Heyns product the respective peaks were relatively more intense, as compared to the Amadori product (Figure 3.4). We assume that the observed retro-aldolization of ARP at C2-C3 carbon bond occurred after retro-isomerization of ARP into Schiff base. (Scheme 3.2) Furthermore, only the spectra of the Amadori product contained peaks, albeit in low abundances, that were ascribed to its dehydration under neutral conditions.



**Scheme 3.2** Proposed diagnostic collision-induced fragmentations of the glycine Schiff base and Amadori or Heyns rearrangement products under neutral sodiation conditions.

### 3.5 Conclusion

We have demonstrated that ESI-qToF-MS/MS could be used to distinguish between glucose/glycine Schiff base and two most relevant isomers, Amadori and Heyns rearrangement products. Analysis performed under neutral conditions (using sodium formate clusters) is more suitable for identification of the intact sodiated molecular ions, due to lower hydrolysis rates of the Schiff base. On the other hand, MS/MS analysis under acidic conditions (such as in presence of formic acid) offered more informative patterns of characteristic and diagnostic ions for each molecule, thus allowing to discriminate the Schiff base from its corresponding Amadori and Heyns rearrangement products. At higher collision energy (20 eV), both Amadori and Heyns products undergo unique fragmentations that do not involve dehydration. In contrast, the Schiff base generates useful diagnostic ions under low collision energy value (10-15 eV). Loss of water from all three molecules is prominent at energy levels between 10-15 eV.

### 3.6 References

1. Maillard, L., *Action of amino acids on sugars. Formation of melanoidins in a methodical way*. *Compte-Rendu de l'Academie des Sciences*, 1912. **154**: p. 66-68.
2. Nursten, H.E., *The Maillard reaction: chemistry, biochemistry, and implications*. 2005: Royal Society of Chemistry.
3. Hodge, J.E., *Dehydrated foods, chemistry of browning reactions in model systems*. *Journal of agricultural and food chemistry*, 1953. **1**(15): p. 928-943.
4. Høltermand, A., *The browning reaction*. *Starch-Stärke*, 1966. **18**(10): p. 319-328.
5. Herbst, R. and L. Engel, *A reaction between  $\alpha$ -ketonic acids and  $\alpha$ -amino acids*. *Journal of Biological Chemistry*, 1934. **107**(2): p. 505-512.
6. Wnorowski, A. and V.A. Yaylayan, *Monitoring carbonyl-amine reaction between pyruvic acid and  $\alpha$ -amino alcohols by FTIR spectroscopy a possible route to Amadori products*. *Journal of agricultural and food chemistry*, 2003. **51**(22): p. 6537-6543.

7. Chu, F.L. and V.A. Yaylayan, *Post-Schiff Base Chemistry of the Maillard Reaction: Mechanism of Imine Isomerization*. Annals of the New York Academy of Sciences, 2008. **1126**(1): p. 30-37.
8. Chu, F.L. and V.A. Yaylayan, *FTIR monitoring of oxazolidin-5-one formation and decomposition in a glycolaldehyde–phenylalanine model system by isotope labeling techniques*. Carbohydrate research, 2009. **344**(2): p. 229-236.
9. Granvogel, M., S. Bugan, and P. Schieberle, *Formation of Amines and Aldehydes from Parent Amino Acids during Thermal Processing of Cocoa and Model Systems: New Insights into Pathways of the Strecker Reaction*. Journal of Agricultural and Food Chemistry, 2006. **54**(5): p. 1730-1739.
10. Hayashi, T., S. Mase, and M. Namiki, *Formation of the N, N'-Dialkylpyrazine Cation Radical from Glyoxal Dialkylimine Produced on Reaction of a Sugar with an Amine or Amino Acid*. Agricultural and Biological Chemistry, 1985. **49**(11): p. 3131-3137.
11. Glomb, M.A. and V.M. Monnier, *Mechanism of protein modification by glyoxal and glycolaldehyde, reactive intermediates of the Maillard reaction*. Journal of Biological Chemistry, 1995. **270**(17): p. 10017-10026.
12. Manini, P., M. d'Ischi, and G. Prota, *An Unusual Decarboxylative Maillard Reaction between l-DOPA and d-Glucose under Biomimetic Conditions: Factors Governing Competition with Pictet–Spengler Condensation*. The Journal of Organic Chemistry, 2001. **66**(15): p. 5048-5053.
13. Manini, P., A. Napolitano, and M. d'Ischia, *Reactions of d-glucose with phenolic amino acids: further insights into the competition between Maillard and Pictet–Spengler condensation pathways*. Carbohydrate Research, 2005. **340**(18): p. 2719-2727.
14. Demarque, D.P., et al., *Fragmentation reactions using electrospray ionization mass spectrometry: an important tool for the structural elucidation and characterization of synthetic and natural products*. Natural product reports, 2016. **33**(3): p. 432-455.
15. Hemmler, D., et al., *Evolution of complex maillard chemical reactions, resolved in time*. Scientific reports, 2017. **7**(1): p. 1-6.
16. Hemmler, D., et al., *Insights into the Chemistry of Non-Enzymatic Browning Reactions in Different Ribose-Amino Acid Model Systems*. Scientific Reports, 2018. **8**(1): p. 16879.

17. Davidek, T., et al., *Analysis of Amadori compounds by high-performance cation exchange chromatography coupled to tandem mass spectrometry*. Analytical chemistry, 2005. **77**(1): p. 140-147.
18. Hau, J., S. Devaud, and I. Blank, *Detection of Amadori compounds by capillary electrophoresis coupled to tandem mass spectrometry*. Electrophoresis, 2004. **25**(13): p. 2077-2083.
19. Wang, J., et al., *Electrospray positive ionization tandem mass spectrometry of Amadori compounds*. Journal of Mass Spectrometry, 2008. **43**(2): p. 262-264.
20. Yuan, H., et al., *The Comparison of the Contents of Sugar, Amadori, and Heyns Compounds in Fresh and Black Garlic*. Journal of Food Science, 2016. **81**(7): p. C1662-C1668.
21. Mossine, V.V., G.V. Glinsky, and M.S. Feather, *The preparation and characterization of some Amadori compounds (1-amino-1-deoxy-d-fructose derivatives) derived from a series of aliphatic  $\omega$ -amino acids*. Carbohydrate Research, 1994. **262**(2): p. 257-270.
22. Mossine, V.V., et al., *Molecular and crystal structure of N-(2-deoxy-d-aldohexos-2-yl)-glycines (Heyns compounds)*. Carbohydrate Research, 1996. **284**(1): p. 11-24.
23. Mossine, V.V., et al., *Superoxide Free Radical Generation by Amadori Compounds: The Role of Acyclic Forms and Metal Ions*. Chemical Research in Toxicology, 1999. **12**(3): p. 230-236.

### 3.7 Supplementary information

#### Sample preparation

TLC was performed on Merck silica gel 60 plates using the following irrigants: 2-propanol/ 28% aqueous ammonia (4:1, v/v, irrigant A) and pyridine/ acetic acid/ water (9:1:2 v/v, irrigant B). Plates were sprayed with 0.2% ninhydrin in acetone (for detection of amino acid derivatives as well as sugars), followed by heating at 120°C for 2-5 min.

**Preparation of *N*-(1-deoxy-*D*-fructos-1-yl)-glycine.** The procedure for the synthesis of fructose-glycine was as described in [1]: A suspension of 36 g (0.2 moles) of D-glucose and 2.0 g sodium bisulfite in 60 mL of methanol and 30 mL of glycerol was refluxed for 30 min, followed by the addition of 6 g (0.08 moles) of glycine and 8 mL of acetic acid. This solution was refluxed until > 80% of the amino acid had reacted, as evidenced by TLC. The resulting brown, syrupy solution was diluted with 1 volume of water, loaded on a 2 x 30 cm column of Amberlite IRN-77 (H<sup>+</sup>) ion-exchange resin, and the column was eluted with 500 mL of water, followed by 0.2 N ammonium hydroxide. Fractions of 25 mL were collected. Early fractions contained D-glucose, uncharged pigments and D-glucose-derived degradation products. The Amadori compound, along with unreacted amino acid, usually eluted near the end of the water wash and at the beginning of the ammonium hydroxide wash. The combined fractions, which contained fructose-glycine, were evaporated to 100 mL in vacuo and decolorized with charcoal (2.0 g). This solution was placed on a second 2 x 30 cm column of Amberlite IRN-77 (pyridinium form, pretreated with 10 mL of acetic acid). The column was eluted with water, and 25-mL fractions were collected. Fractions containing fructose-glycine were evaporated in vacuo at 30°C to a syrup. The syrup was diluted in methanol to turbidity and left for 3 days to crystallize at room temperature. Resulting colorless prisms were washed with 3:1 methanol-water and dried in vacuo over calcium chloride. An additional crop of crystals was obtained from the mother liquor. Yield 3.4 g (22%, based on starting glycine): mp 146.5-147.5°C (dec) (lit. [2] mp 145°C, dec);  $[\alpha]_D^{25}$  -66° (c 1.0, H<sub>2</sub>O) (lit. [2] -67°). Anal. Calcd for C<sub>8</sub>H<sub>15</sub>NO<sub>7</sub>: C, 40.51; H, 6.33; N, 5.91. Found: C, 40.18; H, 6.70; N, 5.58.

**Preparation of *N*-(1-deoxy-*D*-fructos-1-yl)-*L*-proline.** The procedure for the synthesis of fructose-proline was performed according to Vernin et al. [3] and involved the following steps: A

suspension of 0.1 mol (18 g) of anhydrous D-glucose in 150 mL of methanol was refluxed for 30 min, followed by the addition of 0.1 mol (11.5 g) of L-proline. This solution was refluxed until about 95% of the amino acid had reacted, as evidenced by TLC. Upon cooling, it deposited crystalline mass which was recrystallized from methanol. The crystals were dried at 50-55°C *in vacuo* for 3 hours. Yield 10.8 g (39%): mp 115-118°C (dec.) (lit.[4] mp 119°).  $[\alpha]_D^{25} = -75^\circ$  (c=1.2, water) (lit. [4]:  $[\alpha]_D^{20} = -86^\circ$  (c=2, water)).

**Preparation of *N*-(2-deoxy-D-glucos-2-yl)-glycine (Heyns compound).** The procedure for the synthesis of the Heyns compound glucose-glycine was performed as described in [5]. D-Glucosamine hydrochloride (4 mmol) and glyoxylic acid monohydrate (16 mmol) in 40 mL of 96% formic acid were stirred at 50-60 °C for 8 h. The reaction mixture was evaporated to syrup, dissolved in 8 mL of 1 M hydrochloric acid and hydrolyzed at 100 °C for 2.5 h. After hydrolysis, the hydrochloric acid was removed at reduced pressure with repeated additions of water. The chromatographic purification and crystallization steps were performed exactly as described above for synthesis of fructose-glycine. Yield 85%, white crystalline powder; mp 200-210 °C (dec) (Lit. [6] 180-250 °C (dec));  $[\alpha]_D^{25} +77^\circ$  (c = 1.0, water) (Lit. [6] + 81°). Anal. Calcd for C<sub>8</sub>H<sub>15</sub>NO<sub>7</sub>: C, 40.5; H, 6.37; N, 5.90. Found: C, 39.2; H, 6.44; N, 5.70.

**General procedure for preparation of amino acid *N*-glucosylamines (Schiff bases).** To a solution of 0.23 g Na in 35 ml of methanol, 0.01 mol of glycine or L-proline, and D-glucose (1.80 g, 0.01 mol) were added in the sequence and stirred at room temperature until complete dissolution. The reaction mixture was worked up as specified below. ***N*-D-glucosyl-glycine sodium salt.** The reaction mixture was diluted with 30 ml of diethyl ether and left overnight at room temperature. Crystalline-like material was filtered out, washed with 1:1 methanol/diethyl ether and dried *in vacuo* over CaCl<sub>2</sub>. Yield 1.79 g (69 %) of white powder. It was essentially free (<1%, by TLC) of the starting glycine and fructose-glycine. ***N*-D-glucosyl-L-proline sodium salt.** The reaction mixture was treated overnight with 50 ml of diethyl ether. Crystalline-like material was filtered out, washed with 1:5 methanol/diethyl ether and dried *in vacuo* over CaCl<sub>2</sub>. Yield 1.60 g (54 %) of white powder. It was essentially free (<1%, by TLC) of the starting proline and fructose-L-proline.

**Table S 3.1** Tentative assignments of chemical shifts (ppm) in  $^{13}\text{C}$  NMR spectra and relative populations of the anomeric forms of the compounds in  $\text{D}_2\text{O}$  solutions at  $25^\circ\text{C}$

	Glc-GlyONa (Schiff)		Glc-Gly (Heyns)		Fru-Gly (Amadori)			
	$\alpha$ -pyr	$\beta$ -pyr	$\alpha$ -pyr	$\beta$ -pyr	$\alpha$ -pyr	$\beta$ -pyr	$\alpha$ -fur	$\beta$ -fur
C1	89.00	92.25	90.98	95.40	49.61	54.11	52.14	53.19
C2	73.52	75.64	62.89	65.26	97.03	96.20	102.65	99.66
C3	73.58	79.45	72.48	74.29	72.88	70.84	83.53	78.72
C4	72.75	72.61	72.45	72.75	71.21	70.22	76.93	75.01
C5	75.90	79.54	74.21	78.89	66.81	69.81	83.29	81.82
C6	63.48	63.64	63.16	63.33	63.88	64.82	61.77	62.75
C $\alpha$	51.35	51.27	50.15	51.10	50.51	50.56	50.19	50.40
COOH	182.24	182.74	173.89	174.47	n.r.	171.85	171.90	171.90
<b>%</b>	<b>11</b>	<b>89</b>	<b>80</b>	<b>20</b>	<b>5</b>	<b>69</b>	<b>13</b>	<b>13</b>

	Fru-Pro (Amadori)			
	$\alpha$ -pyr	$\beta$ -pyr	$\alpha$ -fur	$\beta$ -fur
C1	n.r.	58.10	57.96	57.96
C2	n.r.	96.37	102.51	99.64
C3	72.68	70.70	83.40	78.51
C4	71.08	70.13	76.81	74.39
C5	66.21	69.64	83.28	81.50
C6	n.r.	64.48	61.75	62.52
C $\alpha$	71.91	72.18	71.73	71.63
C $\beta$	n.r.	29.01	29.51	29.39
C $\gamma$	n.r.	24.09	23.99	24.02
C $\delta$	58.69	61.42	59.39	60.03
COOH	n.r.	174.59	174.87	174.45
<b>%</b>	<b>4</b>	<b>67</b>	<b>14</b>	<b>15</b>

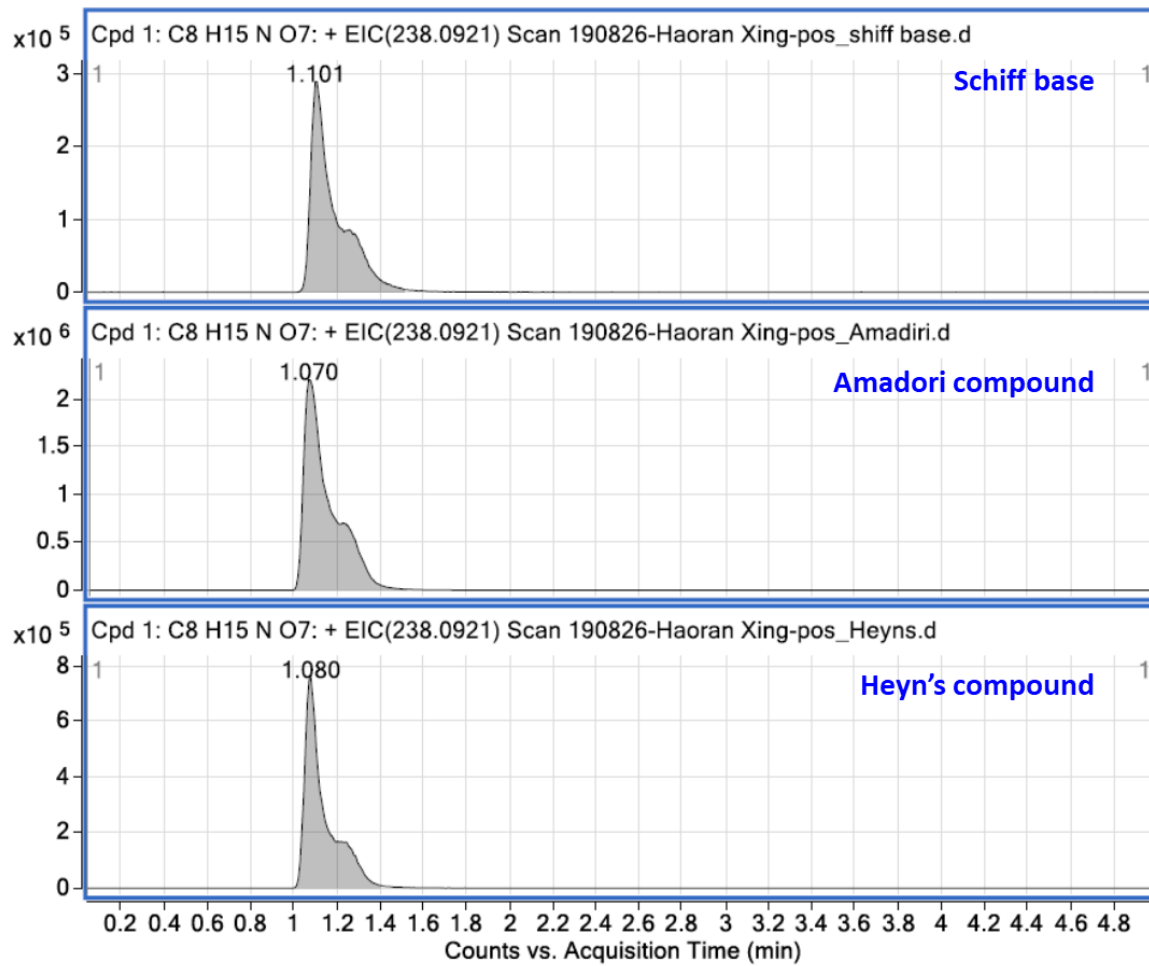


**Figure S 3.1** Extracted ion chromatogram of Schiff base, Amadori, and Heyn's compound under acidic condition.

**Table S 3.2** Summary and comparison of all the product ions from MS/MS of Schiff base, Amadori, and Heyn's compound at different collision energy under acid condition. Numbers reported in the table is the relative abundance.

MF	m/z	ppm	Proposed structure	Schiff base		Amadori			Heyns		
				10 eV	15eV	10 eV	15eV	20 eV	10 eV	15eV	20 eV
C <sub>8</sub> H <sub>16</sub> NO <sub>7</sub>	238.0914	5.783	[M+H] <sup>+</sup>	18.8	0.6	0.8	0.7	0.4	2.1	0.9	0
C <sub>8</sub> H <sub>14</sub> NO <sub>6</sub>	220.0812	0.964	[M+H-H <sub>2</sub> O] <sup>+</sup>	66.7	22.2	<b>100</b>	<b>50.1</b>	<b>10.8</b>	100	59.2	9.1
C <sub>8</sub> H <sub>12</sub> NO <sub>5</sub>	202.0710	1.225	[M+H-2H <sub>2</sub> O] <sup>+</sup>	80.3	71.5	<b>57.2</b>	<b>100</b>	<b>52.0</b>	79.0	95.1	20.8
C <sub>8</sub> H <sub>10</sub> NO <sub>4</sub>	184.0605	5.883	[M+H-3H <sub>2</sub> O] <sup>+</sup>	2.0	3.0	0.7	1.9	2.6	14.3	27.1	12.7
C <sub>7</sub> H <sub>12</sub> NO <sub>4</sub>	174.0757	3.636	[M+H-2H <sub>2</sub> O-CO] <sup>+</sup>	5.1	8.2	3.1	9.3	11.1	8.2	42.5	23.7
C <sub>6</sub> H <sub>8</sub> NO <sub>2</sub>	126.0546	6.374	[M+H-2H <sub>2</sub> O-COOH-H <sub>2</sub> CO] <sup>+</sup>	1.5	2.1	0.4	2.5	7.9	2.5	18.7	14.1
C <sub>7</sub> H <sub>10</sub> NO <sub>3</sub>	156.0652	6.204	[M+H-3H <sub>2</sub> O-CO] <sup>+</sup>	5.8	9.2	1.4	9.5	17.1	5.3	34.8	25.3
C <sub>7</sub> H <sub>8</sub> NO <sub>3</sub>	154.0491	4.662	[M+H-3H <sub>2</sub> O-H <sub>2</sub> CO] <sup>+</sup>	4.5	10.4	1.5	7.4	11.2	<b>16.8</b>	<b>76.8</b>	<b>76.9</b>
<b>Fragments derived from glycine</b>											
C <sub>2</sub> H <sub>6</sub> NO <sub>2</sub>	76.0388	11.224	[AA+H] <sup>+</sup> Glycine	100	100	21.4	44.0	46.0	14.6	46.0	31.5
C <sub>3</sub> H <sub>6</sub> NO <sub>2</sub>	88.0389	8.558	[AA+H+CH <sub>2</sub> ] <sup>+</sup> (C1-C2 fragments)	19.5	42.6	17.4	62.2	<b>100</b>	3.1	21.3	17.3
C <sub>4</sub> H <sub>8</sub> NO <sub>3</sub>	118.0495	6.93	[AA+H+Diose] <sup>+</sup> (C2-C3 fragments)	<b>55.8</b>	<b>58.3</b>	0.8	3.2	4.3	14.9	65.7	42.9
C <sub>3</sub> H <sub>6</sub> NO	72.0443	8.867	[AA+H+Diose-COOH] <sup>+</sup> (C2-C3 fragments)	10.5	33.1	0.3	2.2	11.6	2.5	27.4	42.0
C <sub>5</sub> H <sub>8</sub> NO <sub>3</sub>	130.0501	6.291	[AA+H+Triose-H <sub>2</sub> O] <sup>+</sup> (C3-C4 fragments)	0.4	1.2	0.2	1.1	4.0	<b>18.4</b>	<b>100</b>	<b>100</b>
C <sub>4</sub> H <sub>8</sub> NO <sub>2</sub>	102.0546	8.853	[AA+H+Triose-COOH] <sup>+</sup> (C3-C4 fragments)	0	0.0	0.1	0.4	0.7	3.6	18.1	19.4
C <sub>4</sub> H <sub>6</sub> NO	84.0421	9.981	[AA+H+Triose-COOH-H <sub>2</sub> O] <sup>+</sup> (C3-C4 fragments)	0.3	2.1	0.2	1.1	5.7	3.0	37.5	94.7

C <sub>6</sub> H <sub>8</sub> NO <sub>3</sub>	142.0495	5.759	[AA+H+Tetrose-2H <sub>2</sub> O] <sup>+</sup> (C4-C5 fragments)	2.3	7.1	0.6	2.5	4.7	9.0	39.9	22.1
<b>Fragments derived from sugar</b>											
C <sub>6</sub> H <sub>11</sub> O <sub>5</sub>	163.0598	5.203	[Hexose+H-H <sub>2</sub> O] <sup>+</sup>	1.3	0.9	0	0	0	0	0	0
C <sub>6</sub> H <sub>9</sub> O <sub>4</sub>	145.0498	1.956	[Hexose+H-2H <sub>2</sub> O] <sup>+</sup>	14.1	11.9	1.0	2.1	3.6	1.1	4.2	0
C <sub>6</sub> H <sub>7</sub> O <sub>3</sub>	127.0384	7.235	[Hexose+H-3H <sub>2</sub> O] <sup>+</sup>	13.2	23.5	3.0	11.6	16.0	6.3	24.9	18.4
C <sub>6</sub> H <sub>5</sub> O <sub>2</sub>	109.0279	6.919	[Hexose+H-4H <sub>2</sub> O] <sup>+</sup>	2.9		0.3	1.1	2.9	1.6	11.0	7.4
C <sub>5</sub> H <sub>5</sub> O <sub>2</sub>	97.0279	9.836	[Pentose-3H <sub>2</sub> O] <sup>+</sup> (C1-C2 fragments)	18.5	57.8	9.3	50.2	97.4	4.6	43.4	54.8
C <sub>5</sub> H <sub>7</sub> O <sub>2</sub>	99.0438	9.132	[Furanmethanol+H] <sup>+</sup>	1.4	6.0	0.6	2.8	8.5	2.7	20.7	23.4
C <sub>5</sub> H <sub>9</sub> O <sub>3</sub>	117.0551	4.862	[5-(hydroxymethyl)-2,3-dihydrofuran-2-ol+H] <sup>+</sup>	0.2	0	0.0	0.2	0	4.8	16.0	14.8
C <sub>4</sub> H <sub>5</sub> O <sub>3</sub>	101.0209	11.572	[Tetrose-H <sub>2</sub> O] <sup>+</sup> (C2-C3 fragments)	0.3	1.5	0.0	0.1	0.6	8.7	45.8	28.6
C <sub>4</sub> H <sub>5</sub> O <sub>2</sub>	85.0283	11.224	[Tetrose+H-2H <sub>2</sub> O] <sup>+</sup> (C2-C3 fragments)	<b>26.9</b>	<b>63.6</b>	0.6	3.4	10.2	4.0	37.4	47.1
C <sub>4</sub> H <sub>5</sub> O	69.0326	6.371	[Furan+H] <sup>+</sup>	4.8	16.2	0.8	3.6	11.1	1.0	6.6	17.9
C <sub>2</sub> H <sub>5</sub> O <sub>2</sub>	61.0288	2.53	[Diose+H] <sup>+</sup> (C4-C5 fragments)	2.4	6.9	0.0	0.3	1.4	0.7	5.6	11.0

**Table S 3.3** Summary and comparison of all the product ions from MS/MS of Schiff base, Amadori, and Heyns compound at different collision voltage of 10 eV under neutral condition. Numbers reported in the table is the relative abundance.

MF	m/z	ppm	Proposed structure	Schiff base	Amadori	Heyns
C <sub>8</sub> H <sub>15</sub> NNaO <sub>7</sub>	260.0735	4.312	[M+Na] <sup>+</sup>	38	100	92.8
C <sub>8</sub> H <sub>13</sub> NNaO <sub>6</sub>	242.0631	3.953	[M+Na-H <sub>2</sub> O] <sup>+</sup>	3.3	<b>15.2</b>	7.5
C <sub>8</sub> H <sub>11</sub> NNaO <sub>5</sub>	224.0522	5.767	[M+Na-2H <sub>2</sub> O] <sup>+</sup>	3.3	<b>10.4</b>	0
C <sub>7</sub> H <sub>15</sub> NNaO <sub>5</sub>	216.0842	2.741	[M+Na-COOH] <sup>+</sup>	6.1	1.9	0
C <sub>7</sub> H <sub>13</sub> NNaO <sub>4</sub>	198.0729	6.702	[M+Na-COOH-H <sub>2</sub> O] <sup>+</sup>	2.2	6	3.5
C <sub>7</sub> H <sub>11</sub> NNaO <sub>3</sub>	180.0628	4.792	[M+Na-COOH-2H <sub>2</sub> O] <sup>+</sup>	1.6	3.6	9.8
C <sub>7</sub> H <sub>9</sub> NNaO <sub>2</sub>	162.0516	9.245	[M+Na-COOH-3H <sub>2</sub> O] <sup>+</sup>	1.9	5	0
<b>Fragments derived from Glycine</b>						
C <sub>2</sub> H <sub>5</sub> NNaO <sub>2</sub>	98.0206	12.223	[AA+Na] <sup>+</sup> Glycine	4.2	8.1	1.3
C <sub>3</sub> H <sub>5</sub> NNaO <sub>2</sub>	110.0209	8.163	[AA+Na+CH <sub>2</sub> ] <sup>+</sup> (C1-C2 fragments)	0	0.9	0
C <sub>4</sub> H <sub>7</sub> NNaO <sub>3</sub>	140.0310	9.732	[AA+Na+Diose] <sup>+</sup> (C2-C3 fragments)	<b>100</b>	28.3	100
C <sub>5</sub> H <sub>9</sub> NNaO <sub>4</sub>	170.0417	7.219	[AA+Na+Triose] <sup>+</sup> (C3-C4 fragments)	1.9	5.5	<b>16.8</b>
C <sub>4</sub> H <sub>7</sub> NNaO	108.0426	0.615	[AA+Na+Triose-COOH-H <sub>2</sub> O] <sup>+</sup> (C3-C4 fragments)	0	0.4	3.8
C <sub>6</sub> H <sub>7</sub> NNaO <sub>3</sub>	164.0310	8.308	[AA+Na+Tetrose-2H <sub>2</sub> O] <sup>+</sup> (C4-C5 fragments)	0	0.3	4.4
<b>Fragments derived from sugar</b>						
C <sub>6</sub> H <sub>10</sub> NaO <sub>5</sub>	185.0424	1.044	[Hexose+Na-H <sub>2</sub> O] <sup>+</sup>	0	0.4	0
C <sub>6</sub> H <sub>8</sub> NaO <sub>4</sub>	167.0309	6.756	[Hexose+Na-2H <sub>2</sub> O] <sup>+</sup>	0	3.6	0
C <sub>5</sub> H <sub>10</sub> NaO <sub>5</sub>	173.0415	6.317	[Pentose+Na] <sup>+</sup> (C1-C2 fragments)	0	1.5	0
C <sub>5</sub> H <sub>8</sub> NaO <sub>4</sub>	155.0320	0.183	[Pentose+Na-H <sub>2</sub> O] <sup>+</sup> (C1-C2 fragments)	0	0.3	0
C <sub>4</sub> H <sub>8</sub> NaO <sub>4</sub>	143.0308	8.588	[Tetrose+Na] <sup>+</sup> (C2-C3 fragments)	<b>90.3</b>	32.9	59.2
C <sub>3</sub> H <sub>6</sub> NaO <sub>3</sub>	113.0202	11.181	[Triose+Na] <sup>+</sup> (C3-C4 fragments)	0	1.9	<b>11</b>

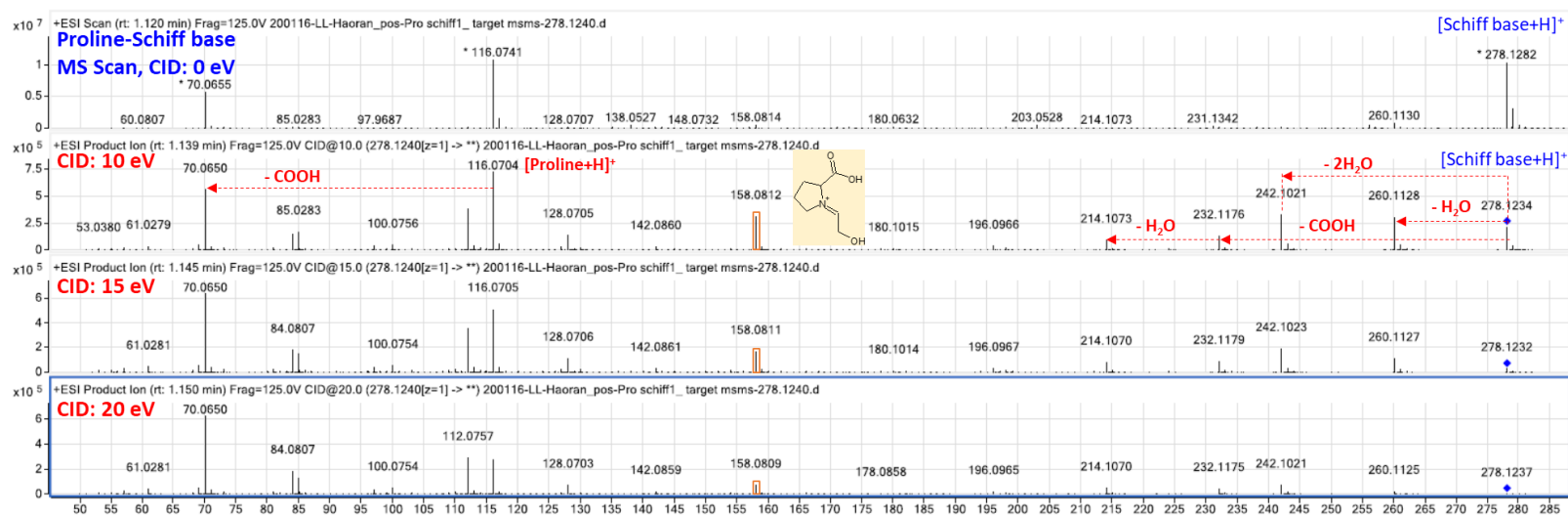


Figure S 3.2 MS and MS/MS spectra acquired at 0, 10, 15, 20 eV of proline Schiff base under acidic conditions.

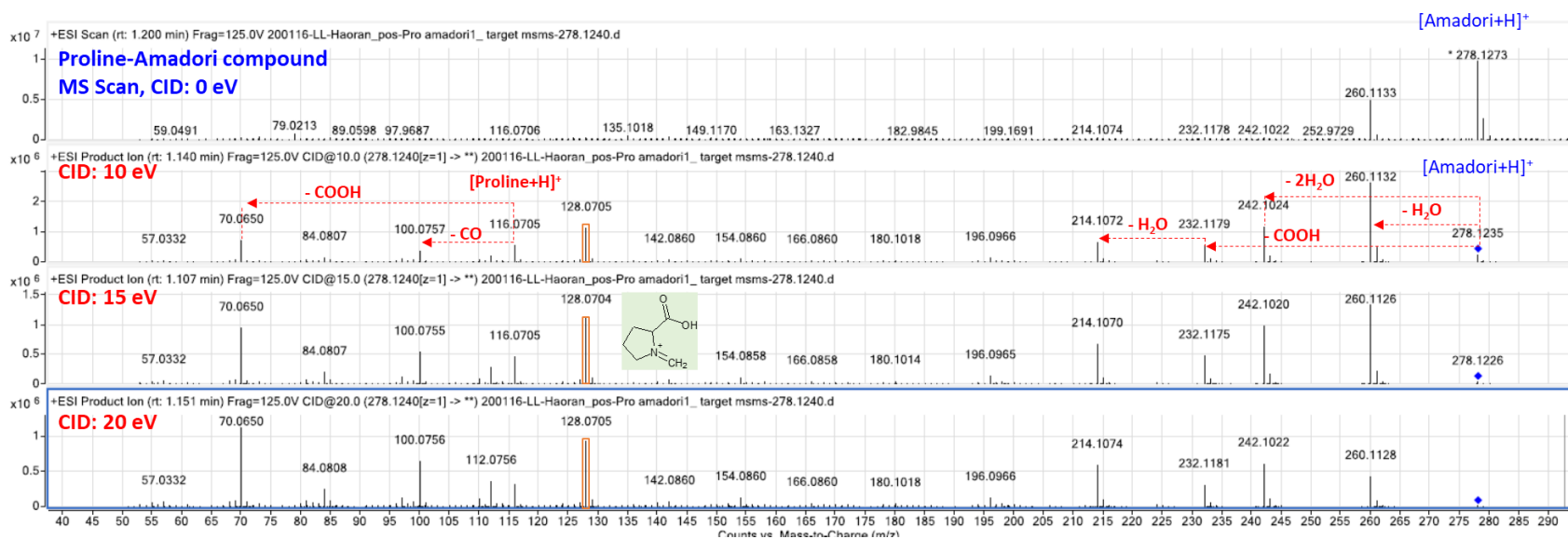
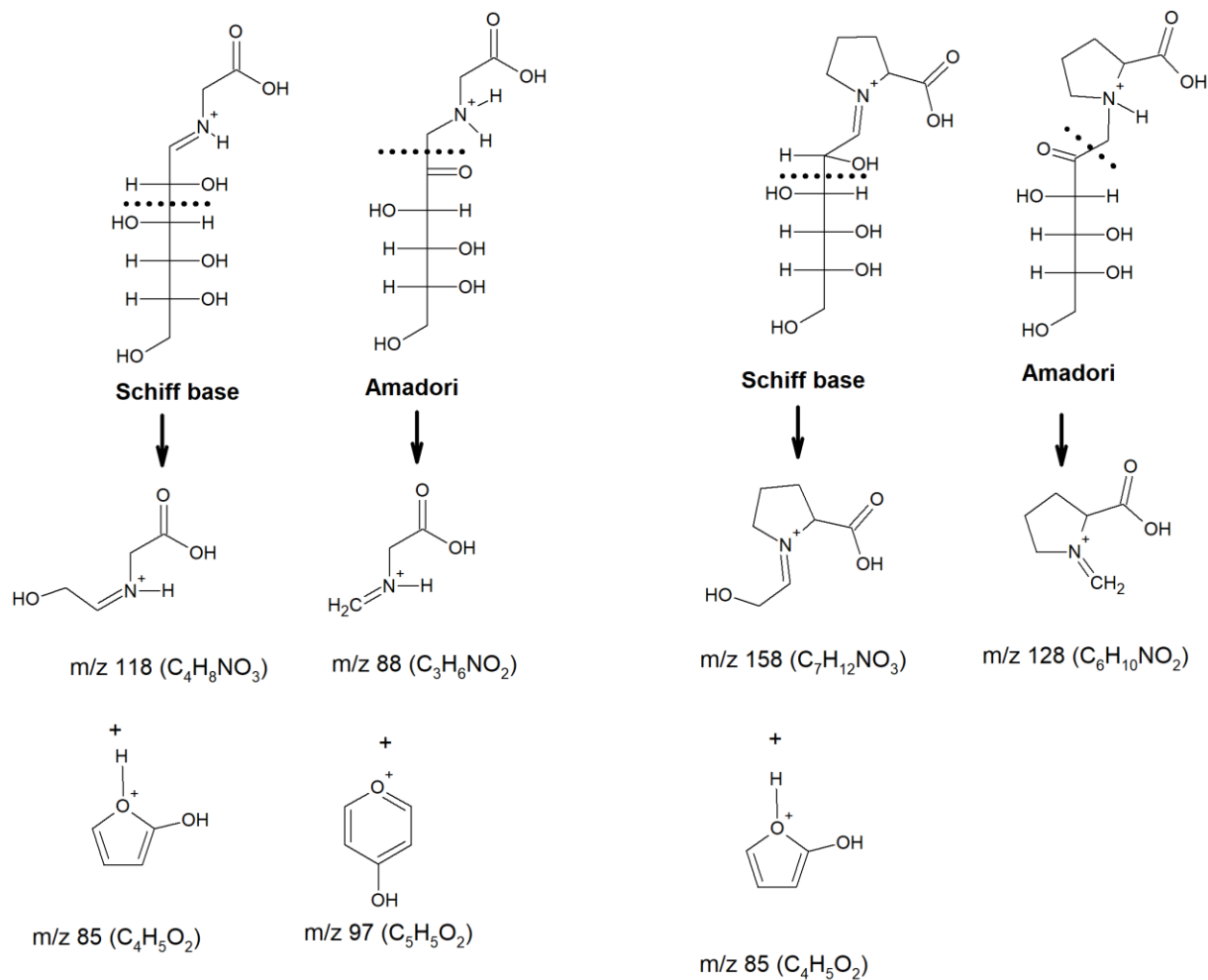
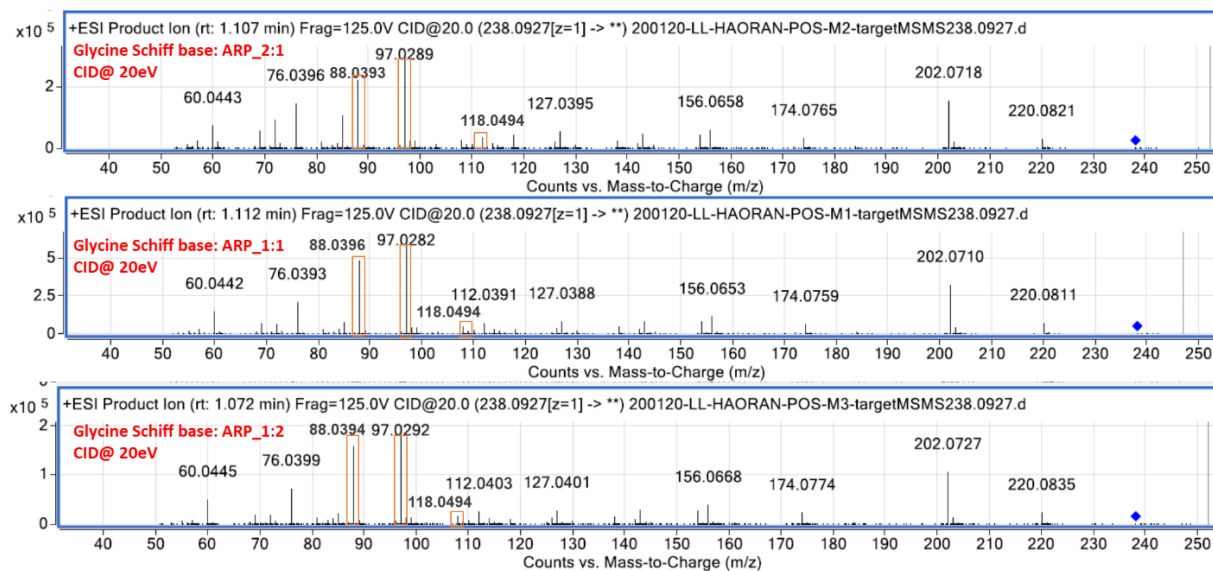


Figure S 3.3 MS and MS/MS spectra acquired at 0, 10, 15, 20 eV of proline ARP under acidic condition.



**Scheme S 3.1** Comparison of the proposed diagnostic collision-induced fragmentations of the proline and glycine Schiff base and Amadori rearrangement products under acidic conditions. The characteristic loss of water molecules from ARP is not shown



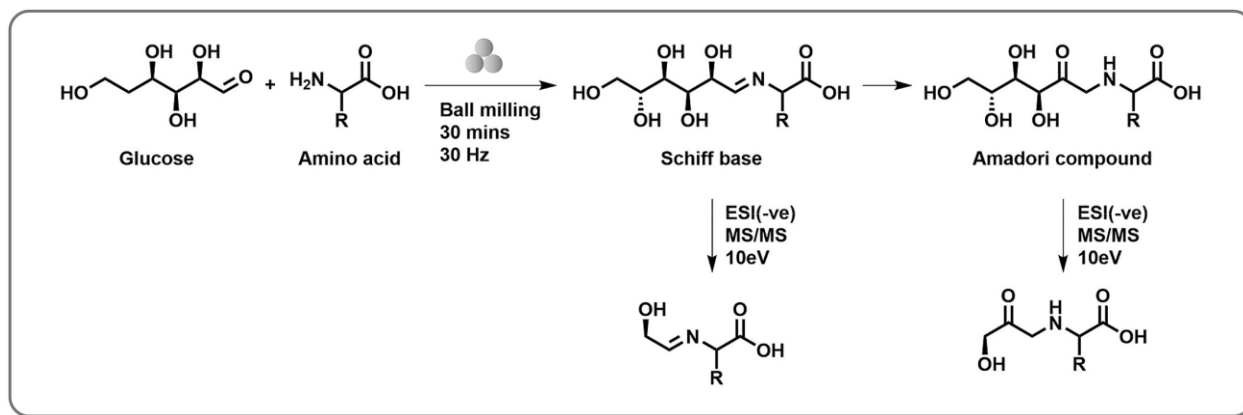
**Figure S 3.4** CID of various mixtures of glycine Schiff base and its ARP at different molar ratios acquired under protonation

## Connecting paragraph

In Chapter 3, we have shown the potential of using diagnostic MS/MS fragmentations for the identification of isomeric Maillard reaction intermediates under ESI positive mode. The results indicated that protonated ions were had more diagnostic value compared to the sodiated ions for distinguishing between Schiff bases and Amadori compounds. In Chapter 4, we further explored the utilization of MS/MS as a diagnostic tool for distinguishing the Schiff bases and their Amadori compounds through fragmentation of the deprotonated ions generated under ESI negative mode. This diagnostic information was subsequently used to study the composition of mechanochemically generated Maillard reaction mixtures through ball milling glucose and various amino acids.

Chapter 4 was published in the *Carbohydrate research*: Xing, H., & Yaylayan, V. (2020). Mechanochemical generation of Schiff bases and Amadori products and utilization of diagnostic MS/MS fragmentation patterns in negative ionization mode for their analysis. *Carbohydrate Research*, **495**, 108091.

## Chapter 4 Mechanochemical generation of Schiff bases and Amadori products and utilization of diagnostic MS/MS fragmentation patterns in negative ionization mode for their analysis



## 4.1 Abstract

The use of tandem mass spectrometry under positive ionization mode was previously developed as a tool for distinguishing isomeric Schiff bases and Amadori products. In this paper, similar diagnostic MS/MS fragmentation patterns were identified under negative ionization mode and was utilized to study the composition of mechanochemically generated Maillard reaction mixtures. The major diagnostic ion of the Schiff base was found to be a diose attached to the amino acid residue, while that of the Amadori compound was a triose. The structures of the diagnostic ions were confirmed through isotope labeling technique and elemental composition. Furthermore, application of this technique showed that ball milling of glucose with different amino acids almost exclusively results in the formation of a mixture of Schiff bases and Amadori compounds, and that amino acids with basic side chains generated more Schiff bases and those with acidic side chains generated more Amadori products.

**Keywords:** Maillard reaction, Mechanochemistry, Ball milling, Schiff base, Amadori compound, ESI-qToF-MS/MS, ESI negative mode, Diagnostic ions, Tandem mass spectrometry (MS/MS)

## 4.2 Introduction

The Maillard reaction has been of great interest over the years in diverse areas of research from human pathology to food chemistry.[1] It is considered as a complex reaction cascade initiated by the condensation of an amino group with an  $\alpha$ -hydroxy carbonyl moiety of a reducing sugar leading to the formation of Schiff base.[2] The formation of this adduct is followed by a well known rearrangement, which produces the Amadori rearrangement product (ARP), a more stable isomer of the Schiff base. Subsequent degradation of the ARPs yields a complex mixture of flavor and aroma-active carbocyclic and heterocyclic compounds, in addition to polymers and oligomers with characteristic yellow-brown colors.[3, 4] The Maillard reaction mixtures have been studied recently using a non-targeted approach based on high-resolution mass spectrometric data.[5] Knowledge of the relative amounts of Schiff bases and their corresponding ARPs in these reaction mixtures can be a useful strategy for estimating their relative importance. Ability to discriminate between the initially formed isomeric intermediates in these reaction mixtures can provide an important tool for the workers in the field of “omics” research on the Maillard reaction. To this end, we recently developed a method based on the diagnostic ions generated from collision-induced dissociation (CID) of Schiff bases and their corresponding Amadori/Heyns products using electrospray ionization (ESI) in positive mode.[6] The CID ions were generated under acidic (formic acid) and under neutral (sodium clusters) conditions. Both conditions provided useful diagnostic ions but more so under protonation.[6] Furthermore, for the purpose of generating flavor precursors from Schiff bases and their Amadori/Heyns rearrangement products, the Maillard reaction is usually carried out under conventional hydrothermal conditions where the reactants (sugar and amino acids) are dissolved in a buffer under controlled pH conditions. The solvent, normally water, needs to be removed after the reaction which is considered as an energy-consuming step.[7] Although there are many recent studies utilizing microemulsions [8] or deep eutectic solvents,[9] addressing the importance of the role of solvents play in the generation of Maillard volatiles and stabilization of the reaction intermediates, in this study, we explore an alternate approach based on high energy mechanochemical ball milling process for the generation of Maillard flavor precursors that eliminates the use of solvents.

There are numerous mechanochemistry-based synthetic strategies of various types of imines reported in the literature with almost quantitative yields, even without acid catalysts.[10, 11] Moreover, mechanochemistry allows various quantitative multistep and sequential reactions to

occur in a solvent free environment, eliminating bulk dissolution problems.[12, 13] Furthermore, despite the fact that during mechanochemical reactions temperature generated is dependent on reaction type, time, and the nature of milling vial etc. [14, 15], the generally observed average reaction temperatures do not exceed ~ 40 to 60 °C minimizing degradations of the target compounds. An additional advantage of using mechanical force to initiate chemical transformations is in its vectorial nature, which, at least in principle, makes it inherently a more controllable process for chemical reactions than that of thermochemistry.[16] The reaction between amino acids and sugar can be quenched easily before it proceeds to the final stages where volatile aroma active compounds are formed from the degradation of Schiff bases and their Amadori/Heyns products. The resulting reaction mixtures can be considered as “activated” or as “dynamic” flavor precursors with enhanced reactivity compared to the initial reactants,[17] since the activated mixtures are readily converted to aroma compounds during thermal treatment of foods and should be compatible with modern food processing techniques such as microwave irradiation. Surprisingly, despite its advantages and to the best of our knowledge, only one example of its application can be found in the literature.[18] The patent literature indicated a facile formation of reactive flavor precursors such as Schiff bases and Amadori products when sugars and amino acids are milled, as evidenced by the generation of Maillard aromas and browning. However, no studies have been reported to confirm this assumption.

In this study, we investigate the potential of ball milling in generating mixtures rich in Schiff bases/Amadori compounds and apply the MS/MS diagnostic ions for their analysis.

## 4.3 Material and Methods

### 4.3.1 Materials and Reagents

Glycine (98%), L-isoleucine (98%), L-phenylalanine (98%), L-aspartic acid (98%), L-glutamic acid (98%), L-histidine (98%), L-arginine (98%), D-glucose (99.5%), AlCl<sub>3</sub>, and Na<sub>2</sub>CO<sub>3</sub> were purchased from Sigma-Aldrich Chemical Co. (Oakville, Ontario, Canada). U-<sup>13</sup>C<sub>6</sub> Glucose (99%) were purchased from Cambridge Isotope Laboratories (Andover, MI). The synthesis and characterization of *N*-carboxymethyl-D-glucosylamine (glycine Schiff base), 1-[(carboxymethyl)amino]-1-deoxy-D-fructose (glycine Amadori compound), 1-[(carboxyethyl)amino]-1-deoxy-D-fructose (alanine Amadori compound), 1-[(2'-

carboxy)pyrrolidinyl]-1-deoxy-D-fructose (proline Amadori compound), and *N*-[(2'-carboxy)pyrrolidinyl]-D-glucosylamine (proline Schiff base) can be found in the supplementary material and previous literature.[6] All other chemicals and reagents were of analytical grade from Fisher Scientific. Ultrapure water was used throughout the study. All materials were used without further purification.

#### **4.3.2 Sample Preparation**

Samples (40 mg) consisting of sugar and amino acid mixtures in a 1:1 molar ratio were milled at ambient temperature. For the mechano-catalytic reactions, 1% (w/w) of AlCl<sub>3</sub> or Na<sub>2</sub>CO<sub>3</sub> were added as acid or base catalysts. All mechanochemical reactions were conducted in a stainless-steel grinding jar (10 mL) with 2 steel balls (3.2 mm in diameter; ball/sample ratio ~32:1) for creating inner friction. The jars were seated in the Retsch Mixer Mill (MM 400, Newtown, PA, US) that performs radial oscillations in a horizontal position without coolant (the external jar temperature was ~25 °C) at a frequency of 30 Hz for 30 mins (M30). Samples collected after milling were stored at -20°C for further analysis.

#### **4.3.3 ESI-qToF-MS/MS under sodium formate condition**

The diluted sample solutions (1 µL) in water/ methanol (10%/ 90%) were supplied to the source directly via a syringe. The analysis was performed on a Bruker Maxis Impact quadrupole time of flight mass spectrometer (Bruker Daltonics, Bremen, Germany) operated in both positive and negative ion modes. Instrument calibration was performed using sodium formate clusters. The electrospray interphase settings were as follows: nebulizer pressure, 0.6 bar; drying gas, 4 L/min; temperature, 180 °C; and capillary voltage, 4500 V. The scan range was from *m/z* 50 to 800. Tandem mass spectrometry (MS/MS) for the ions [M+Na]<sup>+</sup> under positive mode and [M-H]<sup>-</sup> under negative mode was carried out in MRM mode using collision energy ranging from 5 to 15 eV. The data were analyzed using Bruker Compass Data Analysis software, version 4.2.

#### **4.3.4 LC-ESI-qToF-MS/MS under formic acid condition**

Samples were analyzed using an Agilent 1290 Infinity II LC system coupled to the 6545 qToF - MS (Agilent Technologies, Santa Clara, USA). The LC separation was conducted on a Poreshell120 EC-C18 analytical column (Agilent Technologies; 2.7 µm × 3 mm × 100 mm) connected with a Poreshell120 EC-C18 guard column (Agilent Technologies; 2.7 µm × 3 mm × 5 mm). The elution condition was at a flow rate of 0.4 ml/min with the mobile phase as the mixture

of 0.1% (V/V) aqueous formic acid (40%) with methanol (60%). The injection volume was 1  $\mu\text{L}$ , and the column temperature was set to 20  $^{\circ}\text{C}$ . The samples were analyzed in both positive and negative electrospray ionization mode using product ion (MS/MS) experiment. The drying gas temperature was at 275  $^{\circ}\text{C}$  with a flow of 10 mL/min, the sheath gas temperature was at 300  $^{\circ}\text{C}$  with a flow of 12 mL/min, the pressure on the nebulizer at 45 psi, the capillary voltage at 4500 V, the fragmentor voltage at 1000 V, the skimmer voltage at 50 V, and the nozzle voltage at 2000 V. The Tandem mass spectrometry (MS/MS) data was collected by scans between  $m/z$  50 and 1000 at a scan rate of 3 spectra/s for four different collision energies (0 V, 10 V, 15 V, and 20 V) for the ions  $[\text{M}+\text{H}]^{+}$  and  $[\text{M}+\text{Na}]^{+}$  under positive mode and  $[\text{M}-\text{H}]^{-}$  under negative mode. The datasets were processed with MassHunter Profinder B.08.00 software (Agilent Technologies).

#### 4.4 Results and Discussion

The diagnostic MS/MS fragmentation patterns under ESI positive mode that we have recently identified [6] were applied for discriminating between isomeric Schiff bases and their ARPs formed during ball milling of glucose and various amino acids. Despite their usefulness, some of the diagnostic ions under ESI positive ionization mode were not uniquely associated with one isomeric form or the other. Their utility resided in having significantly different relative intensities. For the purpose of identification of MS/MS diagnostic fragmentations with structurally unique identifiers for each of the Schiff bases and Amadori products, ESI under negative ionization mode was also explored to demonstrate their utility in analyzing mechanochemically generated Maillard reaction mixtures for the presence of Amadori and Schiff bases.

#### 4.4.1 Diagnostic MS/MS fragmentations of Schiff bases and ARPs under negative ionization mode

The molecular ions obtained from synthetic standards of Schiff bases and Amadori products of glucose with glycine, proline and alanine under ESI negative ionization mode generated consistent MS/MS fragmentation patterns with high diagnostic value (see Table 4.1 & Figures S4.1 & S4.2) similar to that under ESI positive mode.[6] The diagnostic utility of these ions was determined based on their unique structures associated with only one form of the isomeric precursors (Schiff bases or ARP) and generated from several amino acids in high intensities. The diagnostic ion of the Schiff bases was structurally the same whether generated as sodiated  $[M+Na]^+$ , protonated  $[M+H]^+$ , or deprotonated  $[M-H]^-$  forms having a molecular formula M of  $C_4H_7NO_3$  in the case of glycine. (see Scheme 4.1). The diagnostic ions of Schiff bases were generated through retro-aldol reaction initiated from the C-3 hydroxyl group as shown in Scheme 4.1 (pathway b). Under sodiation conditions both Schiff bases and the ARPs generated diagnostic ions having the same molecular structures (Scheme 4.1,  $m/z$  140 from glycine) but differing only in their relative intensities making utilization of these ions as diagnostic markers less useful. However, under protonation the Schiff bases and their corresponding Amadori compounds generated distinct structures; the former at  $m/z$  118 ( $C_4H_8NO_3$ ) and the latter at  $m/z$  88 ( $C_3H_6NO_2$ ) in the case of glycine as shown in Scheme 4.1.[6] Similar to the diagnostic ions generated under positive ionization mode, negative ionization also generated structurally different diagnostic ions ( $m/z$  116 & 146) from both precursors and at the same time differing structurally from the diagnostic ions generated under sodiation ( $m/z$  140 & 140) and protonation conditions ( $m/z$  118 & 88) (see Scheme 4.1). Scheme 4.1 also shows the bond fissions (**a**, **b**, **c**, **d** and **e**) giving rise to specific diagnostic ions originating from either Schiff bases or ARPs.

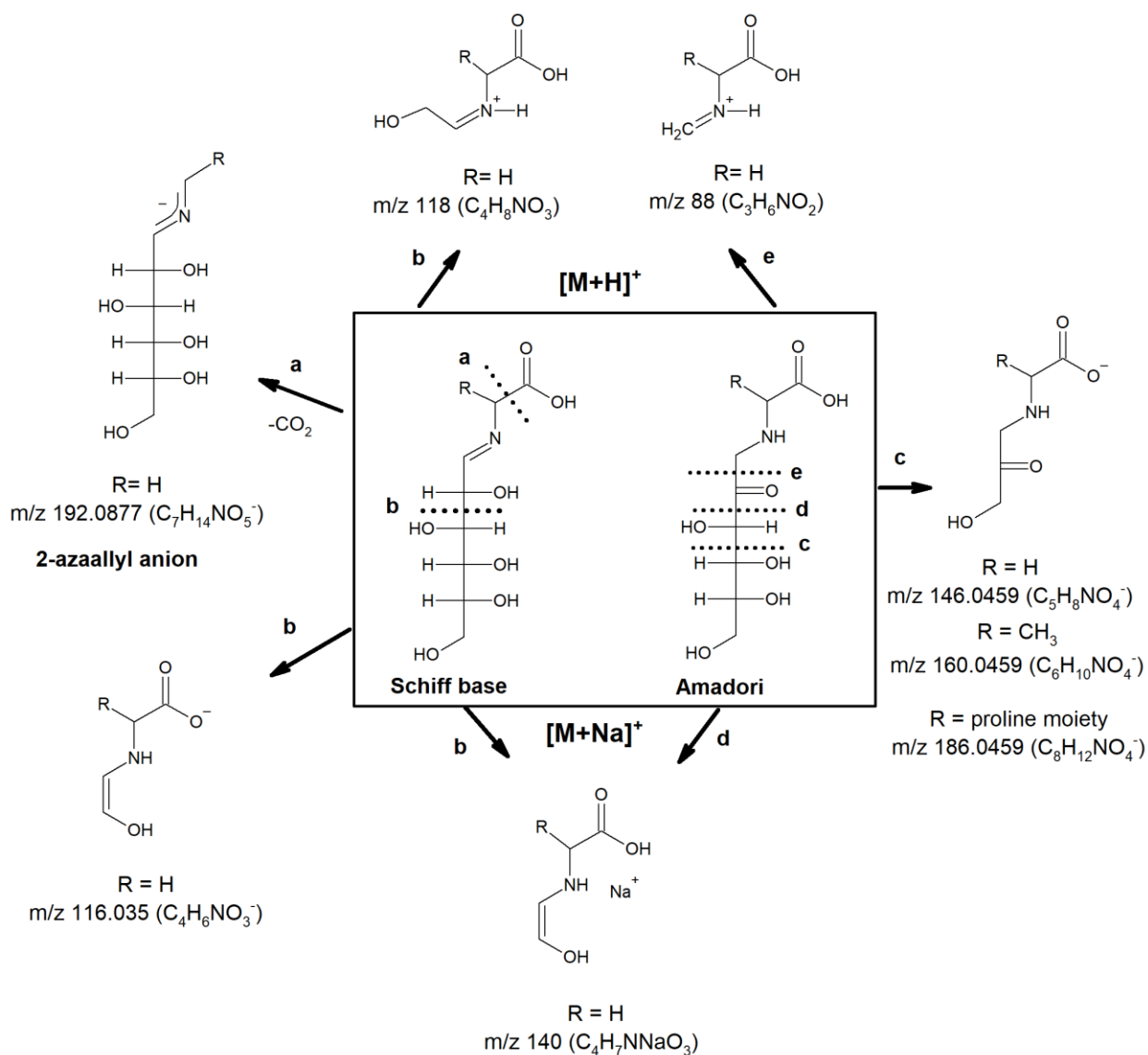
**Table 4.1** ESI-qToF-MS and MS/MS (CID at 10eV) fragmentations under negative ionization mode of standard Schiff bases, and ARPs.

Compound <sup>a</sup>		Significant fragment ions in MS and MS/MS spectra [M-H] <sup>-</sup> (m/z)
Glycine Schiff base	MS	<u>236 (M)</u> <sup>c</sup> , 192 (M-COOH), 116 (Gly+2ose)
	MS/MS <sup>b</sup>	236 (M), <b>192 (M-COOH)</b> <sup>c</sup> , 174 (M-COOH-H <sub>2</sub> O), <b>116 (Gly+2ose)</b>
Glycine ARP	MS	<u>236 (M)</u> , 146 (Gly+3ose)
	MS/MS	236 (M), 176 (M-C <sub>2</sub> H <sub>4</sub> O <sub>2</sub> ), 158 (M-C <sub>2</sub> H <sub>4</sub> O <sub>2</sub> -H <sub>2</sub> O), <b>146 (Gly+3ose)</b>
Proline Schiff base	MS	<u>276 (M)</u> , 179 (Glc), 156 (Pro)
	MS/MS	276 (M), <b>156 (Pro+2ose)</b> , 114 (Pro)
Proline ARP	MS	<u>276 (M)</u>
	MS/MS	276 (M), <b>186 (Pro+3ose)</b> , 114 (Pro)
Alanine ARP	MS	<u>250 (M)</u> , 160 (Ala+3ose)
	MS/MS	250 (M), <b>160 (Ala+3ose)</b>

<sup>a</sup>: The compounds used for MS/MS are synthesized and characterized as reported in [6].

<sup>b</sup>: MS/MS fragmentations were conducted at 5-15 eV in both Bruker and Agilent (LC)-ESI-qToF-MS/MS system. The fragmentation pattern was found reproducible in two replicates.

<sup>c</sup>: Under the MS scanning, the underlined ions are the most abundant; under MS/MS fragmentation, the ion in bold indicates the diagnostic product ion.



**Scheme 4.1** Proposed MS/MS fragmentation patterns under positive and negative ionization modes for the discrimination between Schiff bases and their Amadori rearrangement products modelled after glycine and proline Schiff bases and their Amadori rearrangement products. The fragmentation pattern was tested in mechanochemically generated mixtures of Schiff bases and Amadori products from glucose and various amino acids (including glycine, isoleucine, phenylalanine, aspartic acid, and histidine).

**a** = decarboxylation; **b** = retro aldol C2-C3; **c** = retro aldol C4-C5; **d** = retro-aldol C2-C3; **e** =  $\alpha$ -cleavage

#### 4.4.2 The utility of the MS/MS diagnostic ions generated under ESI negative mode in qualitatively estimating the ratio of glycine Schiff bases and ARPs in prepared mixtures of synthetic standards.

Prepared mixtures of synthetic glycine Schiff base and its ARP with known molar ratios of 1:2 and 2:1 were analyzed by ESI-qTOF/MS/MS to estimate the potential of utilizing relative intensities of diagnostic ions generated from MS/MS in estimating the composition of a mixture of isomers. The three molecular ions, including deprotonated  $[M-H]^-$  (see Figure 4.1 and S4.3-4.4), protonated  $[M+H]^+$  (see Figure S4.5), and sodiated  $[M+Na]^+$ , generated under acidic or neutral conditions and operated under both ESI positive and negative modes were evaluated and compared (see Table S4.2).

The MS/MS fragmentations of the protonated ion  $[M+H]^+$  were demonstrated previously to be suitable for estimating the composition of prepared mixtures of standard glycine Schiff base and its ARP.[6] Despite the fact that Schiff bases were found to be incompatible to be monitored under acidic conditions due to their ease of hydrolysis, however, the relative amounts of only Amadori compounds can be estimated easily through monitoring the relative intensities of  $m/z$  88 (see Figure S4.5). On the other hand, the diagnostic ions originating from the sodiated molecular ions of the Schiff base and its ARP were found to be less informative, due to the fact that they differed only in their relative intensities but sharing a common structure ( $m/z$  140, see Scheme 4.1).

In this study, the utility of the MS/MS diagnostic deprotonated ions  $[M-H]^-$  (see Scheme 4.1) in predicting the presence of Schiff bases and ARPs in prepared mixtures of known molar ratios of 1:2 and 2:1 were also examined (see Figures 4.1 & S4.3-4.4). Analysis under acidic conditions was predictably more favorable to the formation of intense  $[M+H]^+$  ions rather than  $[M-H]^-$  ions when operated under ESI negative mode, thus producing weaker product ions. (see Figure S4.3)

Although both protonated and deprotonated diagnostic ions can also be used as indicators for the presence of glycine Schiff base and its ARP in these standard mixtures, the deprotonated ion  $[M-H]^-$  generated under neutral conditions was found to be the best mode for estimating the composition of a mixture of Schiff bases and their ARPs for several reasons: (1) the MS/MS spectra were less noisy. (2) The intensities of the diagnostic ions were relatively high for both isomers, (3) the hydrolysis of Schiff bases was minimized under neutral MS conditions,[6] and (4) the relative intensities of the diagnostic ions responded well to the known ratio of Schiff base to

ARP (see Figure S4.4). In this study, the application of this analytical method will be illustrated in estimating the relative ratio of the Schiff base and its ARP formed between glucose and various amino acids generated with ball milling. However, the above information can be potentially expanded for quantification of the absolute composition of the two isomers using LC-MS/MS under multiple reaction monitoring mode with appropriate calibration curves (For example, transitions  $m/z236 \rightarrow m/z116$  for glycine Schiff base and  $m/z236 \rightarrow m/z146$  for glycine Amadori compound). It is also worth mentioning that LC conditions should also be optimized to accommodate the instability of Schiff base.[6] In the following section, the MS/MS of mechanochemically generated reaction mixture of glycine and glucose will be discussed.

#### **4.4.3 Application of the MS/MS diagnostic ions generated under ESI negative mode in predicting the formation of Schiff bases and their ARPs in mechanochemically generated reaction mixture from glucose and glycine**

The molecular ions of the Schiff base/Amadori compounds formed in the reaction mixtures generated from ball milling of glucose and glycine (1:1 molar ratio for 30 minutes at 30 Hz) were analyzed under positive and negative electrospray ionization modes using neutral conditions. (see Figures S4.6 & S4.7) Inspection of Figures S4.6 and S4.7 indicated that milling leads to selective formation of Schiff bases and ARPs ( $[M-H]^-$   $m/z$  236;  $[M+Na]^+$   $m/z$  260)) with trace amounts of side reaction products [ $m/z$  282, 360, and 393 (see Figure S4.6) or  $m/z$  265 and 277 (see Figure S4.7)]. The MS/MS data of the common precursor ion at  $[M-H]^-$  236 clearly confirms the presence of  $m/z$  146 (exclusively generated from ARP) and  $m/z$  116 and 192 (exclusively generated from Schiff base). The presence of unreacted free glucose ( $[M-H]^-$   $m/z$  179;  $[M+Na]^+$   $m/z$  203) in the milled samples was also observed.

Under all the reaction conditions that we have investigated (up to 2 hours at 30 Hz), ball milling exclusively resulted in the formation of Schiff bases and ARPs without any other major degradation products. There was no significant color change right after milling indicating the reaction did not proceed to its advanced stages. However, the reaction mixtures did become very hygroscopic after milling and turned into a paste within hours in the reactor when left open at room temperature. As estimated by solid-state NMR, the total conversion after 30 minutes milling at 30 Hz was  $39.3\% \pm 1.7$ . (Figures S4.8 & S4.9)

The condensation adduct was found to be a mixture of Schiff base and ARP through MS/MS analysis by comparing the diagnostic product ions and their relative abundances to those of the standards. (see Figure 4.1) Fragmentation of the condensation adduct generated the diagnostic ions from both Schiff base ( $m/z$  116 and  $m/z$  192) and ARP ( $m/z$  146). (see Figure 4.1e) The elemental composition of the diagnostic ions were consistent with the proposed structures such as  $m/z$  116 ( $C_4H_6NO_3$ ) representing a diose attached to the glycine moiety and  $m/z$  146 ( $C_5H_8NO_4$ ) representing a triose attached to the glycine moiety. Both fragments can be rationalized to be formed through appropriate retro-aldol reactions. Another diagnostic ion of the Schiff base was observed at  $m/z$  192 ( $C_7H_{14}NO_5$ ) which can be generated through decarboxylation, leading to the formation of the 2-azaallyl anion [19, 20] shown in Scheme 4.1. (see Scheme 4.1, pathway a)

Taking advantage of this fast method of generating mixtures of Schiff bases and ARPs, we further provided evidence on the tentative structures of the diagnostic ions proposed earlier by replacing glucose with U- $^{13}C_6$  labeled glucose in the ball milling experiments. As expected, in the glucose-glycine model system, the  $m/z$  at 116 was increased by 2 Da, the  $m/z$  at 192 was increased by 6 Da, and the  $m/z$  at 146 was increased by 3 Da. The increments indicating the number of carbon atoms from sugar that were incorporated in the structures. Together with the elemental composition calculated based on the high-resolution MS results (error < 5ppm), the isotope incorporation data provides further evidence for the structures of proposed diagnostic ions. The results of U- $^{13}C_6$ -glucose-histidine model system were also in accordance with the U- $^{13}C_6$ -glucose-glycine model system. (see Table 4.2)

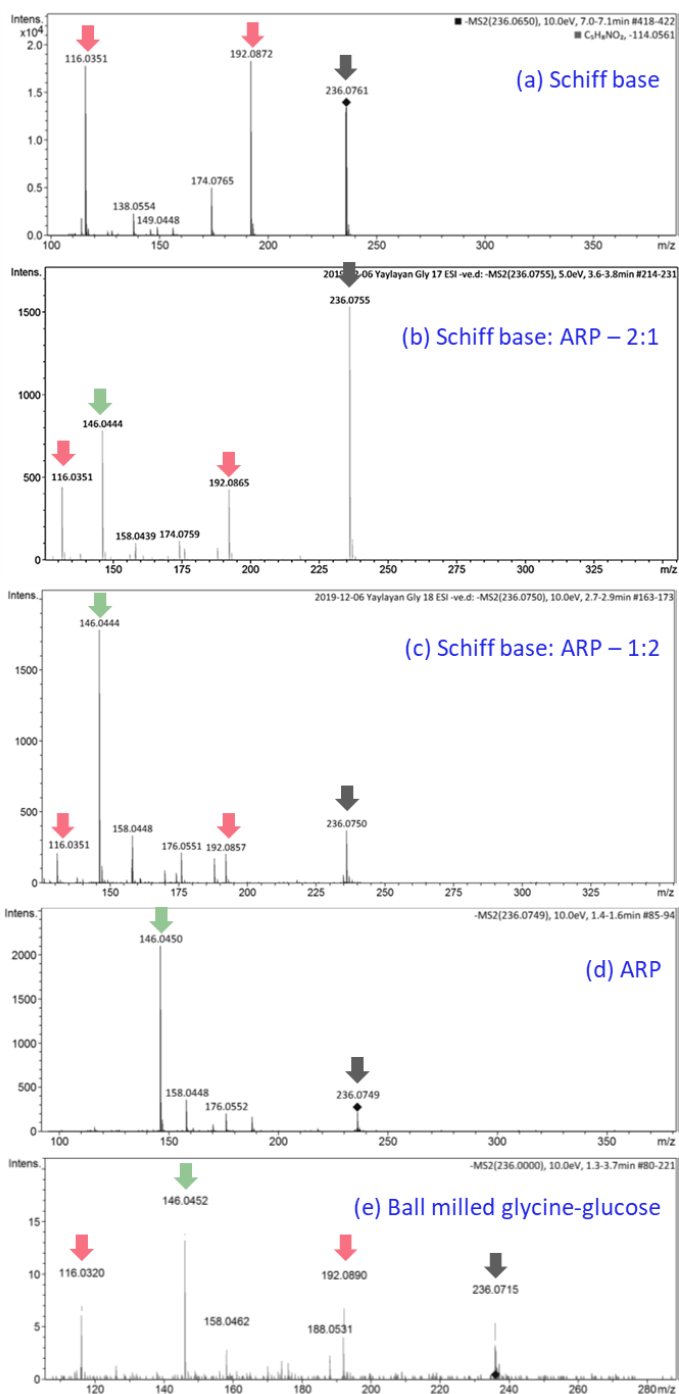


**Figure 4.1** MS/MS fragmentation in negative mode of standard glycine Schiff base and ARP and their mixture at 1:2 and 2:1 molar ratio. The diagnostic ions are indicated with arrows.

Dark grey arrow indicates the precursor ion (i.e. the Schiff base or ARP); Pink arrow indicates diagnostic ion for Schiff base (i.e. decarboxylated Schiff base at  $m/z$  192 and Glycine+diiose at  $m/z$  146); Green arrow indicates diagnostic ion for ARP (i.e. Glycine+triose). Structures are proposed based on elemental composition and evidenced by the isotopically labeled glucose. Milled glycine-glucose (30 mins at 30 Hz) is also incorporated in the graph for comparison.

**Table 4.2** ESI-qToF-MS and MS/MS (CID at 10eV) fragmentations of selected ions in the ball-milled sugar-amino acid model systems under negative ionization mode

Milled <sup>a</sup>		Significant fragment ions in MS and MS/MS spectra [M-H] <sup>-</sup> (m/z)
Gly-Glc	MS <sup>b</sup>	<u>236 (M)</u> <sup>c</sup> , 179 (Glc)
	MS/MS <sup>b</sup>	236 (M), 192 (M-COOH), <b>146 (Gly+3ose)</b> , <b>116 (Gly+2ose)</b>
Gly-(U- <sup>13</sup> C <sub>6</sub> )-Glc	MS	<u>242 (+6, M)</u> , 185 (+6, Glc)
	MS/MS	242 (+6, M), 198 (+6, M-COOH), <b>149 (+3, Gly+3ose)</b> , <b>118 (+2, Gly+2ose)</b>
Ile-Glc	MS	<u>292 (M)</u> , 202 (Ile+3ose), 179 (Glc), 130 (Ile)
	MS/MS	292 (M), <b>202 (Ile+3ose)</b> , 172 (Ile-2ose), <b>130 (Ile)</b>
Phe-Glc	MS	<u>326 (M)</u> , 236 (Phe+3ose), 206 (Phe+2ose), 164 (Phe)
	MS/MS	326 (M), 282 (M-COOH), 236 (Phe-3ose), <b>206 (Phe+2ose)</b> , 186 (Phe-COOH+4ose-2H <sub>2</sub> O) <b>164 (Phe)</b>
Asp-Glc	MS	<u>294 (M)</u> , 179 (Glc), 132 (Asp)
	MS/MS	294 (M), <b>204 (Asp+3ose)</b> , 132 (Asp)
Glu-Glc	MS	308 (M), <u>215 (Glc)</u> , 146 (Glu)
	MS/MS	308 (M), <b>218 (Glu+3ose)</b> , 200 (Glu+3ose-H <sub>2</sub> O), <b>146 (Glu)</b>
His-Glc	MS	316 (M), <u>196 (His+2ose)</u> , 179 (Glc), 154 (His)
	MS/MS	316 (M), <b>196 (His+2ose)</b>
His-(U- <sup>13</sup> C <sub>6</sub> )-Glc	MS	<u>322 (+6, M)</u> , 229 (+3, His+3ose), 198 (+2, His+2ose), 185 (+6, Glc), 154 (His)
	MS/MS	322 (+6, M), <b>229 (+3, His+3ose)</b> , <b>198 (+2, His+2ose)</b> , 154 (His)
Arg-Glc	MS	335 (M), 215 (Arg+2ose), <u>179 (Glc)</u> , 173 (Arg)
	MS/MS	335 (M), 291 (M-COOH), <b>215 (Arg+2ose)</b> , 195 (M-COOH+4ose)

<sup>a</sup>: All samples were prepared by milling sugar with different amino acids at 1:1 molar ratio at 30 Hz for 30 minutes;

<sup>b</sup>: MS scan with the Bruker system was conducted under both ESI positive and negative mode to generate sodiated and deprotonated ions; all MS/MS fragmentation was conducted at 10-15 eV.

<sup>c</sup>: Under the MS scanning, the underlined ions are the most abundant; under MS/MS fragmentation, the ion in bold indicates the diagnostic product ions.

#### 4.4.4 The effect of the side chain of the amino acid on the formation of the Schiff base/ARP and the analysis through MS/MS fragmentation

In addition to glycine, different amino acids were also selected and milled with glucose at a 1:1 molar ratio, including L-isoleucine, L-phenylalanine, L-aspartic acid, L-glutamic acid, L-histidine, and L-arginine. Ball milling was conducted at 30 Hz for 30 minutes in all cases. The resulting reaction mixtures were scanned by MS under both ESI positive and negative mode. The sodiated and deprotonated ions of the condensation adducts were fragmented at CID of 10 eV, except glucose-aspartic acid model where 15 eV was utilized. (see Tables 4.2 & S4.3)

Similar to glycine, ball milled glucose with other amino acids also selectively generated under ESI(-ve)/MS scanning mode, the condensation adducts as one of the major abundant ions together with the unreacted amino acid and glucose ions. (see Table 4.2 & Figure S4.10) The mechanochemical reaction mixtures were found to be faint-yellow colored solids with increasing hygroscopicity similar to what we observed in the case of glucose-glycine model system. Although all the amino acids used exclusively produced mixtures rich in Schiff base/Amadori compounds with very little of advanced reaction products, however, the amino acid side chain had significant influence on the composition of the reaction mixture based on MS/MS study.

The fragmentation of the deprotonated condensation adducts  $[M-H]^-$  generated two major diagnostic ions specific to either Schiff base ( $[M-C_4H_8O_4-H]^-$ ) or ARP ( $[M-C_3H_6O_3-H]^-$ ) and the free amino acid ( $[M-C_6H_{10}O_5-H]^-$ ). (see Figure 4.2) On the other hand, the 2-azaallyl anion, diagnostic ion for glycine Schiff base, which was generated through decarboxylation was also found in L-phenylalanine, L-histidine, and L-arginine model systems, indicating the prevalence of Schiff bases in these amino acid with basic side chains. (see Figure 4.2)

Based on the MS/MS analysis, we propose that amino acids bearing basic side chains tend to generate more Schiff bases due to the observation of significant higher abundances of the diagnostic ions at  $[M-C_4H_8O_4-H]^-$ . (see Figures 4.2e & 4.2f) On the other hand, the amino acids bearing acidic side chains tend to generate ARP due to the higher intensity of the diagnostic ions at  $[M-C_3H_6O_3-H]^-$ . (see Figures 4.2c & 4.2d) In the case of neutral amino acids, both diagnostic ions were present in more or less equal intensities, (see Figures 4.2a & 4.2b) similar to what we observed for glycine model system. In order to confirm the above hypothesis on the effect of side chain on the selectivity of forming Schiff bases or ARPs, we conducted mechano-catalytic

reactions using glycine-glucose model system with the addition of 1% (w/w)  $\text{AlCl}_3$  or  $\text{Na}_2\text{CO}_3$  as acidic and basic catalysts respectively. However, the addition of these catalysts suppressed the formation of Schiff/ARP and generated more side products (see Figure S4.11-4.12) such as the disaccharide-glycine condensation adduct at  $m/z$  398 ( $\text{C}_{14}\text{H}_{24}\text{NO}_{12}$ ) when  $\text{AlCl}_3$  was added (see Figure S4.11).  $\text{AlCl}_3$  have been reported previously [21] to catalyze the formation of glycosidic bonds during mechano-catalytical reaction. This ion has also been confirmed through U- $^{13}\text{C}_6$  labeled glucose study, where the molecular weight increased by 12 Da. (see Table S4.3) However, by examining the MS/MS spectra we found that  $\text{AlCl}_3$  catalysed reactions only generated ARP diagnostic ions while the Schiff base diagnostic ion was absent. (see Figure S4.11-4.12)

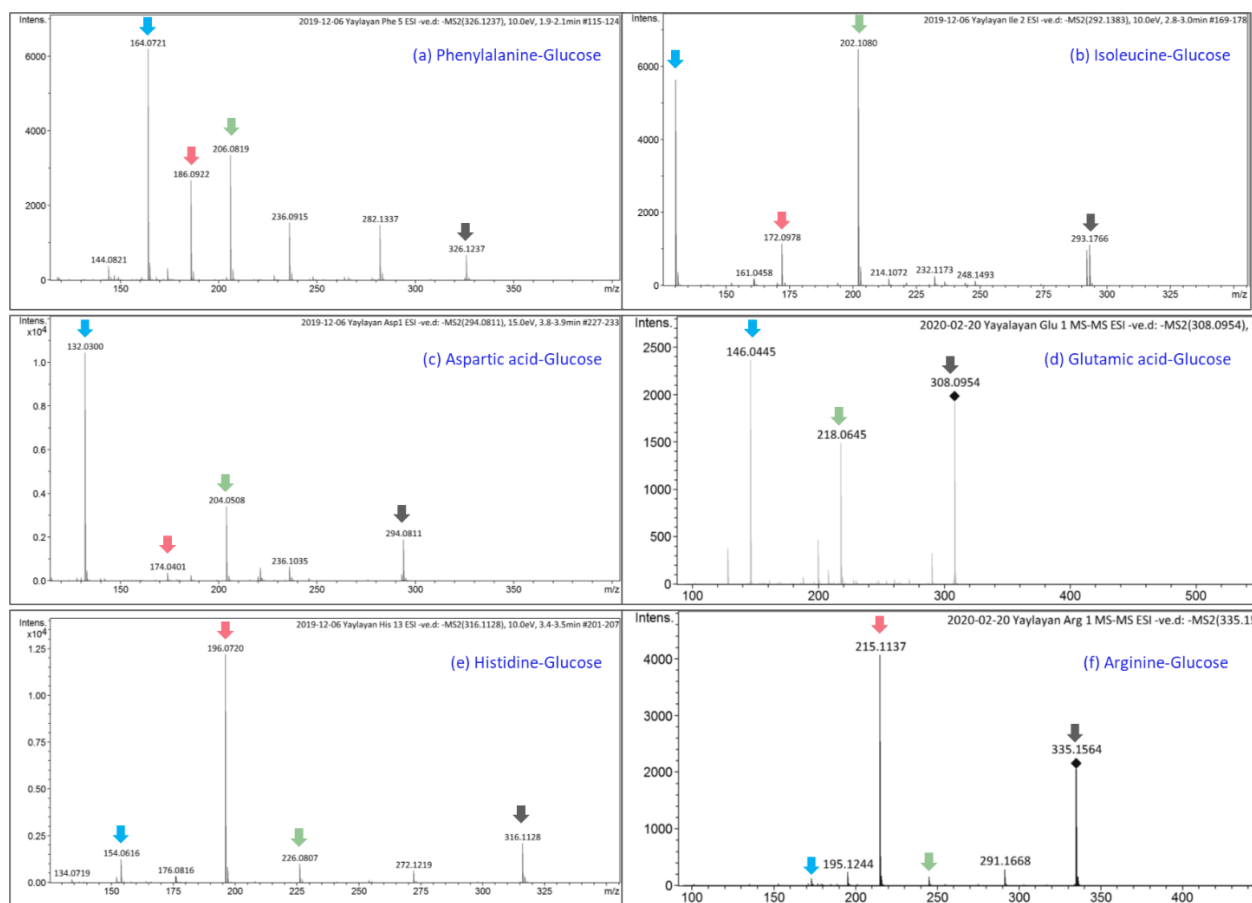


**Figure 4.2** MS/MS fragmentation in negative mode of ball-milled amino acid and glucose adducts. All the mechanochemical mixtures were prepared by ball mill glucose with the amino acid at 1:1 molar ratio for 30 mins at 30 Hz. The diagnostic ions are indicated with arrows.

Dark grey arrow indicates the precursor ion (i.e. the condensation adducts of glucose with different amino acids); Pink arrow indicates diagnostic ion for Schiff base (i.e. amino acids + diose); Green arrow indicates diagnostic ion for ARP (i.e. amino acids + triose); blue arrow indicates the amino acid. Structures are proposed based on elemental composition.

## 4.5 Conclusion

Overall, the diagnostic ions generated from both protonated and deprotonated ion can be used for distinguishing Schiff bases from ARPs. Their composition can be estimated by the relative abundances of the corresponding diagnostic ions. The mechanochemical induced Maillard reaction selectively results in the fast formation of the Schiff base/ARP or a mixture of both depending on the side chain properties of the amino acid used. The resulting material has a potential application in food as a flavor precursor.

## 4.6 References

1. Maillard, L., *Action of amino acids on sugars. Formation of melanoidins in a methodical way*. Comptes-Rendus de l'Académie des Sciences, 1912. **154**: p. 66-68.
2. Nursten, H.E., *The Maillard reaction: chemistry, biochemistry, and implications*. 2005: Royal Society of Chemistry.
3. Hodge, J.E., *Dehydrated foods, chemistry of browning reactions in model systems*. Journal of agricultural and food chemistry, 1953. **1**(15): p. 928-943.
4. Yaylayan, V.A., *Classification of the Maillard reaction: A conceptual approach*. Trends in Food Science & Technology, 1997. **8**(1): p. 13-18.
5. Hemmler, D., et al., *Evolution of complex maillard chemical reactions, resolved in time*. Scientific reports, 2017. **7**(1): p. 1-6.
6. Xing, H., V.V. Mossine, and V. Yaylayan, *Diagnostic MS/MS fragmentation patterns for the discrimination between Schiff bases and their Amadori or Heyns rearrangement products*. Carbohydrate Research, 2020. **491**: p. 107985.
7. Sukan, M.K. and D.K. Weerasinghe, *Process and reaction flavors: An overview*. 2005, ACS Publications.
8. Garti, N., *Microemulsions as microreactors for food applications*. Current opinion in colloid & interface science, 2003. **8**(2): p. 197-211.
9. Kranz, M. and T. Hofmann, *Food-grade synthesis of maillard-type taste enhancers using natural deep eutectic solvents (NADES)*. Molecules, 2018. **23**(2): p. 261.

10. Schmeyers, J., et al., *Quantitative solid–solid synthesis of azomethines*. Journal of the Chemical Society, Perkin Transactions 2, 1998(4): p. 989-994.
11. Kaupp, G., J. Schmeyers, and J. Boy, *Quantitative Solid-State Reactions of Amines with Carbonyl Compounds and Isothiocyanates*. Tetrahedron, 2000. **56**(36): p. 6899-6911.
12. Kaupp, G., et al., *Cascade Reactions in Quantitative Solid-State Syntheses*. Angewandte Chemie International Edition, 1999. **38**(19): p. 2896-2899.
13. Kaupp, G., J. Schmeyers, and J. Boy, *Iminium Salts in Solid-State Syntheses Giving 100% Yield*. Journal für praktische Chemie, 2000. **342**(3): p. 269-280.
14. Schmidt, R., H. Martin Scholze, and A. Stolle, *Temperature progression in a mixer ball mill*. International Journal of Industrial Chemistry, 2016. **7**(2): p. 181-186.
15. Kulla, H., et al., *Warming up for mechanosynthesis – temperature development in ball mills during synthesis*. Chemical Communications, 2017. **53**(10): p. 1664-1667.
16. James, S.L., et al., *Mechanochemistry: opportunities for new and cleaner synthesis*. Chemical Society Reviews, 2012. **41**(1): p. 413-447.
17. Cui, H., et al., *Controlled formation of flavor compounds by preparation and application of Maillard reaction intermediate (MRI) derived from xylose and phenylalanine*. RSC Advances, 2017. **7**(72): p. 45442-45451.
18. Viton, F., H.R. Oertling, and R. Fumeaux, *Mechanical generation of flavour compositions*. 2017, U.S. Patent US20170079316A1.
19. Chu, F.L. and V.A. Yaylayan, *Post-Schiff Base Chemistry of the Maillard Reaction: Mechanism of Imine Isomerization*. Annals of the New York Academy of Sciences, 2008. **1126**(1): p. 30-37.
20. Yaylayan, V.A., *Acrylamide formation and its impact on the mechanism of the early Maillard reaction*. Journal of Food & Nutrition Research, 2009. **48**(1).
21. Xing, H. and V.A. Yaylayan, *Mechanochemical depolymerization of inulin*. Carbohydrate Research, 2018. **460**: p. 14-18.

## 4.7 Supplementary information

### 4.7.1 Material and Method

#### 1. Preparation of standard Schiff base and Amadori product

*N-(1-deoxy-D-fructos-1-yl)-glycine*. The procedure for the synthesis of fructose-glycine was as described in (*Carbohydrate Research*, 1994. 262(2): p. 257-270.): A suspension of 36 g (0.2 moles) of D-glucose and 2.0 g sodium bisulfite in 60 mL of methanol and 30 mL of glycerol was refluxed for 30 min, followed by the addition of 6 g (0.08 moles) of glycine and 8 mL of acetic acid. This solution was refluxed until > 80% of the amino acid had reacted, as evidenced by TLC. The resulting brown, syrupy solution was diluted with 1 volume of water, loaded on a 2 x 30 cm column of Amberlite IRN-77 (H+) ion-exchange resin, and the column was eluted with 500 mL of water, followed by 0.2 N ammonium hydroxide. Fractions of 25 mL were collected. Early fractions contained D-glucose, uncharged pigments and D-glucose-derived degradation products. The Amadori compound, along with unreacted amino acid, usually eluted near the end of the water wash and at the beginning of the ammonium hydroxide wash. The combined fractions, which contained fructose-glycine, were evaporated to 100 mL in vacuo and decolorized with charcoal (2.0 g). This solution was placed on a second 2 x 30 cm column of Amberlite IRN-77 (pyridinium form, pretreated with 10 mL of acetic acid). The column was eluted with water, and 25-mL fractions were collected. Fractions containing fructose-glycine were evaporated in vacuo at 30°C to a syrup. The syrup was diluted in methanol to turbidity and left for 3 days to crystallize at room temperature. Resulting colorless prisms were washed with 3:1 methanol-water and dried in vacuo over calcium chloride. An additional crop of crystals was obtained from the mother liquor. Yield 3.4 g (22%, based on starting glycine): mp 146.5-147.5°C (dec) (lit. [2] mp 145°C, dec);  $[\alpha]_D^{25}$  -66° (c 1.0, H<sub>2</sub>O) (lit. [2] -67°). Anal. Calcd for C<sub>8</sub>H<sub>15</sub>NO<sub>7</sub>: C, 40.51; H, 6.33; N, 5.91. Found: C, 40.18; H, 6.70; N, 5.58.

*N-(1-deoxy-D-fructos-1-yl)-L-proline*. The procedure for the synthesis of fructose-proline was performed according to Vernin et al. (*Developments in Food Science*, G. Charalambous, Editor. 1992, Elsevier. p. 567-623.) and involved the following steps: A suspension of 0.1 mol (18 g) of anhydrous D-glucose in 150 mL of methanol was refluxed for 30 min, followed by the addition of 0.1 mol (11.5 g) of L-proline. This solution was refluxed until about 95% of the amino acid had reacted, as evidenced by TLC. Upon cooling, it deposited crystalline mass which was

recrystallized from methanol. The crystals were dried at 50-55°C in vacuo for 3 hours. Yield 10.8 g (39%): mp 115-118°C (dec.) (lit.[4] mp 119°).  $[\alpha]_{\text{D}}^{25} = -75^{\circ}$  (c=1.2, water) (lit. [4]:  $[\alpha]_{\text{D}}^{20} = -86^{\circ}$  (c=2, water)).

**General procedure for preparation of amino acid N-glucosylamines (Schiff bases).** To a solution of 0.23 g Na in 35 ml of methanol, 0.01 mol of glycine or L-proline, and D-glucose (1.80 g, 0.01 mol) were added in the sequence and stirred at room temperature until complete dissolution. The reaction mixture was worked up as specified below.

**N-D-glucosyl-glycine sodium salt.** The reaction mixture was diluted with 30 ml of diethyl ether and left overnight at room temperature. Crystalline-like material was filtered out, washed with 1:1 methanol/diethyl ether and dried *in vacuo* over CaCl<sub>2</sub>. Yield 1.79 g (69 %) of white powder. It was essentially free (<1%, by TLC) of the starting glycine and fructose-glycine.

**N-D-glucosyl-L-proline sodium salt.** The reaction mixture was treated overnight with 50 ml of diethyl ether. Crystalline-like material was filtered out, washed with 1:5 methanol/diethyl ether and dried *in vacuo* over CaCl<sub>2</sub>. Yield 1.60 g (54 %) of white powder. It was essentially free (<1%, by TLC) of the starting proline and fructose-L-proline.

**Thin-layer chromatography.** TLC was performed on Merck silica gel 60 plates using the following irrigants: 2-propanol/ 28% aqueous ammonia (4:1, v/v, irrigant A) and pyridine/ acetic acid/ water (9:1:2 v/v, irrigant B). Plates were sprayed with 0.2% ninhydrin in acetone (for detection of amino acid derivatives as well as sugars), followed by heating at 120°C for 2-5 min.

**Table S 4.1** Tentative assignments of chemical shifts (ppm) in  $^{13}\text{C}$  NMR spectra and relative populations of the anomeric forms of the compounds in  $\text{D}_2\text{O}$  solutions at  $25^\circ\text{C}$

	Glc-GlyONa (Schiff)		Fru-Gly (Amadori)			
	$\alpha$ -pyr	$\beta$ -pyr	$\alpha$ -pyr	$\beta$ -pyr	$\alpha$ -fur	$\beta$ -fur
C1	89.00	92.25	49.61	54.11	52.14	53.19
C2	73.52	75.64	97.03	96.20	102.65	99.66
C3	73.58	79.45	72.88	70.84	83.53	78.72
C4	72.75	72.61	71.21	70.22	76.93	75.01
C5	75.90	79.54	66.81	69.81	83.29	81.82
C6	63.48	63.64	63.88	64.82	61.77	62.75
C $\alpha$	51.35	51.27	50.51	50.56	50.19	50.40
COOH	182.24	182.74	n.r.	171.85	171.90	171.90
<b>%</b>	<b>11</b>	<b>89</b>	<b>5</b>	<b>69</b>	<b>13</b>	<b>13</b>

Table S 4.1 (continued)

	Fru-Pro (Amadori)			
	$\alpha$ -pyr	$\beta$ -pyr	$\alpha$ -fur	$\beta$ -fur
C1	n.r.	58.10	57.96	57.96
C2	n.r.	96.37	102.51	99.64
C3	72.68	70.70	83.40	78.51
C4	71.08	70.13	76.81	74.39
C5	66.21	69.64	83.28	81.50
C6	n.r.	64.48	61.75	62.52
C $\alpha$	71.91	72.18	71.73	71.63
C $\beta$	n.r.	29.01	29.51	29.39
C $\gamma$	n.r.	24.09	23.99	24.02
C $\delta$	58.69	61.42	59.39	60.03
COOH	n.r.	174.59	174.87	174.45
<b>%</b>	<b>4</b>	<b>67</b>	<b>14</b>	<b>15</b>

## 2. Solid-state magic-angle spinning NMR experiments

Solid-state  $^{13}\text{C}$  NMR spectra were acquired through  $^1\text{H}$ - $^{13}\text{C}$  cross-polarization (CP) on a 400 MHz Varian VNMRS spectrometer using a 4 mm double-resonance Varian Chemagnetics T3 probe (Agilent, Santa Clara, CA). 50 mg of sample were center packed into  $\text{ZrO}_2$  rotors and spun at 13 kHz. The  $^{13}\text{C}$  chemical shifts were referenced to TMS, and the COO- resonance of R-glycine at 176.49 ppm as a secondary reference. The CP contact time was 1.5 ms, and the recycle delay was 5 s with total 300 scans for 25 mins.

## 4.7.2 Tables and figures

**Table S 4.2** Comparing different ions from different systems on predicting the prepared mixtures.

	[M+H] <sup>+</sup>	[M+Na] <sup>+</sup>	[M-H] <sup>-</sup>
Acidic condition	<ul style="list-style-type: none"> <li>- Low stability of Schiff base during ESI;</li> <li>- Unique MS/MS fragmentation pattern (presence and absence type of difference);</li> <li>- Low stability of Schiff base during MS/MS (completely gone at high CID voltage).</li> </ul>	<ul style="list-style-type: none"> <li>- Low stability of Schiff base during ESI;</li> <li>- Less unique fragmentation pattern (differ only in intensity);</li> <li>- Higher stability during MS/MS (ARP reluctant to be fragmented);</li> <li>- Only present when Schiff base is sodium salt.</li> </ul>	<ul style="list-style-type: none"> <li>- Low stability of Schiff base during ESI;</li> <li>- Less abundant (low intensities of daughter ions);</li> <li>- Unique MS/MS fragmentation pattern.</li> </ul>
Neutral condition	<ul style="list-style-type: none"> <li>- Low abundance (too low to perform MS/MS).</li> </ul>	<ul style="list-style-type: none"> <li>- Less unique fragmentation pattern (differ only in intensity);</li> <li>- Higher stability during MS/MS (ARP reluctant to be fragmented).</li> </ul>	<ul style="list-style-type: none"> <li>- Unique MS/MS fragmentation pattern;</li> <li>- Clean MS/MS spectrum.</li> </ul>

**Table S 4.3** ESI-qToF-MS in positive mode and MS/MS (CID 10 eV) study on the ball milled sugar-amino acid model systems.

Milled <sup>a</sup>		Significant fragment ions in MS and MS/MS spectra [M+Na] <sup>+</sup> (m/z)
Gly-Glc	MS <sup>b</sup>	<b>260 (M)</b> <sup>c</sup> , <b>203 (Glc)</b> ,
	MS/MS <sup>b</sup>	260 (M), 242 (M-H <sub>2</sub> O), 224 (M-2H <sub>2</sub> O), 198 (M-COOH-H <sub>2</sub> O), <b>143 (4ose)</b> , <b>140 (Gly+2ose)</b> <sup>c</sup> , 98 (Gly)
Ile-Glc	MS	<b>316 (M)</b> , <b>203 (Glc)</b> , 154 (Ile)
	MS/MS	316 (M), 280, 236, 202, <b>196 (Ile+2ose)</b> , 154 (Ile), <b>143 (4ose)</b> , 113 (3ose)
Phe-Glc	MS	350 (M), <b>203 (Glc)</b> , 188 (Phe)
	MS/MS	350 (M), <b>230 (Phe+2ose)</b> , 188 (Phe), <b>143 (4ose)</b>
Asp-Glc	MS	318 (M), 203 (Glc), 156 (Asp)
	MS/MS	318 (M), <b>198 (Asp+2ose)</b> , <b>143 (4ose)</b>
His-Glc	MS	<b>340 (M)</b> , 220 (His+2ose), 203 (Glc), 178 (His)
	MS/MS	340 (M), 296 (M-COOH), <b>220 (His+2ose)</b> , 158 (His+2ose-H <sub>2</sub> O), <b>143 (4ose)</b>
His-( <sup>13</sup> C <sub>2</sub> )-Glc	MS	341 (+1, M), 178 (His)
	MS/MS	341 (+1, M), <b>221 (+1, His+2ose)</b> , 178 (His), <b>143 (4ose)</b>
His-( <sup>13</sup> C <sub>3</sub> )-Glc	MS	341 (+1, M), 178 (His)
	MS/MS	341 (+1, M), <b>220 (His+2ose)</b> , 178 (His), <b>144 (+1, 4ose)</b>

<sup>a</sup>: All the milled samples are prepared by milling sugar and different amino acids at 1:1 molar ratio at 30 Hz for 30 minutes;

<sup>b</sup>: MS scan with the Bruker system was conducted under both ESI positive and negative mode to generate sodiated and deprotonated ions; all MS/MS fragmentation was conducted at 10 eV.

<sup>c</sup>: Under the MS scanning, the ion in bold indicates the most abundant ion; under MS/MS fragmentation, the ion in bold indicates the diagnostic daughter ions.

**Table S 4.4** Elemental composition of reported m/z.

m/z	Elemental composition [M-H] <sup>-</sup>	Error (ppm)
<b>Glycine</b>		
116.0348	C <sub>4</sub> H <sub>6</sub> NO <sub>3</sub>	0.275
146.0444	C <sub>5</sub> H <sub>8</sub> NO <sub>4</sub>	6.387
158.0439	C <sub>6</sub> H <sub>8</sub> NO <sub>4</sub>	9.065
174.0759	C <sub>7</sub> H <sub>12</sub> NO <sub>4</sub>	4.21
176.0551	C <sub>6</sub> H <sub>10</sub> NO <sub>5</sub>	4.529
192.0865	C <sub>7</sub> H <sub>14</sub> NO <sub>5</sub>	3.632
236.0755	C <sub>8</sub> H <sub>14</sub> NO <sub>7</sub>	6.467
118.0415 <sup>a</sup>	C <sub>2</sub> H <sub>6</sub> NO <sub>3</sub> [ <sup>13</sup> C] <sub>2</sub>	0.19
149.0557 <sup>a</sup>	C <sub>2</sub> H <sub>8</sub> NO <sub>4</sub> [ <sup>13</sup> C] <sub>3</sub>	2.03
185.0759 <sup>a</sup>	H <sub>10</sub> O <sub>6</sub> [ <sup>13</sup> C] <sub>6</sub>	1.84
198.1077 <sup>a</sup>	CH <sub>14</sub> NO <sub>5</sub> [ <sup>13</sup> C] <sub>6</sub>	1.89
242.0979 <sup>a</sup>	C <sub>2</sub> H <sub>14</sub> NO <sub>7</sub> [ <sup>13</sup> C] <sub>6</sub>	5.6
398.1302	C <sub>14</sub> H <sub>24</sub> NO <sub>12</sub>	0.88
410.1715 <sup>a</sup>	C <sub>2</sub> H <sub>24</sub> NO <sub>12</sub> [ <sup>13</sup> C] <sub>12</sub>	3.39
<b>Isoleucine</b>		
130.0876	C <sub>6</sub> H <sub>12</sub> NO <sub>2</sub>	6.122
172.0978	C <sub>8</sub> H <sub>14</sub> NO <sub>3</sub>	2.508
179.056	C <sub>6</sub> H <sub>11</sub> O <sub>6</sub>	2.44
202.1080	C <sub>9</sub> H <sub>16</sub> NO <sub>4</sub>	0.331
292.1383	C <sub>12</sub> H <sub>22</sub> NO <sub>7</sub>	4.543
<b>Phenylalanine</b>		
164.0721	C <sub>9</sub> H <sub>10</sub> NO <sub>2</sub>	5.768
186.0922	C <sub>12</sub> H <sub>12</sub> NO	1.671
206.0819	C <sub>11</sub> H <sub>12</sub> NO <sub>3</sub>	0.882
236.0915	C <sub>12</sub> H <sub>14</sub> NO <sub>4</sub>	3.316
282.1337	C <sub>14</sub> H <sub>20</sub> NO <sub>5</sub>	1.587
326.1237	C <sub>15</sub> H <sub>20</sub> NO <sub>7</sub>	0.849
<b>Aspartic acid</b>		
132.0300	C <sub>4</sub> H <sub>6</sub> NO <sub>4</sub>	2.403
204.0508	C <sub>7</sub> H <sub>10</sub> NO <sub>6</sub>	0.059
294.0811	C <sub>10</sub> H <sub>16</sub> NO <sub>9</sub>	4.781
<b>Glutamic acid</b>		
146.0445	C <sub>5</sub> H <sub>8</sub> NO <sub>4</sub>	5.7
200.0546	C <sub>8</sub> H <sub>10</sub> NO <sub>5</sub>	6.49
218.0645	C <sub>8</sub> H <sub>12</sub> NO <sub>6</sub>	9
308.0954	C <sub>11</sub> H <sub>18</sub> NO <sub>9</sub>	8.95

<b>Histidine</b>		
154.0616	C <sub>6</sub> H <sub>8</sub> N <sub>3</sub> O <sub>2</sub>	0.334
196.0720	C <sub>8</sub> H <sub>10</sub> N <sub>3</sub> O <sub>3</sub>	1.103
226.0807	C <sub>9</sub> H <sub>12</sub> N <sub>3</sub> O <sub>4</sub>	9.204
316.1128	C <sub>12</sub> H <sub>18</sub> N <sub>3</sub> O <sub>7</sub>	0.87
198.0795 <sup>a</sup>	C <sub>6</sub> H <sub>10</sub> N <sub>3</sub> O <sub>3</sub> [ <sup>13</sup> C] <sub>2</sub>	6.43
229.0927 <sup>a</sup>	C <sub>6</sub> H <sub>11</sub> N <sub>3</sub> O <sub>4</sub> [ <sup>13</sup> C] <sub>3</sub>	3.03
322.1350 <sup>a</sup>	C <sub>6</sub> H <sub>17</sub> N <sub>3</sub> O <sub>7</sub> [ <sup>13</sup> C] <sub>6</sub>	0.47
<b>Arginine</b>		
173.1035	C <sub>6</sub> H <sub>13</sub> N <sub>4</sub> O <sub>2</sub>	2.03
195.1244	C <sub>9</sub> H <sub>15</sub> N <sub>4</sub> O	0.954
215.1137	C <sub>8</sub> H <sub>15</sub> N <sub>4</sub> O <sub>3</sub>	3.33
291.1668	C <sub>11</sub> H <sub>23</sub> N <sub>4</sub> O <sub>5</sub>	0.15
335.1564	C <sub>12</sub> H <sub>23</sub> N <sub>4</sub> O <sub>7</sub>	0.82
<b>Alanine</b>		
250.0932	C <sub>9</sub> H <sub>16</sub> NO <sub>7</sub>	2.09
160.0615	C <sub>6</sub> H <sub>10</sub> NO <sub>4</sub>	3.23
<b>Proline</b>		
276.1069	C <sub>11</sub> H <sub>18</sub> NO <sub>7</sub>	5.17
186.077	C <sub>8</sub> H <sub>12</sub> NO <sub>4</sub>	1.97
156.0667	C <sub>7</sub> H <sub>10</sub> NO <sub>3</sub>	4.05
114.056	C <sub>5</sub> H <sub>8</sub> NO <sub>2</sub>	4.35

<sup>a</sup>: isotope labelled m/z.

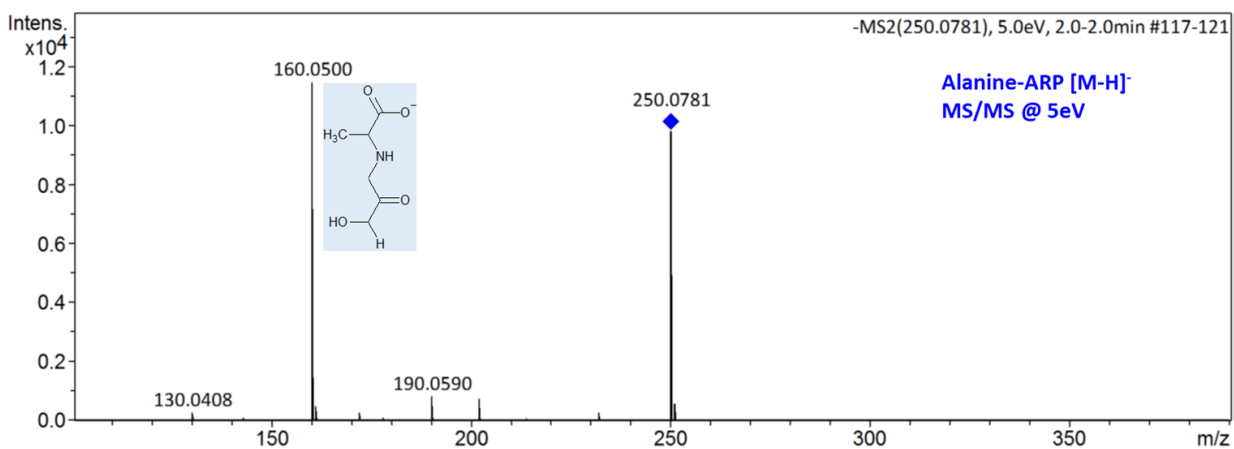
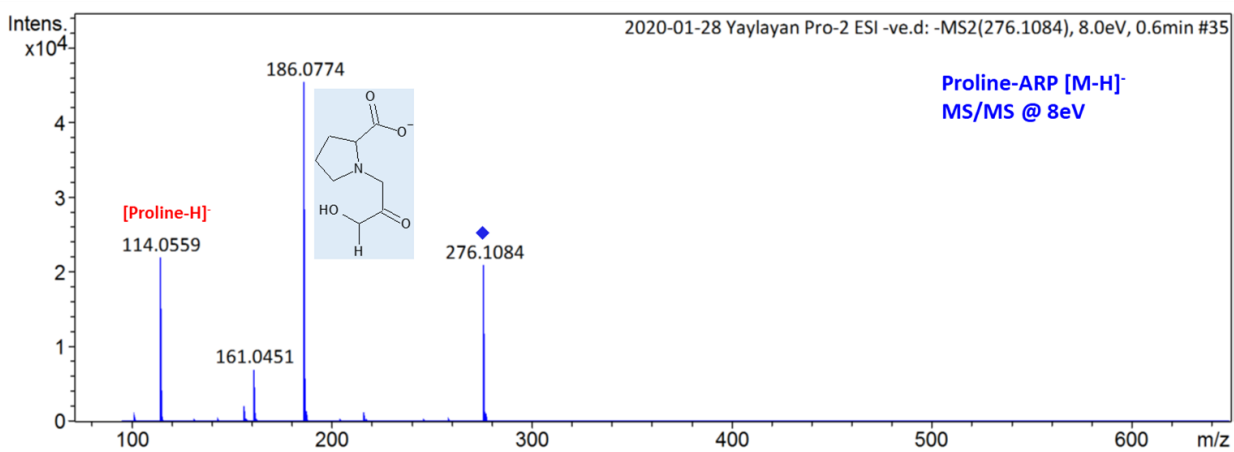
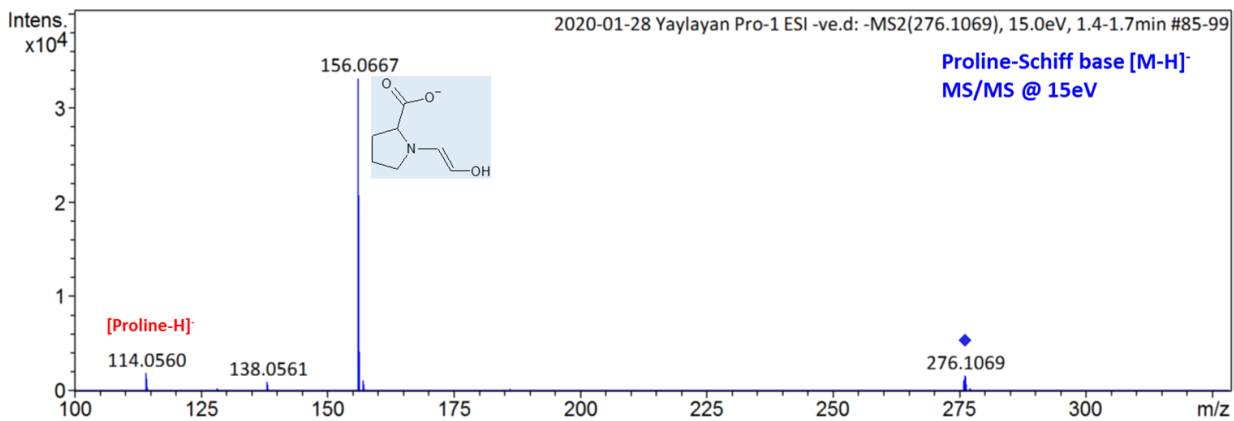


**Figure S 4.1** MS/MS (neutral condition) of the deprotonated ion of the standard pure proline Schiff base, proline ARP, and alanine ARP.

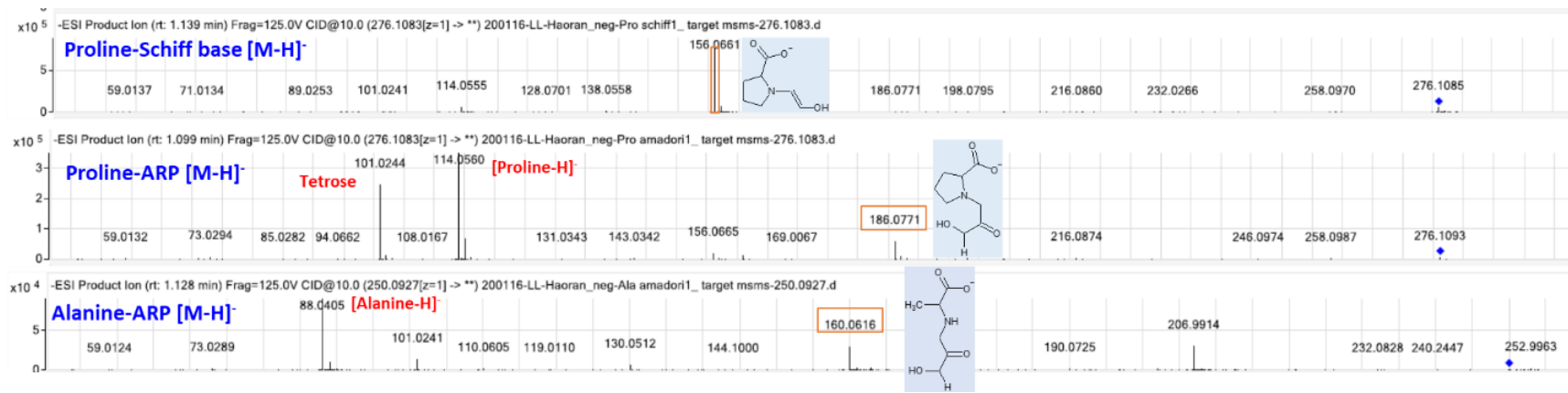


**Figure S 4.2** MS/MS (acidic condition) of the deprotonated ion of the standard pure proline Schiff base, proline ARP, and alanine ARP

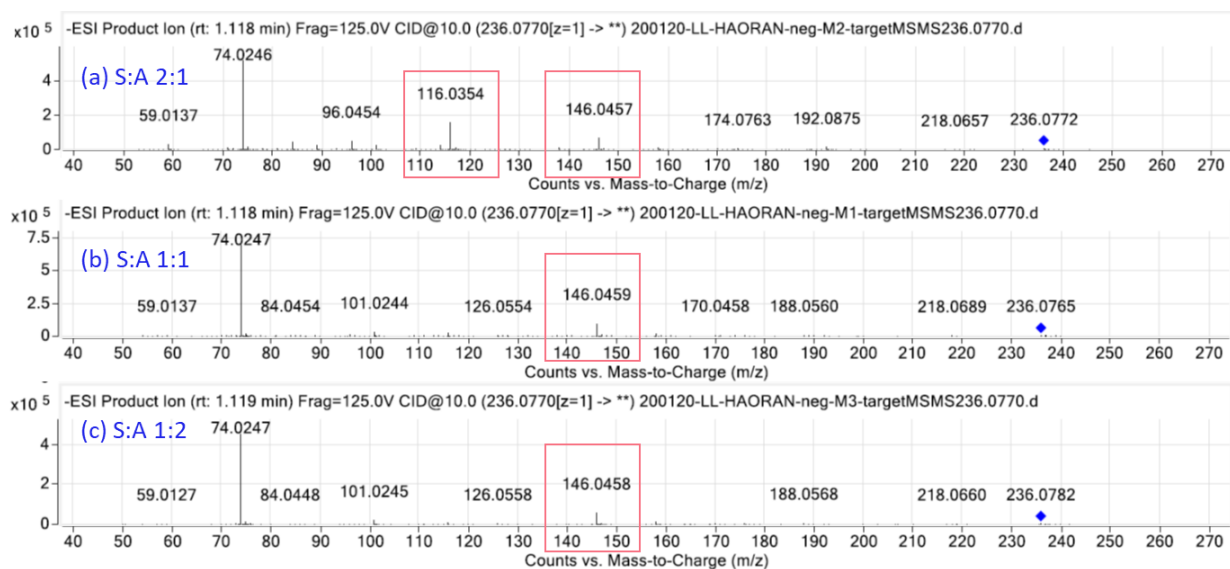


**Figure S 4.3** MS/MS spectra of a mixture of standard glycine Schiff base (S) and its ARP (A) at molar ratio of (a) 2:1, (b) 1:1, and (c) 1:2. The spectra were recorded under MS acidic condition at CID 10 eV on the deprotonated ion  $[M-H]^-$  at m/z 236. The m/z at 116 is the diagnostic ion for Schiff base, and the m/z at 146 is the diagnostic ion for ARP.

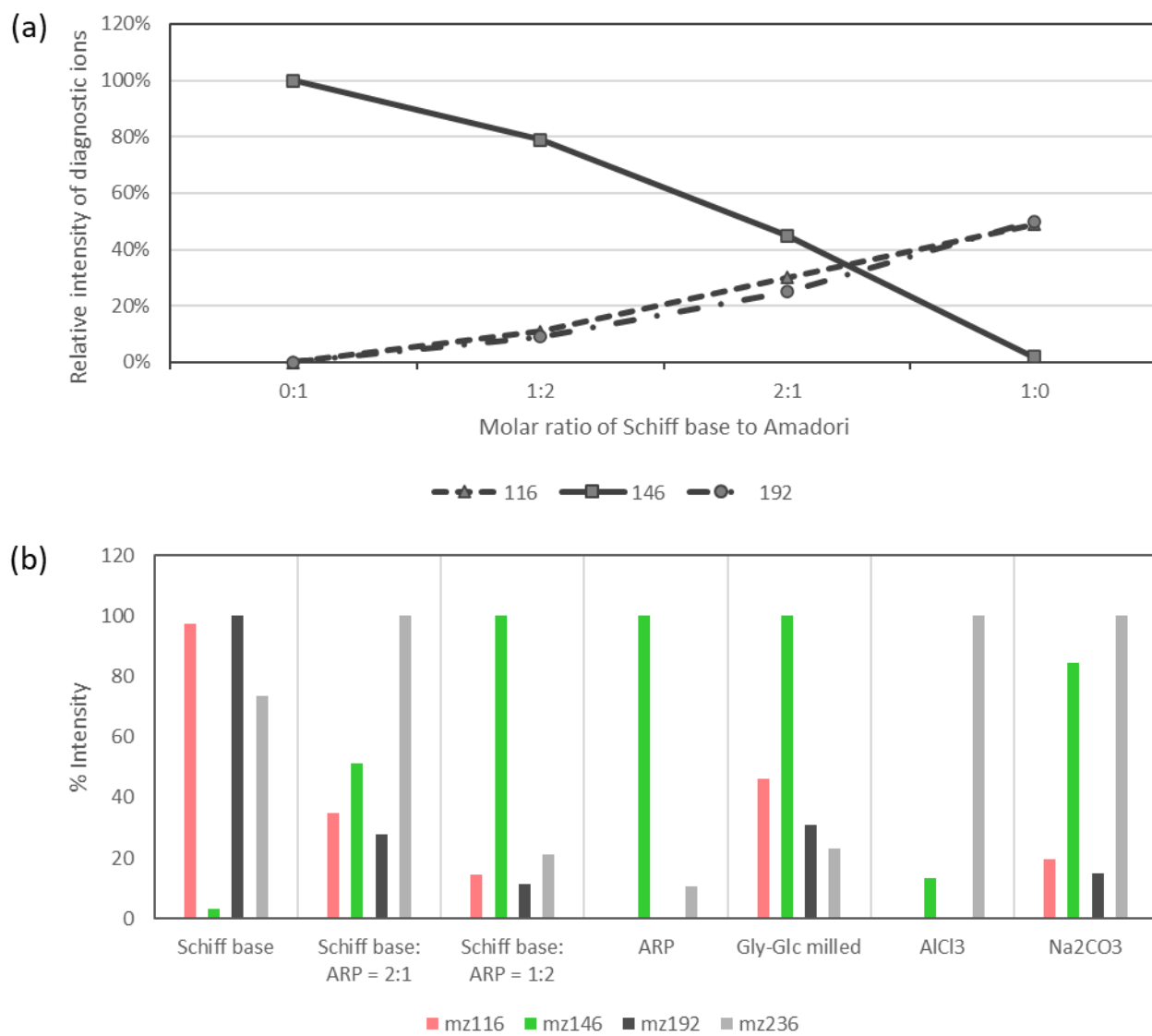


**Figure S 4.4** MS/MS of prepared mixture of glycine Schiff base and ARP at molar ratio of 1:2 and 2:1. (a) Relative intensities of the diagnostic ions. (b) Comparison of diagnostic ions from the ball-milled glucose-glycine-(AlCl<sub>3</sub>/Na<sub>2</sub>CO<sub>3</sub>) sample to the prepared mixtures.

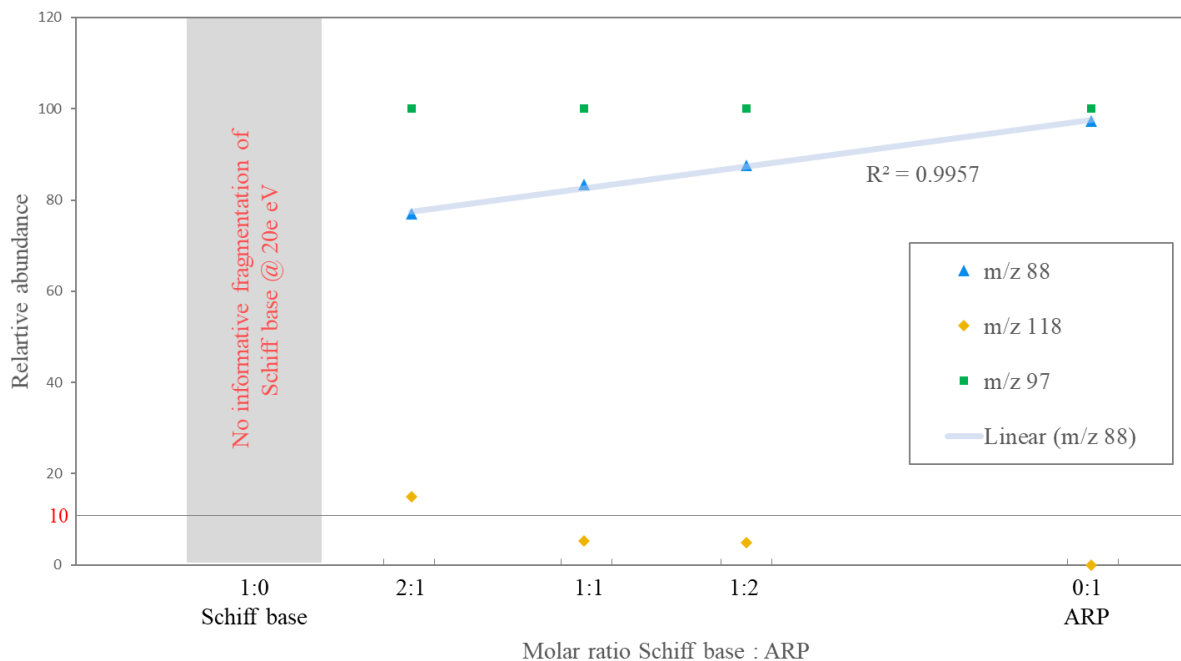


**Figure S 4.5** MS/MS CID fragmentation at 20 eV of the mixture of glycine Schiff base and ARP at 5 different molar ratios. All models have m/z 97 as the most abundant product ion. The ion at m/z 88 is diagnostic for ARP, the ion at m/z 118 is diagnostic for Schiff base.

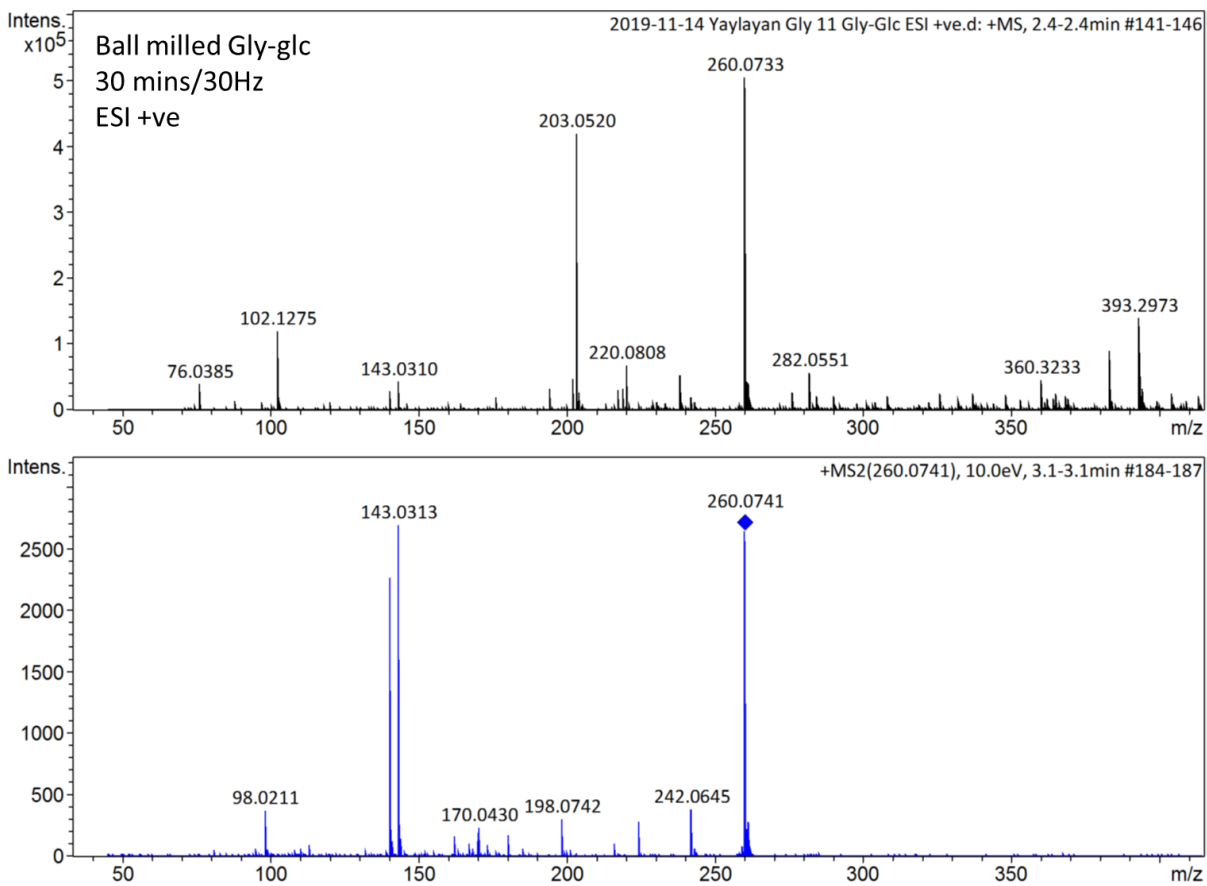


**Figure S 4.6** MS (top, ESI +ve) and MS/MS (bottom, sodiated adduct peak, 10eV) spectra of ball milled glucose and glycine model system.

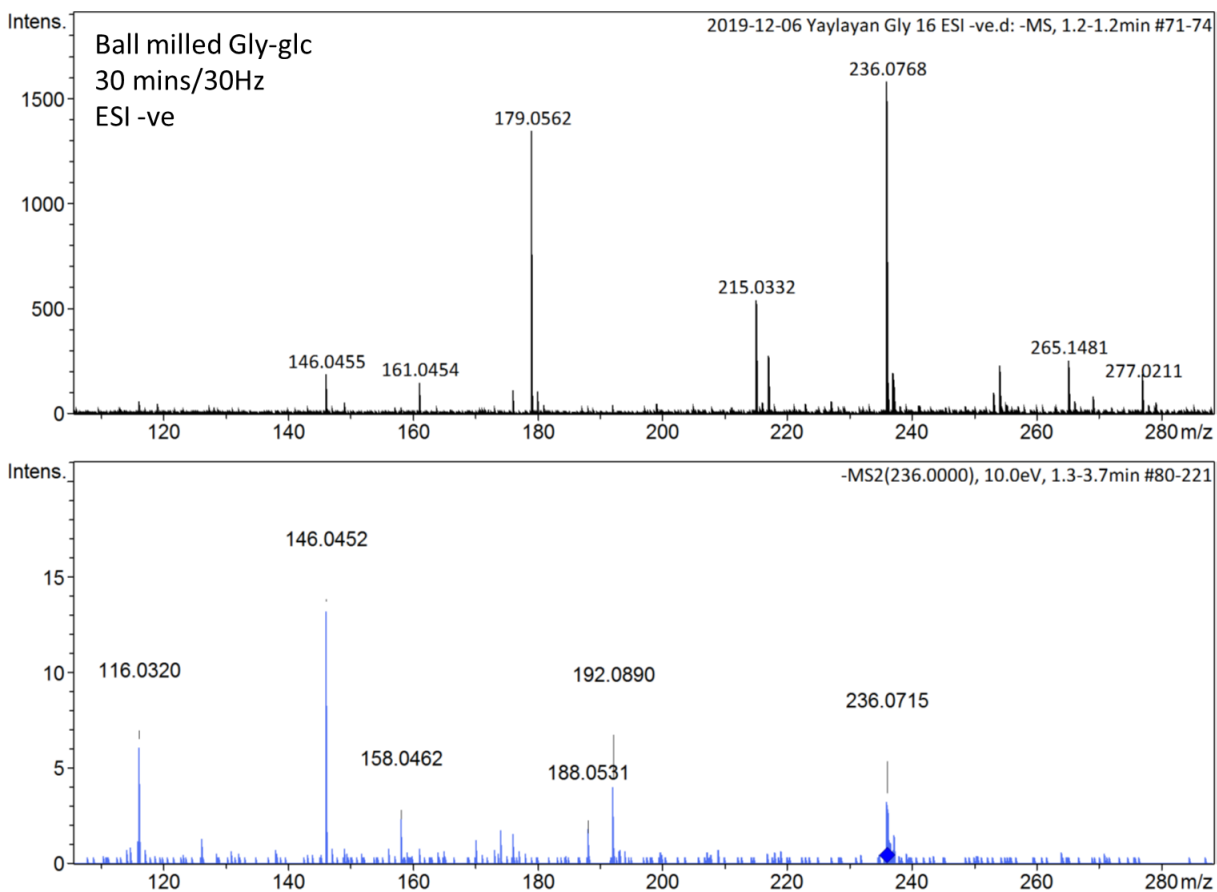


**Figure S 4.7** MS (top, ESI -ve) and MS/MS (bottom, deprotonated adduct peak, 10eV) spectra of ball milled glucose and glycine model system.

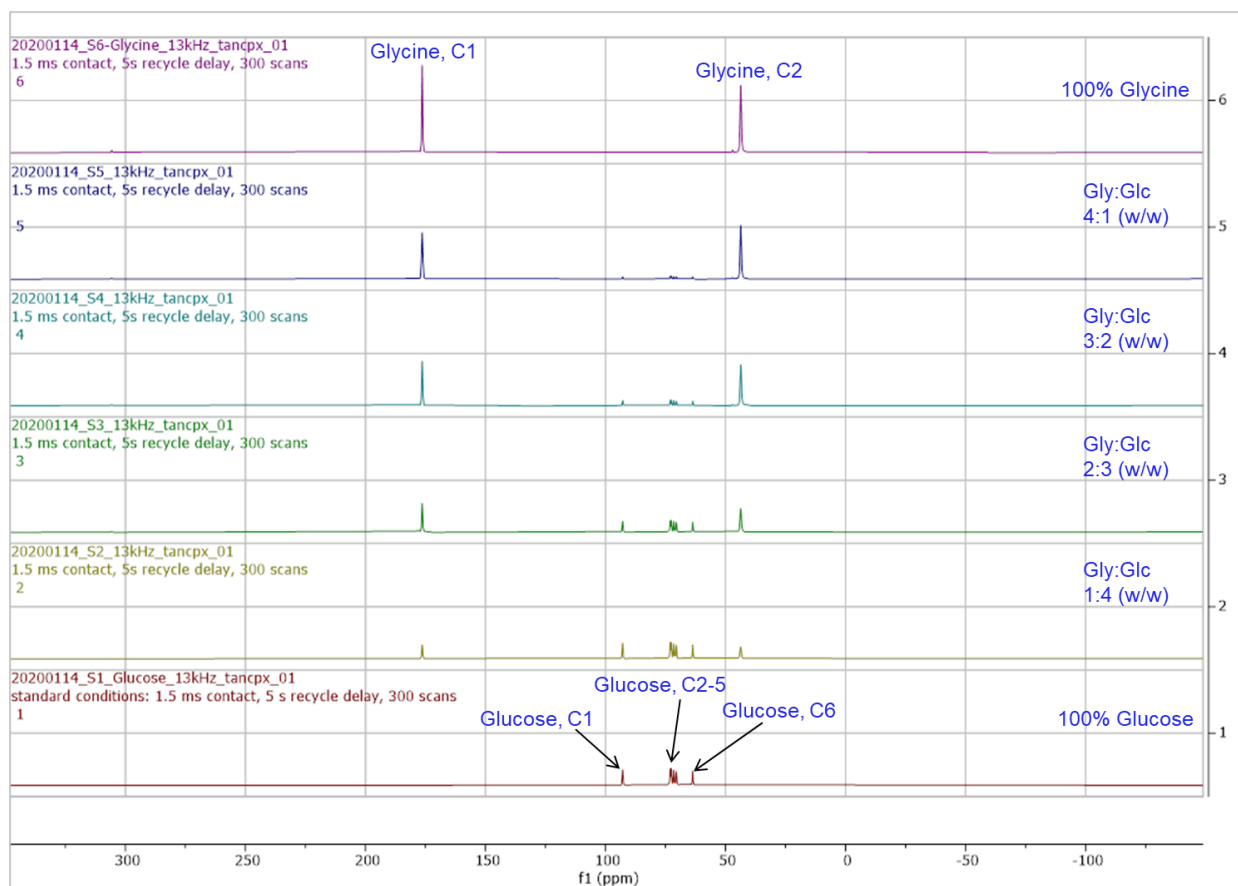


**Figure S 4.8** ssNMR spectra of standard mixtures of milled glucose and milled glycine to verify CP-MAS NMR response to the mixture of glucose and glycine at different ratio (from top to bottom (Gly-Glc %): 100%-0%; 80%-20%; 60%-40%; 40%-60%; 20%-80%; 0%-100%).

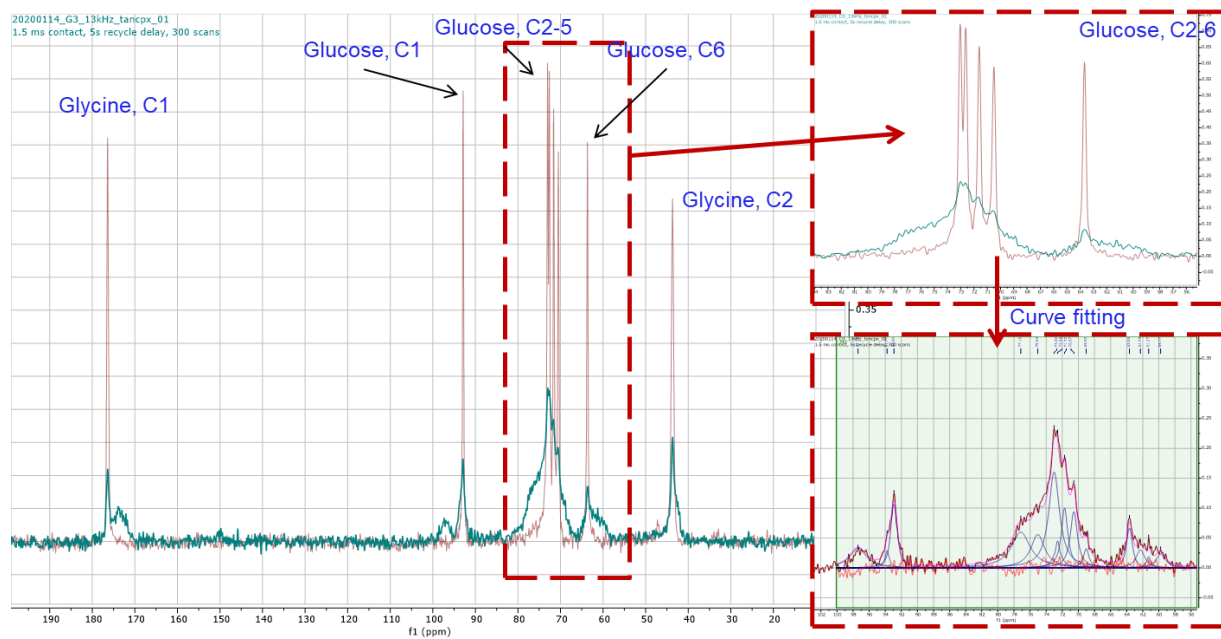


**Figure S 4.9** Superimposed ssNMR spectra. Green: ball milled glucose-glycine (30 mins/ 30Hz); Red: Standard mixture of glucose and glycine (Glc:Gly 4:1). The total conversion was estimated by curve fitting.



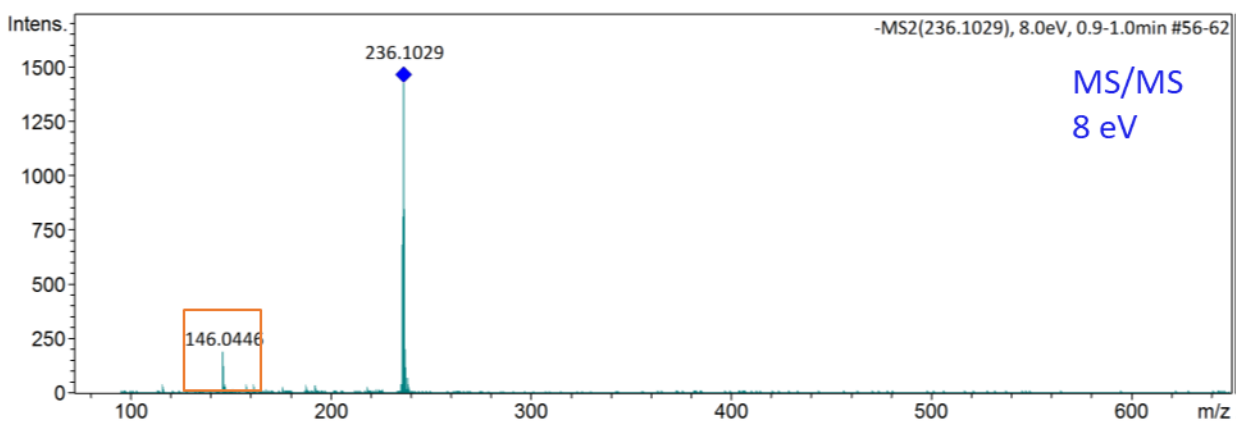
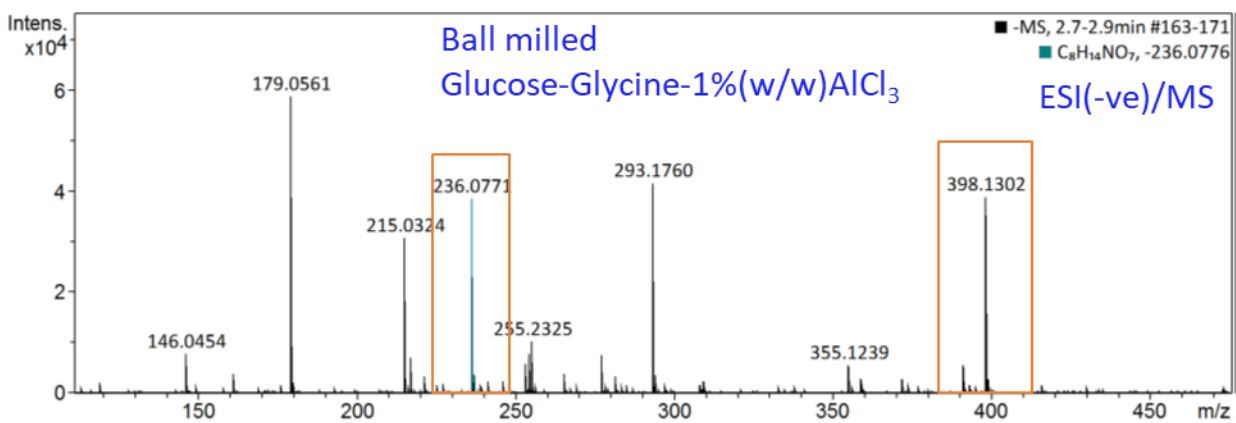


**Figure S 4.11** ESI(-ve)/MS (top) and MS/MS (bottom, [M-H]<sup>-</sup> @ m/z 236, 10eV) spectra of ball milled glucose and glycine model system and AlCl<sub>3</sub> (1% w/w).

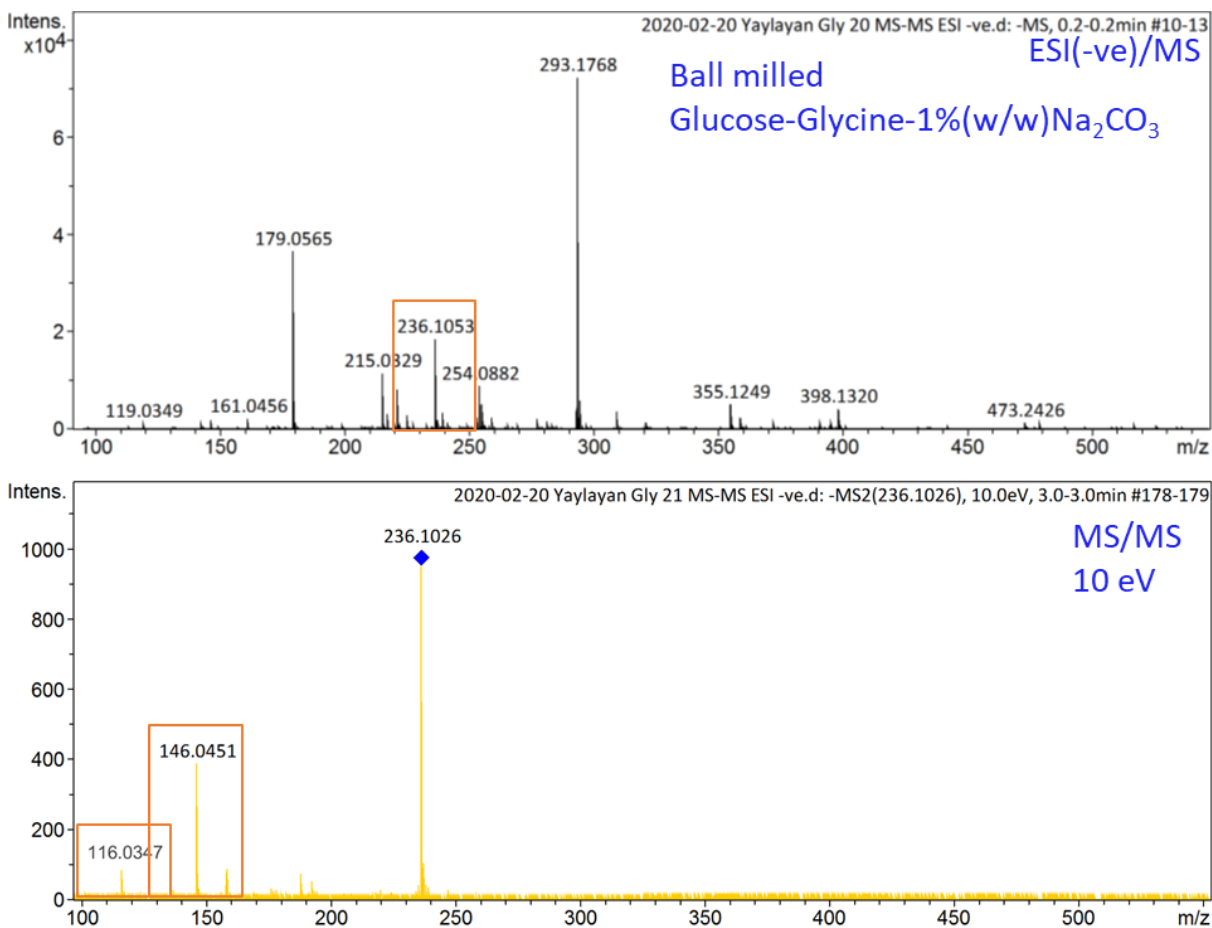


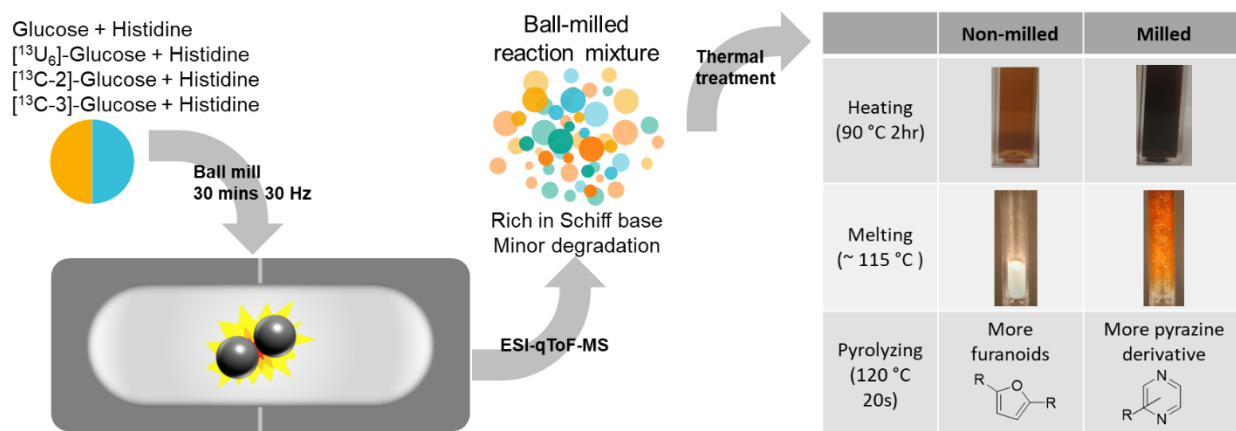
**Figure S 4.12** ESI(-ve)/MS (top) and MS/MS (bottom, [M-H]<sup>-</sup> @ m/z 236, 10eV) spectra of ball milled glucose and glycine model system and Na<sub>2</sub>CO<sub>3</sub> (1% w/w).

## Connecting paragraph

In chapter 4, we reported that ball milling of glucose with various amino acids selectively lead to the formation of the Schiff bases and its Amadori compounds. The ratio of the two isomeric intermediates was dependent on the acidity of the amino acid sidechain. In chapter 5, we investigated the thermochemical properties of the mechanochemical reaction mixtures through heating, melting, and pyrolysis for their potential applications in food as flavor precursors. We selected the histidine-glucose model system as an example due to its ability to generate more Schiff base than the Amadori compound.

Chapter 5 was published in the *European Food Research and Technology*: Xing, H., & Yaylayan, V. (2020). Investigation of thermo-chemical properties of mechanochemically generated glucose–histidine Maillard reaction mixtures. *European Food Research and Technology*, **247(1)**, 111-120.

# Chapter 5 Investigation of thermo-chemical properties of mechanochemically generated glucose–histidine Maillard reaction mixtures



## 5.1 Abstract

Mechanochemistry is gaining increasing interest as an efficient tool for solvent-free organic transformations. Recently, it was applied to perform the Maillard reaction of glucose with various amino acids that lead to the selective formation of Schiff bases and their Amadori rearrangement products. In this study, we report the thermal properties of the mechanochemically generated glucose-histidine reaction mixtures. Direct video recordings of their melting behavior show that the browning of the ball-milled mixtures starts at lower temperatures and proceed more slowly compared to the non-milled mixtures. Furthermore, pyrolysis of ball-milled mixtures generated more pyrazines and fewer furan derivatives compared to the non-milled mixtures. The chemical composition of the ball-milled glucose-histidine was also investigated in depth by high-resolution mass spectrometry. The decarboxylation and C2-C3 sugar chain cleavage reactions were identified as the most important transformations during ball milling. These findings further support the utility of mechanochemically generated mixtures as potential Maillard flavor and browning precursors.

**Keywords:** Mechanochemistry, Ball milling, Maillard reaction, Browning, Pyrazine, High-resolution mass spectrometry

## 5.2 Introduction

The Maillard reaction is considered as one of the main chemical transformations that is responsible for the generation of flavors and aromas in thermally processed foods in addition to lipid oxidation and caramelization.[1-3] It is considered as a complex reaction cascade initiated by the condensation of an amino group with an  $\alpha$ -hydroxy carbonyl moiety of reducing sugars leading to the formation of Schiff bases.[4] The formation of this adduct is followed by a well-known rearrangement, which produces the Amadori rearrangement product (ARP), a more stable isomer of the Schiff base. Subsequent degradation of the ARPs yields a complex mixture of flavor and aroma-active carbocyclic and heterocyclic compounds, in addition to polymers and oligomers with characteristic yellow-brown colors.[5, 6]

The Maillard reaction is naturally initiated during cooking; but it can also be performed outside of the food environment from a “well-formulated” mixtures of precursors that mimic the real food system under carefully controlled reaction conditions such as time, temperature, and pH.[2] The reaction products generated is often termed as ‘processed flavors’ or ‘reaction flavors’. Many techniques were developed over the past decades such as extrusion,[7] microwave irradiation,[8] ultrasound,[9] and ball milling [10], to meet the increasing demand for flavors of ready-to-eat food market and for new aroma compounds as well as to gain control over the Maillard reaction.

The mechanochemical approach using high energy ball milling has received increasing interest over the past few years for its ability to induce chemical reactions in a fast and yet efficient way.[11] It gained particular interest in organic synthesis for its “green” properties due to the elimination of bulk dissolution and solvent-free conditions. Ball milling has been successfully employed for numerous organic transformations.[12] However, a theoretical understanding of mechanochemical processes for conducting the Maillard reaction is still poorly understood. Fortunately, the Maillard reaction can be considered as a collection of fundamental organic transformations occurring consecutively and in parallel,[6] many of which have been studied outside the context of the Maillard reaction using mechanochemistry.[13, 14]

Furthermore, the mechanochemical approach is most suited for the purpose of generating reaction flavors compared to the conventional methods, for many reasons; firstly, the reaction can be carried out under solid-state in a solvent-free environment compared to the conventional hydrothermal conditions where the reactants (sugar and amino acids) are dissolved in a buffer under controlled

pH conditions. Using the conventional method, the solvent, normally water, needs to be removed after the reaction which is not only an energy-consuming process but also may cause degradation or loss of aroma active compounds.[2] Secondly, the ball-milling can be considered as a non-thermal process, although during mechanochemical reactions limited amount of generated heat is dependent on the reaction type, time, and the nature of milling vessels [15, 16], the generally observed average reaction temperatures do not exceed ~ 40 to 60 °C minimizing degradations of the target compounds. An additional advantage of using mechanical force to initiate chemical transformations is its vectorial nature, which, at least in principle, makes it inherently a more controllable process than that of thermochemistry.[11] Consequently, the reaction between amino acids and sugars can be quenched easily before it proceeds to the later stages where volatile aroma active compounds are formed from the degradation of Schiff bases and their Amadori/Heyns products. Surprisingly, despite its advantages and to our best knowledge only one example of its application can be found and that is in the patent literature.[10] The patent describes a flavor composition for wafers that were generated mechanochemically from rhamnose and proline. According to the sensory panel, the use of ball-milled sugars and amino acid mixtures as flavor precursors generated higher aroma intensity in the baked wafers compared to the non-milled control samples, indicating a further need to investigate the thermo-chemical properties of the mechanochemically generated flavor mixtures. Such mixtures have been reported to be a rich source of Schiff bases and Amadori compounds.[17]

## **5.3 Material and Methods**

### **5.3.1 Material**

L-Histidine (98%), D-glucose (99.5%), and deuterated NMR solvent (D<sub>2</sub>O and MeOD) were purchased from Sigma-Aldrich Chemical Co. (Oakville, Ontario, Canada). [<sup>13</sup>C<sub>2</sub>-, <sup>13</sup>C<sub>3</sub>-, and U-<sup>13</sup>C<sub>6</sub>-] Glucose (99%) were purchased from Cambridge Isotope Laboratories (Andover, MI). All other chemicals and reagents were of analytical grade from Fisher Scientific. Ultrapure water was used throughout the study. All materials were used without further purification.

### 5.3.2 Sample preparation

*Mechanochemistry:* Samples (30 mg powder) were prepared through ball milling at ambient temperature. The D-glucose and L-histidine mixture was at a 1:1 molar ratio. All mechanochemical reactions were conducted in a stainless-steel grinding jars (10 mL) with 2 steel balls (3.2 mm in diameter; ball/sample ratio ~32:1) for the creation of inner friction. The jars were seated in the Retsch Mixer Mill (MM 400, Newtown, PA, US) that performs radial oscillations in a horizontal position without coolant (the external jar temperature was ~ 25 °C) at a frequency of 30 Hz for 30 minutes for the mixture of glucose and histidine, and 60 minutes for the glucose or histidine alone. Samples collected after milling were stored at -20°C for further analysis.

*Aging* of the ball-milled samples was carried out directly in the milling vial (left open) at room temperature. Samples were taken out for UV-Vis measurements at 1 hr, 6 hrs, 1 day, 2 days, 3 days, 7 days, and 14 days intervals. As a control, the non-milled samples were manually mixed using mortar and pestle to ensure homogeneity.

*Thermal* treatments were carried out by dissolving the solid samples (30 mg) in 2 mL methanol and heating in an open vial (5 mL capacity) at 90 °C for 1 h until dry. The dry residues were then re-dissolve in 4 mL methanol for UV-Vis analysis. UV-Vis measurements were run at a single wavelength of 420 nm using an Evolution 300 scanning spectrophotometer from Thermo Electron Corp.

### 5.3.3 Melting studies

Melting studies were performed on an SRS OptiMelt MPA100 apparatus (Stanford Research Systems) with 90 mm × 1 mm sampling tubes. The samples were packed approximately to 4 – 5 mm in height. A moistened pH paper was inserted in the opening of the tube just before the melting started. The packed tube was placed in the melting chamber and heated with a rate of 10 °C/min. The reflectance of the solid samples during melting was continuously measured and recorded using the built-in detector and a video camera. Data were automatically recorded and analyzed with the help of the melting point software (MeltView v. 2.0.7; Stanford Research Systems). The videos are uploaded to “YouTube” and can be accessed through the links provided.

**Table 5.1** Video demonstrations of the melting behavior of glucose histidine models

Video	Samples and tube position in the video	Melting range °C (10 °C/min increase)
1	Native glucose (left), Manually ground glucose (middle), Milled glucose (right) (1hr 30Hz) – MeltView video*	100 – 200
	<b>Video 1 link:</b> <a href="https://youtu.be/p6z1H0ScxqA">https://youtu.be/p6z1H0ScxqA</a>	
2	Native histidine (left), Manually ground histidine (middle), Milled histidine (right) (1hr 30Hz) – MeltView video*	200 – 350
	<b>Video 2 link:</b> <a href="https://youtu.be/g5GofFaLCkQ">https://youtu.be/g5GofFaLCkQ</a>	
3	Manually mixed glucose-histidine (left), Milled glucose-histidine (middle), Empty tube (right) – MeltView video*	50 – 150
	<b>Video3 link:</b> <a href="https://youtu.be/cWW4DHd292g">https://youtu.be/cWW4DHd292g</a>	
4	Manually mixed glucose-histidine (left), Milled glucose-histidine (middle), Empty tube (right) - Cell phone video	~50 – ~150
	<b>Video 4 link:</b> <a href="https://youtu.be/WpWyVr2gfsk">https://youtu.be/WpWyVr2gfsk</a>	

\*In the intensity vs temperature graph shown in the video, intensity refers to the intensity of the reflected light that measures the loss of crystallinity of the sample, not the browning.

### 5.3.4 Scanning electron microscope (SEM)

The surface morphology and microstructure of the solid samples from ball milling and in their native state were recorded by a Hitachi TM-3000 scanning electron microscope (Tokyo, Japan) with resolution varying from 50× to 1500×.

### 5.3.5 ESI-qToF-MS study

The diluted sample solutions (1 µL) in water/ methanol (10%/ 90%) were supplied to the source directly via a syringe. The analysis was performed on a Bruker Maxis Impact quadrupole time of flight mass spectrometer (Bruker Daltonics, Bremen, Germany) operated in both positive and negative ion modes. Instrument calibration was performed using sodium formate clusters. The electrospray interphase settings were as follows: nebulizer pressure, 0.6 bar; drying gas, 4 L/min; temperature, 180 °C; and capillary voltage, 4500 V. The full scan MS range was from  $m/z$  50 to 800. The data were analyzed using Bruker Compass Data Analysis software (version 4.2). The sample was analyzed in triplicate. MS/MS was performed on  $m/z$  340  $[M+Na]^+$  under ESI positive mode and  $m/z$  316  $[M-H]^-$  under ESI negative mode at CID 10eV.

### 5.3.6 NMR

The  $^1\text{H}$  NMR spectra of ball-milled glucose-histidine mixtures were collected on an 800 MHz Bruker Avance III HD spectrometer in both  $\text{D}_2\text{O}$  and MeOD at 25 °C in the quantitative mode in the Quebec/Eastern Canada High Field NMR Facility. The quantitative  $^{13}\text{C}$  NMR spectra were recorded at a relaxation delay of 6.5s where only the U- $^{13}\text{C}$  labelled carbon from glucose are recovered in DMSO-*d*<sub>6</sub>. The spectra were processed and analyzed using TopSpin 3.6.2 and MestReNova 14.1.1.

### 5.3.7 FTIR

The FTIR spectra were acquired on a Bruker Alpha-P FTIR spectrometer (Bruker Optic GmbH, Ettlingen, Germany) equipped with a deuterated triglycine sulfate (DTGS) detector, a single-bounce diamond attenuated total reflectance (ATR) crystal, and a pressure application device for solid samples. A total of 32 scans at 4  $\text{cm}^{-1}$  resolution were co-added. The data were recorded and processed using Bruker OPUS software.

### 5.3.8 Pyrolysis-GC/MS

Pyrolysis GC/MS (Py-GC/MS) analyses were conducted using a Varian CP-3800 GC coupled to a Varian Saturn 2000 ion trap mass spectrometric detector (Varian, Walnut Creek, CA). The pyrolysis unit included a CDS 1500 valved interface and a CDS Pyroprobe 2000 unit (CDS Analytical, Oxford, PA) was installed onto the GC injection port. The solid samples (3 mg) were introduced inside a quartz tube (0.3 mm thickness) plugged with quartz wool, and inserted inside the coil probe and pyrolyzed for a total heating time of 20 s at 120 °C. The GC column was a fused silica DB-5 column (50 m length  $\times$  0.2 mm i.d.  $\times$  0.33  $\mu\text{m}$  film thickness, J&W Scientific). The pyroprobe interface temperature was set at 250 °C. The capillary direct MS interface temperature was 280 °C, and the ion source temperature was 180 °C. The ionization voltage was 70 eV, and the electron multiplier was 2471 V. The mass range analyzed was 20-650 m/z. The initial temperature of the column was set at -5 °C for 2 min and was increased to 50 °C at a rate of 30 °C/min; immediately the temperature was further increased to 250 °C at a rate of 8 °C/min and kept at 250 °C for 5 min. Compound identification was performed by using AMDIS (v 2.62) and the National Institute of Standards and Technology (NIST) Standard Reference Database (v 05). All samples are analyzed in duplicates and the results are reported as average  $\pm$  standard deviation in mole/area.

## 5.4 Results and Discussion

The use of the mechanochemical approach for generating Maillard reaction flavors from sugars and amino acids through ball milling was first reported in the patent literature.[10] Subsequently, it was shown that ball milling glucose and various amino acids lead to selective formation of Schiff bases and their Amadori products based on MS/MS diagnostic ions.[17, 18] The ratio of the two intermediates was dependent on the acidity/ basicity of the side chain of the amino acid used. The application of ball milling for conducting chemical reactions not only can generate novel structures as end-products but also, the imparted mechanical energy may alter the microstructure of the reactants, and possibly results in the formation of an activated state, where, after a brief period of milling, the reaction continues to proceed even without further supply of mechanical energy under mild conditions.[19, 20] The thermal properties of ball milled and control samples were investigated by direct observation of their melting behaviour using video recording, and their browning intensities were used as an indication of their thermal reactivity, in addition, their volatile profiles were also analyzed and used as an indication of the chemical changes induced by milling.

In general, flavor active compounds generated from the Maillard reaction are highly dependent on the type of amino acids used and the reaction conditions. With the prospect of studying various amino acids, glucose/histidine model system was chosen to demonstrate the potential of using ball milling for controlled generation of Maillard reaction products under mild conditions. The histidine was chosen because its higher reactivity, and its ability to generate more Schiff base.[17]

### 5.4.1 Histidine/ glucose milled separately

The D-glucose and L-Histidine were milled separately to examine their reactivities and stability under ball milling conditions.

#### 5.4.1.1 Chemical changes after milling

Ball milling of glucose or histidine alone (1h, 30 Hz) did not cause any significant chemical changes. (see Figures S5.1-S5.4) ESI(+ve)/MS scanning of ball-milled glucose generated as expected only its sodiated ion at  $m/z$  203 as a major product. There were no degradation or polymerization products that can be observed from the MS spectrum. (see Figure S5.1) On the other hand, scanning of ball-milled histidine generated its protonated, sodiated, and potassiated molecular ions. Oxidative-decarboxylation of histidine was also observed through detection of ion

at  $m/z$  110 with an elemental composition of  $[C_5H_7N_3+H]^+$ . (see Figure S5.2,  $[M+H]^+$  110) Other chemical modifications of histidine included dipeptide formation and de-amination but only in trace amounts ( $<1\%$  relative abundance). (see Table S5.1) The FTIR spectrum did not indicate any changes or shifts from the observed absorption wavelengths of the untreated samples. (Figures S5.3-S5.4)

#### 5.4.1.2 Morphology after milling

Although ball milling of glucose or histidine separately did not alter their chemical composition, however, based on the scanning electron microscopy data (see Figure 5.1) their morphology has been changed. Loss of crystallinity and size reduction were observed for both glucose and histidine after ball milling.

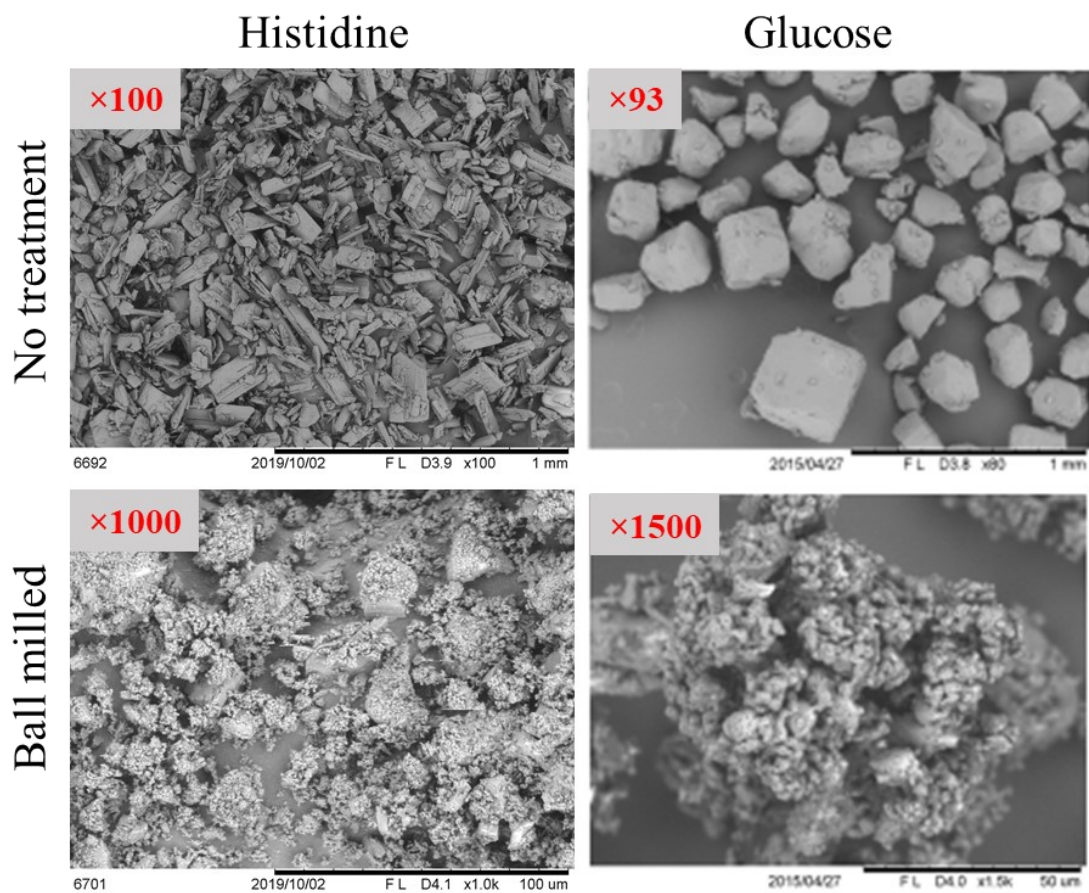


**Figure 5.1** SEM micrographs of native histidine, native glucose, milled histidine, and milled glucose

### 5.4.1.3 Melting behaviour

The melting behavior was assessed through a SRS OptiMelt melting point apparatus. Direct observation of the melting behaviour was recorded by a built in-system camera and the results can be viewed through the following YouTube links listed in Table 5.1.

In order to eliminate the effect of crystal size on the melting behavior, the solid samples were also manually ground by mortar and pestle as a control (the middle tubes in Videos 1-2). The native crystal samples were placed in the left tube, and the ball-milled sample were placed in the right tube. (see Table 5.1 and Videos 1-2) The temperature ramping for the melting experiments was set at a rate of 10 °C per minute to get a rough estimation of the onset of melting range and the changing of the physical state and color. For glucose, there was no significant difference in the onset of the melting temperature. However, the native glucose crystals transformed into a clear and transparent appearance after melting, the manually ground glucose also exhibited the same tendency of forming clear liquid over the course of temperature ramping; the milled glucose, on the other hand, liquefied into an opaque slurry. (See Video 1) This could probably indicate an altered crystal structure due to milling, that affected the appearance of the melt. Milled histidine on the other hand (see Video 2) was found to be more susceptible to heating as was indicated by the rapid release of gases at the moment the tightly packed sample was inserted inside the heating chamber which was set at 200 °C. (see Video 2, right tube) The gas produced turned the moist litmus paper into blue, such an effect was observed only at the later stages of melting process of the native and manually ground histidine samples. These observations indicate that milled histidine decomposes more easily during melting and produces carbon dioxide and an alkaline gas which was assumed to be ammonia, these gases are generated through decarboxylation of histidine followed by deamination as confirmed by the observation of the residual ions at  $m/z$  112 ( $C_5H_{10}N_3$ ) and at  $m/z$  95 ( $C_5H_7N_2$ ) in the milled histidine samples (see Table S5.1).

### 5.4.1.4 Thermal reactivity

The thermal reactivity of the individually milled glucose or histidine was assessed by the intensity of the Maillard browning developed when milled and not-milled reactants (see below) were heated at 90 °C for 1 hour and resulting brown color was measured at 420 nm (see Figure 5.2a, section T60) Three mixtures were tested (1) milled glucose and native histidine, (2) native glucose and milled histidine, and (3) milled glucose and milled histidine. There were no significant differences

in observed thermal reactivity of the three mixtures. Overall, glucose and histidine were assumed to be stable when ball-milled separately.

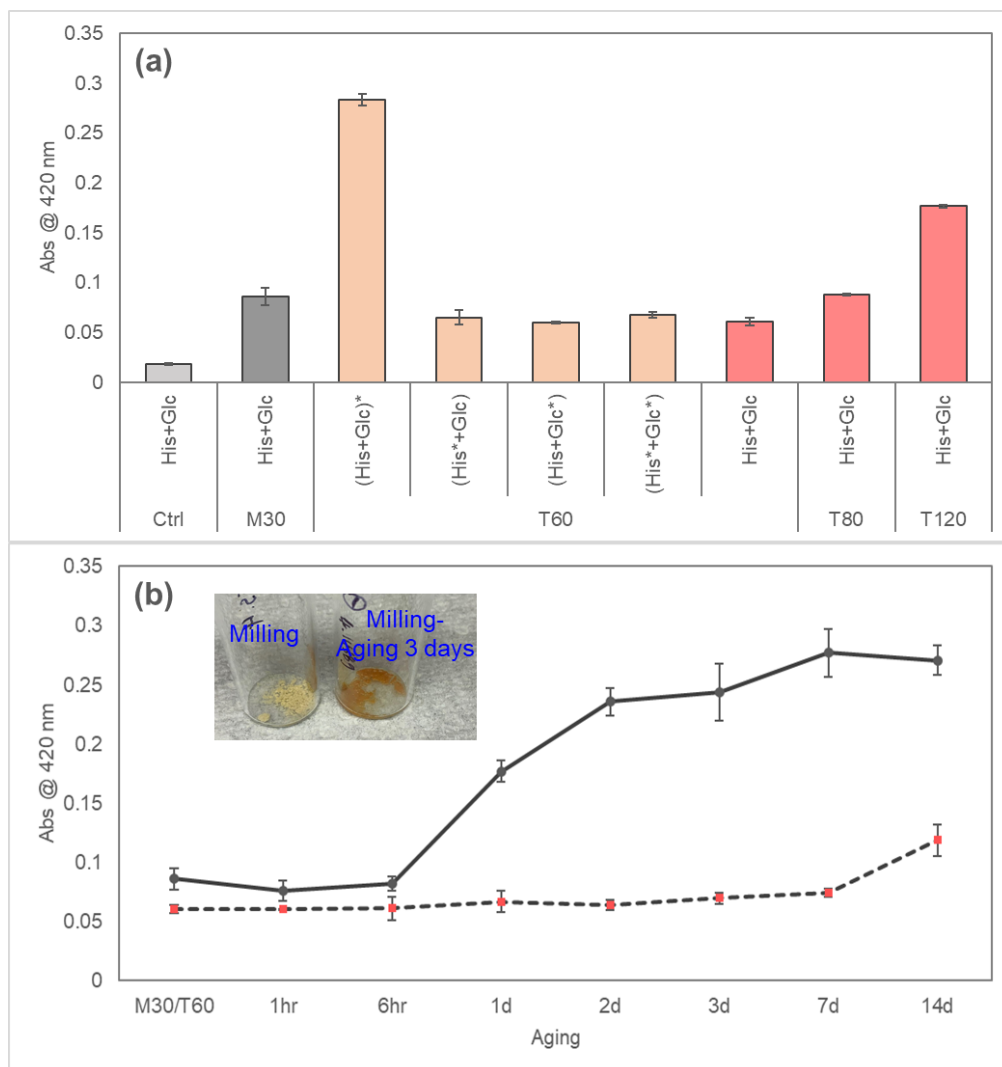


**Figure 5.2** Evaluation of thermal reactivity of glucose/histidine model systems based on browning measurement at 420 nm under various conditions.

**(a)** Comparison of browning intensities of milled glucose/histidine (1:1, 30 min, 30 Hz, M30); non-milled mixtures upon heating at 90°C in methanol for 60 min (T60), 80 min (T80), and for 120 min (T120), and various mechanochemically activated or partially activated glucose-histidine mixtures. (\* Mechanochemically activated.)

**(b)** Browning intensities as a function of aging at room temperature of milled glucose/histidine (1:1, 30 min, 30 Hz (M30), solid line) and heated glucose/histidine (90°C in methanol, 60 min (T60), dashed line)

## 5.4.2 Histidine and glucose milled together

### 5.4.2.1 Analysis of the chemical composition of ball-milled glucose-histidine mixtures using high-resolution mass spectrometry and NMR spectroscopy

The chemical composition of ball-milled (30 min, 30 Hz) glucose-histidine mixtures, was explored using high-resolution mass spectrometry, MS/MS analysis and NMR spectroscopy. Table S5.2 lists all the ions observed that are related to the molecular ion species of the reactants and the main adduct, the Schiff base, at  $m/z$  317. This adduct was characterized using MS/MS diagnostic ions [17] and NMR spectroscopy. The yield of this adduct was estimated by  $^1\text{H}$  NMR in both  $\text{D}_2\text{O}$  and MeOD using the integrated intensities of the two aromatic protons of the imidazole side chain of histidine with chemical shifts in the range of 6.9 – 8.19 ppm, shown in Figures S5.5-S5.6. Inspection of the NMR spectra have indicated the presence of three sets of such aromatic proton signals that were attributed to the Schiff base, the ARP, and the free histidine. (see Figures S5.5-S5.6) The chemical shift assignments of the free histidine was based on the standard, ARP was based on the literature report, [21] and the remaining pair of proton signal was tentatively assigned to the Schiff base since the condensation adduct was the major reaction product generated based on the HRMS results. Further evidence of the Schiff base chemical shift assignment was supported by the observation of the intensity loss when analyzed in  $\text{D}_2\text{O}$  compared to in MeOD due to hydrolysis. (Table S5.3) Based on this assignment, we estimated the yield of Schiff base to be  $35.692\% \pm 1.134\%$ , and that of ARP  $7.299\% \pm 1.567\%$ . This estimation were also agrees with our previous report where more Schiff base was generated relative to its ARP through MS/MS study. [17] The observed increased in Schiff base intensity relative to Amadori product could be attributed to the absence of water during ball milling that prevents the proton transfer during the rearrangement, as well as the basicity of the histidine side chain.[17]

On the other hand, the milled mixtures were also analyzed using high-resolution mass spectrometry (HRMS). The MS scanning and MS/MS fragmentation spectra under both ESI positive and negative mode are shown in Figure S5.7-S5.8. Under ESI positive mode the detected molecular ions were categorized into four types;  $[\text{M}+\text{H}]^+$ ,  $[\text{M}+\text{Na}]^+$ ,  $[\text{M}+\text{K}]^+$ , and  $[\text{M}-\text{H}+2\text{Na}]^+$ ; while under the negative ionization mode, deprotonated ion  $[\text{M}-\text{H}]^-$  was the predominant molecular ion. (see Table S5.2). Analysis of the mass spectral data generated under both positive and negative ionization modes have indicated that the ion at  $[\text{M}+\text{Na}]^+ = 340$  regardless of its charged state whether  $[\text{M}+\text{H}]^+$ ,  $[\text{M}+\text{Na}]^+$  or  $[\text{M}-\text{H}]^-$  can undergo two major degradation pathways, a retro-aldol

cleavage at the C2-C3 carbon bond of the sugar, generating an ion at  $[M+Na]^+ = 220$  and a sugar fragment at  $[M+Na]^+ = 143$ . (see Figure 5.3 and Figures S5.9-S5.10). The other degradation pathway involves decarboxylation of  $[M+Na]^+ = 340$  to generate a decarboxylated Schiff base at  $[M+Na]^+ = 296$ . Similarly the ion at  $[M+Na]^+ = 220$  can also undergo decarboxylation to generate the ion at  $[M+Na]^+ = 176$  (see Figures 5.3, S5.9-S5.10). The chemical identity of these ions were confirmed through assignment of their elemental composition, and through isotopic labeling technique using  $^{13}C$ -2 and  $^{13}C$ -3 glucoses under ESI positive ionization mode (due to the particular interests on the C2-C3 sugar carbon cleavage) and U- $^{13}C_6$ -glucose under negative ionization mode. (see Table S5.4-S5.5). For example, under negative ionization mode, both ions at  $m/z$  316 and  $m/z$  272 incorporated six carbon atoms from glucose, thus increasing their masses to  $m/z$  322 and  $m/z$  278 respectively (see Table S5.5); under ESI positive ionization mode the ion at  $[M+Na]^+ = 220$  had only one labeled atom incorporated from glucose (C2 atom) and on the other hand, the sugar residue at  $[M+Na]^+ = 143$  had only C3 of glucose atom incorporated in its structure, confirming the proposed fragmentation. (see Table S5.4)

Overall, the ball-milled glucose/histidine model system did not generate a complex reaction mixture. There was no observed significant degradation of the Schiff base or ARP based on the number of detectable ions and their relative abundances. Although formed in smaller amounts, such degradation products could have a significant impact on the sensory properties since most aroma active compounds only occur at the sub-ppm levels.

#### **5.4.2.2 Melting behavior of ball-milled glucose-histidine**

The melting behaviour of ball-milled glucose/histidine was studied using SRS OptiMelt apparatus, equipped with video recording capability to give a direct view of its thermal reactivity as compared to the non-milled sample. Non-milled samples were prepared by manually mixing equal molar amounts of glucose and histidine to obtain a homogenous mixture. As shown in videos 3 and 4, where the middle tube contains the ball-milled sample, while the left side contains the manually mixed sample. Inspection of the melting experiments, as shown in videos 3 and 4, indicated that the ball-milled glucose/histidine mixtures exhibited extreme heat sensitivities and earlier onset of browning at temperatures  $\sim 68$  °C and vigorous evolution of gases starting at  $\sim 100$  °C relative to the non-milled samples that started browning at  $\sim 125$  °C and showed vigorous evolution of gases

only around 131°C. (see Videos 3 & 4 in Table 5.1). These observations corroborate the use of such mixtures to accelerate the Maillard reaction.

### 5.4.2.3 Reactivity

The thermal reactivity of the milled glucose/histidine mixtures (30 mg dissolved in 4 mL methanol) were also assessed by the intensity of the browning observed when heated in methanol at 90 °C for 1 hour in a sand bath. (see Figure 5.2a) There was a light-yellow color formation directly after 30 minutes of milling of histidine and glucose together. The color was significantly intensified upon heating for 1 hour at 90 °C in methanol.

On the other hand, heating of the non-milled mixture for 80 mins at 90 °C generate the same level of browning compared to the 30 minutes milled sample. (see Figure 5.2a) The 80 minutes heated sample was also scanned by HRMS and compared with the Maillard reaction products generated through 30 minutes ball milling. Despite at the same browning intensity, we observed that there were much less reaction products generated by heating compared to ball milling especially for the relative intensity of the condensation adduct at  $m/z$  340. (see Figure S5.9) This observation agrees with literature reports on the relatively low reactivity of glucose where even heating glucose and glycine for 24 hours at 100 °C where only limited number of reaction products detected by HRMS. [22]

The enhanced reactivity of the milled mixtures was further demonstrated through storage experiments where samples were stored in open vials at room temperature. This practice is also known as “aging” in the context of mechanochemistry. Over two weeks of storage time the mechanochemically “activated” mixtures continued to develop brown color (see Figure 5.2b).

The most significant color changes were observed within the first 3 days of the storage. Consequently, 1 day and 3 days aged samples were analyzed through HRMS and NMR to study the evolution of reaction products over the 3-day storage time. Surprisingly, the overall reaction profile developed over the 3-day storage period did not become more complex relative to the 1 day stored samples. Instead, we observed the accumulation of the condensation adducts at  $m/z$  318 and 340, and their dehydrated counterparts at  $m/z$  300, 282, and 322. (see Table S5.6 and Figure S5.10) Furthermore, a significant decrease in the relative intensities of the free sugar ( $m/z$  203) and the C2–C3 cleavage products ( $m/z$  198 and 220) were observed (see Figure 5.3) indicating the high reactivity of the histidine-diose adducts as browning precursors.

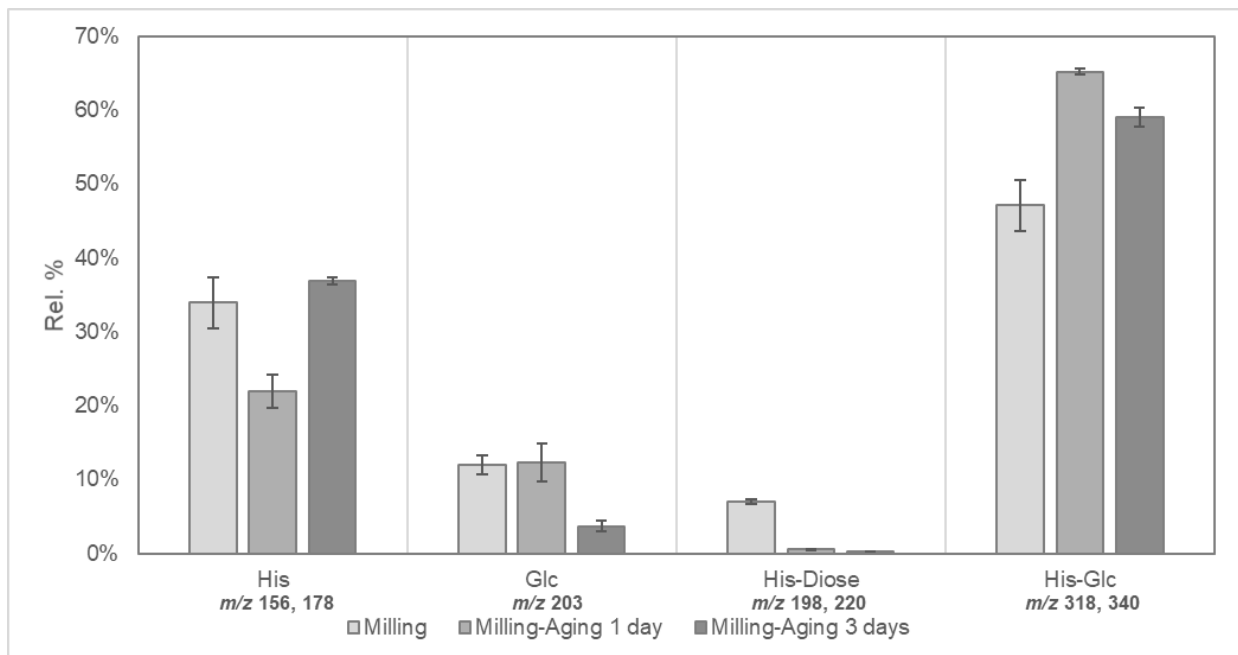


**Figure 5.3** Changing of the relative intensities of selected ions during storage at 1 day and 3 days at room temperature. Results obtained from HRMS are from two independent trial (n=2).

To selectively study the evolving profile of the glucose during the storage, we recorded the quantitative  $^{13}\text{C}$  NMR spectra at a relaxation delay of 6.5 s where only the U- $^{13}\text{C}$  labeled carbon from glucose were recovered. (see Figure S5.11) The results agree with the observation from HRMS. There was ~ 80% sugar conversion at the end of the 3-day aging period compared to ~ 50% directly after milling (the conversion was estimated based on intensities of the chemical shifts of C1, C3, C5, and C6). Furthermore, the  $^{13}\text{C}$  NMR spectra of the 3-day aged sample also indicated that the reaction mixture did not increase in complexity, although there were more peaks observed in the chemical shift range between 64 and 78 ppm. Furthermore, there was a clear tendency of increased intensities of certain carbon signals (e.g. at 102.5, 95.65, 61.25, and 51.89 ppm) accompanied with the significant decrease in the free glucose signal (e.g. at 97.41, 92.73, 77.17, and 61.71). (see Table S5.7 and Figure S5.11) In this experiment, only indicated glucose carbon signals were unequivocally assigned, other chemical shifts were tentatively assigned based on most relevant literatures listed in the Table S5.7.

Overall, ball milling of sugars and amino acids seems more efficient in selectively generating their condensation adducts compared to heating. Furthermore, the mechanochemical reaction mixture

was found have enhanced reactivity based on the observed browning. Despite the intensified browning during storage at room temperature, generally, its chemical profile remained unchanged except for the accumulation of the presumed browning precursors Schiff base or its Amadori rearrangement product.

#### **5.4.3 Comparison of the volatiles formed in milled and not-milled glucose/histidine mixtures.**

Due to the importance of the volatiles in the Maillard reaction, the milled glucose-histidine mixtures were pyrolyzed and the volatiles generated were compared to the non-milled mixtures. (see Table 5.2). Considering the heat sensitivity of the milled samples, the pyrolysis was conducted at a relatively low temperature (120 °C for 20 s). The main difference between the samples was the intensity of the volatiles generated (see Table 5.2). The milled glucose/histidine mixtures produced more pyrazine derivatives than furan derivatives compared to the non-milled mixtures. For example, milled glucose-histidine produced significantly more 2,5-dimethylparazine, while lacking 2-furanmethanol and 5-methyl-2-furancarboxaldehyde compared to the non-milled mixture. (see Table 5.2)

To rationalize these differences, we further investigated the chemical composition of the ball-milled glucose-histidine mixtures by HRMS, for the presence of potential precursors. Figure 5.3 shows the major sodiated ions and Figures S5.12 to S5.14 shows protonated and deprotonated ions observed in glucose-histidine milled mixtures. Of particular importance to browning and pyrazine formation are the ions observed at  $m/z$  340, 280, 250 and 220 that are not expected to be found in the non-milled mixture, (see Figure 5.4) due to lack of any chemical reaction occurring when two solids are mixed at room temperature. The ions at  $m/z$  340, 280 and 250 after appropriate dehydration steps can undergo Strecker reaction generating various  $\alpha$ -amino carbonyl moieties that are considered the direct precursors of pyrazines. The formation of higher amounts of pyrazines relative to non-milled samples were demonstrated above when the volatiles from the two mixtures were compared (Table 5.2). Furthermore, under pyrolytic conditions, the ion at  $m/z$  220 can release the potent browning precursor glyoxal or glycolaldehyde [23] depending on the redox environment the reaction. The presence of this browning precursor can rationalize the thermal reactivity and more intense browning observed in the milled samples. Furthermore, the

ion at  $m/z$  220 can be directly generated from the Schiff base through retro-aldol cleavage of C2-C3 carbon atoms and was detected in relatively high abundances under both ESI positive and negative ionization modes. (see Table S5.4-S5.5) In fact, this ion was proposed as one of the MS/MS diagnostic ions for the Schiff bases in negative ionization mode. [17]. (see Figure S5.8 and Table S5.5)

Under ball milling conditions, the Maillard reaction effectively slows down at the Schiff base/Amadori stage with only a smaller percentage degrading through decarboxylation, dehydration and retro-aldol reactions (see Figure 5.3) relative to non-milled samples. With basic amino acids such as histidine this stage is characterized by a high content of Schiff bases relative to the Amadori products.[17]

**Table 5.2** Comparison of volatiles<sup>a</sup> generated from milled (30 mins, 30 Hz) and non-milled glucose-histidine (1:1) mixtures when pyrolyzed at 120 °C for 20 s.

Category	Compounds	Retention time (min)	Major ions	Not-milled (area per mole)	Mill (area per mole)
Pyrazines	Methylpyrazine	12.628	94, 67, 39, 26	1.918 ± 0.005	4.048 ± 0.362
	2,5-dimethylparazine	14.473	108, 42	3.960 ± 0.197	17.295 ± 1.542
	2-ethyl-3-methylpyrazine	16.361	122, 112, 84, 55, 42, 29	2.805 ± 0.758	8.878 ± 0.572
<b>Sum</b>				<b>8.683</b>	<b>30.222</b>
O-heterocycles	furfural	12.714	95, 39	9.306 ± 0.886	0
	2-furanmethanol	13.18	81, 98, 39	63.378 ± 0.431	1.825 ± 0.082
	5-methyl-2-furanmethanol	15.213	95, 112	27.307 ± 4.247	20.125 ± 0.605
	5-methyl-2-furancarboxaldehyde	15.476	110, 53	12.166 ± 0.486	1.475 ± 0.185
	2,4-dihydroxy-2,5-dimethyl-furanone	15.896	144, 101, 55, 43	8.783 ± 1.340	6.347 ± 0.123
	2,3-dihydro-3,5-dihydroxy-6-methyl-pyranone	23.099	144, 101, 43	14.630 ± 3.573	6.707 ± 0.237
<b>Sum</b>				<b>135.569</b>	<b>36.478</b>

<sup>a</sup> Results are reported as area per mole of histidine or glucose with at least two replicates.

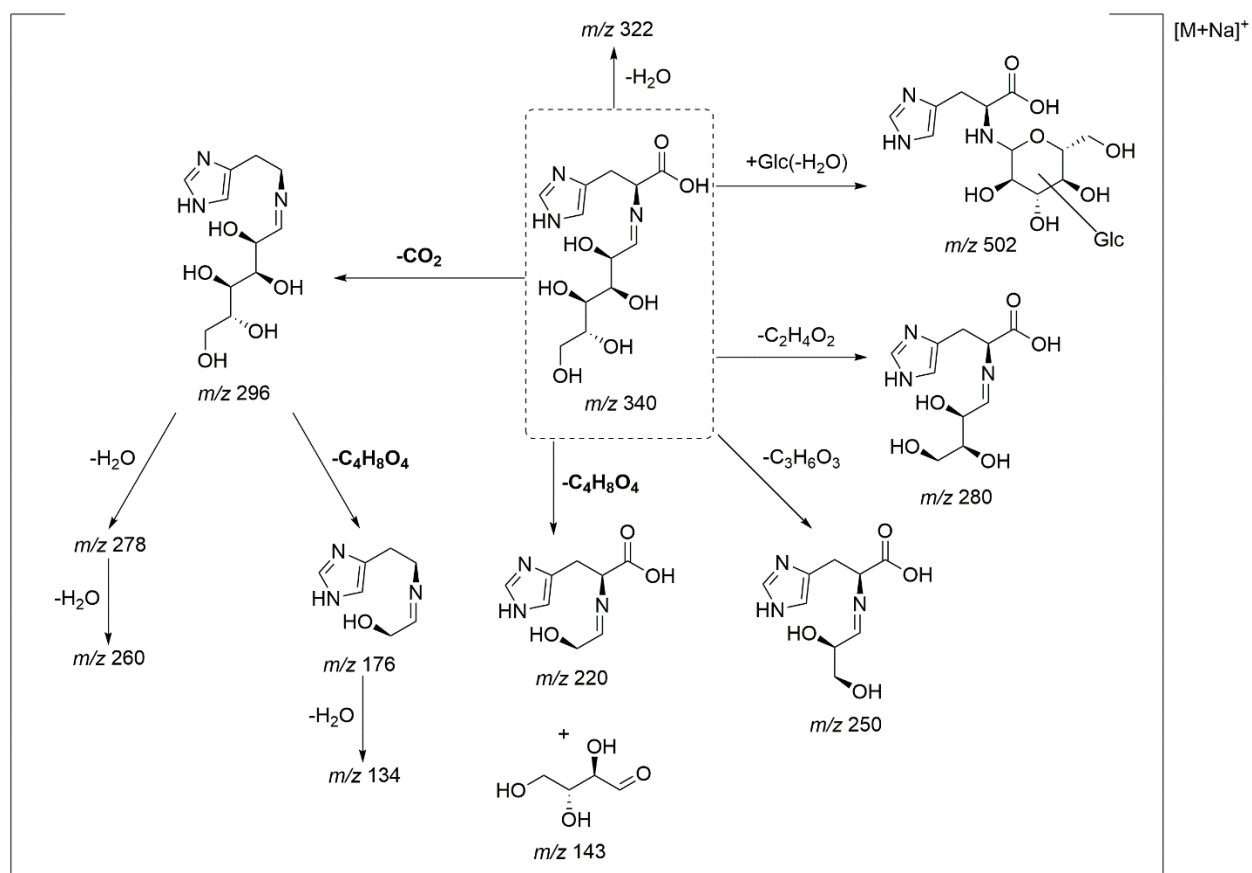


**Figure 5.4** Maillard reaction products generated from ball milling of glucose and histidine (30 mins, 30 Hz) under positive ionization mode showing sodiated ions. The glycosidic linkage of the disaccharide-histidine condensation adduct at  $m/z$  502 is unknown. (see also Table S5.4)

## 5.5 References

1. Mottram, D.S., *Flavor compounds formed during the Maillard reaction*. 1994, ACS Publications.
2. Sukan, M.K. and D.K. Weerasinghe, *Process and reaction flavors: An overview*. 2005, ACS Publications.
3. Kerler, J., et al., *Basic chemistry and process conditions for reaction flavours with particular focus on Maillard-type reactions*. Food flavour technology, 2010. **2**.
4. Nursten, H.E., *The Maillard reaction: chemistry, biochemistry, and implications*. 2005: Royal Society of Chemistry.
5. Hodge, J.E., *Dehydrated foods, chemistry of browning reactions in model systems*. Journal of agricultural and food chemistry, 1953. **1**(15): p. 928-943.
6. Yaylayan, V.A., *Classification of the Maillard reaction: A conceptual approach*. Trends in Food Science & Technology, 1997. **8**(1): p. 13-18.
7. Yaylayan, V., J. Fichtali, and F. Van de Voort, *Production of Maillard reaction flavour precursors by extrusion processing*. Food Research International, 1992. **25**(3): p. 175-180.
8. Yaylayan, V.A., et al., *Microwave-assisted synthesis and extraction of selected Maillard reaction products*. Journal of agricultural and food chemistry, 1997. **45**(1): p. 149-152.
9. Ong, O.X., et al., *High-intensity ultrasound production of Maillard reaction flavor compounds in a cysteine-xylose model system*. Ultrasonics sonochemistry, 2015. **26**: p. 399-407.
10. Viton, F., H.R. Oertling, and R. Fumeaux, *Mechanical generation of flavour compositions*. 2017, U.S. Patent US20170079316A1.
11. James, S.L., et al., *Mechanochemistry: opportunities for new and cleaner synthesis*. Chemical Society Reviews, 2012. **41**(1): p. 413-447.
12. Margetic, D. and V. Štrukil, *Mechanochemical Organic Synthesis*. 2016: Elsevier.
13. Schmeyers, J., et al., *Quantitative solid-solid synthesis of azomethines*. Journal of the Chemical Society, Perkin Transactions 2, 1998(4): p. 989-994.
14. Kaupp, G., J. Schmeyers, and J. Boy, *Quantitative Solid-State Reactions of Amines with Carbonyl Compounds and Isothiocyanates*. Tetrahedron, 2000. **56**(36): p. 6899-6911.

15. Schmidt, R., H. Martin Scholze, and A. Stolle, *Temperature progression in a mixer ball mill*. International Journal of Industrial Chemistry, 2016. **7**(2): p. 181-186.
16. Kulla, H., et al., *Warming up for mechanosynthesis – temperature development in ball mills during synthesis*. Chemical Communications, 2017. **53**(10): p. 1664-1667.
17. Xing, H. and V. Yaylayan, *Mechanochemical generation of Schiff bases and Amadori products and utilization of diagnostic MS/MS fragmentation patterns in negative ionization mode for their analysis*. Carbohydrate Research, 2020. **495**: p. 108091.
18. Xing, H., V.V. Mossine, and V. Yaylayan, *Diagnostic MS/MS fragmentation patterns for the discrimination between Schiff bases and their Amadori or Heyns rearrangement products*. Carbohydrate Research, 2020. **491**: p. 107985.
19. Hammerer, F., et al., *Solvent-free enzyme activity: quick, high-yielding mechano-enzymatic hydrolysis of cellulose into glucose*. Angewandte Chemie International Edition, 2018.
20. Descamps, M., et al., *The amorphous state of pharmaceuticals obtained or transformed by milling: Sub-Tg features and rejuvenation*. Journal of Non-Crystalline Solids, 2015. **407**: p. 72-80.
21. Röper, H., et al., *N.m.r. spectroscopy of N-(1-deoxy-d-fructos-1-yl)-l-amino acids (“fructose-amino acids”)*. Carbohydrate Research, 1983. **116**(2): p. 183-195.
22. Hemmler, D., et al., *Insights into the Chemistry of Non-Enzymatic Browning Reactions in Different Ribose-Amino Acid Model Systems*. Scientific Reports, 2018. **8**(1): p. 16879.
23. Hofmann, T., *Quantitative studies on the role of browning precursors in the Maillard reaction of pentoses and hexoses with L-alanine*. European food research and technology, 1999. **209**(2): p. 113-121.

## 5.6 Supplementary information

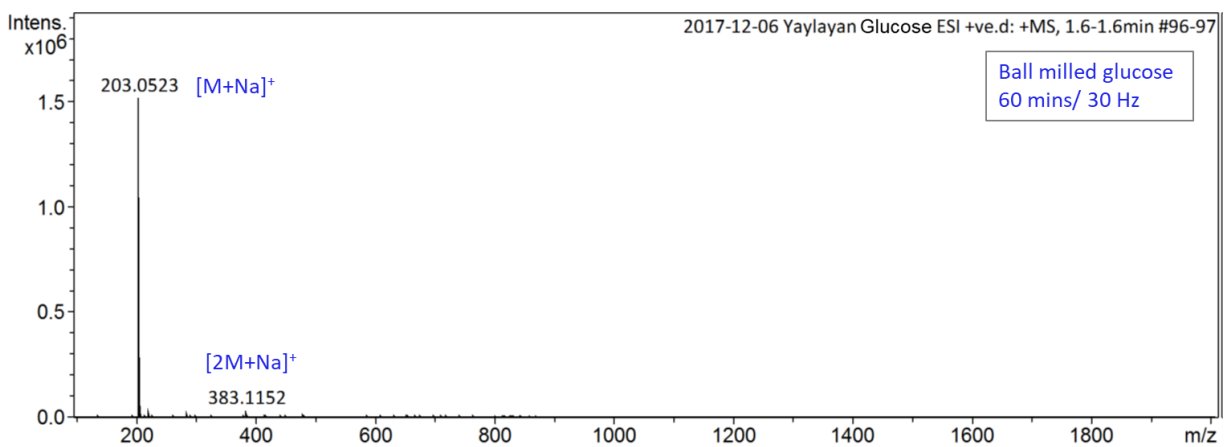


Figure S 5.1 ESI (+ve)/MS spectra of ball-milled glucose for 60 min, 30Hz.

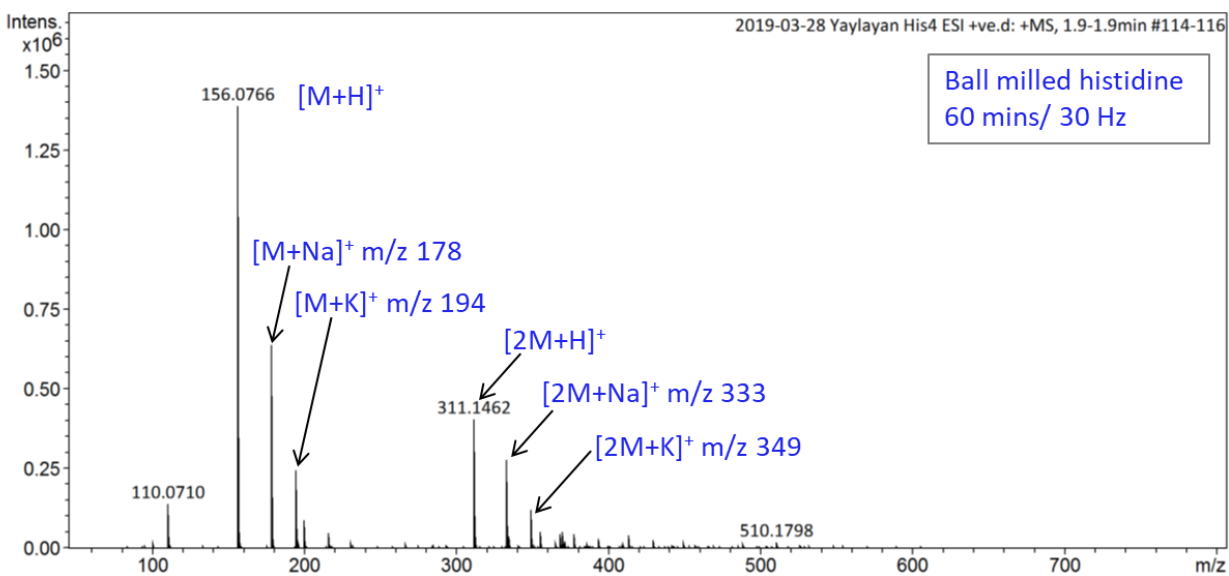
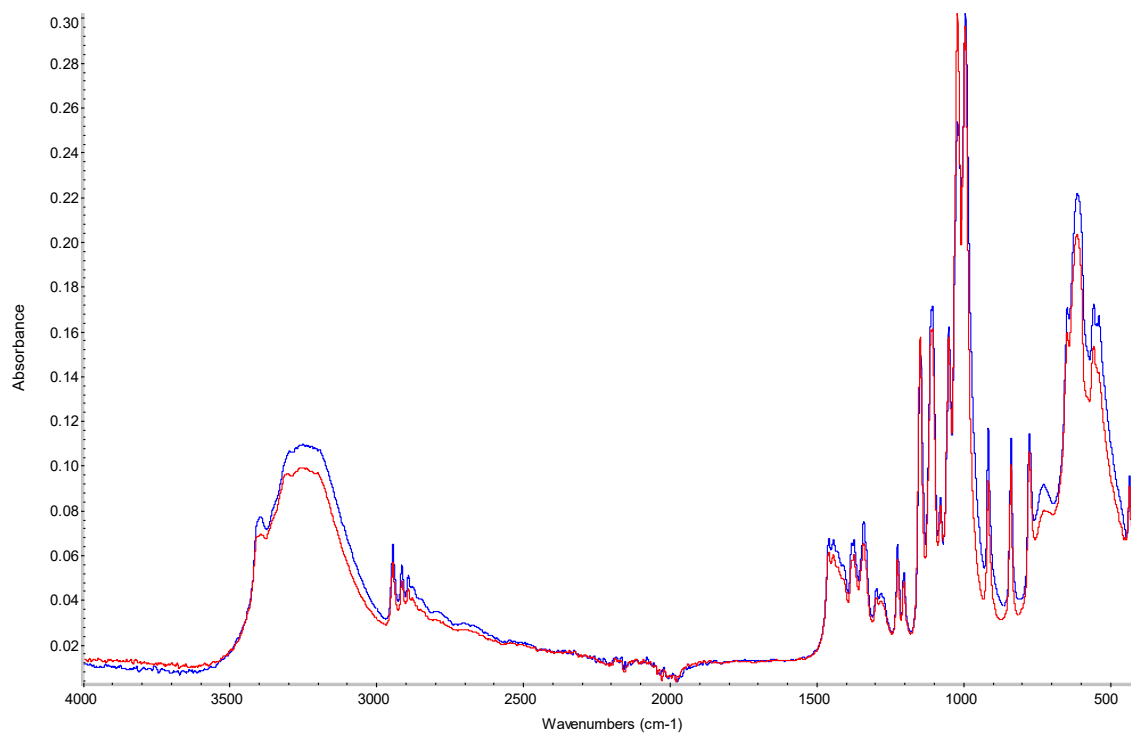
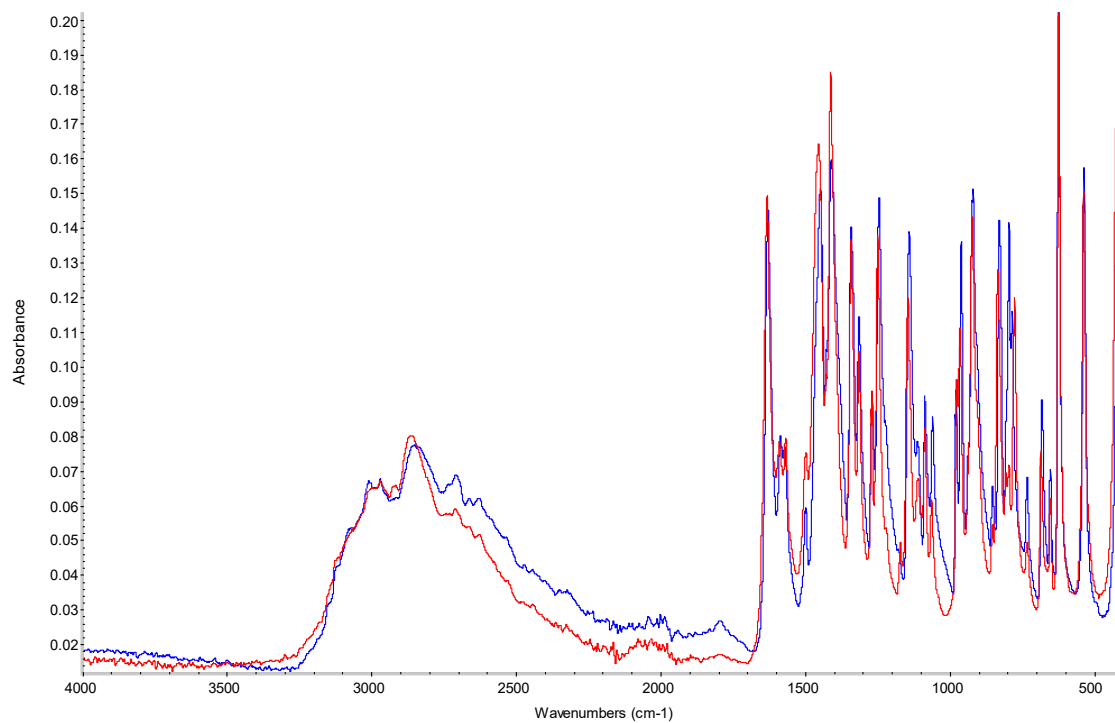


Figure S 5.2 ESI (+ve)/MS spectra of ball-milled histidine for 60 min, 30Hz.



**Figure S 5.3** Superimposed FTIR spectra of glucose (blue) and ball-milled glucose (red, 60 min, 30Hz).



**Figure S 5.4** Superimposed FTIR spectra of histidine (blue) and ball-milled histidine (red, 60 min, 30Hz).

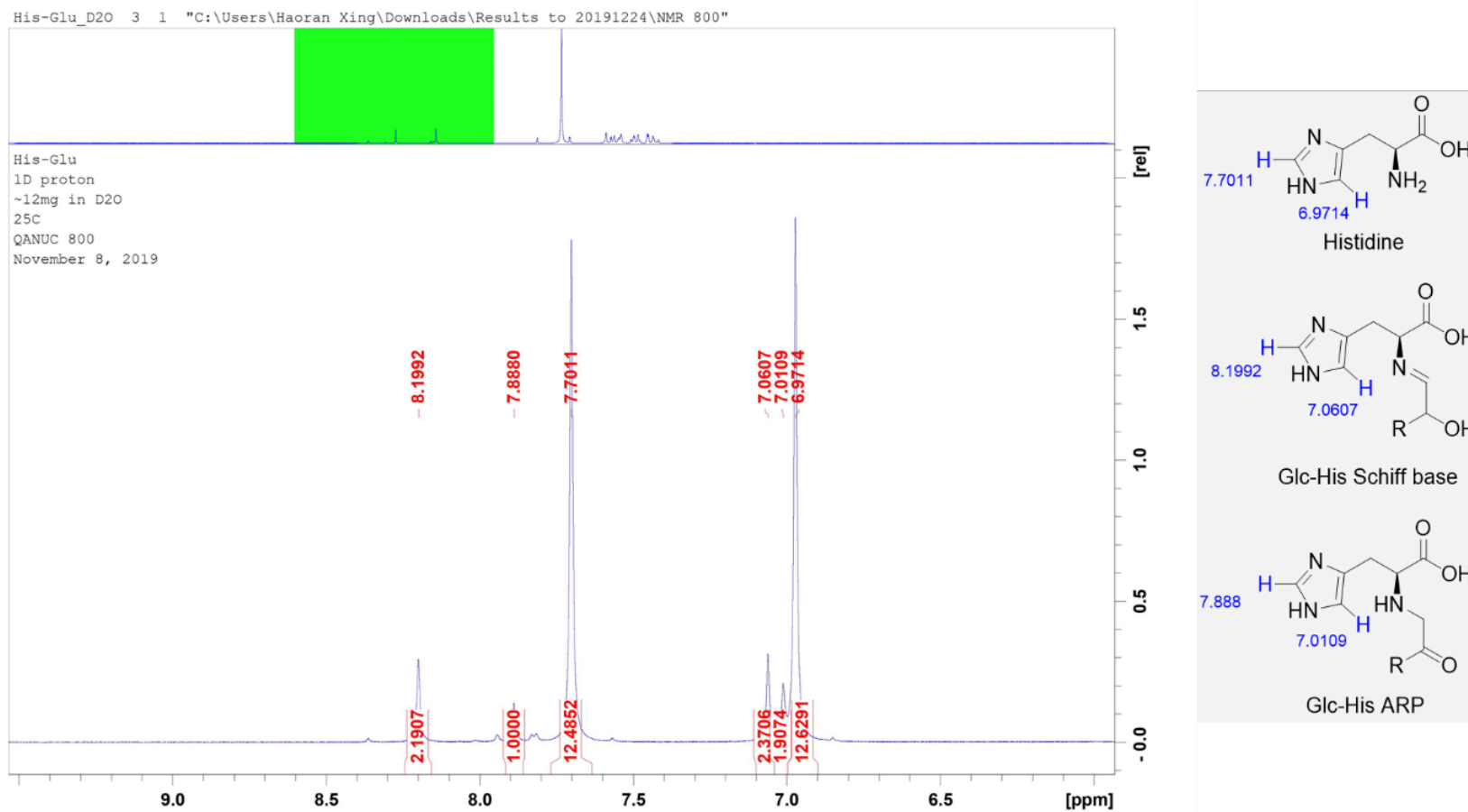


**Figure S 5.5** The aromatic proton region of  $^1\text{H}$  NMR Spectrum of ball-milled glucose-histidine in  $\text{D}_2\text{O}$ . The tentative assignments are annotated on the structures shown.

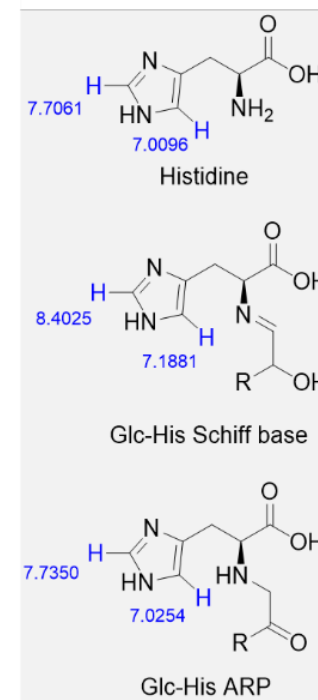
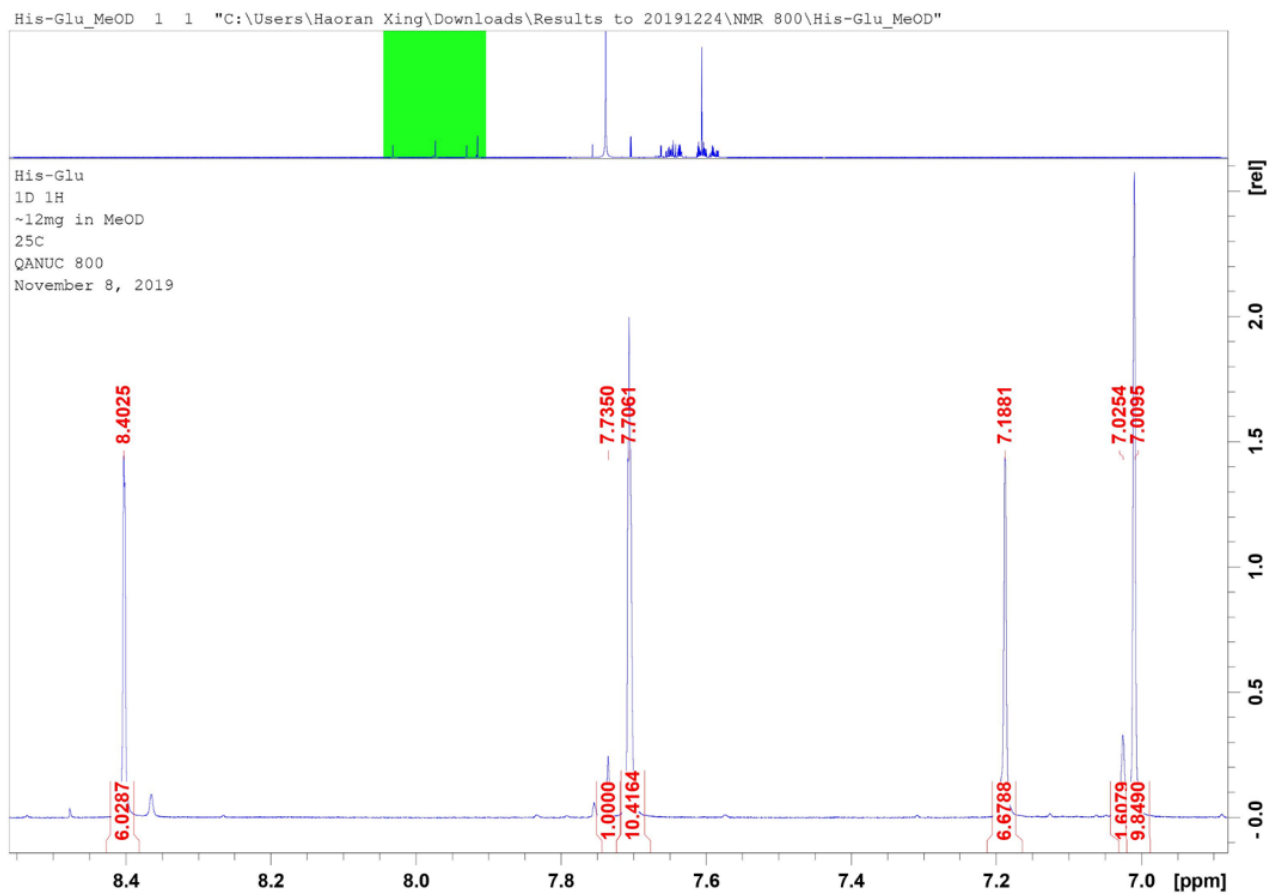


**Figure S 5.6** The aromatic proton region of  $^1\text{H}$  NMR Spectrum of ball-milled glucose-histidine in MeOD. The tentative assignments are annotated on the structures shown

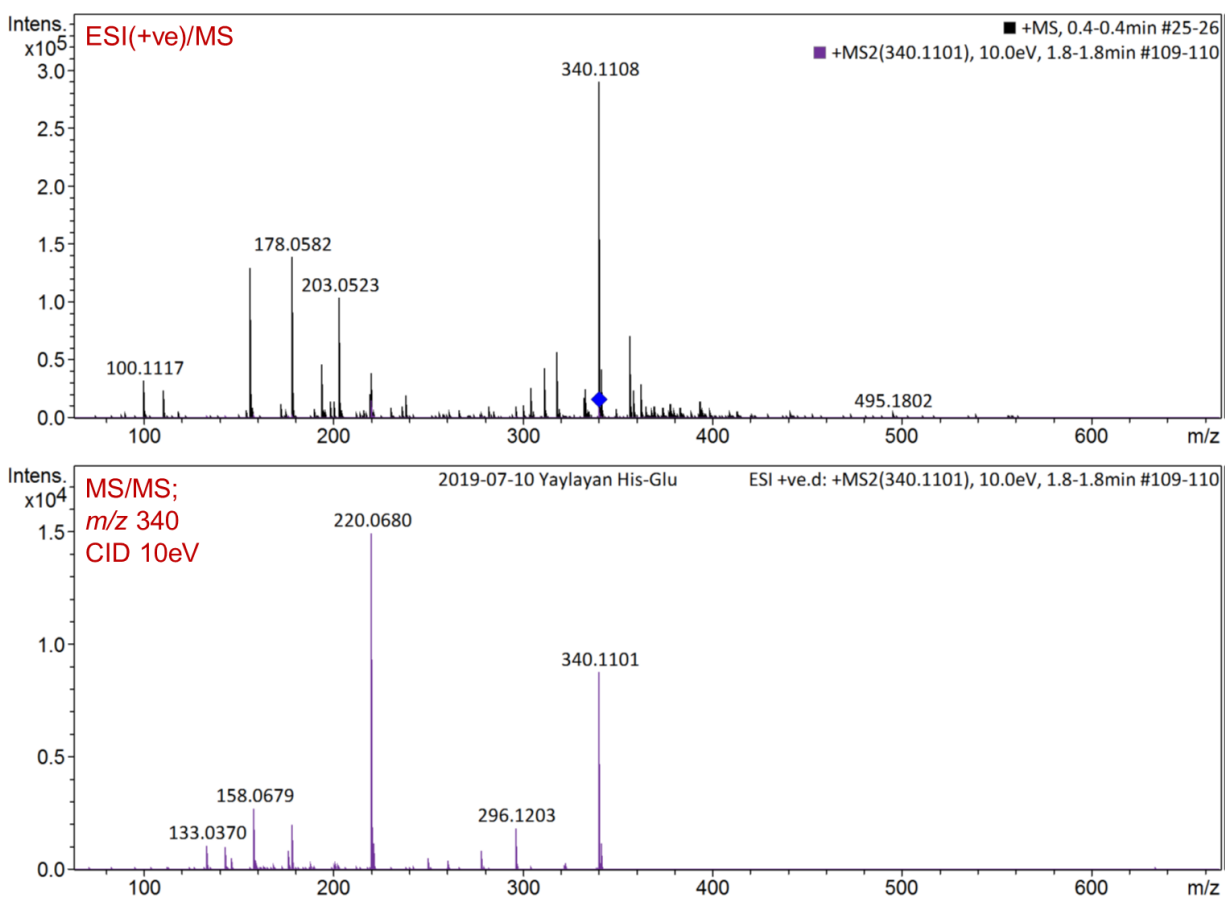


**Figure S 5.7** ESI (+ve)/MS/MS spectra of the ball-milled glucose-histidine mixture (30 min, 30Hz).

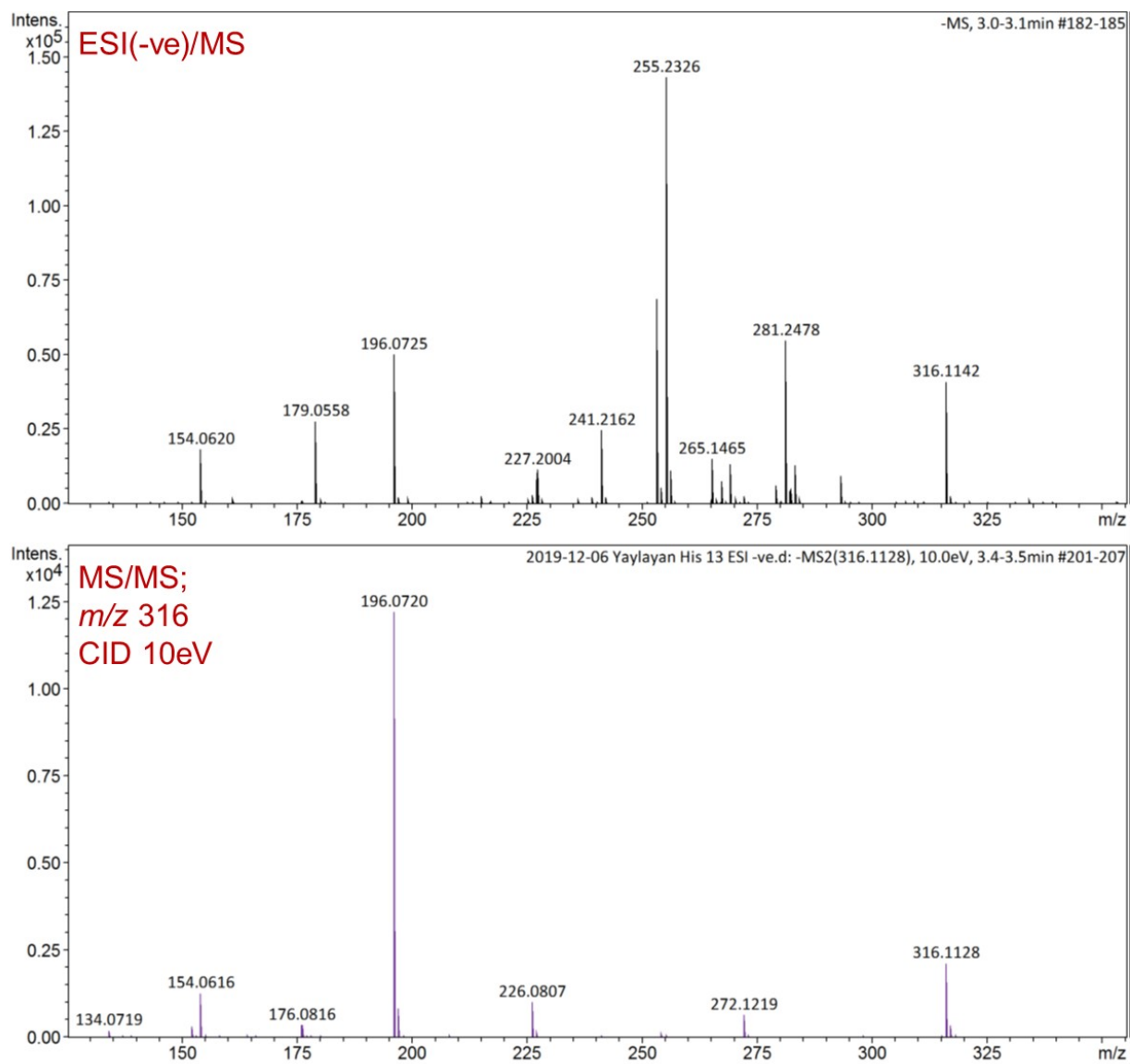


**Figure S 5.8** ESI(-ve)/MS/MS spectra of the ball-milled glucose-histidine mixture (30 min, 30Hz).

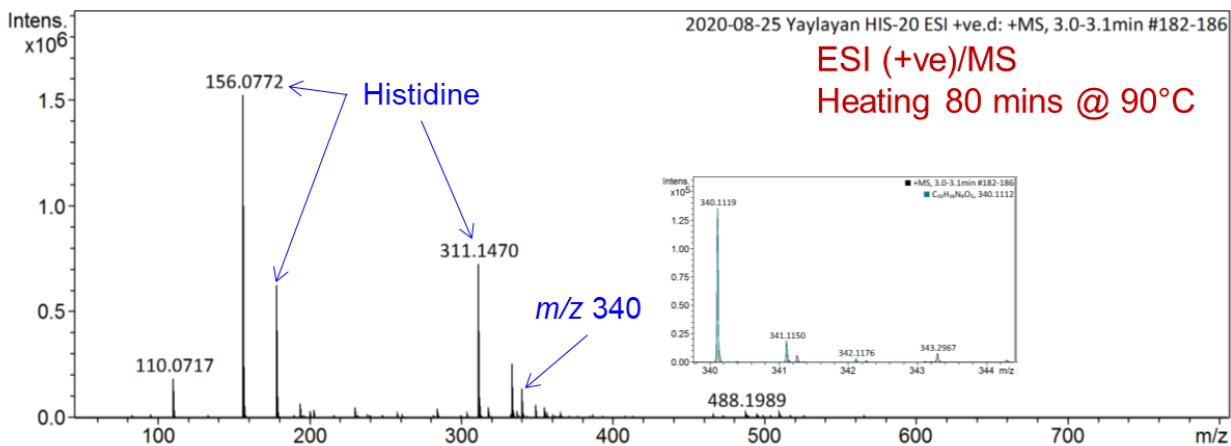


**Figure S 5.9** ESI(+ve)/MS spectra of the heated sample (80 mins at 90 °C).

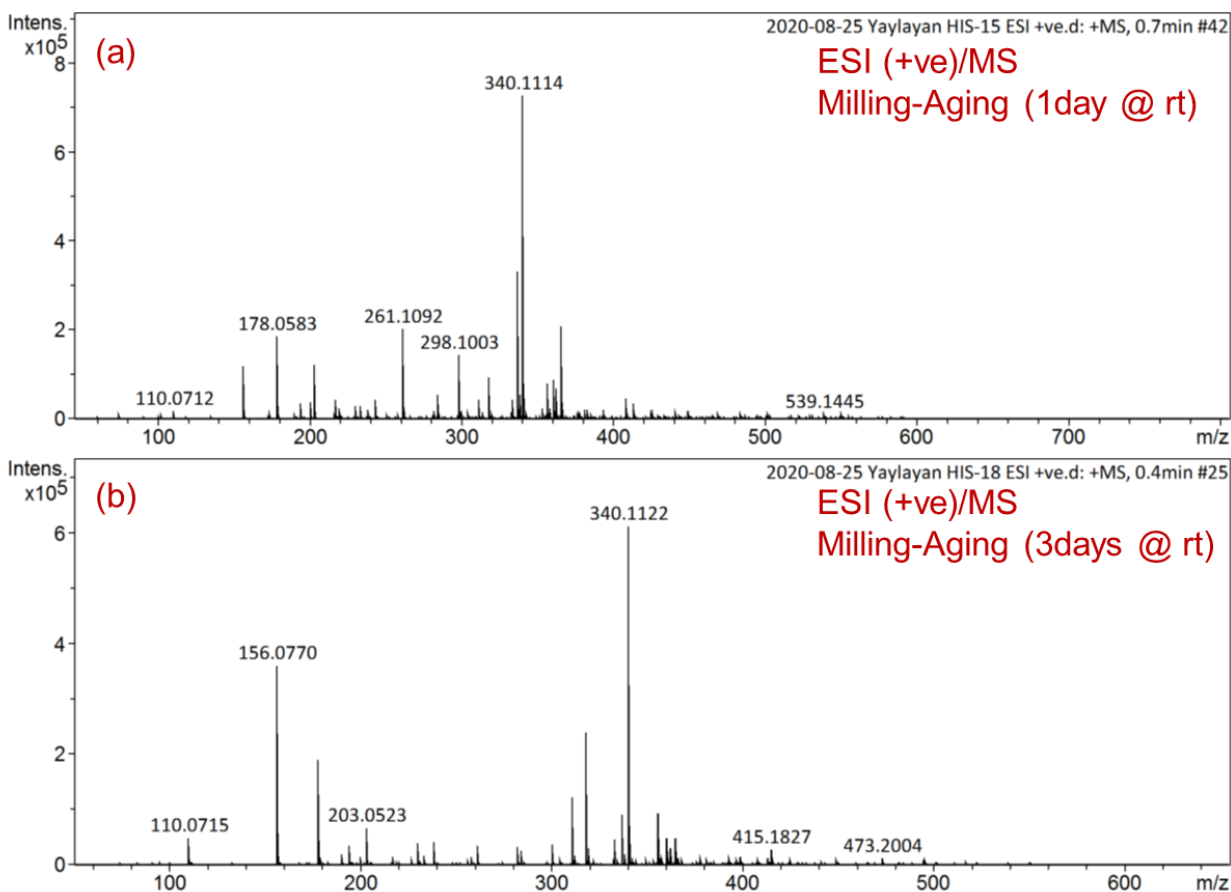


**Figure S 5.10** ESI(+ve)/MS spectra of (1) 1 day aging of milled sample (30 min, 30Hz), and (b) 3 days aging of milled sample (30 min, 30Hz).



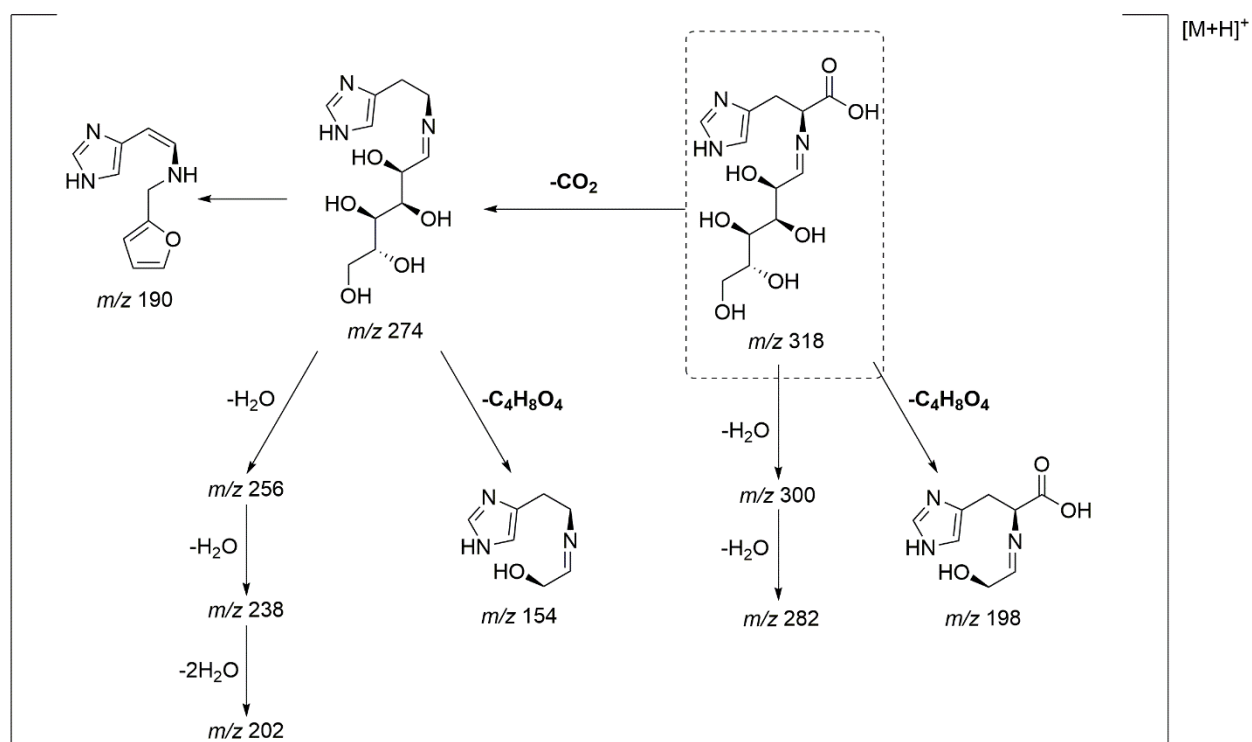


**Figure S 5.12** Maillard reaction products generated from ball milled glucose and histidine (30 min, 30 Hz) under positive ionization mode showing protonated ions. (see also Table S5.4)

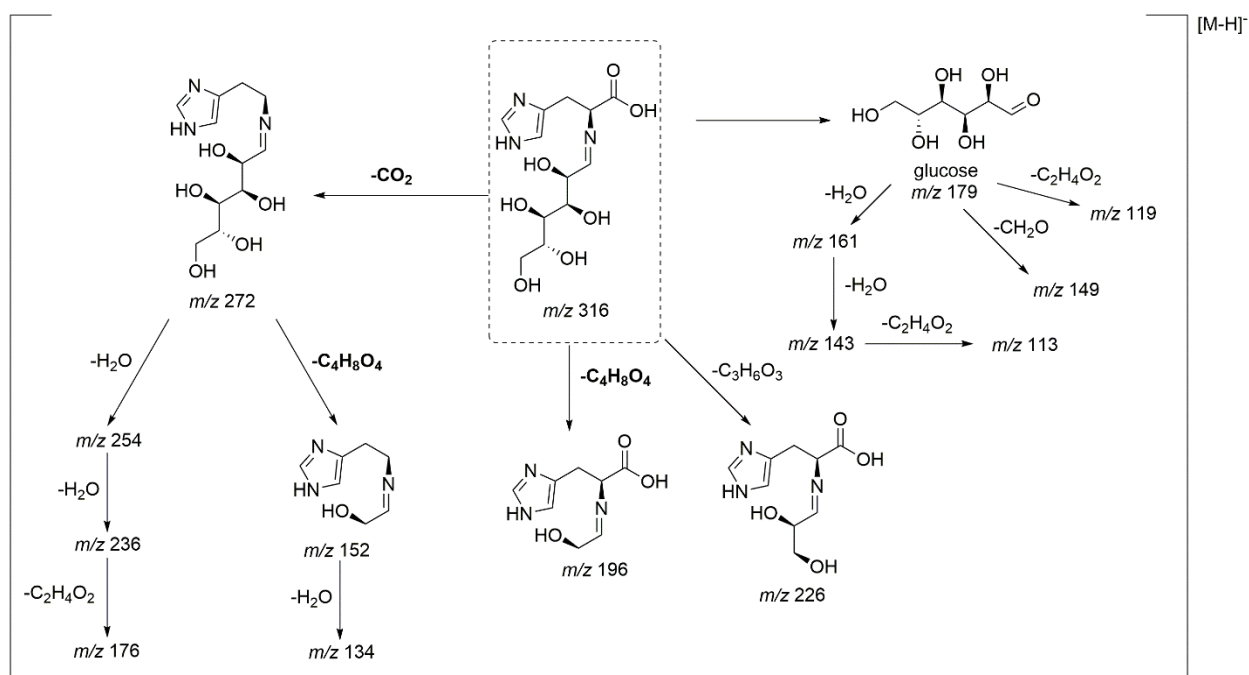


**Figure S 5.13** Maillard reaction products generated from ball milled glucose and histidine (30 min, 30 Hz) under negative ionization mode showing deprotonated ions. (see also Table S5.5).



**Table S 5.1** Elemental composition of selected  $m/z$  s from ball-milled histidine (60 min, 30Hz).

<i>m/z</i>		Elemental composition	I%	Rel. error [ppm]
Exp.	Theor.			
95.0600	95.0604	C <sub>5</sub> H <sub>7</sub> N <sub>2</sub>	0.6	4.452
110.0710	110.0712	C <sub>5</sub> H <sub>8</sub> N <sub>3</sub>	10	1.45
112.0866	112.0875	C <sub>5</sub> H <sub>10</sub> N <sub>3</sub>	0.6	7.783
133.0370	133.0378	C <sub>5</sub> H <sub>6</sub> N <sub>2</sub> NaO	0.4	5.882
156.0766	156.0773	C <sub>6</sub> H <sub>10</sub> N <sub>3</sub> O <sub>2</sub>	100	4.495
178.0585	178.0592	C <sub>6</sub> H <sub>9</sub> N <sub>3</sub> NaO <sub>2</sub>	46	4.191
194.0323	194.0332	C <sub>6</sub> H <sub>9</sub> KN <sub>3</sub> O <sub>2</sub>	17.6	4.553
293.1361	293.1362	C <sub>12</sub> H <sub>17</sub> N <sub>6</sub> O <sub>3</sub>	0.5	0.387
311.1462	311.1468	C <sub>12</sub> H <sub>19</sub> N <sub>6</sub> O <sub>4</sub>	29.1	1.858
315.1175	315.1182	C <sub>12</sub> H <sub>16</sub> N <sub>6</sub> NaO <sub>3</sub>	0.5	2.088
331.0924	331.0927	C <sub>12</sub> H <sub>16</sub> KN <sub>6</sub> O <sub>3</sub>	0.2	0.92
333.1278	333.1287	C <sub>12</sub> H <sub>18</sub> N <sub>6</sub> NaO <sub>4</sub>	20	2.77
349.1000	349.1027	C <sub>12</sub> H <sub>18</sub> KN <sub>6</sub> O <sub>4</sub>	8.8	7.62

**Table S 5.2** Ions related to molecular species observed in milled histidine/glucose under ESI(+ve/-ve)/ionization modes. (see Figures S5.7-S5.8)

ESI (+ve)	<i>m/z</i>		I%	Adducts	Elemental composition	Rel. error [ppm]
	Exp.	Theor.				
Histidine						
M = 155	139.0491	139.0508	0.1	[M+H-NH <sub>3</sub> ] <sup>+</sup>	C <sub>6</sub> H <sub>7</sub> N <sub>2</sub> O <sub>2</sub>	-11.88
	156.0763	156.0773	48.7	[M+H] <sup>+</sup>	C <sub>6</sub> H <sub>10</sub> N <sub>3</sub> O <sub>2</sub>	-6.42
	178.0582	178.0592	51.7	[M+Na] <sup>+</sup>	C <sub>6</sub> H <sub>9</sub> N <sub>3</sub> NaO <sub>2</sub>	-5.87
	194.0320	194.0332	29.2	[M+K] <sup>+</sup>	C <sub>6</sub> H <sub>9</sub> KN <sub>3</sub> O <sub>2</sub>	-6.1
	200.0403	200.0412	9.9	[M+2Na-H] <sup>+</sup>	C <sub>6</sub> H <sub>8</sub> N <sub>3</sub> Na <sub>2</sub> O <sub>2</sub>	-4.45
	231.9894	231.9897	0.6	[M+2K-H] <sup>+</sup>	C <sub>6</sub> H <sub>8</sub> K <sub>2</sub> N <sub>3</sub> O <sub>2</sub>	1.45
	333.1277	333.1287	10.4	[2M+Na] <sup>+</sup>	C <sub>12</sub> H <sub>18</sub> N <sub>6</sub> NaO <sub>4</sub>	-3.07
	349.1010	349.1027	3.6	[2M+K] <sup>+</sup>	C <sub>12</sub> H <sub>18</sub> KN <sub>6</sub> O <sub>4</sub>	-4.75
	355.1076	355.1107	1.1	[2M+2Na-H] <sup>+</sup>	C <sub>12</sub> H <sub>17</sub> N <sub>6</sub> Na <sub>2</sub> O <sub>4</sub>	-8.64
Glucose						
M = 180	203.0523	203.0532	27.4	[M+Na] <sup>+</sup>	C <sub>6</sub> H <sub>12</sub> NaO <sub>6</sub>	-4.22
	219.0261	219.0271	14.8	[M+K] <sup>+</sup>	C <sub>6</sub> H <sub>12</sub> KO <sub>6</sub>	-4.54
	225.0344	225.0351	1.1	[M+2Na-H] <sup>+</sup>	C <sub>6</sub> H <sub>11</sub> Na <sub>2</sub> O <sub>6</sub>	-3.12
	399.0888	399.0905	2.9	[2M+K] <sup>+</sup>	C <sub>12</sub> H <sub>24</sub> KO <sub>12</sub>	-4.22
Schiff base/Amadori						
M = 317	300.1183	300.1196	5.1	[M+H-H <sub>2</sub> O] <sup>+</sup>	C <sub>12</sub> H <sub>18</sub> N <sub>3</sub> O <sub>6</sub>	-4.2
	318.1290	318.1301	18.3	[M+H] <sup>+</sup>	C <sub>12</sub> H <sub>20</sub> N <sub>3</sub> O <sub>7</sub>	-3.54
	340.1108	340.1121	100.0	[M+Na] <sup>+</sup>	C <sub>12</sub> H <sub>19</sub> N <sub>3</sub> NaO <sub>7</sub>	-3.73
	356.0845	356.0860	25.0	[M+K] <sup>+</sup>	C <sub>12</sub> H <sub>19</sub> KN <sub>3</sub> O <sub>7</sub>	-4.23
	362.0926	362.0940	12.4	[M+2Na-H] <sup>+</sup>	C <sub>12</sub> H <sub>18</sub> N <sub>3</sub> Na <sub>2</sub> O <sub>7</sub>	-3.9
Schiff base/Amadori						
Schiff base/Amadori						
ESI (-ve)	<i>m/z</i>		I%	Adducts	Elemental composition	Rel. error [ppm]
	Exp.	Theor.				
Histidine						
M = 155	154.062	154.0623	12.5	[M-H] <sup>-</sup>	C <sub>6</sub> H <sub>8</sub> N <sub>3</sub> O <sub>2</sub>	2.26
	309.128	309.1309	0.1	[2M-H] <sup>-</sup>	C <sub>12</sub> H <sub>17</sub> N <sub>6</sub> O <sub>4</sub>	-9.47
	331.111	331.1134	0.2	[2M-2H+Na] <sup>-</sup>	C <sub>12</sub> H <sub>16</sub> N <sub>6</sub> NaO <sub>4</sub>	-7.16
Glucose						
M = 180	179.056	179.0562	19.1	[M-H] <sup>-</sup>	C <sub>6</sub> H <sub>11</sub> O <sub>6</sub>	1.32
	215.031	215.0322	1.8	[M+Cl] <sup>-</sup>	C <sub>6</sub> H <sub>12</sub> ClO <sub>6</sub>	-5.77
	359.116	359.1194	0.2	[2M-H] <sup>-</sup>	C <sub>12</sub> H <sub>23</sub> O <sub>12</sub>	-9.33
Schiff base/Amadori						
M = 317	316.114	316.1143	28.6	[M-H] <sup>-</sup>	C <sub>12</sub> H <sub>18</sub> N <sub>3</sub> O <sub>7</sub>	-0.87
	338.094	338.0961	0.2	[M-2H+Na] <sup>-</sup>	C <sub>12</sub> H <sub>17</sub> N <sub>3</sub> NaO <sub>7</sub>	-6.27
	633.235	633.2371	0.2	[2M-H] <sup>-</sup>	C <sub>24</sub> H <sub>37</sub> N <sub>6</sub> O <sub>14</sub>	-3.28
	655.217	655.2184	0.3	[2M-2H+Na] <sup>-</sup>	C <sub>24</sub> H <sub>36</sub> N <sub>6</sub> NaO <sub>14</sub>	-2.17



**Table S 5.3** Estimation of the yields<sup>a</sup> of Schiff base and ARP formed in milled glucose/histidine model system using <sup>1</sup>H NMR (in D<sub>2</sub>O and MeOD).

	D <sub>2</sub> O	MeOD
Schiff base	13.998% ± 0.023%	35.692% ± 1.134%
ARP	8.830% ± 2.451%	7.299% ± 1.567%
Free Histidine	77.171% ± 2.474%	57.008% ± 2.701%

<sup>a</sup> based on integration of aromatic protons. (See Figures S5.5 & S5.6)

**Table S 5.4** Elemental composition of all the ions observed in ball-milled glucose-histidine sample under ESI positive ionization mode.

<i>m/z</i>		Elemental composition	%I	Rel. error [ppm]
Exp.	Theor.			
<b>[M+H]<sup>+</sup></b>				
112.0865	112.0875	C <sub>5</sub> H <sub>10</sub> N <sub>3</sub>	1.0	-8.67
156.0763	156.0773	C <sub>6</sub> H <sub>10</sub> N <sub>3</sub> O <sub>2</sub>	48.7	-6.42
154.0968	154.0980	C <sub>7</sub> H <sub>12</sub> N <sub>3</sub> O	4.1	-8.03
155.1004 <sup>a</sup>	155.1014	C <sub>6</sub> H <sub>12</sub> N <sub>3</sub> O[ <sup>13</sup> C]	0.3	-6.39
198.0868	198.0879	C <sub>8</sub> H <sub>12</sub> N <sub>3</sub> O <sub>3</sub>	7.8	-5.38
199.0922 <sup>a</sup>	199.0932	C <sub>7</sub> H <sub>12</sub> N <sub>3</sub> O <sub>3</sub> [ <sup>13</sup> C]	0.2	4.92
190.0973	190.0980	C <sub>10</sub> H <sub>12</sub> N <sub>3</sub> O	3.3	-3.88
202.0968	202.0980	C <sub>11</sub> H <sub>12</sub> N <sub>3</sub> O	0.3	-6.12
238.1181	238.1192	C <sub>11</sub> H <sub>16</sub> N <sub>3</sub> O <sub>3</sub>	8.3	-4.48
256.1289	256.1297	C <sub>11</sub> H <sub>18</sub> N <sub>3</sub> O <sub>4</sub>	1.6	-3.24
274.1397	274.1403	C <sub>11</sub> H <sub>20</sub> N <sub>3</sub> O <sub>5</sub>	1.1	-2.17
275.1431 <sup>a</sup>	275.1437	C <sub>10</sub> H <sub>20</sub> N <sub>3</sub> O <sub>5</sub> [ <sup>13</sup> C]	1.3	-2.00
275.1419 <sup>b</sup>	275.1436	C <sub>10</sub> H <sub>20</sub> N <sub>3</sub> O <sub>5</sub> [ <sup>13</sup> C]	1.0	-6.36
282.1081	282.1090	C <sub>12</sub> H <sub>16</sub> N <sub>3</sub> O <sub>5</sub>	4.0	-3.17
300.1183	300.1196	C <sub>12</sub> H <sub>18</sub> N <sub>3</sub> O <sub>6</sub>	5.1	-4.2
318.1290	318.1301	C <sub>12</sub> H <sub>20</sub> N <sub>3</sub> O <sub>7</sub>	18.3	-3.54
319.1333 <sup>a</sup>	319.1335	C <sub>11</sub> H <sub>20</sub> N <sub>3</sub> O <sub>7</sub> [ <sup>13</sup> C]	2.4	-0.56
319.1324 <sup>b</sup>	319.1335	C <sub>11</sub> H <sub>20</sub> N <sub>3</sub> O <sub>7</sub> [ <sup>13</sup> C]	5.5	-3.38
473.2000	473.2004	C <sub>18</sub> H <sub>29</sub> N <sub>6</sub> O <sub>9</sub>	0.5	0.84
<b>[M+Na]<sup>+</sup></b>				
143.0317	143.0320	C <sub>4</sub> H <sub>8</sub> NaO <sub>4</sub>	0.4	-2.29
144.0348 <sup>b</sup>	144.0354	C <sub>3</sub> H <sub>8</sub> NaO <sub>4</sub> [ <sup>13</sup> C]	0.1	-4.05
133.0368	133.0378	C <sub>5</sub> H <sub>6</sub> N <sub>2</sub> NaO	0.5	-7.38
178.0582	178.0592	C <sub>6</sub> H <sub>9</sub> N <sub>3</sub> NaO <sub>2</sub>	51.7	-5.87
203.0523	203.0532	C <sub>6</sub> H <sub>12</sub> NaO <sub>6</sub>	27.4	-4.22
176.0784	176.0800	C <sub>7</sub> H <sub>11</sub> N <sub>3</sub> NaO	0.2	-8.98
205.0582	205.0589	C <sub>8</sub> H <sub>10</sub> N <sub>2</sub> NaO <sub>3</sub>	0.7	-3.47
220.0688	220.0698	C <sub>8</sub> H <sub>11</sub> N <sub>3</sub> NaO <sub>3</sub>	12.2	-4.59
221.0712 <sup>a</sup>	221.0731	C <sub>7</sub> H <sub>11</sub> N <sub>3</sub> NaO <sub>3</sub> [ <sup>13</sup> C]	1.0	8.73
250.0807	250.0810	C <sub>9</sub> H <sub>13</sub> N <sub>3</sub> NaO <sub>4</sub>	0.5	1.3
280.0889	280.0909	C <sub>10</sub> H <sub>15</sub> N <sub>3</sub> NaO <sub>5</sub>	0.3	-7.28
260.1003	260.1011	C <sub>11</sub> H <sub>15</sub> N <sub>3</sub> NaO <sub>3</sub>	0.2	-3.12
277.1045	277.1051	C <sub>11</sub> H <sub>16</sub> N <sub>3</sub> NaO <sub>4</sub>	0.3	2.34

278.1101	278.1117	C <sub>11</sub> H <sub>17</sub> N <sub>3</sub> NaO <sub>4</sub>	1.1	-5.66
296.1211	296.1222	C <sub>11</sub> H <sub>19</sub> N <sub>3</sub> NaO <sub>5</sub>	2.8	-3.85
297.1273 <sup>a</sup>	297.1278	C <sub>10</sub> H <sub>19</sub> N <sub>3</sub> NaO <sub>5</sub> [ <sup>13</sup> C]	1.1	1.71
297.1259 <sup>b</sup>	297.1262	C <sub>10</sub> H <sub>19</sub> N <sub>3</sub> NaO <sub>5</sub> [ <sup>13</sup> C]	1.1	1.03
333.1277	333.1287	C <sub>12</sub> H <sub>18</sub> N <sub>6</sub> NaO <sub>4</sub>	10.4	-3.07
322.1015	322.1015	C <sub>12</sub> H <sub>17</sub> N <sub>3</sub> NaO <sub>6</sub>	0.3	-0.01
340.1108	340.1121	C <sub>12</sub> H <sub>19</sub> N <sub>3</sub> NaO <sub>7</sub>	100.0	-3.73
341.1142 <sup>a</sup>	341.1155	C <sub>11</sub> H <sub>19</sub> N <sub>3</sub> NaO <sub>7</sub> [ <sup>13</sup> C]	39.3	-3.95
341.1144 <sup>b</sup>	341.1154	C <sub>11</sub> H <sub>19</sub> N <sub>3</sub> NaO <sub>7</sub> [ <sup>13</sup> C]	100	-3.00
358.1214	358.1226	C <sub>12</sub> H <sub>21</sub> N <sub>3</sub> NaO <sub>8</sub>	8.9	-3.45
495.1802	495.1815	C <sub>18</sub> H <sub>28</sub> N <sub>6</sub> NaO <sub>9</sub>	1.5	-2.72
502.1628	502.1649	C <sub>18</sub> H <sub>29</sub> N <sub>3</sub> NaO <sub>12</sub>	0.2	-4.17
MS/MS of <i>m/z</i> 340				
133.0370	133.0376	C <sub>5</sub> H <sub>6</sub> N <sub>2</sub> ONa	7.2	4.37
143.0307	143.0314	C <sub>4</sub> H <sub>8</sub> O <sub>4</sub> Na	6.6	5.09
146.0688	146.0695	C <sub>6</sub> H <sub>9</sub> N <sub>3</sub> Na	3.3	4.90
158.0679	158.0687	C <sub>7</sub> H <sub>9</sub> N <sub>3</sub> Na	18.1	5.16
176.0798	176.0808	C <sub>7</sub> H <sub>11</sub> N <sub>3</sub> ONa	5.6	5.57
178.0585	178.0594	C <sub>6</sub> H <sub>9</sub> N <sub>3</sub> O <sub>2</sub> Na	13.2	5.31
220.0680	220.0688	C <sub>8</sub> H <sub>11</sub> N <sub>3</sub> O <sub>3</sub> Na	100	3.68
260.0987	260.0990	C <sub>11</sub> H <sub>15</sub> N <sub>3</sub> O <sub>3</sub> Na	2.8	1.19
278.1091	278.1097	C <sub>11</sub> H <sub>17</sub> N <sub>3</sub> O <sub>4</sub> Na	5.4	2.07
296.1203	296.1210	C <sub>11</sub> H <sub>17</sub> N <sub>3</sub> O <sub>5</sub> Na	12.3	2.50
340.1101	340.1108	C <sub>12</sub> H <sub>19</sub> N <sub>3</sub> O <sub>7</sub> Na	58.8	1.96
<b>[M-H+2Na]<sup>+</sup></b>				
135.0024	135.0034	C <sub>3</sub> H <sub>5</sub> Na <sub>2</sub> O <sub>3</sub>	1.5	-7.46
165.0138	165.0140	C <sub>4</sub> H <sub>7</sub> Na <sub>2</sub> O <sub>4</sub>	0.3	-1.04
200.0403	200.0412	C <sub>6</sub> H <sub>8</sub> N <sub>3</sub> Na <sub>2</sub> O <sub>2</sub>	9.9	-4.45
225.0344	225.0351	C <sub>6</sub> H <sub>11</sub> Na <sub>2</sub> O <sub>6</sub>	1.1	-3.12
242.0515	242.0518	C <sub>8</sub> H <sub>10</sub> N <sub>3</sub> Na <sub>2</sub> O <sub>3</sub>	1.4	-1.05
272.0618	272.0623	C <sub>9</sub> H <sub>12</sub> N <sub>3</sub> Na <sub>2</sub> O <sub>4</sub>	0.2	-1.91
355.1076	355.1107	C <sub>12</sub> H <sub>17</sub> N <sub>6</sub> Na <sub>2</sub> O <sub>4</sub>	1.1	-8.64
362.0926	362.0940	C <sub>12</sub> H <sub>18</sub> N <sub>3</sub> Na <sub>2</sub> O <sub>7</sub>	12.4	-3.9
363.0962 <sup>a</sup>	363.0974	C <sub>11</sub> H <sub>18</sub> N <sub>3</sub> Na <sub>2</sub> O <sub>7</sub> [ <sup>13</sup> C]	8.8	-3.22
363.0959 <sup>b</sup>	363.0974	C <sub>11</sub> H <sub>18</sub> N <sub>3</sub> Na <sub>2</sub> O <sub>7</sub> [ <sup>13</sup> C]	15.6	-4.04
517.1630	517.1635	C <sub>18</sub> H <sub>27</sub> N <sub>6</sub> Na <sub>2</sub> O <sub>9</sub>	0.8	-0.95
<b>[M+K]<sup>+</sup></b>				

194.0320	194.0332	$C_6H_9KN_3O_2$	29.2	-6.1
219.0261	219.0271	$C_6H_{12}KO_6$	14.8	-4.54
236.0424	236.0437	$C_8H_{11}KN_3O_3$	3.0	-5.71
312.0947	312.0962	$C_{11}H_{19}KN_3O_5$	0.6	-4.73
349.1010	349.1027	$C_{12}H_{18}KN_6O_4$	3.6	-4.75
356.0845	356.0860	$C_{12}H_{19}KN_3O_7$	25.0	-4.23
357.0885 <sup>a</sup>	357.0894	$C_{11}H_{19}N_3KO_7[^{13}C]$	1.9	-2.41
357.0881 <sup>b</sup>	357.0894	$C_{11}H_{19}N_3KO_7[^{13}C]$	4.9	-3.53
399.0888	399.0905	$C_{12}H_{24}KO_{12}$	2.9	-4.22

<sup>a</sup>: Elemental composition of ions from ball-milled ( $^{13}C_2$ )-glucose-histidine.

<sup>b</sup>: Elemental composition of ions from ball-milled ( $^{13}C_3$ )-glucose-histidine.

**Table S 5.5** Elemental composition of all the ions observed in ball-milled glucose-histidine sample under ESI negative ionization mode.

<i>m/z</i>		Elemental composition	% I	Rel. error [ppm]
Exp.	Theor.			
113.0242	113.0245	C <sub>5</sub> H <sub>5</sub> O <sub>3</sub>	0.1	2.93
119.0345	119.0346	C <sub>4</sub> H <sub>7</sub> O <sub>4</sub>	0.3	0.56
123.0474 <sup>a</sup>	123.0479	H <sub>7</sub> O <sub>4</sub> [ <sup>13</sup> C] <sub>4</sub>	0.2	-3.68
128.0347	128.0348	C <sub>5</sub> H <sub>6</sub> NO <sub>3</sub>	0.1	-0.53
134.0714	134.0718	C <sub>7</sub> H <sub>8</sub> N <sub>3</sub>	0.2	-3.15
143.0348	143.0352	C <sub>6</sub> H <sub>7</sub> O <sub>4</sub>	0.1	2.56
146.0452	146.0453	C <sub>5</sub> H <sub>8</sub> NO <sub>4</sub>	0.2	-0.91
149.0450	149.0450	C <sub>5</sub> H <sub>9</sub> O <sub>5</sub>	0.2	0.01
154.0622 <sup>a</sup>	154.0626	H <sub>9</sub> O <sub>5</sub> [ <sup>13</sup> C] <sub>5</sub>	10.5	2.77
152.0821	152.0824	C <sub>7</sub> H <sub>10</sub> N <sub>3</sub> O	0.2	-1.89
161.0449	161.0450	C <sub>6</sub> H <sub>9</sub> O <sub>5</sub>	1	-0.61
167.0655 <sup>a</sup>	167.0659	H <sub>9</sub> O <sub>5</sub> [ <sup>13</sup> C] <sub>6</sub>	0.7	2.23
176.0816	176.0824	C <sub>9</sub> H <sub>10</sub> N <sub>3</sub> O	0.5	-4.47
180.0949 <sup>a</sup>	180.0958	C <sub>5</sub> H <sub>10</sub> N <sub>3</sub> O[ <sup>13</sup> C] <sub>4</sub>	0.3	-5.03
196.0725	196.0728	C <sub>8</sub> H <sub>10</sub> N <sub>3</sub> O <sub>3</sub>	35	1.45
198.0795 <sup>a</sup>	198.0801	C <sub>6</sub> H <sub>10</sub> N <sub>3</sub> O <sub>3</sub> [ <sup>13</sup> C] <sub>2</sub>	11.3	2.9
226.0815	226.0828	C <sub>9</sub> H <sub>12</sub> N <sub>3</sub> O <sub>4</sub>	2.1	-5.67
229.0927 <sup>a</sup>	229.0928	C <sub>6</sub> H <sub>12</sub> N <sub>3</sub> O <sub>4</sub> [ <sup>13</sup> C] <sub>3</sub>	6.5	-0.63
236.1023	236.1035	C <sub>11</sub> H <sub>14</sub> N <sub>3</sub> O <sub>3</sub>	0.7	-5.15
254.1110	254.1141	C <sub>11</sub> H <sub>16</sub> N <sub>3</sub> O <sub>4</sub>	0.1	-12.12
266.0724	266.0753	C <sub>9</sub> H <sub>13</sub> N <sub>3</sub> NaO <sub>5</sub>	0.2	-10.86
269.0851	269.0873	C <sub>9</sub> H <sub>17</sub> O <sub>9</sub>	0.4	-8.02
272.1229	272.1246	C <sub>11</sub> H <sub>18</sub> N <sub>3</sub> O <sub>5</sub>	1.9	-6.42
278.1435 <sup>a</sup>	278.1448	C <sub>5</sub> H <sub>18</sub> N <sub>3</sub> O <sub>5</sub> [ <sup>13</sup> C] <sub>6</sub>	0.7	-4.58
316.1142	316.1145	C <sub>12</sub> H <sub>18</sub> N <sub>3</sub> O <sub>7</sub>	28.6	-0.87
322.1350 <sup>a</sup>	322.1352	C <sub>6</sub> H <sub>17</sub> N <sub>3</sub> O <sub>7</sub> [ <sup>13</sup> C] <sub>6</sub>	20	0.47
338.0940	338.0961	C <sub>12</sub> H <sub>17</sub> N <sub>3</sub> NaO <sub>7</sub>	0.2	-6.27
344.114 <sup>a</sup>	344.1165	C <sub>6</sub> H <sub>17</sub> N <sub>3</sub> NaO <sub>7</sub> [ <sup>13</sup> C] <sub>6</sub>	0.2	-7.41
374.0709	374.0731	C <sub>12</sub> H <sub>18</sub> N <sub>3</sub> ClNaO <sub>7</sub>	0.5	-5.87
413.1255	413.1295	C <sub>15</sub> H <sub>25</sub> O <sub>13</sub>	0.1	-9.72
428.1239	428.1281	C <sub>15</sub> H <sub>23</sub> N <sub>3</sub> NaO <sub>10</sub>	0.1	-9.84
493.1633	493.1659	C <sub>18</sub> H <sub>26</sub> N <sub>6</sub> NaO <sub>9</sub>	0.4	-5.26
MS/MS of <i>m/z</i> 316				
134.0719	134.0720	C <sub>7</sub> H <sub>8</sub> N <sub>3</sub>	1.7	0.58

154.0616	154.0617	C <sub>6</sub> H <sub>8</sub> N <sub>3</sub> O <sub>2</sub>	10.4	0.33
176.0816	176.0824	C <sub>9</sub> H <sub>10</sub> N <sub>3</sub> O	2.8	4.46
196.0720	196.0722	C <sub>8</sub> H <sub>10</sub> N <sub>3</sub> O <sub>3</sub>	100	1.10
226.0807	226.0828	C <sub>9</sub> H <sub>12</sub> N <sub>3</sub> O <sub>4</sub>	8.3	9.20
272.1219	272.1220	C <sub>8</sub> H <sub>20</sub> N <sub>2</sub> O <sub>8</sub>	5.2	0.24
316.1128	316.1131	C <sub>12</sub> H <sub>18</sub> N <sub>3</sub> O <sub>7</sub>	17.4	0.87

<sup>a</sup>: Elemental composition of ions from ball-milled (U-<sup>13</sup>C<sub>6</sub>)-glucose-histidine.

**Table S 5.6** HRMS study of the milled and aged samples. The average relative intensities (n=2) of selected ions are compared at different aging time. (n.d. indicates not detected).

Entry	MF	Theor. $m/z$	Average experimental $m/z$ (n=2) (rel. error [ppm])			Average relative intensity $\pm$ SD (n=2)		
			Milling	Milling-Aging 1 day	Milling-Aging 3 days	Milling	Milling-Aging 1 day	Milling-Aging 3 days
	<b>[M+H]<sup>+</sup></b>							
1	C <sub>5</sub> H <sub>10</sub> N <sub>3</sub>	112.0875	112.0864 (9.52)	112.0866 (8.03)	112.0871 (4.01)	0.5333 $\pm$ 0.3300	0.1500 $\pm$ 0.0500	0.5000 $\pm$ 0.1000
2	C <sub>7</sub> H <sub>12</sub> N <sub>3</sub> O	154.0980	154.0966 (8.87)	154.0965 (10.06)	154.0978 (0.97)	2.7000 $\pm$ 1.0198	0.1000 $\pm$ 0.0000	0.2500 $\pm$ 0.0500
3	C <sub>6</sub> H <sub>10</sub> N <sub>3</sub> O <sub>2</sub>	156.0773	156.0762 (7.26)	156.0765 (5.13)	156.0771 (1.28)	40.1000 $\pm$ 9.2891	13.4000 $\pm$ 2.8000	72.9500 $\pm$ 14.0500
4	C <sub>8</sub> H <sub>12</sub> N <sub>3</sub> O <sub>3</sub>	190.0980	190.0968 (6.49)	190.0969 (5.79)	190.0975 (2.89)	2.4667 $\pm$ 0.7409	1.2000 $\pm$ 0.1000	4.4500 $\pm$ 1.4500
5	C <sub>10</sub> H <sub>12</sub> N <sub>3</sub> O	198.0879	198.0864 (7.57)	198.0862 (8.58)	198.0875 (2.02)	5.2333 $\pm$ 1.9431	0.2000 $\pm$ 0.0000	0.4000 $\pm$ 0.1000
6	C <sub>11</sub> H <sub>12</sub> N <sub>3</sub> O	202.0980	202.0966 (7.09)	202.0976 (2.23)	202.0978 (0.74)	0.2000 $\pm$ 0.0816	0.1500 $\pm$ 0.0500	0.4500 $\pm$ 0.1500
7	C <sub>11</sub> H <sub>16</sub> N <sub>3</sub> O <sub>3</sub>	238.1192	238.1177 (6.44)	238.1179 (5.46)	238.1187 (2.31)	6.2000 $\pm$ 1.9511	2.6000 $\pm$ 0.3000	9.8000 $\pm$ 3.2000
8	C <sub>11</sub> H <sub>18</sub> N <sub>3</sub> O <sub>4</sub>	256.1297	256.1283 (5.60)	256.1287 (3.90)	256.1292 (1.95)	1.1333 $\pm$ 0.4110	0.5500 $\pm$ 0.0500	1.7500 $\pm$ 0.5500
9	C <sub>11</sub> H <sub>20</sub> N <sub>3</sub> O <sub>5</sub>	274.1403	274.1392 (4.01)	274.1394 (3.28)	274.1401 (0.73)	0.8000 $\pm$ 0.2944	0.2000 $\pm$ 0.0000	1.0500 $\pm$ 0.3500
10	C <sub>12</sub> H <sub>16</sub> N <sub>3</sub> O <sub>5</sub>	282.1090	282.1075 (5.44)	282.1080 (3.54)	282.1089 (0.35)	2.9667 $\pm$ 0.9534	2.0000 $\pm$ 0.2000	7.5500 $\pm$ 2.3500
11	C <sub>12</sub> H <sub>18</sub> N <sub>3</sub> O <sub>6</sub>	300.1196	300.1178 (5.89)	300.1173 (7.50)	300.1194 (0.67)	3.7333 $\pm$ 1.1898	2.3500 $\pm$ 0.2500	8.6000 $\pm$ 2.8000
12	C <sub>12</sub> H <sub>20</sub> N <sub>3</sub> O <sub>7</sub>	318.1301	318.1284 (5.24)	318.1291 (2.99)	318.1303 (-0.63)	16.0333 $\pm$ 4.1588	11.1500 $\pm$ 1.5500	59.9500 $\pm$ 21.0500
13	C <sub>18</sub> H <sub>29</sub> N <sub>6</sub> O <sub>9</sub>	473.1996	473.1988 (1.62)	473.1991 (0.95)	473.2006 (-2.01)	0.5333 $\pm$ 0.0471	0.5000 $\pm$ 0.1000	2.6000 $\pm$ 0.9000
	<b>[M+Na]<sup>+</sup></b>							
14	C <sub>5</sub> H <sub>6</sub> N <sub>2</sub> NaO	133.0378	133.0368 (7.77)	133.0371 (5.26)	133.0377 (0.38)	0.5000 $\pm$ 0.0816	0.3000 $\pm$ 0.0000	0.3000 $\pm$ 0.0000
15	C <sub>4</sub> H <sub>8</sub> NaO <sub>4</sub>	143.0320	143.0308 (8.16)	n.d.	n.d.	0.3667 $\pm$ 0.0471	n.d.	n.d.
16	C <sub>7</sub> H <sub>11</sub> N <sub>3</sub> NaO	176.0800	176.0777 (13.25)	n.d.	n.d.	0.2667 $\pm$ 0.0943	n.d.	n.d.
17	C <sub>6</sub> H <sub>9</sub> N <sub>3</sub> NaO <sub>2</sub>	178.0592	178.0580 (6.93)	178.0582 (5.62)	178.0588 (2.53)	44.9333 $\pm$ 7.1760	24.0000 $\pm$ 1.4000	26.4500 $\pm$ 4.4500
18	C <sub>6</sub> H <sub>12</sub> NaO <sub>6</sub>	203.0532	203.0518 (6.89)	203.0520 (5.91)	203.0524 (3.69)	29.6000 $\pm$ 4.3688	20.9000 $\pm$ 4.2000	9.8000 $\pm$ 0.9000
19	C <sub>8</sub> H <sub>10</sub> N <sub>2</sub> NaO <sub>3</sub>	205.0589	205.0607 (-8.78)	205.0574 (7.56)		0.5333 $\pm$ 0.1247	0.3000 $\pm$ 0.1000	
20	C <sub>8</sub> H <sub>11</sub> N <sub>3</sub> NaO <sub>3</sub>	220.0698	220.0683 (6.97)	220.0687 (5.00)	220.0693 (2.27)	12.3333 $\pm$ 0.9031	0.8000 $\pm$ 0.1000	0.5000 $\pm$ 0.0000
21	C <sub>9</sub> H <sub>13</sub> N <sub>3</sub> NaO <sub>4</sub>	250.0804	250.0807 (-1.33)	250.0796 (3.40)	250.0800 (1.60)	0.3000 $\pm$ 0.1414	0.3000 $\pm$ 0.0000	0.4000 $\pm$ 0.0000
22	C <sub>11</sub> H <sub>15</sub> N <sub>3</sub> NaO <sub>3</sub>	260.1011	260.1000 (4.36)	260.1001 (3.65)	260.1014 (-0.96)	0.2333 $\pm$ 0.0471	0.2000 $\pm$ 0.0000	0.2000 $\pm$ 0.0000
23	C <sub>11</sub> H <sub>16</sub> N <sub>3</sub> NaO <sub>4</sub>	277.1039	277.1038 (0.48)	n.d.	n.d.	0.4000 $\pm$ 0.2944	n.d.	n.d.
24	C <sub>11</sub> H <sub>17</sub> N <sub>3</sub> NaO <sub>4</sub>	278.1117	278.1099 (6.35)	278.1084 (11.87)	278.1119 (-0.54)	1.0000 $\pm$ 0.1414	0.2000 $\pm$ 0.0000	0.2000 $\pm$ 0.0000

25	C <sub>10</sub> H <sub>15</sub> N <sub>3</sub> NaO <sub>5</sub>	280.0909	280.0883 (9.28)	n.d.	280.0922 (-4.46)	0.3000±0.0816	n.d.	0.1000±0.0000
26	C <sub>11</sub> H <sub>19</sub> N <sub>3</sub> NaO <sub>5</sub>	296.1222	296.1207 (5.18)	296.1218 (1.52)	296.1230 (-2.87)	2.8667±0.4922	0.3000±0.0000	0.3500±0.0500
27	C <sub>12</sub> H <sub>17</sub> N <sub>3</sub> NaO <sub>6</sub>	322.1015	322.1007 (2.38)	322.1006 (2.79)	322.1017 (-0.47)	0.3333±0.0471	0.6500±0.0500	1.1000±0.1000
28	C <sub>12</sub> H <sub>18</sub> N <sub>6</sub> NaO <sub>4</sub>	333.1287	333.1270 (5.20)	333.1279 (2.40)	333.1288 (-0.30)	7.5667±2.7741	4.5500±1.4500	6.0500±1.2500
29	C <sub>12</sub> H <sub>19</sub> N <sub>3</sub> NaO <sub>7</sub>	340.1121	340.1104 (5.00)	340.1113 (2.35)	340.1125 (-1.03)	100.0000±0.0000	100.0000±0.0000	100.0000±0.0000
30	C <sub>12</sub> H <sub>21</sub> N <sub>3</sub> NaO <sub>8</sub>	358.1226	358.1204 (6.05)	358.1218 (2.23)	358.1200 (7.12)	6.7333±2.5850	2.6000±0.6000	1.2000±0.3000
31	C <sub>18</sub> H <sub>28</sub> N <sub>6</sub> NaO <sub>9</sub>	495.1815	495.1796 (3.90)	495.1815 (0.00)	495.1821 (-1.11)	1.3667±0.1247	0.8500±0.1500	1.2500±0.0500
32	C <sub>18</sub> H <sub>29</sub> N <sub>3</sub> NaO <sub>12</sub>	502.1649	502.1631 (3.65)	502.1640 (1.69)	n.d.	0.2000±0.0000	1.6500±0.3500	n.d.

**Table S 5.7**  $^{13}\text{C}$  NMR (quantitative) peak assignment and integration.

Entry	ppm	Assignment <sup>[b]</sup>	Integrated peak area <sup>[a]</sup>		
			Glc	Milled	Milled-Aged (3 days)
1	102.50	Ama- $\beta$ -f-C2	n.d.	11	13
2	100.83	Ama- $\beta$ -p-C2	n.d.	4	5
<b>3</b> <sup>[c]</sup>	<b>97.41</b>	<b>Glc-<math>\beta</math>-p-C1</b>	<b>24</b>	<b>11</b>	<b>5</b>
4	96.65	Ama or Schiff-C2	n.d.	6	7
5	95.93	Ama or Schiff-C2	n.d.	2	2
<b>6</b>	<b>92.73</b>	<b>Glc-<math>\alpha</math>-p-C1</b>	<b>27</b>	<b>8</b>	<b>2</b>
7	89.97	Schiff- $\alpha$ -p-C1	n.d.	2	n.d.
8	83.59	Ama or Schiff-C3&C5	n.d.	11	13
9	82.68	Ama or Schiff-C3&C5	n.d.	5	7
10	81.91	Ama or Schiff-C3&C5	n.d.	12	14
<b>11</b>	<b>77.17</b>	<b>Glc-<math>\beta</math>-p-C3&amp;C5</b>	<b>50</b>	<b>24</b>	<b>8</b>
12	76.01	Schiff- $\alpha$ -p-C5	n.d.	12	11
13	64.09	Ama-C6	n.d.	11	12
14	63.30	Schiff-C6	n.d.	7	9
<b>15</b>	<b>61.71</b>	<b>Glc-<math>\alpha</math>&amp;<math>\beta</math>-p-C6</b>	<b>53</b>	<b>22</b>	<b>9</b>
16	61.25	Ama-C6	n.d.	12	13
17	53.20	Ama-C1	n.d.	5	8
18	52.48	Ama-C1	n.d.	5	6
19	51.89	Ama-C1	n.d.	9	12

<sup>[a]</sup>: the areas are normalized to the solvent  $\text{DSMO-}d_6$ . The integer is reported. N.d. indicates not detected.

<sup>[b]</sup>: assignment to glucose was based on: Hopley, P., Howarth, O. and Ibbett, R.N., 1996.  $^1\text{H}$  and  $^{13}\text{C}$  NMR shifts for aldopyranose and aldofuranose monosaccharides: Conformational analysis and solvent dependence. *Magnetic resonance in chemistry*, 34(10), pp.755-760.

assignment to ARP was based on: Röper, H., Röper, S., Heyns, K. and Meyer, B., 1983. NMR spectroscopy of N-(1-deoxy-D-fructos-1-yl)-L-amino acids ("fructose-amino acids"). *Carbohydrate Research*, 116(2), pp.183-195.

assignment to Schiff base was based on: Xing, H. and Yaylayan, V., 2020. Mechanochemical generation of Schiff bases and Amadori products and utilization of diagnostic MS/MS fragmentation patterns in negative ionization mode for their analysis. *Carbohydrate Research*, p.108091.

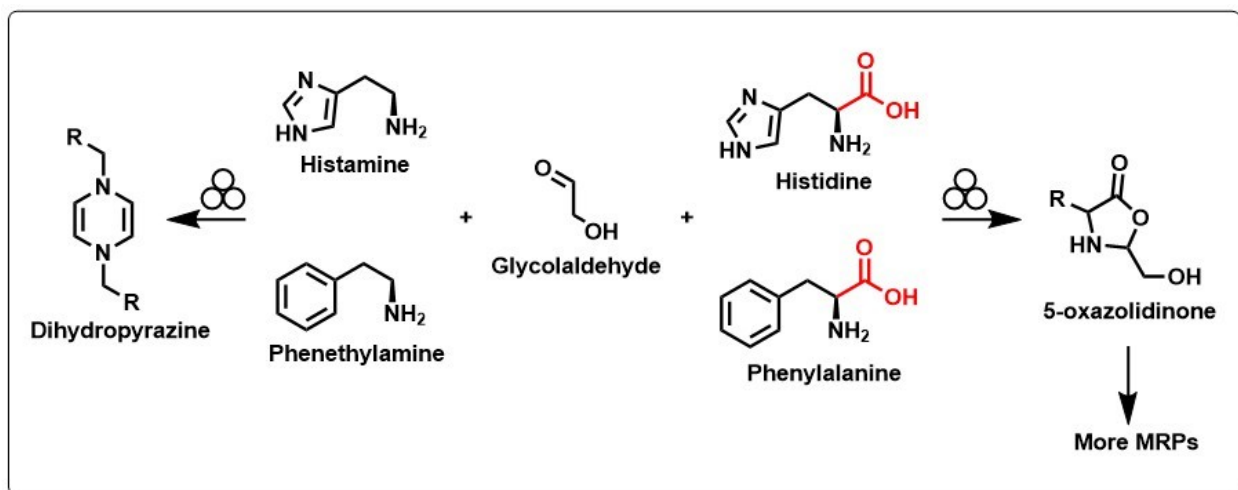
<sup>[c]</sup>: Unequivocal assignment to glucose were highlighted in bold.

## Connecting paragraph

In chapter 5, we observed an enhanced reactivity associated with the mechanochemical reaction mixtures compared to non-milled control. Upon subsequent heat treatment, the mechanochemical reaction mixtures started reacting at a lower temperature and generating more browning and pyrazine-rich volatiles relative to non-milled samples. Those observations were rationalized based on a detailed investigation of the chemical composition of the ball-milled glucose-histidine mixtures using ESI/qToF/MS/MS where the decarboxylation and retro-aldolization at C2-C3 of glucose were identified as the most important transformations during ball milling. In chapter 6, we provided the mechanistic insight into the mechanochemistry of the Maillard reaction through the investigation of model systems containing glycolaldehyde and histidine or phenylalanine as well as their corresponding amines (histamine and phenethylamine).

Chapter 6 was published in *European Food Research and Technology*: Xing, H., & Yaylayan, V. (2021). Insight into the mechanochemistry of the Maillard reaction: Degradation of Schiff bases via 5-oxazolidinone intermediate, **247**, 1095-1106. *European Food Research and Technology*.

## Chapter 6 Insight into the mechanochemistry of the Maillard reaction: Degradation of Schiff bases via 5-oxazolidinone intermediate



## 6.1 Abstract

With the emergence of mechanochemistry as a fast and efficient synthetic methodology, we reported earlier that ball milling of glucose with histidine leads to the formation of reaction mixtures rich in Schiff bases. Upon subsequent thermal treatments, these mixtures exhibited enhanced reactivity generating more browning and pyrazine-rich volatiles, compared to non-milled samples. To rationalize these observations, we further investigated the mechanochemistry of the Maillard reaction using glycolaldehyde and histidine or phenylalanine as model systems. The conversion of Schiff bases into reactive 5-oxazolidinone in these model systems was proposed as the basis of the observed enhanced reactivity. Furthermore, the formation of 5-oxazolidinone in the ball-milled samples was verified through direct spectroscopic observation of its characteristic FTIR absorption band between  $1780\text{ cm}^{-1}$  and  $1810\text{ cm}^{-1}$  and through the identification of its specific degradation products. The important role of the carboxylic acid moiety in enabling the formation of reactive 5-oxazolidinone intermediate that facilitates its subsequent decarboxylation and formation of downstream degradation products such as dihydropyrazines and Strecker aldehydes were elucidated.

**Keywords:** Mechanochemistry, Maillard reaction, Schiff base, 5-oxazolidinone, Dihydropyrazine, High-resolution mass spectrometry.

## 6.2 Introduction

Understanding the Maillard reaction has been of great interest in areas as diverse as human pathology and food chemistry for more than a century. [1] It is often referred to as a complex reaction cascade initiated by the condensation of an amino group with an  $\alpha$ -hydroxy carbonyl moiety of a reducing sugar leading to the formation of Schiff bases. [2] The commonly accepted reaction pathway was proposed by Hodge in 1953, [3] involving the Amadori rearrangement as a key step in the early stage of the reaction. The rearrangement produces a so-called Amadori compound, which is the first stable intermediate in this sequence. Subsequent degradation of the Amadori compound yields a complex mixture of aroma active carbocyclic and heterocyclic compounds and the characteristic yellow-brown oligomers and polymers. [3] However, the critical role of Schiff bases for initiating and propagating the Maillard reaction has attracted less attention since the Amadori rearrangement preferentially occurs under conditions commonly encountered in food systems such as intermediate moisture content and slightly acidic pH (5-7). [3, 4] Before the formation of the Amadori compound, the initially formed Schiff bases can also undergo several transformations depending on the reaction conditions. For example, the base-catalyzed transamination, [5-7] the intramolecular cyclization with either the side chain or the carboxylic moiety of the amino acid leading to, for example, 5-oxazolidinone moiety, [4, 8-10] and the Namiki pathway. [11, 12] We have recently reported that ball milling of glucose with the basic amino acids such as histidine selectively leads to the formation of mixtures rich in Schiff bases; [13] these mixtures were found to have enhanced thermal reactivity generating more browning and pyrazine rich volatiles during subsequent thermal treatments and as such can be considered as potential flavor precursor systems. [14] Other degradation products were also detected in relatively low intensities in the ball-milled reaction mixtures based on high-resolution mass spectrometric (HRMS) analysis. These studies have indicated that these Schiff base-rich mixtures undergo two major degradation pathways one initiated by the retro-aldol reaction at C2-C3 position and the other through decarboxylation. The former pathway leads to the formation of the two and four carbon-containing sugar fragments, where a C2 fragment is attached to histidine (structurally equivalent to the glycolaldehyde-histidine condensation adduct) and a C4 sugar fragment with no amino acid residues attached. The HRMS analysis of these mixtures has indicated that the intensities of histidine-glycolaldehyde adducts have decreased during the subsequent room-temperature storage experiments (known as aging), accompanied by a significant increase in

browning. [14] Furthermore, the decarboxylation pathway was also found to be one of the prominent chemical transformations in these mixtures. These observations were considered to be the main contributing factors to the enhanced thermal reactivity and particularly, the diose-histidine condensation product was envisaged as a potent browning precursor. [14]

In this study, we selected histidine-glycolaldehyde and phenylalanine-glycolaldehyde model systems to gain more detailed mechanistic insight into the mechanochemistry of the Maillard reaction.

## **6.3 Material and methods**

### **6.3.1 Materials**

The paraformaldehyde, glycolaldehyde dimer, histamine, and 20 L-amino acids including glycine, L-alanine, L-valine, L-leucine, L-isoleucine, L-methionine, L-proline, L-phenylalanine, L-tryptophan, L-tyrosine, L-serine, L-threonine, L-cystine, L-glutamine, L-asparagine, L-glutamine acid, L-aspartic acid, L-lysine, L-histidine, and L-arginine were purchased from Sigma-Aldrich Chemical Co. (Oakville, Ontario, Canada). The  $^{15}\text{N}$ - and  $^{13}\text{C}_1$ -phenylalanine (99%) was purchased from Cambridge Isotope Laboratories (Andover, MI). All other chemicals and reagents were of analytical grade from Fisher Scientific. Ultrapure water was used throughout the study. All materials were used without further purification.

### **6.3.2 Sample preparation**

Samples (30 mg powder) were prepared through ball milling at ambient temperature. The glycolaldehyde dimer and L-histidine, L-phenylalanine, histamine, and phenethylamine mixture were at a 1:2 molar ratio. The paraformaldehyde and 20 amino acids were mixed at a ratio of 1:1. All mechanochemical reactions were conducted in the stainless-steel grinding jars (10 mL) with 2 steel balls (3.2 mm in diameter; ball/sample ratio  $\sim$ 32:1) for creating inner friction. The jars were seated in the Retsch Mixer Mill (MM 400, Newtown, PA, US) that performs radial oscillations in a horizontal position without coolant (the external jar temperature was  $\sim$  25 °C) at a frequency of 30 Hz for 30 minutes. Samples collected after milling were stored at  $-20^\circ\text{C}$  for further analysis.

### 6.3.3 FTIR

The solid reaction mixtures from ball milling were directly applied and tightly pressed against a single-bounce diamond attenuated total reflectance (ATR) crystal and scanned over the spectral range of 4000 – 500  $\text{cm}^{-1}$  at room temperature. The spectra were recorded on a Bruker Alpha-P FTIR spectrometer (Bruker Optic GmbH, Ettlingen, Germany) equipped with a deuterated triglycine sulfate (DTGS) detector, a temperature-controlled ATR crystal, and a pressure application device for solid samples. A total of 32 scans at 4  $\text{cm}^{-1}$  resolution were co-added. Processing of the FTIR data was performed using Bruker OPUS 4.2 software (Bruker, Germany).

### 6.3.4 Electrospray ionization/quadrupole time of flight/mass spectrometry (ESI/qTOF/MS)

The diluted sample solutions (1  $\mu\text{L}$ ; 0.1 mg/ml) in water/ methanol (10%/ 90%) were supplied to the source directly via a syringe. The analysis was performed on a Bruker Maxis Impact qTOF mass spectrometer (Bruker Daltonics, Bremen, Germany) operated in positive ion modes. Instrument calibration was performed using sodium formate clusters. The electrospray interphase settings were as follows: nebulizer pressure, 0.6 bar; drying gas, 4 L/min; temperature, 180  $^{\circ}\text{C}$ ; and capillary voltage, 4500 V. The full scan MS range was from  $m/z$  50 to 800. The data were analyzed using Bruker Compass Data Analysis software (version 4.2), R language (version 3.6.3), and Microsoft Excel (2009). Each sample was analyzed in duplicates from independent trials.

## 6.4 Results and Discussion

Previous studies on mechanochemically induced Maillard reaction have indicated that the nature of the side chain of the amino acids determined the relative ratio of Schiff base to Amadori products. [13, 14] Amino acids with basic side chains generated more Schiff bases than Amadori products, and amino acids with neutral side chains generated comparable intensities of the diagnostic ions of Schiff bases and Amadori products. [13] In this study, we have selected L-histidine and L-phenylalanine as model amino acids for their ability to generate Schiff bases under ball milling conditions.

#### **6.4.1 Data mining: Comparing the specific masses generated by equivalent chemical transformations from the amino acid side chains in L-histidine and L-phenylalanine**

Ball milling (30 min/ 30 Hz) of glycolaldehyde with L-histidine or L-phenylalanine at room temperature rapidly leads to color development in both samples. The MS scan of the milled samples generated extremely complex spectra with over 1000 masses detected. (Figure 6.1) A data analysis pipeline (Figure S6.1) was specifically developed to analyze these complex reaction mixtures and to extract masses related to amino acid side chain-specific reaction products generated by equivalent chemical transformations in histidine and phenylalanine. This strategy was achieved through mass corrections based on the difference in the masses between the two side chains. (Figure S6.1). Due to the complexity of the systems, only masses with one and two side chain equivalent mass differences were extracted. Furthermore, due to the presence of heteroatoms, that significantly increases the number of possible molecular formulas, [15] the number of nitrogen atoms extracted from the histidine model system was limited to 3 and 6 and for the phenylalanine model system to 1 and 2. (see Figure S6.1 for details) Following this analytical pipeline, we were able to extract 97 masses generated by equivalent chemical transformations in histidine and phenylalanine model systems. (Table S6.1) Reaction pathways have been proposed (Figures 6.2) based on the extracted mass list shown in Table S6.1 and the proposed pathways can be considered common to both histidine and phenylalanine model systems.

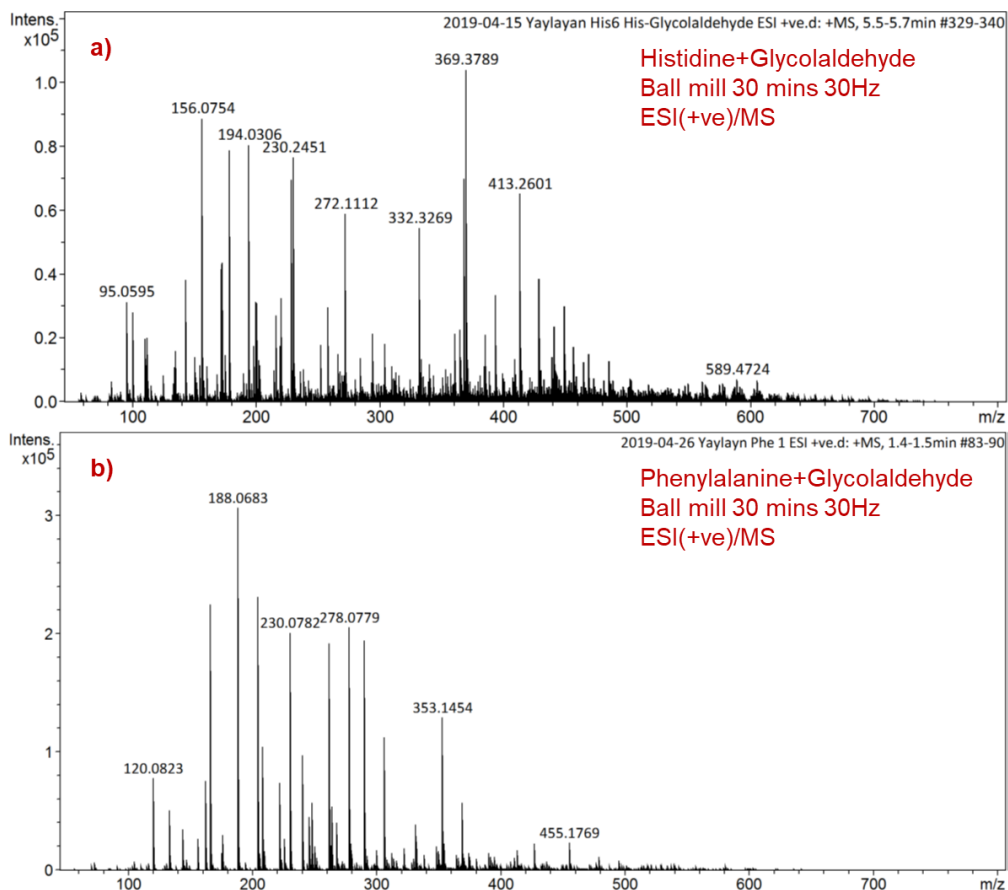


**Figure 6.1** MS spectra of ball-milled (30 min, 30 Hz) (a) histidine-glycolaldehyde and (b) phenylalanine-glycolaldehyde.

**Table 6.1** The number of incidences observed of selected transformations in both histidine- and phenylalanine- glycolaldehyde (GA) model systems.

Transformations	Formula	Monoisotopic mass	Incidences
+ GA-H <sub>2</sub> O	C <sub>2</sub> H <sub>2</sub> O	42.01059	33
± GA	C <sub>2</sub> H <sub>4</sub> O <sub>2</sub>	60.02115	28
± H <sub>2</sub> O	H <sub>2</sub> O	18.01056	20
+ 2GA-H <sub>2</sub> O	C <sub>4</sub> H <sub>6</sub> O <sub>3</sub>	102.0317	21
+ AA-H <sub>2</sub> O	C <sub>6</sub> H <sub>7</sub> N <sub>3</sub> O (Histidine-H <sub>2</sub> O)	137.0589	11
	C <sub>9</sub> H <sub>9</sub> NO (Phenylalanine-H <sub>2</sub> O)	147.0684	
Decarboxylation	CO <sub>2</sub>	43.9898	8
± 2GA	C <sub>4</sub> H <sub>8</sub> O <sub>4</sub>	120.0423	7

+ addition; - elimination; AA amino acid

### 6.4.2 Exploratory analysis

To obtain chemical transformation-specific information, the extracted masses were subjected to mass difference analysis where every mass in the list was compared to every other mass for differences. If a known mass difference occurred between two masses, such as  $\Delta m/z$  at 18.01056, the pair was considered to represent a hypothetical chemical transformation, in this case, dehydration/hydration reactions. The incidences of each transformation type were counted and used to indicate the importance of each transformation occurring in the reaction mixture. (Table 6.1) In this study, we identified seven types of common transformations such as the addition of amino acids or glycolaldehyde/glycolaldehyde dimer, decarboxylation, and dehydration. (Table 6.1) The seven transformations listed in Table 6.1 can successfully connect 72 masses out of 97 masses listed in Table S6.1, of which 58 masses belonged to clusters with more than 5 members as exemplified in Figure S6.2 for the histidine model system. The paired masses with known mass differences were further validated by their mass defects to eliminate false positives. For example, a pair of masses that have  $\Delta m/z$  at 18.01056 should also have the same Kendrick mass defect when scaled by water. [16] When visualized in the Kendrick mass ( $H_2O$ ) plot, those (de)hydration masses should be lined up horizontally. [16] Similarly, for a mass difference of  $\Delta m/z$  at 42.01059 ( $C_2H_2O$ ) representing glycolaldehyde addition reactions, mathematically, the second mass should be able to be defined by vector addition to the first mass at (42, 0.0142). When visualized in the Kendrick mass ( $H_2O$ ) plot, all the masses related to glycolaldehyde addition can be lined up at a slope of 0.0003 and a Kendrick mass difference at 42. (Figure S6.3a) Other transformations can also be corrected and validated in the same way. Since the addition of glycolaldehyde through condensation was identified as a major transformation in both histidine- and phenylalanine-glycolaldehyde model systems, (Table 6.1) those masses are highlighted in green and visualized in Figure S6.3a.

Furthermore, a mass difference network (Figure S6.2) was also constructed using the seven transformations shown in Table 6.1 where each node represents one  $m/z$  value (from Table S6.1), and the edges between the two nodes are one of the predefined transformations (from Table 6.1). For example, the histidine has been indicated in the graph at  $m/z$  156 (protonated), and  $m/z$  178 (sodiated). The relationship between the histidine addition (red edges), the decarboxylation (blue edges), and the addition/ elimination of glycolaldehyde or water (grey edges) can be visualized from the mass difference network. For example, the mass difference between  $m/z$  238 and  $m/z$  375

is 137, which is considered as histidine addition through condensation. This provided a holistic overview of the transformations that had occurred in a mechanochemical reaction mixture.

Finally, the assigned elemental compositions for the 97 masses were examined and visualized for the histidine model system through the Van Krevelen diagrams. [16] (Figure S6.3b) By plotting the elemental composition of each  $m/z$  based on their O/C and H/C ratios, it serves as a quick diagnostic tool to examine the accuracy of the automated elemental composition assignments. As expected, the results agree with the mass difference analysis. For example, the masses involved in the hypothetical glycolaldehyde addition appear in lines, which has been highlighted in circles in Figure S6.3b. Overall, through the exploratory analysis by mass differences, mass defects, and Van Krevelen diagrams, it can be concluded that the main reaction type that was common between the ball-milled histidine- and phenylalanine-glycolaldehyde model systems were the glycolaldehyde addition reactions, although, the importance of decarboxylation reaction cannot be overlooked, despite its relatively low incidence values.

Analyzing the high-resolution MS data reported in Tables 6.2 and S1 for the masses involved in the common transformations shown in Table 6.1, appropriate structures were proposed and used to construct common reaction pathways shown in Figure 6.2.

### 6.4.3 Glycolaldehyde-amino acid model systems

The initially formed important intermediates, the Schiff bases and Amadori products, from the interaction of amino acids with sugars are isomeric in nature and cannot be distinguished by their elemental composition (HRMS data). (see Figure 6.2) Furthermore, for a complex reaction mixture such as glycolaldehyde-histidine, some targeted masses only occurred in relatively low intensities that made the application of MS/MS for structural elucidation not feasible. Instead, a strategy based on the utilization of unique downstream reaction products derived from these isomeric intermediates was employed, such as the reaction products shown in Figure 6.2 in dashed boxes.

The Schiff bases can either rearrange into Amadori products or undergo reversible dimerization into 1,4-dioxane derivatives or undergo intramolecular cyclization to form 5-oxazolidinone. [4, 8] On the other hand, the Amadori products can also dimerize into dihydropyrazine derivatives but cannot undergo intramolecular cyclization into 5-oxazolidinone. Consequently, the dimerization

products along with 5-oxazolidinone and its degradation products were used as unique markers for the formation of Schiff bases and Amadori compounds.

According to our previous study, [13] ball-milled glucose with histidine or phenylalanine generated more Schiff bases than Amadori products, and the two isomers were the main observed reaction products. [14] However, replacing glucose with glycolaldehyde, significantly increased the number of reaction products detected. It is reasonable to assume that these products were generated from the degradation of the Schiff bases rather than that of the Amadori products (see also section 3.4) due to the fact that the Schiff bases were the major products in such mixtures. [13, 14] Several pathways have been proposed in the literature for the chemical transformations of Schiff bases including (i) transamination under basic pH, [7] (ii) side chain cyclization, [17] (iii) 5-oxazolidinone formation. [4, 8] In the case of phenylalanine, the post-Schiff base transformations to produce side chain specific reaction products (see section 3.1) can be limited only to 5-oxazolidinone formation and dimerization reactions, [4] considering the absence of nucleophilic centers in the side chain. Generally, if the reacting sugar is a hexose, the initially formed Schiff bases are expected to undergo cyclization to form more stable glycosylamine or undergo Amadori rearrangement. In the case of glycolaldehyde, where cyclization is not possible to generate a stable ring system, we observed instead of the formation of *N*-substituted 1,4-dioxane at  $[M+H]^+$  395.1679 from the dimerization of the Schiff bases. (Figure 6.2) On the other hand, dimerization of the Amadori compound followed by dehydration generated the dihydropyrazine at  $[M+H]^+$  381.1271 (Figure 6.2). [18] By observing the formation of these two dimers (having different *m/z* and elemental compositions), we were able to tentatively confirm the presence of both the Schiff base and its Amadori compound in the reaction mixtures. Furthermore, as an estimation, the relative intensities of the Schiff base dimers were higher than their Amadori counterparts (~7.7% and ~5.3% for histidine; ~2.5% and ~0.4% for phenylalanine) in agreement with our previous report. [13] (Table 6.2).

As mentioned above, in these reaction mixtures some of the monomeric Schiff bases could also exist as isomeric 5-oxazolidinones promoting subsequent decarboxylation reactions leading to the formation of *N*-protonated azomethine ylides. These ylides are known to undergo a 1,2-prototropic shift leading to the formation of two decarboxylated and isomeric Schiff bases – Schiff base A and B. [4, 8] (Figure 6.2) The Schiff base A, if formed, can rearrange into its Amadori product followed

by dimerization to form the decarboxylated dihydropyrazine observed at  $[M+H]^+$  271.1660, this dimer cannot be generated from Schiff base B. The Schiff base B, on the other hand, can hydrolyze easily to generate Strecker aldehydes at  $[M+Na]^+$  133.0369 (His) and  $[M+Na]^+$  143.0477 (Phe). However, oxidation of the 1,2-enaminol and subsequent 5-oxazolidinone assisted decarboxylation and hydrolysis can also lead to Strecker aldehyde formation. (Figure 6.2) One of the reaction intermediates in this route can be detected at  $[M+H]^+$  152.0814 (His) and 162.0919 (Phe), (Figure 6.2) Elementally, this ion also represents the 3-oxazoline which is an important cyclic intermediate leading to Strecker aldehydes that is favored under dry conditions. [19] The Schiff base B can also undergo dehydration leading to the dehydrated reaction product at  $[M+Na]^+$  158.0690 (His) and 168.0809 (Phe), which cannot be derived from the Schiff base A. Therefore, this dehydrated product was considered as the marker compound for Schiff base B. Isotope labeling experiments with  $^{15}\text{N}$ -labeled phenylalanine provided further confirmation for their molecular formulae. (Table 6.3)

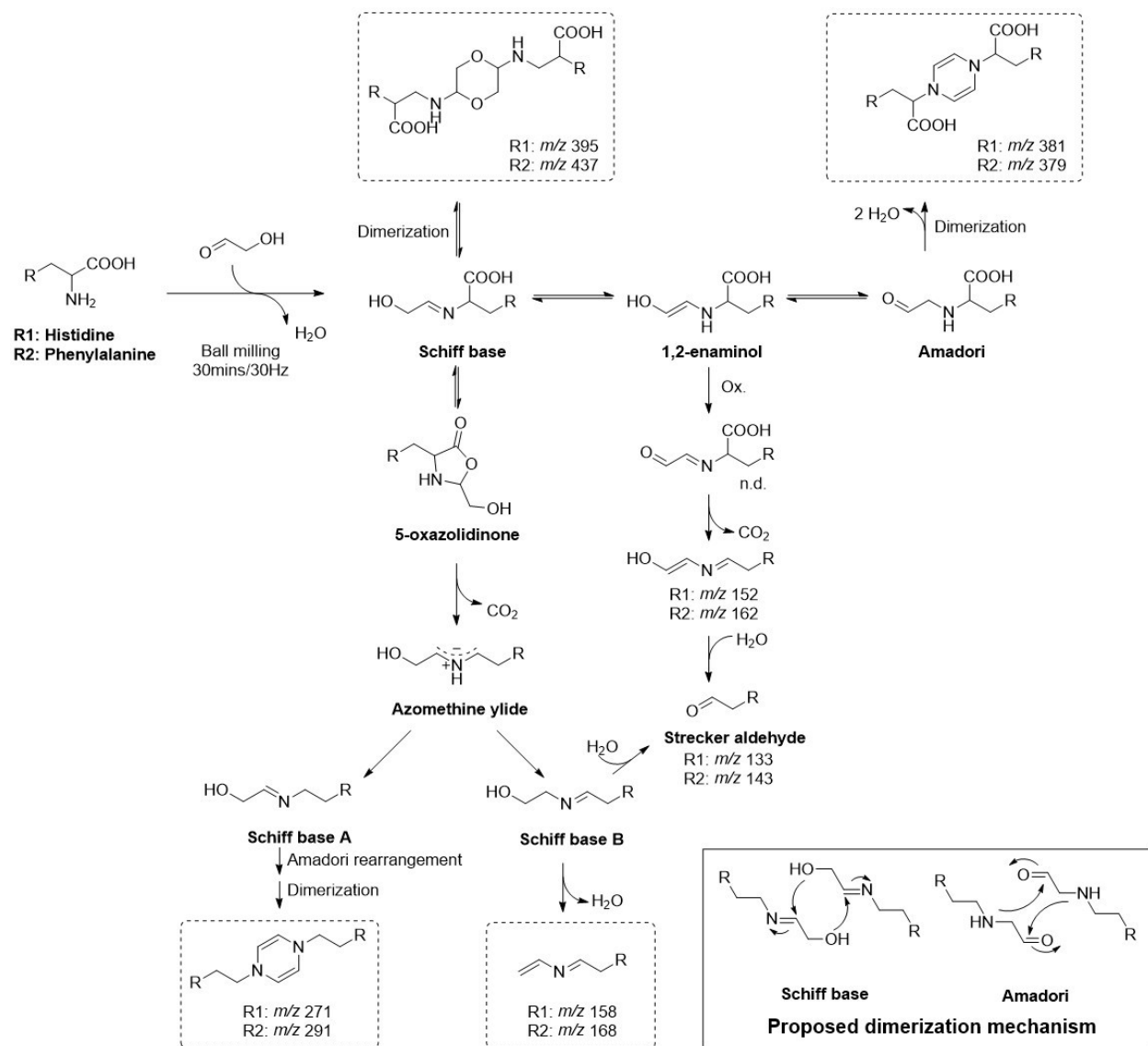


**Figure 6.2** Proposed histidine-glycolaldehyde and phenylalanine-glycolaldehyde reaction pathways and the proposed dimerization mechanism of Schiff base and Amadori compounds (see box with solid lines; n.d.: Not detected).

**Table 6.2** Observed masses from HRMS data from histidine-glycolaldehyde and phenylalanine-glycolaldehyde (GA) model systems corresponding to the structures shown in Figure 6.4.

Structural assignment	Histidine-Glycolaldehyde				Phenylalanine-Glycolaldehyde			
	Molecular formula	Theor. m/z	Exp. m/z (Rel. error, ppm)	Rel. Int. (ave±SD, n=2)	Molecular formula	Theor. m/z	Exp. m/z (Rel. error, ppm)	Rel. Int. (ave±SD, n=2)
AA	C <sub>6</sub> H <sub>10</sub> N <sub>3</sub> O <sub>2</sub>	156.0773	156.0765 (5.1)	92.7±7.3	C <sub>9</sub> H <sub>12</sub> NO <sub>2</sub>	166.0868	166.0868 (0.0)	61.8±11.6
AA	C <sub>6</sub> H <sub>9</sub> N <sub>3</sub> O <sub>2</sub> Na	178.0592	178.0583 (5.3)	73.1±2.7	C <sub>9</sub> H <sub>11</sub> NO <sub>2</sub> Na	188.0687	188.0683 (2.4)	92.4±7.6
AA+GA	C <sub>8</sub> H <sub>12</sub> N <sub>3</sub> O <sub>3</sub>	198.0879	198.0869 (4.9)	25.2±8.3	C <sub>11</sub> H <sub>14</sub> NO <sub>3</sub>	208.0974	208.0966 (3.7)	27.9±6.1
AA+GA	C <sub>8</sub> H <sub>11</sub> N <sub>3</sub> O <sub>3</sub> Na	220.0698	220.0688 (4.6)	36.0±5.8	C <sub>11</sub> H <sub>13</sub> NO <sub>3</sub> Na	230.0793	230.0782 (4.8)	64.1±1.5
Schiff base dimer	C <sub>16</sub> H <sub>23</sub> N <sub>6</sub> O <sub>6</sub>	395.1679	395.1673 (1.5)	4.2±1.1	C <sub>22</sub> H <sub>26</sub> N <sub>2</sub> O <sub>6</sub> Na	437.1689	437.1675 (3.1)	2.5±0.0
Schiff base dimer	C <sub>16</sub> H <sub>22</sub> N <sub>6</sub> O <sub>6</sub> Na	417.1499	417.1492 (1.6)	3.5±0.8	n.d.	n.d.	n.d.	n.d.
Amadori dimer	C <sub>16</sub> H <sub>18</sub> N <sub>6</sub> O <sub>4</sub> Na	381.1287	381.1271 (4.3)	5.3±2.2	C <sub>22</sub> H <sub>23</sub> N <sub>2</sub> O <sub>4</sub>	379.1658	379.1641 (4.4)	0.4±0.0
AA-CO <sub>2</sub> +GA	C <sub>7</sub> H <sub>11</sub> N <sub>3</sub> ONa	176.0800	176.0796 (2.2)	2.2±0.8	C <sub>10</sub> H <sub>13</sub> NONa	186.0895	186.0881 (7.4)	0.4±0.0
AA-CO <sub>2</sub>	C <sub>5</sub> H <sub>10</sub> N <sub>3</sub>	112.0875	112.0862 (11.4)	17.2±2.3	C <sub>8</sub> H <sub>12</sub> N	122.0970	122.0963 (5.5)	3.9±0.4
AA-CO <sub>2</sub> +GA-H <sub>2</sub> O	C <sub>7</sub> H <sub>9</sub> N <sub>3</sub> Na	158.0694	158.0690 (2.6)	6.8±0.2	C <sub>10</sub> H <sub>11</sub> NNa	168.0789	168.0809 (-11.8)	1.1±0.0
AA-CO <sub>2</sub> +GA-2H	C <sub>7</sub> H <sub>10</sub> N <sub>3</sub> O	152.0824	152.0814 (6.5)	6.4±0.6	C <sub>10</sub> H <sub>12</sub> NO	162.0919	162.0919 (-0.1)	16.2±8.5
AA-CO <sub>2</sub> +GA-2H	C <sub>7</sub> H <sub>9</sub> N <sub>3</sub> ONa	174.0643	174.0635 (4.8)	0.8±0.0	C <sub>10</sub> H <sub>11</sub> NONa	184.0738	184.0722 (8.9)	0.1±0.0
Schiff base A dimer	C <sub>14</sub> H <sub>19</sub> N <sub>6</sub>	271.1671	271.1691 (7.3)	0.9±0.2	C <sub>20</sub> H <sub>23</sub> N <sub>2</sub>	291.1861	291.1896 (10.5)	0.3±0.2
Schiff base A dimer	C <sub>14</sub> H <sub>18</sub> N <sub>6</sub> Na	293.1491	293.1493 (0.8)	1.1±0.1	n.d.	n.d.	n.d.	n.d.
Strecker aldehyde	C <sub>5</sub> H <sub>6</sub> N <sub>2</sub> ONa	133.0372	133.0369 (2.5)	6.1±1.8	C <sub>8</sub> H <sub>8</sub> ONa	143.0467	143.0477 (6.7)	0.6±0.0

n.d. not detected; AA amino acid

**Table 6.3** Masses observed in ball-milled <sup>15</sup>N-phenylalanine-glycolaldehyde (GA).

Structural assignment	Molecular formula	Theor. m/z	Exp. m/z	Rel. Int.	Rel. error (ppm)
AA	C <sub>9</sub> H <sub>12</sub> O <sub>2</sub> [ <sup>15</sup> N]	167.0838	167.0835	12.9	-2.03
AA	C <sub>9</sub> H <sub>11</sub> O <sub>2</sub> Na[ <sup>15</sup> N]	189.0658	189.0655	100	-1.5
AA+GA	C <sub>11</sub> H <sub>14</sub> O <sub>3</sub> [ <sup>15</sup> N]	209.0944	209.0940	6.1	-1.93
AA+GA	C <sub>11</sub> H <sub>13</sub> O <sub>3</sub> Na[ <sup>15</sup> N]	231.0763	231.0761	86.3	-1.07
Schiff base dimer	C <sub>22</sub> H <sub>26</sub> O <sub>6</sub> Na[ <sup>15</sup> N] <sub>2</sub>	439.1629	439.1641	1.5	2.67
Amadori dimer	C <sub>22</sub> H <sub>23</sub> O <sub>4</sub> [ <sup>15</sup> N] <sub>2</sub>	381.1599	381.1606	0.8	1.96
AA-CO <sub>2</sub> +GA	n.d.	n.d.	n.d.	n.d.	n.d.
AA-CO <sub>2</sub>	C <sub>8</sub> H <sub>12</sub> [ <sup>15</sup> N]	123.0940	123.0938	2.7	-1.7
AA-CO <sub>2</sub> +GA-H <sub>2</sub> O	C <sub>10</sub> H <sub>11</sub> Na[ <sup>15</sup> N]	169.0760	169.0752	1.5	-4.46
AA-CO <sub>2</sub> +GA-2H	C <sub>10</sub> H <sub>12</sub> O[ <sup>15</sup> N]	163.0889	163.0885	4.4	-2.6
Schiff base A dimer	n.d.	n.d.	n.d.	n.d.	n.d.

n.d. not detected; AA amino acid

#### 6.4.4 Glycolaldehyde-histamine and glycolaldehyde-phenethylamine model systems.

To further confirm the downstream degradation products of Schiff base A and its Amadori product and to enhance the signals arising from their further degradation products such as 1,4-dihydropyrazine and 1,4-dioxane dimeric structures, glycolaldehyde was milled with the corresponding decarboxylated amino acids, histamine, and phenethylamine. These model systems are incapable of generating 5-oxazolidinones or 5-oxazolidinone assisted decarboxylation products such as azomethine ylides and Schiff base B, consequently only Schiff base A can be formed through simple condensation. Furthermore, Schiff base B derived degradation products will also be absent from these model systems. As expected, milling of glycolaldehyde with the amines did not generate any dehydrated Schiff base B or the Strecker aldehyde. The reaction almost exclusively generated dihydropyrazines at *m/z* 271 and 291, the Amadori dimer, instead of the Schiff base A dimer. (Figure 6.3-6.5 and Table 6.4) A second reason for the absence of Strecker aldehyde was attributed to the lack of carboxylic acid moiety necessary for the Strecker degradation and for the promotion of 5-oxazolidinone assisted decarboxylation reaction. (Figure 6.5) The results indicated that the absence of the carboxylic acid moiety also eliminated the 5-oxazolidinone pathway as a stabilizing factor, hence the Schiff base mostly rearranged into its stable isomer – the Amadori compound, most likely catalyzed by the *in-situ* generated water from various condensation and dehydration reactions. The MS/MS fragmentations of the

dihydropyrazine ions at  $[M+H]^+$  271.1657 (Histamine) and at 291.1867 (Phenethylamine) showed similar daughter ions consistent with literature reports. (Figure 6.5, 6.3b, and 6.4b) [20] In the case of the phenethylamine model system, the dimer at  $m/z$  291 was not the most intense peak, as in the case of the histamine model system. It appears that the dihydropyrazine dimers can be stabilized further through oxidation and the formation of an extensively conjugated system linking aromatic  $\pi$  electrons to the dihydropyrazine ring. The monohydrated version of this conjugated dimer appeared as the highest peak at  $[M+H]^+$  307 in the mass spectrum. As shown in Figure 6.5 similar transformations can lead to the formation of various hydrated and methanolated adducts of conjugated dihydropyrazine derivatives detected at  $[M+H]^+ = 287, 303, 323, 331, \text{ and } 351$ . (Figure 6.5 and Table 6.4). The decarboxylated amino acid model system further illustrated the importance of carboxylic acid in enhancing the complexity of the Maillard reaction products. It was found that the presence of the carboxylic acid moiety in the amino acids significantly increases the number of Maillard reaction products (Figure 6.1) relative to the decarboxylated amino acid model systems.

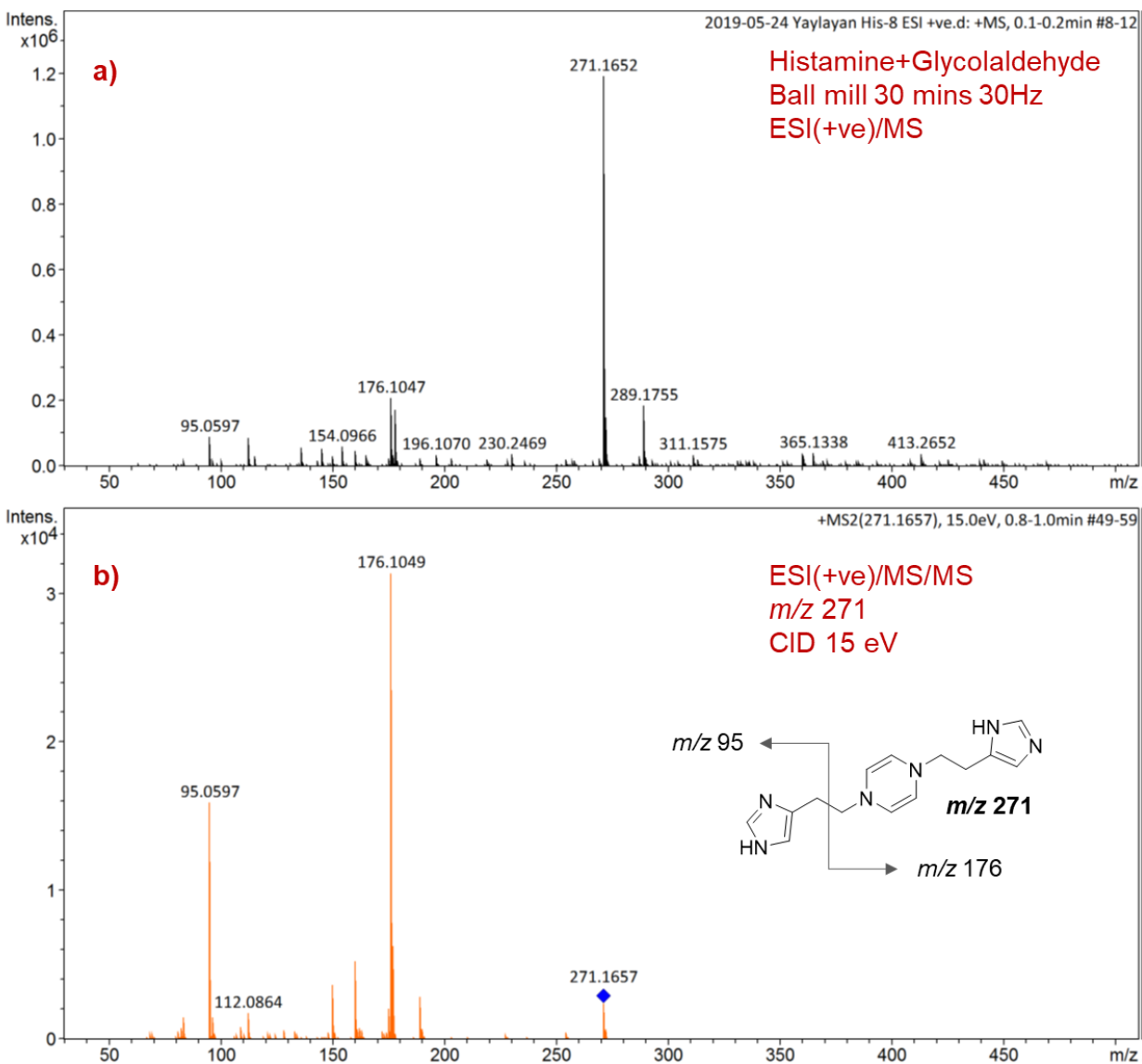


**Figure 6.3** (a) MS spectrum of ball-milled histamine and glycolaldehyde; (b) MS/MS spectrum of the ion at *m/z* 271.

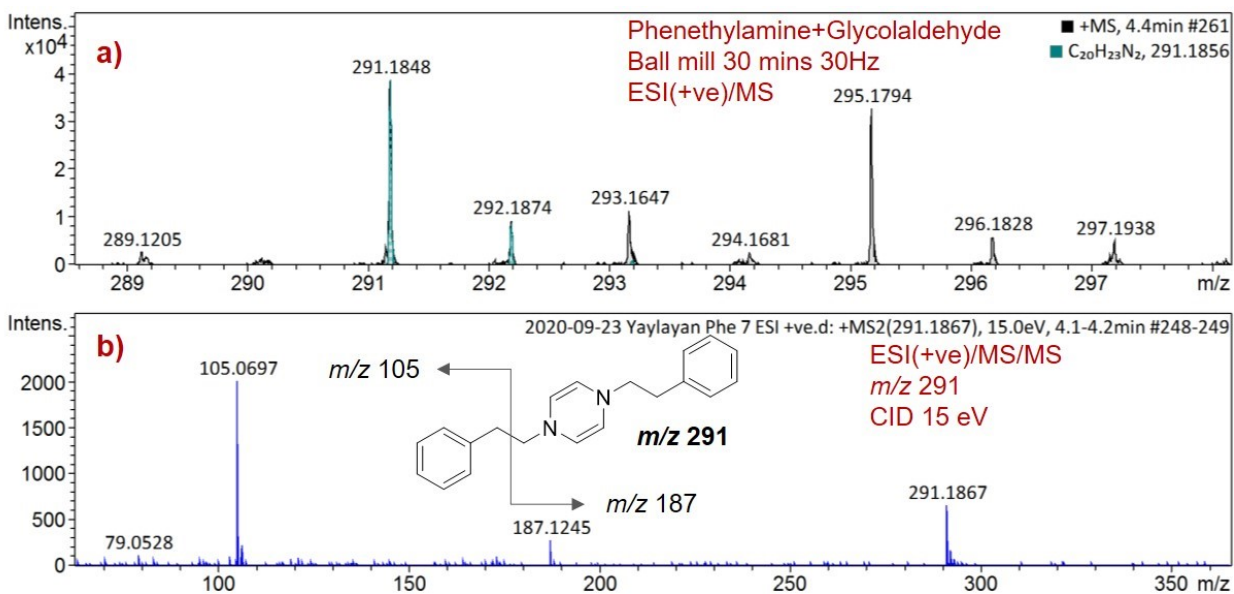


**Figure 6.4** (a) MS spectrum of ball-milled (30 min, 30Hz) phenethylamine and glycolaldehyde shown between  $m/z$  290 and 300; (b) MS/MS spectrum of the ion at  $m/z$  291.

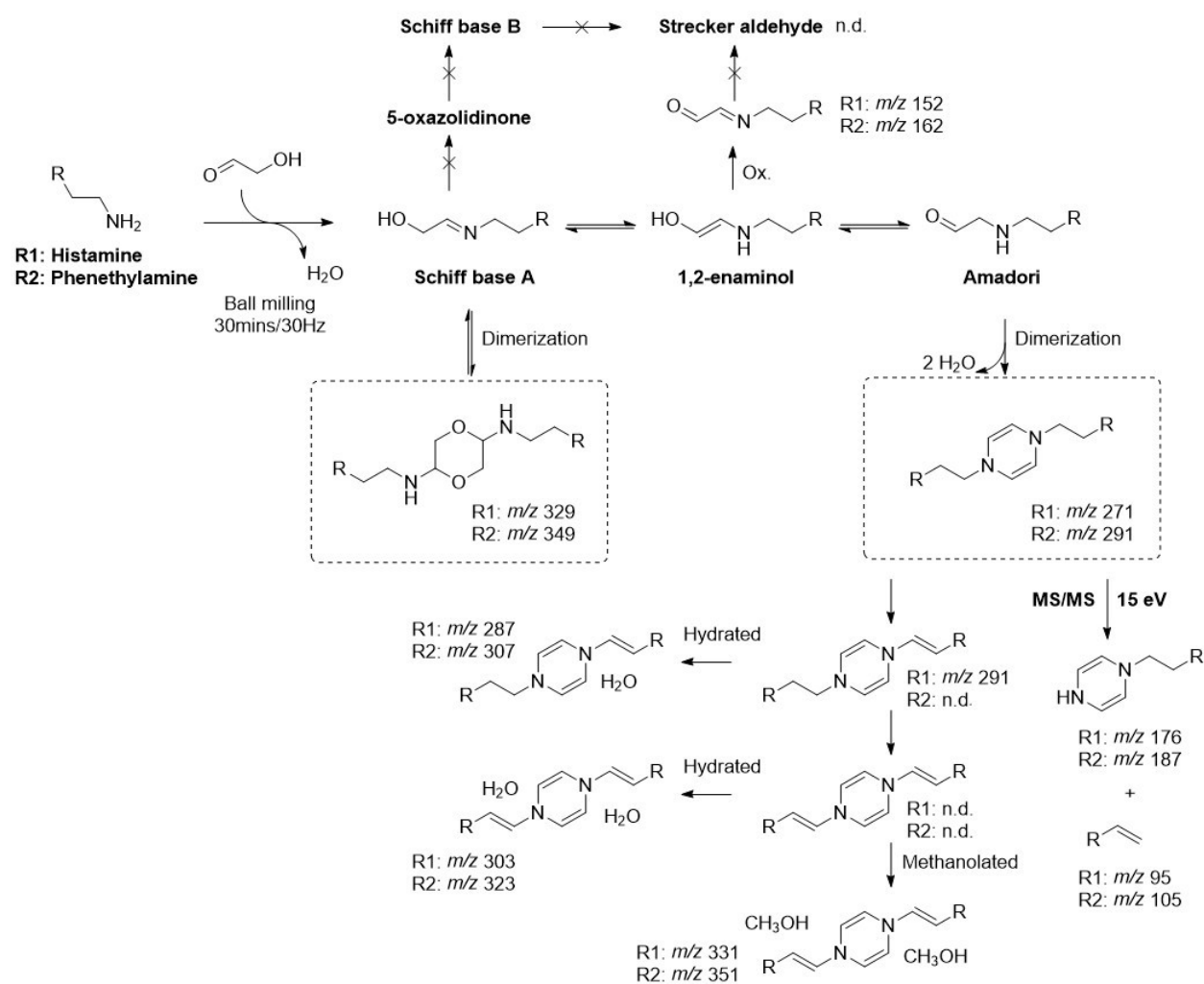


**Figure 6.5** Proposed histamine-glycolaldehyde and phenethylamine-glycolaldehyde reaction pathways and the MS/MS fragmentations of the dihydropyrazine derivatives. (n.d.: not detected)

**Table 6.4** Observed masses from HRMS data from histamine-glycolaldehyde and phenethylamine-glycolaldehyde (GA) model systems corresponding to the structures shown in Figure 6.5.

Structural assignment	Histamine-Glycolaldehyde				Phenethylamine-Glycolaldehyde			
	Molecular formula	Theor. m/z	Exp. m/z (Rel. error, ppm)	Rel. Int. (ave±SD, n=2)	Molecular formula	Theor. m/z	Exp. m/z (Rel. error, ppm)	Rel. Int. (ave±SD, n=2)
Amine	C <sub>5</sub> H <sub>10</sub> N <sub>3</sub>	112.0875	112.0888 (-10.5)	10.0±2.8	C <sub>8</sub> H <sub>12</sub> N	122.0970	122.0966 (3.1)	10.1±1.1
Amine+GA	C <sub>7</sub> H <sub>12</sub> N <sub>3</sub> O	154.0980	154.0982 (-1.1)	6.2±1.3	C <sub>10</sub> H <sub>14</sub> NO	164.1075	164.1069 (3.9)	5.8±1.7
Amine+GA-2H	C <sub>7</sub> H <sub>10</sub> N <sub>3</sub> O	152.0823	152.0825 (-0.7)	0.3±0.0	C <sub>10</sub> H <sub>12</sub> NO	162.0919	162.0913	0.2±0.0
Schiff base dimer	C <sub>14</sub> H <sub>22</sub> N <sub>6</sub> O <sub>2</sub> Na	329.1702	329.1704 (-0.6)	0.5±0.0	C <sub>20</sub> H <sub>26</sub> N <sub>2</sub> O <sub>2</sub> Na	349.1892	349.1895 (-0.9)	0.7±0.3
Amadori dimer	C <sub>14</sub> H <sub>19</sub> N <sub>6</sub>	271.1671	271.1660 (4.1)	100.0±0.0	C <sub>20</sub> H <sub>23</sub> N <sub>2</sub>	291.1861	291.1855 (2.1)	3.4±0.2
Amadori dimer - 2H	C <sub>14</sub> H <sub>17</sub> N <sub>6</sub>	291.1328	291.1309 (-6.8)	1.5±1.0	n.d.	n.d.	n.d.	n.d.
Amadori dimer - 2H +H <sub>2</sub> O	C <sub>14</sub> H <sub>19</sub> N <sub>6</sub> O	287.1620	287.1605 (5.3)	2.3±0.2	C <sub>20</sub> H <sub>23</sub> N <sub>2</sub> O	307.1810	307.1807 (1.1)	100.0±0.0
Amadori dimer - 4H +2H <sub>2</sub> O	C <sub>14</sub> H <sub>19</sub> N <sub>6</sub> O <sub>2</sub>	303.1569	303.1576 (-2.1)	0.2±0.0	C <sub>20</sub> H <sub>23</sub> N <sub>2</sub> O <sub>2</sub>	323.1760	323.1764 (-1.4)	0.9±0.1
Amadori dimer - 4H +2CH <sub>3</sub> OH	C <sub>16</sub> H <sub>23</sub> N <sub>6</sub> O <sub>2</sub>	331.1882	331.1862 (6.2)	1.6±0.2	C <sub>22</sub> H <sub>27</sub> N <sub>2</sub> O <sub>2</sub>	351.2073	351.2055 (5.0)	1.7±1.0

n.d. not detected

#### **6.4.5 FTIR spectroscopic evidence for the formation 5-oxazolidinone during ball milling of paraformaldehyde with 20 common amino acids**

Due to the reactivity of 5-oxazolidinone, this moiety is difficult to be observed and studied using chromatographic systems. So far, its formation and degradation have been studied only in few model systems consisting of amino acids and simple aldehydes. [21, 22] In the context of the Maillard reaction, direct FTIR spectroscopic evidence was reported with model systems containing glyceraldehyde and asparagine, [23] or phenylalanine; [4] and glycolaldehyde and phenylalanine [8] due to its characteristic carbonyl absorption band between  $1780\text{ cm}^{-1}$  and  $1810\text{ cm}^{-1}$ . [21] In this study, due to the reactivity of glycolaldehyde, the paraformaldehyde (PFA) was chosen as a more stable precursor in ball-milling experiments with 20 common amino acids to provide direct FTIR spectroscopic evidence on their ability to form 5-oxazolidinone. Analysis of the data have indicated that only 7 out of 20 amino acids were able to form stable oxazolidinone moieties to be detected by FTIR when milled at 30 Hz for 30 min. (see Table 6.5) Taking the PFA-phenylalanine model system as an example (Figure 6.6), a strong absorption band was observed at  $1775\text{ cm}^{-1}$  after milling, the formation of this band was accompanied by the loss of carboxylate band of the amino acid. Its identity was further confirmed through the observation of the expected  $40\text{ cm}^{-1}$ -downshifting of the peak when phenylalanine was replaced with  $^{13}\text{C}$ -1-phenylalanine. (Figure 6.6) This characteristic band was then integrated, and the peak areas were reported for all the amino acids studied in Table 6.5. These peak areas can be useful indicators of the effect of amino acid side chains on the stability of 5-oxazolidinones. (Table 6.5) It seems that alkyl and aromatic electron-donating groups as amino acid side chains stabilize the 5-oxazolidinone ring systems more than others.

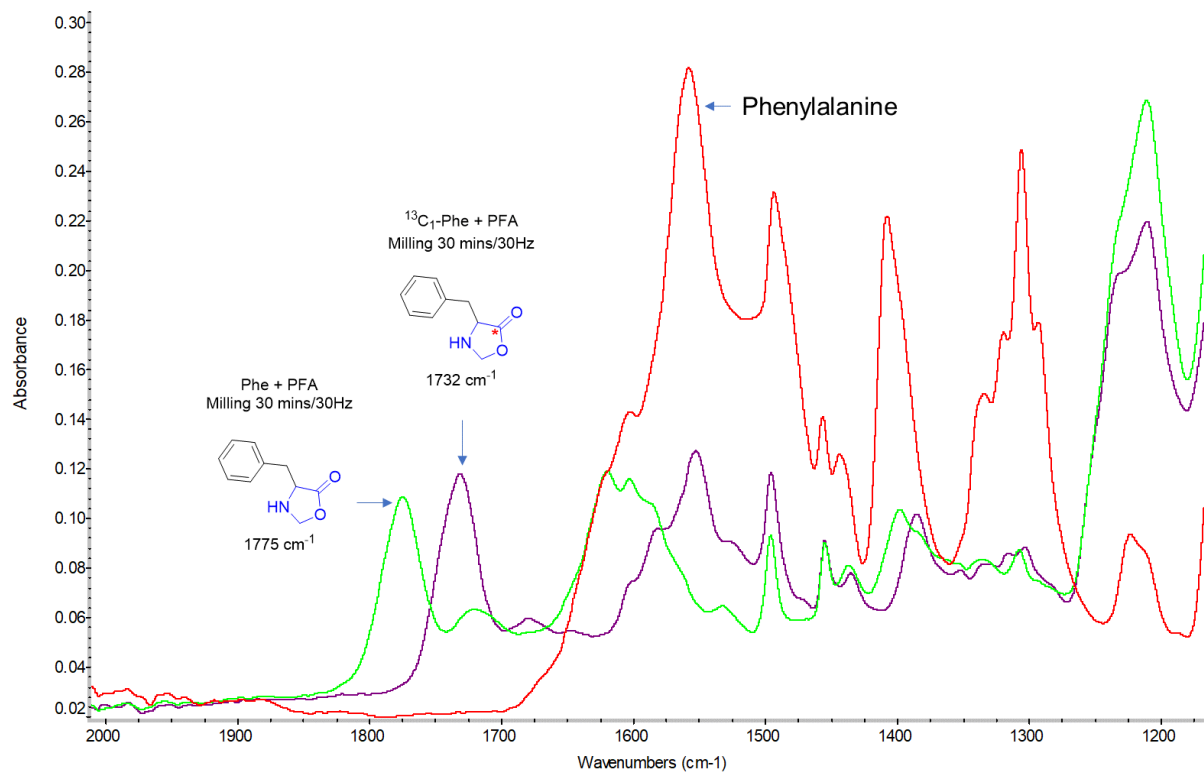


**Figure 6.6** Superimposed FTIR spectra of ball-milled (30 min, 30Hz) phenylalanine alone (red), paraformaldehyde (PFA)/phenylalanine (green) and PFA/[<sup>13</sup>C-1]-phenylalanine (purple).

**Table 6.5** Amino acids that exhibit stable 5-oxazolidinone absorption bands in the FTIR spectrum when ball milled with paraformaldehyde (30 min, 30 Hz).

Amino acids	Wavenumber (cm <sup>-1</sup> ) of the 5-oxazolidinone peak	Peak area (average ± SD; n=3)
Alanine (Ala)	1783	0.106 ± 0.006
Valine (Val)	1776	0.855 ± 0.070
Leucine (Leu)	1778	0.604 ± 0.049
Isoleucine (Ile)	1774	1.512 ± 0.053
Methionine (Met)	1777	0.887 ± 0.119
Phenylalanine (Phe)	1775	0.863 ± 0.005
Tyrosine (Tyr)	1776	0.243 ± 0.019

This study demonstrates the important role that the carboxylic acid moiety of the amino acids can play in the Maillard reaction in enabling the formation of the reactive 5-oxazolidinone intermediate. This intermediate can facilitate subsequent decarboxylation reaction and formation of two isomeric Schiff bases of which one can be converted into Strecker aldehyde. Under solvent-free ball milling conditions, the conventional Amadori rearrangement following the carbonyl-amine condensation step may not be the preferred route in the progression of the Maillard reaction. Instead, various other post-Schiff base transformations can take precedence, for example with longer chain sugars C2-C3 retro-aldolization can be observed as a major pathway of degradation, and with shorter chain sugars such as glycolaldehyde, the transition from 5-oxazolidinone intermediate to decarboxylated Schiff bases was observed as a prominent process in determining the reaction profile. With the emergence of mechanochemical methodology as a cleaner and faster route for generating Maillard reaction intermediates as flavor precursors or other functional food ingredients, these findings can provide important insight into their formulation and processing strategies. [14]

## 6.5 References

1. Maillard, L., *Action of amino acids on sugars. Formation of melanoidins in a methodical way*. *Compte-Rendu de l'Academie des Sciences*, 1912. **154**: p. 66-68.
2. Nursten, H.E., *The Maillard reaction: chemistry, biochemistry, and implications*. 2005: Royal Society of Chemistry.
3. Hodge, J.E., *Dehydrated foods, chemistry of browning reactions in model systems*. *Journal of agricultural and food chemistry*, 1953. **1**(15): p. 928-943.
4. Chu, F.L. and V.A. Yaylayan, *Post-Schiff Base Chemistry of the Maillard Reaction: Mechanism of Imine Isomerization*. *Annals of the New York Academy of Sciences*, 2008. **1126**(1): p. 30-37.
5. Høltermand, A., *The browning reaction*. *Starch-Stärke*, 1966. **18**(10): p. 319-328.
6. Herbst, R. and L. Engel, *A reaction between  $\alpha$ -ketonic acids and  $\alpha$ -amino acids*. *Journal of Biological Chemistry*, 1934. **107**(2): p. 505-512.

7. Wnorowski, A. and V.A. Yaylayan, *Monitoring carbonyl-amine reaction between pyruvic acid and  $\alpha$ -amino alcohols by FTIR spectroscopy a possible route to Amadori products*. Journal of agricultural and food chemistry, 2003. **51**(22): p. 6537-6543.
8. Chu, F.L. and V.A. Yaylayan, *FTIR monitoring of oxazolidin-5-one formation and decomposition in a glycolaldehyde–phenylalanine model system by isotope labeling techniques*. Carbohydrate research, 2009. **344**(2): p. 229-236.
9. Manini, P., M. d'Ischi, and G. Prota, *An Unusual Decarboxylative Maillard Reaction between l-DOPA and d-Glucose under Biomimetic Conditions: Factors Governing Competition with Pictet–Spengler Condensation*. The Journal of Organic Chemistry, 2001. **66**(15): p. 5048-5053.
10. Manini, P., A. Napolitano, and M. d'Ischia, *Reactions of d-glucose with phenolic amino acids: further insights into the competition between Maillard and Pictet–Spengler condensation pathways*. Carbohydrate Research, 2005. **340**(18): p. 2719-2727.
11. Hayashi, T., S. Mase, and M. Namiki, *Formation of the N, N'-Dialkylpyrazine Cation Radical from Glyoxal Dialkylimine Produced on Reaction of a Sugar with an Amine or Amino Acid*. Agricultural and Biological Chemistry, 1985. **49**(11): p. 3131-3137.
12. Glomb, M.A. and V.M. Monnier, *Mechanism of protein modification by glyoxal and glycolaldehyde, reactive intermediates of the Maillard reaction*. Journal of Biological Chemistry, 1995. **270**(17): p. 10017-10026.
13. Xing, H. and V. Yaylayan, *Mechanochemical generation of Schiff bases and Amadori products and utilization of diagnostic MS/MS fragmentation patterns in negative ionization mode for their analysis*. Carbohydrate Research, 2020. **495**: p. 108091.
14. Xing, H. and V. Yaylayan, *Investigation of thermo-chemical properties of mechanochemically generated glucose–histidine Maillard reaction mixtures*. European Food Research and Technology, 2020.
15. Koch, B.P., et al., *Fundamentals of Molecular Formula Assignment to Ultrahigh Resolution Mass Data of Natural Organic Matter*. Analytical Chemistry, 2007. **79**(4): p. 1758-1763.
16. Kim, S., R.W. Kramer, and P.G. Hatcher, *Graphical Method for Analysis of Ultrahigh-Resolution Broadband Mass Spectra of Natural Organic Matter, the Van Krevelen Diagram*. Analytical Chemistry, 2003. **75**(20): p. 5336-5344.

17. Kaupp, G., J. Schmeyers, and J. Boy, *Quantitative Solid-State Reactions of Amines with Carbonyl Compounds and Isothiocyanates*. Tetrahedron, 2000. **56**(36): p. 6899-6911.
18. Namiki, M. and T. Hayashi, *A new mechanism of the Maillard reaction involving sugar fragmentation and free radical formation*. 1983, ACS Publications.
19. Granvogel, M., E. Beksan, and P. Schieberle, *New Insights into the Formation of Aroma-Active Strecker Aldehydes from 3-Oxazolines as Transient Intermediates*. Journal of Agricultural and Food Chemistry, 2012. **60**(25): p. 6312-6322.
20. Hofmann, T., W. Bors, and K. Stettmaier, *Studies on Radical Intermediates in the Early Stage of the Nonenzymatic Browning Reaction of Carbohydrates and Amino Acids*. Journal of Agricultural and Food Chemistry, 1999. **47**(2): p. 379-390.
21. Tsuge, O., et al., *Simple generation of nonstabilized azomethine ylides through decarboxylative condensation of  $\alpha$ -amino acids with carbonyl compounds via 5-oxazolidinone intermediates*. Bulletin of the Chemical Society of Japan, 1987. **60**(11): p. 4079-4089.
22. Aurelio, L., et al., *An efficient synthesis of N-methyl amino acids by way of intermediate 5-oxazolidinones*. The Journal of organic chemistry, 2003. **68**(7): p. 2652-2667.
23. Perez Locas, C. and V.A. Yaylayan, *Further Insight into Thermally and pH-Induced Generation of Acrylamide from Glucose/Asparagine Model Systems*. Journal of Agricultural and Food Chemistry, 2008. **56**(15): p. 6069-6074.

## 6.6 Supplementary information

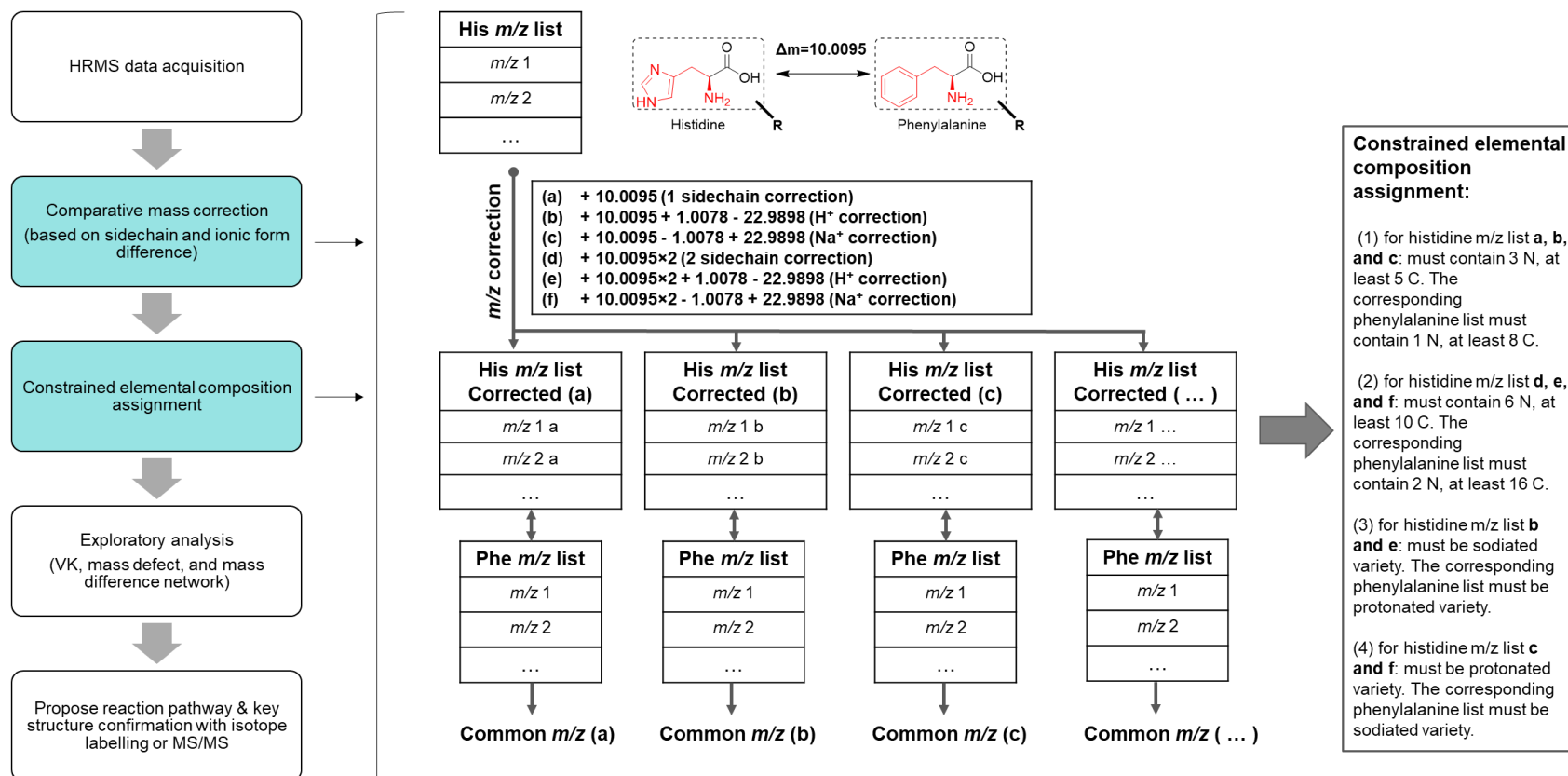


**Figure S 6.1** Data analysis pipeline: extraction of amino acid side chain specific reaction products. VK=Van Krevelen. (Note: For the *m/z* correction rules, (b)&(e) assuming all the ions from histidine model are sodiated, and all the ions from phenylalanine model are protonated; (c)&(f) assuming all the ions from histidine model are protonated, and all the ions from phenylalanine model are sodiated.)



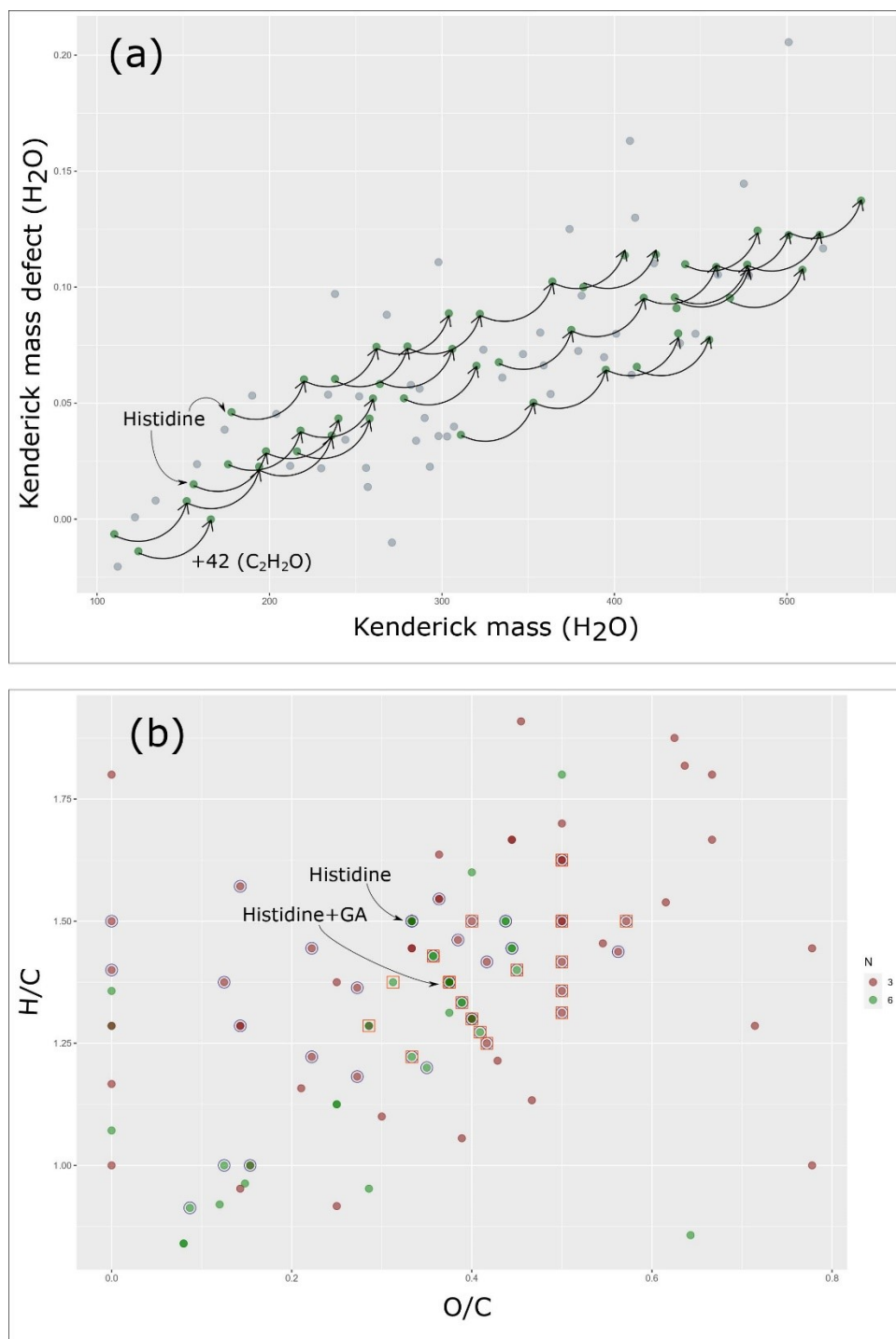


**Figure S 6.3** MS data visualization using (a) Kendrick mass defect plot (scaled by water) and (b) Van Krevelen diagrams. Masses involved in glycolaldehyde addition are highlighted in green in (a), and as circles in (b). Masses involved in histidine addition are highlighted in squares in (b). (The graphs are generated by R language (version 3.6.3) package *ggplot2* (version 3.2.3))

**Table S 6.1** Extracted equivalent masses ( $m/z$ ) from histidine and phenylalanine model systems.

	Histidine - Glycolaldehyde				Phenylalanine - Glycolaldehyde			
	Elemental composition	Theor. m/z	Exp. m/z	Rel. error (ppm)	Elemental composition	Theor. m/z	Exp. m/z	Rel. error (ppm)
1	C5H8N3	110.0718	110.0710	7.47	C8H10N	120.0813	120.0823	-8.12
2	C5H10N3	112.0875	112.0862	11.35	C8H12N	122.0970	122.0963	5.52
3	C6H8N3	122.0718	122.0708	8.37	C9H10N	132.0813	132.0818	-3.60
4	C6H10N3	124.0875	124.0866	7.03	C9H12N	134.0970	134.0989	-14.36
5	C7H8N3	134.0718	134.0706	9.12	C10H10N	144.0813	144.0816	-1.91
6	C7H10N3O	152.0824	152.0814	6.49	C10H12NO	162.0919	162.0919	-0.07
7	C6H10N3O2	156.0773	156.0765	5.14	C9H12NO2	166.0868	166.0868	0.02
8	C7H9N3Na	158.0694	158.0690	2.63	C10H11NNa	168.0789	168.0809	-11.80
9	C8H12N3O	166.0980	166.0975	3.23	C11H14NO	176.1075	176.1074	0.79
10	C7H9N3ONa	174.0643	174.0635	4.77	C10H11NONa	184.0738	184.0722	8.86
11	C7H11N3ONa	176.0800	176.0796	2.16	C10H13NONa	186.0895	186.0881	7.43
12	C6H9N3O2Na	178.0592	178.0583	5.30	C9H11NO2Na	188.0687	188.0683	2.37
13	C7H9N3O2Na	190.0592	190.0582	5.49	C10H11NO2Na	200.0687	200.0679	4.23
14	C9H12N3O2	194.0930	194.0912	9.02	C12H14NO2	204.1025	204.1019	2.71
15	C8H12N3O3	198.0879	198.0869	4.88	C11H14NO3	208.0974	208.0966	3.69
16	C8H11N3O2Na	204.0749	204.0743	2.91	C11H13NO2Na	214.0844	214.0843	0.45
17	C9H14N3O3	212.1035	212.1014	9.98	C12H16NO3	222.1130	222.1121	4.14
18	C8H14N3O4	216.0984	216.0975	4.31	C11H16NO4	226.1079	226.1070	4.13
19	C9H13N3O2Na	218.0905	218.0897	3.87	C12H15NO2Na	228.1000	228.1013	-5.50
20	C8H11N3O3Na	220.0698	220.0688	4.58	C11H13NO3Na	230.0793	230.0782	4.83
21	C9H16N3O4	230.1141	230.1130	4.70	C12H18NO4	240.1236	240.1224	4.93
22	C9H13N3O3Na	234.0855	234.0836	7.94	C12H15NO3Na	244.0950	244.0933	6.81
23	C11H14N3O3	236.1035	236.1024	4.73	C14H16NO3	246.1130	246.1113	6.98
24	C7H9N3O5Na	238.0440	238.0425	6.25	C10H11NO5Na	248.0535	248.0519	6.41
25	C8H13N3O4Na	238.0804	238.0792	4.93	C11H15NO4Na	248.0899	248.0886	5.14
26	C10H14N3O4	240.0984	240.0974	4.29	C13H16NO4	250.1079	250.1065	5.73
27	C13H14N3O2	244.1086	244.1089	-1.22	C16H16NO2	254.1181	254.1159	8.67
28	C9H15N3O4Na	252.0960	252.0949	4.46	C12H17NO4Na	262.1055	262.1042	5.06
29	C11H18N3O4	256.1297	256.1281	6.37	C14H20NO4	266.1392	266.1372	7.64
30	C11H19N3O4	257.1376	257.1369	2.55	C14H21NO4	267.1471	267.1486	-5.77
31	C10H16N3O5	258.1090	258.1080	3.86	C13H18NO5	268.1185	268.1173	4.47
32	C11H15N3O3Na	260.1011	260.1005	2.34	C14H17NO3Na	270.1106	270.1097	3.37
33	C10H13N3O4Na	262.0804	262.0794	3.72	C13H15NO4Na	272.0899	272.0888	3.95
34	C10H15N3O4Na	264.0960	264.0966	-2.18	C13H17NO4Na	274.1055	274.1051	1.55

35	C12H11N3O3Na	268.0698	268.0691	2.64	C15H13NO3Na	278.0793	278.0779	5.07
36	C14H19N6	271.1671	271.1691	7.30	C20H23N2	291.1861	291.1896	10.50
37	C11H17N3O4Na	278.1117	278.1110	2.42	C14H19NO4Na	288.1212	288.1213	-0.43
38	C10H15N3O5Na	280.0909	280.0898	4.06	C13H17NO5Na	290.1004	290.0987	6.00
39	C10H17N3O5Na	282.1066	282.1076	-3.59	C13H19NO5Na	292.1161	292.1153	2.71
40	C10H17N6O4	285.1311	285.1334	-7.97	C16H21N2O4	305.1501	305.1514	-4.15
41	C11H17N3O6	287.1117	287.1121	-1.27	C14H19NO6	297.1212	297.1237	-8.29
42	C14H15N6Na	290.1256	290.1265	-3.15	C20H20N2	288.1626	288.1647	-7.12
43	C14H18N6Na	293.1491	293.1493	0.81	C20H23N2	291.1861	291.1896	10.50
44	C9H13N3O7Na	298.0651	298.0640	3.75	C12H15NO7Na	308.0746	308.0724	7.20
45	C11H21N3O5Na	298.1379	298.1390	-3.73	C14H23NO5Na	308.1474	308.1465	2.89
46	C10H19N6O5	303.1417	303.1421	-1.34	C16H22N2O5Na	345.1426	345.1419	2.14
47	C12H15N3O5Na	304.0909	304.0896	4.40	C15H17NO5Na	314.1004	314.0985	6.18
48	C12H17N3O5Na	306.1066	306.1061	1.60	C15H19NO5Na	316.1161	316.1168	-2.24
49	C11H21N3O7	307.1380	307.1402	-7.33	C14H23NO7	317.1475	317.1459	4.89
50	C12H19N6O4	311.1468	311.1461	2.18	C18H22N2O4Na	353.1477	353.1454	6.58
51	C13H19N3O5Na	320.1222	320.1216	1.99	C16H21NO5Na	330.1317	330.1303	4.36
52	C12H17N3O6Na	322.1015	322.1004	3.42	C15H19NO6Na	332.1110	332.1099	3.33
53	C14H18N3O6	324.1196	324.1170	7.90	C17H20NO6	334.1291	334.1305	-4.30
54	C12H18N6O4Na	333.1287	333.1277	3.06	C18H22N2O4Na	353.1477	353.1454	6.58
55	C12H21N3O8	335.1329	335.1355	-7.86	C15H23NO8	345.1424	345.1419	1.35
56	C13H21N3O8	347.1329	347.1324	1.34	C16H23NO8	357.1424	357.1432	-2.33
57	C14H21N6O5	353.1573	353.1569	1.25	C20H24N2O5Na	395.1583	395.1589	-1.54
58	C14H18N6O4Na	357.1287	357.1290	-0.78	C20H22N2O4Na	377.1477	377.1502	-6.56
59	C16H19N6O4	359.1468	359.1443	6.90	C22H23N2O4	379.1658	379.1641	4.44
60	C21H21N3O3	363.1583	363.1590	-1.95	C24H23NO3	373.1678	373.1699	-5.64
61	C14H19N3O7Na	364.1121	364.1111	2.66	C17H21NO7Na	374.1216	374.1213	0.72
62	C15H17N3O7Na	374.0964	374.0943	5.66	C18H19NO7Na	384.1059	384.1036	6.04
63	C14H20N6O5Na	375.1393	375.1384	2.36	C20H24N2O5Na	395.1583	395.1589	-1.54
64	C19H22N3O4Na	379.1508	379.1498	2.63	C22H24NO4Na	389.1603	389.1625	-5.65
65	C16H18N6O4Na	381.1287	381.1271	4.25	C22H23N2O4	379.1658	379.1641	4.44
66	C14H21N3O8Na	382.1226	382.1240	-3.58	C17H23NO8Na	392.1321	392.1302	4.93
67	C16H22N6O6	394.1601	394.1613	-3.09	C22H25N2O6Na	436.1610	436.1609	0.30
68	C16H23N6O6	395.1679	395.1673	1.54	C22H26N2O6Na	437.1689	437.1675	3.10
69	C16H22N6O5Na	401.1549	401.1553	-0.91	C22H26N2O5Na	421.1739	421.1734	1.28
70	C16H21N3O8Na	406.1226	406.1244	-4.35	C19H23NO8Na	416.1321	416.1331	-2.32
71	C14H13N6O9	409.0744	409.0768	-5.86	C20H16N2O9Na	451.0753	451.0756	-0.56
72	C15H28N3O10	410.1775	410.1783	-2.03	C18H30NO10	420.1870	420.1894	-5.78
73	C18H19N3O7Na	412.1121	412.1117	0.89	C21H21NO7Na	422.1216	422.1213	0.64
74	C16H25N6O7	413.1785	413.1766	4.53	C22H28N2O7Na	455.1794	455.1769	5.53

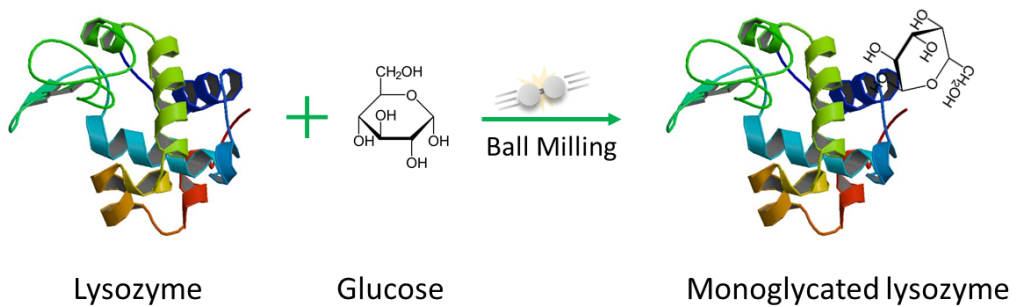
75	C16H22N6O6Na	417.1499	417.1492	1.56	C22H26N2O6Na	437.1689	437.1675	3.10
76	C20H22N3O6Na	423.1406	423.1378	6.68	C23H24NO6Na	433.1501	433.1475	6.07
77	C16H23N3O9Na	424.1332	424.1346	-3.31	C19H25NO9Na	434.1427	434.1439	-2.77
78	C16H24N6O7Na	435.1604	435.1596	1.87	C22H28N2O7Na	455.1794	455.1769	5.53
79	C23H21N6O2Na	436.1624	436.1648	-5.58	C29H25N2O2Na	456.1814	456.1801	2.79
80	C18H25N6O7	437.1785	437.1763	4.97	C24H28N2O7Na	479.1794	479.1775	4.00
81	C25H22N6O2	438.1804	438.1811	-1.54	C31H25N2O2Na	480.1814	480.1812	0.36
82	C18H22N6O6Na	441.1499	441.1488	2.38	C24H26N2O6Na	461.1689	461.1708	-4.22
83	C16H30N3O10Na	447.1829	447.1823	1.31	C19H32NO10Na	457.1924	457.1911	2.82
84	C18H27N6O8	455.1890	455.1896	-1.24	C24H30N2O8Na	497.1900	497.1899	0.17
85	C18H24N6O7Na	459.1604	459.1605	-0.19	C24H28N2O7Na	479.1794	479.1775	4.00
86	C25H21N6O2Na	460.1624	460.1644	-4.42	C31H25N2O2Na	480.1814	480.1812	0.36
87	C24H24N6O3Na	467.1808	467.1786	4.62	C30H29N2O3	465.2178	465.2159	4.12
88	C21H20N6O6Na	475.1342	475.1340	0.42	C27H24N2O6Na	495.1532	495.1517	3.04
89	C18H26N6O8Na	477.1710	477.1701	1.84	C24H30N2O8Na	497.1900	497.1899	0.17
90	C25H23N6O3Na	478.1729	478.1753	-4.95	C31H27N2O3Na	498.1919	498.1932	-2.54
91	C20H24N6O7Na	483.1604	483.1589	3.14	C26H28N2O7Na	503.1794	503.1811	-3.34
92	C18H19N3O14	501.0867	501.0882	-2.99	C21H21NO14	511.0962	511.0982	-3.90
93	C20H26N6O8Na	501.1710	501.1714	-0.84	C26H30N2O8Na	521.1900	521.1900	-0.03
94	C26H26N6O4Na	509.1913	509.1911	0.43	C32H31N2O4	507.2284	507.2302	-3.58
95	C20H28N6O9Na	519.1815	519.1819	-0.68	C26H32N2O9Na	539.2005	539.1998	1.39
96	C27H26N6O4Na	521.1913	521.1889	4.65	C33H30N2O4Na	541.2103	541.2126	-4.20
97	C22H28N6O9Na	543.1815	543.1812	0.63	C28H32N2O9Na	563.2005	563.2013	-1.33

## Connecting paragraph

In the previous chapters 4 to 6, we investigated the Maillard reaction from reducing sugars and amino acids under ball milling conditions. Ball milling has been identified as a fast and efficient method for selectively generating a mechanochemical reaction mixture rich in Schiff bases and the Amadori compounds, which during subsequent heat treatment reacted in a controlled manner generating more aroma-active compounds than the control samples. In chapter 7, the mechanochemical method is further extended to include protein glycation using reducing sugars with lysozyme.

Chapter 7 was published in the *Journal of agricultural and food chemistry*: Xing, H., & Yaylayan, V. (2019). Mechanochemically Induced Controlled Glycation of Lysozyme and Its Effect on Enzymatic Activity and Conformational Changes. *Journal of agricultural and food chemistry*, **67(11)**, 3249-3255.

## Chapter 7 Mechanochemically Induced Controlled Glycation of Lysozyme and Its Effect on Enzymatic Activity and Conformational Changes



## 7.1 Abstract

Protein glycation through heating of a mixture of protein and reducing sugars is one of the most commonly used methods of protein modification, however, in most cases, this approach can lead to uncontrolled glycation. The hypothesis that mechanical energy supplied through ball milling can induce glycation of proteins was tested using a well-characterized enzyme lysozyme. The Q-TOF/MS analysis of the milled samples has indicated that milling of sugar-protein mixtures in stainless steel jars for 30 min and at a frequency of 30 Hz generated mainly mono-glycated proteins even with the highly reactive ribose. Increasing the sugar concentration or the milling time did not influence the overall yield or generated more glycoforms. Enzymatic activity measurements, FTIR and fluorescence spectroscopic studies have indicated that milling of lysozyme alone leads to a significant loss in enzymatic activity and structural integrity in contrast to milling in the presence of sugars.

**Keywords:** Glycation, Lysozyme, Mechanochemistry, Ball milling, Enzymatic activity, Conformational changes.

## 7.2 Introduction

Non-enzymatic glycation can lead to a complex mixture of the protein-sugar adducts through the Maillard reaction. The early stage of the reaction is initiated by the condensation between a carbonyl group of reducing sugars and an amino group of proteins to form the Schiff base, the subsequent rearrangement of this intermediate yields an Amadori or Heyn's product depending on whether aldose or ketose sugar is involved.[1] Further degradation of the rearrangement products can lead to the formation of reactive carbonyl compounds via dehydration and oxidation, the interaction of these reactive intermediates can lead to cross-linking and the formation of advanced glycation end products (AGEs).[2] Protein glycation through Maillard reaction is one of the most commonly used methods for protein modification.[3] Its effect on protein functionality can be either beneficial or detrimental. Under controlled conditions, the glycation can be limited to the stage of Amadori rearrangement and the resulting glycated proteins are reported to have improved functionalities.[4-7] However, extensive and uncontrolled glycation may result in protein cross-linking and loss of nutritional value by blocking lysine residues [8] and damaging other essential amino acids.[9] Solid state incubation or heating of a mixture of protein and reducing sugars is the most commonly used method of protein glycation, however, in most cases, this approach can lead to uncontrolled glycation, browning and cross-linking requiring the use of anti-glycation reagents and modification of time-temperature exposure. In recent years, novel techniques such as microwave,[10, 11] and ultrasound [12-15] have been also employed to affect protein glycation to shorten the incubation times, with no specific advantages gained in the controlled generation of glycated proteins, except in increasing the yields. Although ball milling can promote the condensation between reducing sugars and amino acids, [16] and has been reported as a means of modification of protein functionalities in the absence of sugars [17, 18] through size reduction, however, glycation induced by ball milling has not been reported. Generally, reactions that proceed in the solid-state with mechanical energy is categorized as part of mechanochemistry. This branch of chemistry is emerging as a cleaner route for a wide range of transformations, featuring a means to avoid bulk solvent consumption and conduct chemical reactions between poorly soluble reactants quickly and quantitatively. Based on the reported stability of enzymes under the seemingly harsh ball milling conditions developments have been made on mechanoenzymatic reactions, where enzymes are used as biocatalysts during milling, for example, the use of immobilized lipase for catalyzing the stereoselective acetylation of several secondary alcohols,[19]

the use of papain in amide synthesis, [20, 21] and the depolymerization of cellulose catalyzed by cellulase.[22] Ball milling has also been used in pharmaceutical and food industries for protein size reduction [17, 23] and modification of protein functionalities [17, 18] and digestibility.[24, 25] In this study, lysozyme (LZM) was used as a model protein to demonstrate for the first time the ability of mechanochemical energy to induce glycation of proteins. Furthermore, the effect of milling of lysozyme alone and in the presence of glucose on the structural and conformational changes in the lysozyme was investigated and its residual enzymatic activity was measured.

## **7.3 Materials and Methods**

### **7.3.1 Materials**

Lysozyme from chicken egg white (L6876, purity, >90%; MW 14,307 Da), D-glucose (purity, 99.5%), D-ribose (purity, 99%), D-sorbitol (purity,  $\geq 98\%$ ) *Micrococcus lysodeikticus*, potassium phosphate monobasic, potassium phosphate dibasic were purchased from Sigma-Aldrich Chemicals (St. Louis, MO). All other chemicals and reagents were of analytical grade from Fisher Scientific. Ultrapure water was used throughout the study. All materials were used without further purification.

### **7.3.2 Sample Preparation**

Ball milling was conducted at ambient temperature by mixing 0.1 g of lysozyme and 0.009g of D-glucose or 0.006g of D-ribose or 0.009g of D-sorbitol (lysozyme/sugar molar ratio of 1:6 to give approximately 1:1 molar ratio of lysine residue to sugar carbonyl) in a stainless-steel grinding jar (10 mL) with 2 steel balls (3.2 mm in diameter; ball/sample ratio  $\sim 32:1$ ) for creating inner friction. The jars were seated in the Retsch Mixer Mill (MM 400, Newtown, PA, US) that performs radial oscillations in a horizontal position without coolant (the external jar temperature was  $\sim 25$  °C) at a frequency of 30 Hz for 30 or 60 min (M30 or M60). For acid/base catalyzed reactions,  $\text{AlCl}_3$  and KOH were added respectively at 1% (w/w) to lysozyme. Samples collected after milling were stored at  $-20^\circ\text{C}$  for further analysis. Repeated milling and heating cycles at different time combinations were performed at a frequency of 30 Hz and at  $50^\circ\text{C}$ . After milling treatment, the milling vial was immediately placed in an oven at  $50^\circ\text{C}$ . The time gap between milling and heating was minimized to less than one minute, and the vial was not opened for each cycle in order to eliminated interference from oxygen.

### 7.3.3 Quadruple-time-of-flight-ESI mass spectrometry (Q-TOF-ESI-MS).

The mass spectrometric analysis was performed using a Bruker Maxis Impact quadruple-time-of-flight mass spectrometer (Bruker Daltonics, Bremen, Germany) operating in a positive mode with electrospray ionization as the source type. The dry samples were reconstituted in 70% aqueous acetic acid and were directly introduced into the instrument at a rate of 10  $\mu\text{L}/\text{min}$  using a syringe pump. The electrospray interphase settings were as follows: nebulizer pressure, 0.4 bar; drying gas, 6.0 L/min; temperature, 180  $^{\circ}\text{C}$ ; and capillary voltage, 4500 V. The scan range was from  $m/z$  200 to 3500. Lysozyme and its glycated species were usually detected in the mass range of  $m/z$  1000 – 1700 with different multiple-charged ionization states from +9 to +14, this range was subsequently deconvoluted to simplify data interpretation in ESI-MS. The data were analyzed using Bruker Compass Data Analysis software, version 4.2. The relative proportions of glycated and non-glycated species of lysozyme identified in each sample were estimated from the relative intensities of their corresponding molecular ions in the deconvoluted mass spectrum as a ratio of the total intensity of all identified molecular ion peaks. All samples are analyzed in duplicates and the results are reported as average  $\pm$  standard deviation.

### 7.3.4 FTIR

A Bruker Alpha-P spectrometer (Bruker Optic GmbH, Ettlingen, Germany) equipped with a deuterated triglycine sulfate (DTGS) detector was used to record the FTIR spectra in the transmission mode. A demountable  $\text{CaF}_2$  transmission flow cell with an injection volume of 100  $\mu\text{l}$  (Dwight Analytical, Toronto, ON, Canada) was used for all measurements. A total of 32 scans at 4  $\text{cm}^{-1}$  resolution were co-added. The spectrometer was run under the Bruker OPUS 4.2 software (Bruker, Germany). For analysis, the flow cell was filled with an adequate amount of sample solution and scanned over the spectral range of 4000–500  $\text{cm}^{-1}$ . Samples were generally prepared as solutions in  $\text{D}_2\text{O}$  with a protein concentration of 5% (w/v). In order to obtain information on amide II band shifting, a series of 4 spectra were recorded for each sample during the H/D exchange process over a 1-hour period with 20 minutes interval at room temperature. Background spectra were collected in the absence of the transmission cell. The second-derivative analysis of the amide I region (1700 – 1600  $\text{cm}^{-1}$ ) of the infrared spectrum was performed as per the method of Dong et al.[26] After subtracting the background and water vapor contributions, the second derivative spectrum was generated using a nine-point Savitsky-Golay transformation. All the second-derivative plots were area normalized (1700–1600  $\text{cm}^{-1}$ ) for comparison. The second

derivative band assignments were based on Byler et al. [27] and Sethuraman and Belfort [28] where  $\alpha$ -helical structure was assigned to the band at  $1656\text{ cm}^{-1}$ , intramolecular  $\beta$ -sheet at  $1693$  and  $1633\text{ cm}^{-1}$ , unordered and ordered helix at  $1672$ ,  $1648$ , and  $1620\text{ cm}^{-1}$ , and turn structures at  $1720$ ,  $1668$ ,  $1630$ , and  $1617\text{ cm}^{-1}$ .

### **7.3.5 Residual Lysozyme Activity**

The activity of lysozyme was analyzed using a method described by Shugar [29] with minor modifications. Briefly, milled or native lysozyme samples were dissolved in  $0.1\text{ M}$  potassium phosphate buffer at  $\text{pH } 7.0$  ( $25\mu\text{g/ml}$ ),  $40\ \mu\text{L}$  of this solution was mixed with  $170\ \mu\text{L}$  ( $3\text{mg/ml}$ ) cell suspension of *Micrococcus lysodeikticus* in a 96-well plate. The decrease in absorption at  $450\text{ nm}$  wavelength due to lysis of the cells was measured in 10-second intervals for 2 min using SpectraMax i3x microplate reader (Molecular Devices, Sunnyvale, CA, USA). The kinetic rate, indicating the enzyme activity, was obtained from the slope of the linear part of the curve. Activity was calculated using a calibration curve measured with a solution of native lysozyme at a concentration of  $1.3$ ,  $1.8$ ,  $2.5$ ,  $3.1$ ,  $3.8$ ,  $4.4$ , and  $5.0\ \mu\text{g/mL}$ . Samples from milling were measured in triplicates. The residual enzymatic activity was calculated based on the method previously reported by Gao and Yaylayan.[30]

### **7.3.6 Intrinsic Fluorescence Spectroscopy**

The intrinsic emission fluorescence spectra of the protein samples ( $0.5\text{ mg/mL}$ ;  $0.1\text{ M}$  phosphate buffer,  $\text{pH } 7$ ) were obtained with a SpectraMax i3x microplate reader (Molecular Devices, Sunnyvale, CA, USA) at an excitation wavelength of  $290$ . The emission spectra were recorded from  $300$  to  $400\text{ nm}$  at a constant slit width of  $10\text{ nm}$  for both excitation and emission. Samples from milling were measured in triplicates.

### **7.3.7 Statistical analyses**

Sample preparation and their analyses were performed in three independent replicates. One-way analysis of variance (one-way ANOVA) was performed followed by the least significant difference (LSD) test to establish the significance in differences among the mean values using the SPSS 22.0 program (SPSS Inc., Chicago, IL, USA) statistical analysis package and the level of significance was determined at  $p < 0.05$ .

## 7.4 Results and Discussion

Hen egg white lysozyme is a relatively small globular protein containing 129 amino acids (8 lysine residual) with an average molecular mass of 14307 Da. Using lysozyme as a model protein, we investigated the advantages of mechanochemically induced solid-state glycation over thermal glycation employing ESI-qToF-MS to estimate the distribution of various glycoforms. This technique has been proven to be a precise method for monitoring protein glycation and for quantitative and qualitative analysis of glycoconjugate profile distribution. [2, 31, 32] During the ESI-MS analysis, the diluted protein solutions were directly infused under conditions that will preserve its native structure in multiply-charged states. The native spectrum produced from ESI-MS of glycated LZM revealed a heterogeneous distribution of glycoforms in the charge states ranging from +9 to +14 within  $m/z$  range of 1000-1700 amu. In this case, the interpretation of the spectral information can be challenging due to the low signal-to-noise ratio and broad peak shapes resulting from residual solvation and adduct formation during the ionization process.[33] In order to simplify data interpretation from ESI-MS, deconvolution of each spectrum was performed before the glycoconjugate profile was evaluated.

### 7.4.1 Analysis of the distribution of glycoconjugate profile

The preliminary glycation experiments were performed with aged lysozyme samples (stored in the freezer for over 10 years and indicated as LZM\* in Table 7.1). These preliminary trials have indicated that the mechanical energy supplied through ball milling at the frequency of 30 Hz for 1 hour was sufficient to overcome the energy barrier for initiating the condensation reaction between a carbonyl group of glucose and an amino moiety of lysozyme. Increasing the sugar concentration from 9% (w/w; approximately 1:1 molar ratio of lysine residue of lysozyme to sugar carbonyl) to 30% (w/w; approximately 1:1 molar ratio of lysine, arginine, glutamine, and asparagine residue of lysozyme to sugar carbonyl), lead to a decrease in the percentage of glycation from 31.91% to 10.15% (see Table 7.1). This could be attributed to the protective role of sugar on the solid-state stability of enzymes.[34] Furthermore, due to the intense mixing effect produced during the milling process, comparable glycation efficiencies and glycoform profiles were obtained regardless whether the reaction mixtures were dissolved in water and lyophilized or just mixed prior to milling experiments. Consequently, all the experiments were performed by simply mixing the sugar with lysozyme. The milling frequency was kept at 30Hz and 30- or 60-min durations representing the low and high mechanical energy input. Milling experiments performed with a

recently purchased lysozyme showed significantly lower glycation efficiency compared to aged lysozyme (Table 7.1, entries 1 & 6). This could be attributed to the conformational changes during storage and possibly results in more exposed lysine groups which are more accessible to glucose. To test this hypothesis, we heated the fresh lysozyme (LZM) at 76°C for 1 hour in a closed glass vial in the sand bath before mechanochemical glycation to mimic the aging process. [35] The deliberately denatured fresh lysozyme was denoted as LZM\*\* (Table 7.1, entry 3). Interestingly, a significant and comparable increase in the glycation efficiency was observed to that of LZM\* as shown in Table 7.1. Another interesting observation was that 60 min of milling time did not alter the glycation efficiency and glycoform distribution relative to 30 min (see Table 7.1, entries 5 & 6). High impact milling reactions where water is released as an internal solvent such as glycation, may alter the reaction phase from a dry powdery solid into a moist semi-solid, causing the mechanical energy supplied through impact to shift to mainly kneading. This results in decreased efficiency of absorption of mechanical energy, longer reaction times, low yields and poor scalability.[36] On the other hand, prolonged milling times (more than 60 min) at high frequency might result in a substantial increase in temperature due to friction especially for milling vials made from stainless steel.[37] Therefore, milling times longer than 30 min are not appropriate parameters for improving glycation yield or changing the glycoform distribution. Under these conditions (30 min milling at 30 Hz) mechanochemical induced glycation mainly results in mono-glycated lysozyme with minimal increase in frictional temperature during the reaction.

#### **7.4.2 Investigation of the factors influencing the efficiency of mechanochemical glycation**

We investigated further the effect of using solid acid or solid base as catalysts for mechanochemical glycation reactions. Both  $\text{AlCl}_3$  and KOH failed in initiating glycation in the solid state (see Table 7.1, entries 9 & 10). Most likely KOH degraded sugar and  $\text{AlCl}_3$  catalyzed the conversion of glucose into oligosaccharides as demonstrated before. [38] [39] Using more reactive sugars was also investigated as a means of improving the yields. Usually, thermally induced glycation with reactive sugars such as ribose often proceed in an uncontrollable manner [38], requiring the use of anti-glycating agents to control the extent of glycation and browning.[30] Interestingly, with ball milling, the glycation with ribose also proceeded in a controlled manner producing mainly mono-glycated lysozyme with a higher conversion factor (see Table 7.1, entry 8) indicating that mechanochemical glycation in the solid state could be used as a promising tool

for controlled glycation of proteins with highly reactive sugars without the need for chemical control.

Limited accessibility of  $\epsilon$ -amino groups of lysine to the surrounding sugars in the solid state was considered as one of the reasons behind controlled glycation under solid state milling conditions. In an attempt to increase the flexibility of protein and to have more accessible amino groups, water (200% w/w) was introduced into the reaction system as a solvent before milling to perform liquid assisted grinding. However, the results showed that, on the contrary, the addition of water even prevented the glycation (Table 7.1, entry 7) either through hydrolysis of the initially formed Schiff base or through hydrophobic effect shielding the reducing sugars from the amino groups.

Furthermore, inspired by an innovative milling process reported by Hammerer et al. (2018),[22] where repeated milling and aging/heating cycles have improved the efficiency of the mechanochemical transformations, we investigated the utility of such an approach on the glycation process of lysozyme (Table 7.1, entries 11 &12) through implementation of such as cycle where lysozyme was milled for 30 min at 30Hz followed by heating at 50°C for 30 min. The results have indicated that two such consecutive treatment cycles were able to increase the total conversion of lysozyme to 40.6 % from 18.8% at the same time increasing the percentage of dehydrated monoglycated product and even inducing the formation of a trace amount of triglycated product (1.58%). However, when the number of cycles was increased to three, a complete loss of MS protein signal was observed and neither lysozyme nor its glycated products were detected by the ESI-MS. The samples obtained from such a high intense treatment displayed a dark brown char-like texture instead of yellowish-white powder as was observed in other cases due to the total degradation of reactants.

Overall, it was observed that mechanical energy supplied via ball milling could initiate the condensation between sugars and lysozyme. Under all treatment conditions (see Table 7.1), the glycoconjugates formed always consisted of mainly monoglycated product and a small amount of dehydrated monoglycated and diglycated products. Therefore, mechanochemical glycation could be a potentially promising method for introducing controlled and limited mono-glycation, especially with highly reactive sugars.

**Table 7.1** ESI/MS based calculated values of glycoform distribution in mechanochemically-induced glycosylated lysozyme a

	Reactants	Milling time (min)	% LZM <sup>b</sup> conversion	% LZM+S	% LZM+S - H <sub>2</sub> O	% LZM+2S
1	LZM* + 9% Glu <sup>c</sup>	60	31.25 ± 0.66%	23.48 ± 0.80%	3.75 ± 0.52%	3.72 ± 0.36%
2	LZM* + 30% Glu <sup>c</sup>	60	10.75 ± 0.60%	9.59 ± 0.18%	0	0.83 ± 0.09%
3	LZM** + 9% Glu <sup>d</sup>	60	39.16 ± 0.55%	25.11 ± 0.17%	6.60 ± 1.10%	6.04 ± 0.06%
4	LZM <sup>e</sup> + 4% Glu	30	9.34 ± 1.35%	8.77 ± 1.42%	0	0.58 ± 0.07%
5	LZM + 9% Glu	30	18.83 ± 1.14%	14.14 ± 0.83%	2.35 ± 0.05%	2.35 ± 0.35%
6	LZM + 9% Glu	60	19.72 ± 0.59%	13.67 ± 0.14%	5.14 ± 1.93%	1.48 ± 0.92%
7	LZM + 9% Glu+200% water	60	11.54 ± 0.20%	10.76 ± 0.99%	0	0.46 ± 0.46%
8	LZM + 7.5% Ribose	30	30.37 ± 3.95%	24.33 ± 2.26%	0	4.93 ± 1.23%
9	LZM + 9% Glu + 1% KOH	30	0	0	0	0
10	LZM + 9% Glu+1% AlCl <sub>3</sub>	30	0	0	0	0
11	LZM + 9% Glu	(Cycle) <sup>f</sup> ×2	40.57 ± 0.86%	24.53 ± 0.76%	7.54 ± 2.04%	6.40 ± 0.31%
12	LZM + 9% Glu	(Cycle) <sup>f</sup> ×3	No protein signal	No protein signal	No protein signal	No protein signal
13	LZM + 9% Glu	(Cycle) <sup>g</sup> ×2	9.67 ± 0.54%	9.07 ± 0.07%	0	0.38 ± 0.38%

<sup>a</sup> all values represent the average of two replicate experiments ± standard deviation, % compositions are w/w basis and S = Sugar

<sup>b</sup> based on the ESI/MS intensity of the unreacted LZM

<sup>c</sup> LZM\* = aged lysozyme;

<sup>d</sup> LZM\*\* = fresh lysozyme heated at 76°C for 1 hour before mechanochemical treatment

<sup>e</sup> LZM = fresh lysozyme;

<sup>f</sup> Cycle = repeated milling and heating cycles where LZM was milled 30 min at 30 Hz followed by heating at 50°C for 30 min, repeated 2 or 3 times.

<sup>g</sup> Cycle = repeated milling and heating cycles where LZM was milled 15 min at 30 Hz followed by heating at 50°C for 45 min, repeated 2 times.

### 7.4.3 Effect of milling on conformational changes and the residual enzymatic activity

The effect of mechanical stress and mechanochemical glycation on the secondary structure and conformational changes of lysozyme were studied using Fourier transform infrared (FTIR) spectroscopy and fluorescence spectroscopy. FTIR is one of the most commonly used techniques for the determination of protein secondary structure featuring fast and non-destructive approach. According to literature, the structural information obtained from FTIR are in a good agreement with the values determined using X-ray crystallography and ultraviolet circular dichroism spectroscopy.[26, 27] The amide I band ( $1700\text{ cm}^{-1} - 1600\text{ cm}^{-1}$ ), which arises mainly from the C=O stretching vibration, was used for the elucidation of the changes in the secondary structure induced by milling. Second derivative spectra of the amide I bands were used to resolve the superimposed bands representing the four most common structural motifs of lysozyme;  $\alpha$ -helix,  $\beta$ -sheet,  $\beta$ -turns, and unordered/random coils. The second derivative is the most common band narrowing technique for effectively removing sloping baselines and broad spectral features of a spectrum. It also permits direct quantitative analysis of the components of the secondary structure of proteins by revealing the unresolved bands in the original spectrum.[26] Structurally, lysozyme is a helix-rich globular protein consisting of  $\sim 40\%$  or  $\sim 46\%$  of the  $\alpha$ -helical structure as reported in the literature by using ATR/FTIR [40] and X-ray [41] respectively. In this study, the most significant changes of lysozyme secondary structure in terms of milling time occurred within the helical region, where a downshifting of the most intense peak from  $1656\text{ cm}^{-1}$  ( $\alpha$ -helix) to  $\sim 1650\text{ cm}^{-1}$  (unordered helix) was observed (Figure 7.1) for all samples milled with and without sugar. The loss of  $\alpha$ -helix results in loss of the active conformation and a decrease in enzymatic activity. The residual enzymatic activity of lysozyme milled for 30 min and 60 min were  $67.53 \pm 3.26\%$  and  $38.22 \pm 4.33\%$  respectively relative to the activity of native lysozyme (Figure 7.2a). There was a significant increase ( $p < 0.05$ ) in the residual enzymatic activity of lysozyme milled in the presence of sugar compared to that milled without sugar. For 30 min milling with glucose, the measured activity value was  $84.13 \pm 5.20\%$  and for 60 min milling, the value was  $59.37 \pm 5.76\%$ . Although the second derivative spectrum of amide I band did not indicate any specific differences between samples milled with and without sugar (Figure 7.1), however, analysis of amide II band was more informative. FTIR analysis was performed in  $\text{D}_2\text{O}$  due to the strong interference of H–O–H bending vibrations from  $\text{H}_2\text{O}$  overlapping with the amide I band of protein.[27] Compared to amide I band, the IR absorption bands of amide II band ( $\sim 1550\text{ cm}^{-1}$ ), are mainly due to in-

plane N–H bending (40–60%) and C–N stretching (20–40%) vibrations that shift towards  $\sim 1450\text{ cm}^{-1}$  and  $\sim 940\text{--}1040\text{ cm}^{-1}$  respectively upon H/D exchange.[42] In this experiment, a series of 4 spectra were recorded for each sample during the H/D exchange process over a one hour period with 20 minutes intervals at room temperature. As shown in Figure 7.3, amide II band shifted towards amide II' upon H/D exchange, the intensity was used as an index of deuteration level. As shown in Figure 7.3, the sample M60 (lysozyme milled for 60 minutes), underwent H/D exchange almost instantaneously upon addition of  $\text{D}_2\text{O}$  and the intensity of the amide II' increased significantly over the one hour period compared to the native lysozyme, indicating milling disrupted the ordered structure of lysozyme since the kinetics of H/D exchange relies on the strength of hydrogen bonding and the accessibility of the external amide protons.[43] On the other hand, because of the inherently ordered structure of lysozyme where exchangeable protons are buried in the less accessible domains, native lysozyme went through a very slow H/D exchange process which is consistent with literature observations where complete H/D exchange takes up to 24 hours under room temperature.[27] Surprisingly, mechanochemically glycosylated lysozyme (M60+Glu) showed even more reluctance to H/D exchange compared to native lysozyme due to the stabilizing effect of sugar on maintaining protein tertiary structure via either the formation of cross-linking or H-bonding leading to a more compact conformation and prevention of isotopic exchange.[34] The presence of monoglycosylated adducts with loss of one-mole water (see Table 7.1, entry 5) implies the formation of a potential carbonyl moiety on the glycosylated lysozyme able to cross-link. In addition, the intrinsic fluorescence spectra of lysozyme samples were also recorded ( $\lambda_{\text{ex}} = 290\text{ nm}$ ;  $\lambda_{\text{em}} = 300\text{--}400\text{ nm}$ ) as an indication of the chemical environment of the six tryptophan residues and their specific interactions. The results are in good agreement with the observation made in the FTIR H/D exchange experiments and the residual enzymatic activity assays results. Lysozyme milled for 60 minutes showed a drastic decrease in the fluorescence intensity at 350 nm indicating significant structural modification induced by milling (Figure 7.2b). The decrease in the fluorescence intensity suggested the disruption of the tertiary structure and subsequent exposure of tryptophyl residues to the solvent.[44] Similarly, the increase in intrinsic fluorescence of lysozyme upon glycosylation with glucose suggests partial recovery of the tertiary structure due to the interaction with sugar as discussed in H/D exchange process. In all cases, the maxima of the emission peaks were not shifted. The intrinsic fluorescence results, in conjunction with those obtained using FTIR and enzymatic activity assays, suggest that mechanical stress

supplied through ball milling results in enzymatic activity loss of lysozyme due to disruption of its structural integrity. Milling in the presence of glucose had a positive effect on the preservation of the tertiary structure of the lysozyme and its enzymatic activity through either cross-linking by glycation or the formation of H-bonding. The effect of the formation of H-bonding on the stability of the enzymatic activity was evaluated by replacing glucose with sorbitol, a nonreducing sugar. After 30 min of milling with sorbitol, the residual enzymatic activity measured was  $65.71 \pm 2.07\%$  indicating that the formation of glycoconjugates is necessary to retain the enzymatic activity. Furthermore, replacing glucose with ribose similarly retained the enzymatic activity of lysozyme at the same level as that of glucose.

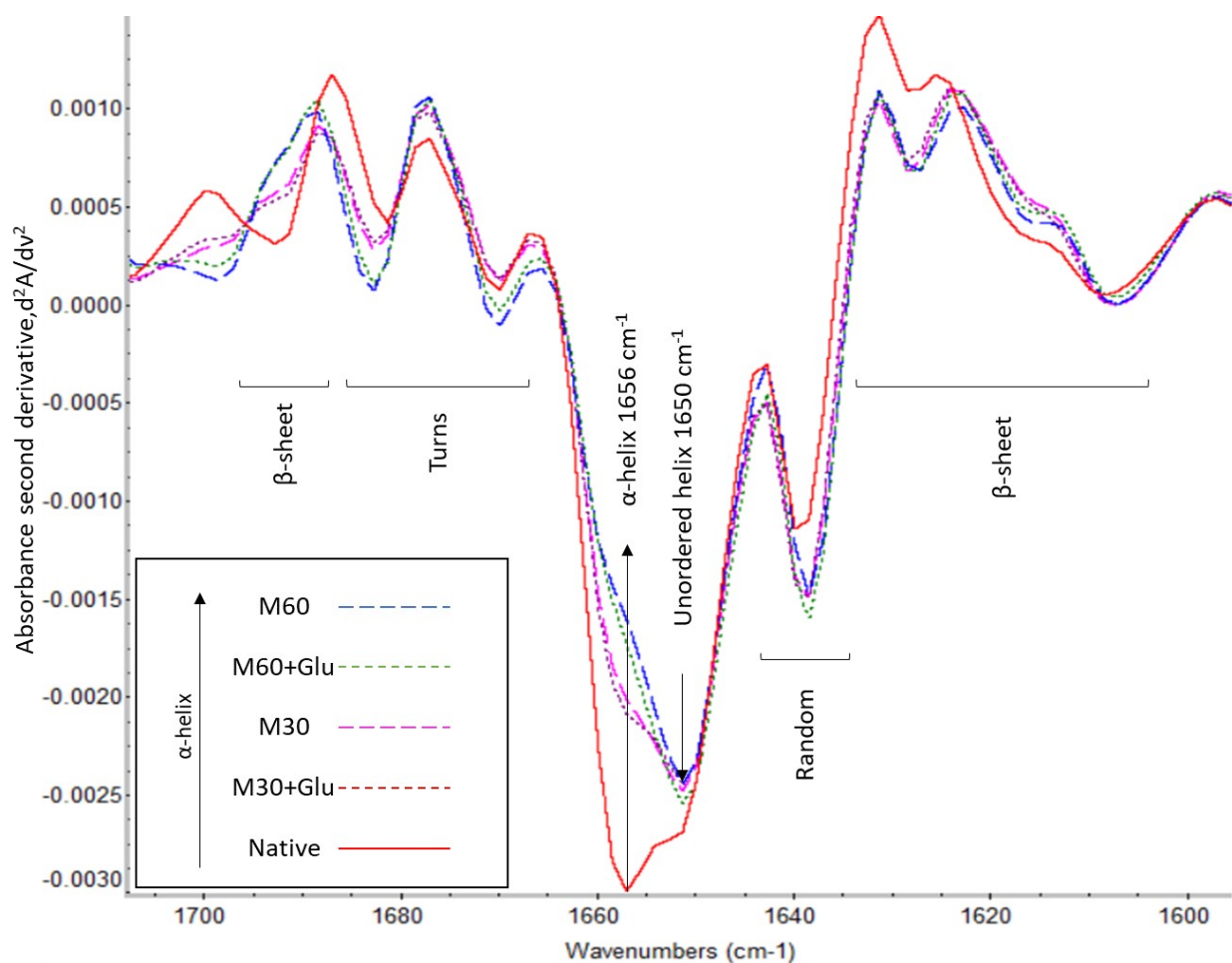


**Figure 7.1** Superimposed second derivative FTIR spectra of amide I region of native lysozyme (Native, red solid line), 30 minutes milled lysozyme (M30, magenta dashed line), and 60 minutes milled lysozyme (M60, blue dashed line) with/without 9% glucose.

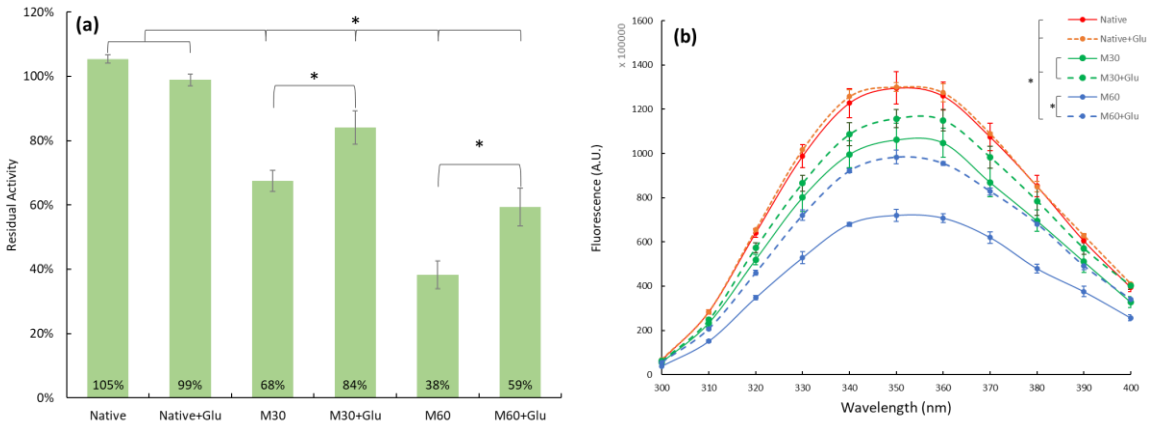


**Figure 7.2** (a) Residual lysozyme activity and (b) intrinsic fluorescence ( $\lambda_{ex}=290$  nm) before and after milling at 30 minutes (M30) and 60 minutes (M60) with and without glucose (Glu); the values are reported as the mean  $\pm$  standard deviation of triplicates; \* indicates significant difference at  $p < 0.05$ .

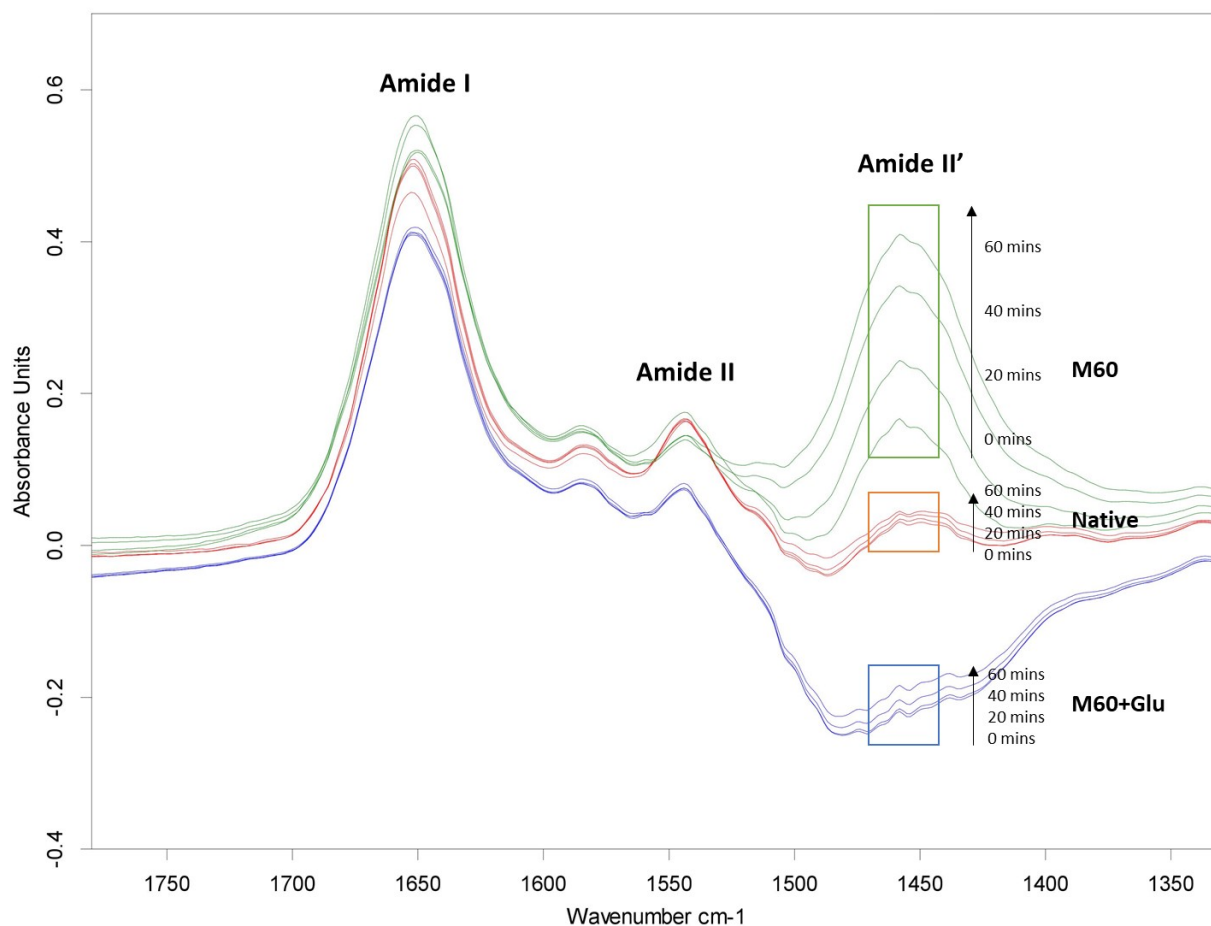


**Figure 7.3** Time-dependent superimposed FTIR spectra of amide I, amide II and amide II' which appear upon H/D exchange of amide II, a series of 4 spectra were recorded for lysozyme (Native, red lines) and 60 minutes milled lysozyme (M60, green lines) with/without 9% glucose (M60+Glu, blue lines) during the H/D exchange process over 1-hour period with 20 minutes interval at room temperature.

In recent years, there is considerable interest in the use of denatured globular proteins as excipients in pharmaceutical formulations with improved emulsion stability and targeted delivery of active pharmaceutical ingredient.[45] For this purpose, milling would be a perfect solution for fast denaturation and modification of protein conformation and eliminate the use of solvents.

Overall, ball milling was shown to be a fast, efficient, solvent-free process to induce controlled glycation of lysozyme even in the presence of reactive sugars, generating a mainly mono-glycated product. Extensive milling of lysozyme in the absence of sugars results in significant loss of

enzymatic activity as evidenced by the loss of  $\alpha$ -helix and other conformational changes as measured by FTIR spectroscopy and intrinsic fluorescence spectroscopy. On the other hand, milling in the presence of sugars was found to have a positive effect on the stabilization of protein conformation and on the preservation of enzymatic activity.

## 7.5 References

1. Nursten, H.E., *The Maillard reaction: chemistry, biochemistry, and implications*. 2005: Royal Society of Chemistry.
2. Yeboah, F.K., et al., *Monitoring glycation of lysozyme by electrospray ionization mass spectrometry*. Journal of agricultural and food chemistry, 2000. **48**(7): p. 2766-2774.
3. Wang, Z., et al., *Advanced glycation end-product N  $\epsilon$ -carboxymethyl-Lysine accelerates progression of atherosclerotic calcification in diabetes*. Atherosclerosis, 2012. **221**(2): p. 387-396.
4. Wang, W.-q., Y.-h. Bao, and Y. Chen, *Characteristics and antioxidant activity of water-soluble Maillard reaction products from interactions in a whey protein isolate and sugars system*. Food chemistry, 2013. **139**(1): p. 355-361.
5. Le, T.T., et al., *Maillard reaction and protein cross-linking in relation to the solubility of milk powders*. Journal of agricultural and food chemistry, 2011. **59**(23): p. 12473-12479.
6. Aoki, T., et al., *Improvement of heat stability and emulsifying activity of ovalbumin by conjugation with glucuronic acid through the Maillard reaction*. Food Research International, 1999. **32**(2): p. 129-133.
7. Corzo-Martínez, M., et al., *Assessment of interfacial and foaming properties of bovine sodium caseinate glycated with galactose*. Journal of food engineering, 2012. **113**(3): p. 461-470.
8. Naranjo, G.B., L.S. Malec, and M. Vigo, *Reducing sugars effect on available lysine loss of casein by moderate heat treatment*. Food Chemistry, 1998. **62**(3): p. 309-313.
9. Moreaux, V. and I. Birlouez-Aragon, *Degradation of Tryptophan in Heated  $\beta$ -Lactoglobulin-Lactose Mixtures Is Associated with Intense Maillard Reaction*. Journal of Agricultural and Food Chemistry, 1997. **45**(5): p. 1905-1910.

10. Wang, H., et al., *Comparison of glycation in conventionally and microwave-heated ovalbumin by high resolution mass spectrometry*. Food chemistry, 2013. **141**(2): p. 985-991.
11. Tsubokura, Y., et al., *Glycation of ovalbumin in solid-state by conductive and microwave heating*. Food science and technology research, 2009. **15**(4): p. 377-380.
12. Zhang, N., et al., *Liquid Chromatography High-Resolution Mass Spectrometry Identifies the Glycation Sites of Bovine Serum Albumin Induced by d-Ribose with Ultrasonic Treatment*. Journal of agricultural and food chemistry, 2018. **66**(3): p. 563-570.
13. Mu, L., et al., *Effect of Ultrasonic Treatment on the Graft Reaction between Soy Protein Isolate and Gum Acacia and on the Physicochemical Properties of Conjugates*. Journal of Agricultural and Food Chemistry, 2010. **58**(7): p. 4494-4499.
14. Shi, W.-H., et al., *Study on the characteristic of bovine serum albumin-glucose model system, treated by ultrasonic*. Food research international, 2010. **43**(8): p. 2115-2118.
15. Stanic-Vucinic, D., et al., *Structure and antioxidant activity of  $\beta$ -lactoglobulin-glycoconjugates obtained by high-intensity-ultrasound-induced Maillard reaction in aqueous model systems under neutral conditions*. Food chemistry, 2013. **138**(1): p. 590-599.
16. Viton, F., H.R. Oertling, and R. Fumeaux, *Mechanical generation of flavour compositions*. 2017, U.S. Patent US20170079316A1.
17. Sun, C., et al., *Reduction of particle size based on superfine grinding: Effects on structure, rheological and gelling properties of whey protein concentrate*. Journal of Food Engineering, 2016. **186**: p. 69-76.
18. Ramadhan, K. and T.J. Foster, *Effects of ball milling on the structural, thermal, and rheological properties of oat bran protein flour*. Journal of Food Engineering, 2018. **229**: p. 50-56.
19. Hernández, J.G., M. Frings, and C. Bolm, *Mechanochemical Enzymatic Kinetic Resolution of Secondary Alcohols under Ball-Milling Conditions*. ChemCatChem, 2016. **8**(10): p. 1769-1772.
20. Hernández, J.G., et al., *Mechanoenzymatic peptide and amide bond formation*. Green Chemistry, 2017. **19**(11): p. 2620-2625.

21. Ardila-Fierro, K.J., et al., *Papain-catalysed mechanochemical synthesis of oligopeptides by milling and twin-screw extrusion; application in the Juliá-Colonna enantioselective epoxidation*. Green Chemistry, 2018.
22. Hammerer, F., et al., *Solvent-free enzyme activity: quick, high-yielding mechano-enzymatic hydrolysis of cellulose into glucose*. Angewandte Chemie International Edition, 2018.
23. Ghalanbor, Z., M. Körber, and R. Bodmeier, *Protein release from poly(lactide-co-glycolide) implants prepared by hot-melt extrusion: Thioester formation as a reason for incomplete release*. International Journal of Pharmaceutics, 2012. **438**(1): p. 302-306.
24. Wu, D., et al., *Effect of Ball Mill Treatment on the Physicochemical Properties and Digestibility of Protein Extracts Generated from Scallops (*Chlamys farreri*)*. International journal of molecular sciences, 2018. **19**(2): p. 531.
25. Wang, Z., et al., *Effects of ball milling treatment on physicochemical properties and digestibility of Pacific oyster (*Crassostrea gigas*) protein powder*. Food Science & Nutrition, 2018. **6**(6): p. 1582-1590.
26. Dong, A., P. Huang, and W.S. Caughey, *Protein secondary structures in water from second-derivative amide I infrared spectra*. Biochemistry, 1990. **29**(13): p. 3303-3308.
27. Byler, D.M. and H. Susi, *Examination of the secondary structure of proteins by deconvolved FTIR spectra*. Biopolymers: Original Research on Biomolecules, 1986. **25**(3): p. 469-487.
28. Sethuraman, A. and G. Belfort, *Protein Structural Perturbation and Aggregation on Homogeneous Surfaces*. Biophysical Journal, 2005. **88**(2): p. 1322-1333.
29. Shugar, D., *The measurement of lysozyme activity and the ultra-violet inactivation of lysozyme*. Biochimica et Biophysica Acta, 1952. **8**: p. 302-309.
30. Gao, H.Y., V.A. Yaylayan, and F. Yeboah, *Oxalic acid-induced modifications of postglycation activity of lysozyme and its glycoforms*. Journal of agricultural and food chemistry, 2010. **58**(10): p. 6219-6225.
31. Yeboah, F.K. and V.A. Yaylayan, *Analysis of glycated proteins by mass spectrometric techniques: qualitative and quantitative aspects*. Food / Nahrung, 2001. **45**(3): p. 164-171.

32. Yeboah, F.K., et al., *Effect of limited solid-state glycation on the conformation of lysozyme by ESI-MS/MS peptide mapping and molecular modeling*. *Bioconjugate chemistry*, 2004. **15**(1): p. 27-34.
33. Akıllıoğlu, H.G., et al., *Monitoring protein glycation by electrospray ionization (ESI) quadrupole time-of-flight (Q-TOF) mass spectrometer*. *Food Chemistry*, 2017. **217**: p. 65-73.
34. Mensink, M.A., et al., *How sugars protect proteins in the solid state and during drying (review): Mechanisms of stabilization in relation to stress conditions*. *European Journal of Pharmaceutics and Biopharmaceutics*, 2017. **114**: p. 288-295.
35. Elkordy, A.A., R.T. Forbes, and B.W. Barry, *Study of protein conformational stability and integrity using calorimetry and FT-Raman spectroscopy correlated with enzymatic activity*. *European Journal of Pharmaceutical Sciences*, 2008. **33**(2): p. 177-190.
36. Kaupp, G., *Mechanochemistry: the varied applications of mechanical bond-breaking*. *CrystEngComm*, 2009. **11**(3): p. 388-403.
37. Schneider, F., et al., *Energetic assessment of the Suzuki–Miyaura reaction: a curtate life cycle assessment as an easily understandable and applicable tool for reaction optimization*. *Green Chemistry*, 2009. **11**(11): p. 1894-1899.
38. Xing, H. and V.A. Yaylayan, *Mechanochemical depolymerization of inulin*. *Carbohydrate Research*, 2018. **460**: p. 14-18.
39. Meine, N., R. Rinaldi, and F. Schüth, *Solvent-Free Catalytic Depolymerization of Cellulose to Water-Soluble Oligosaccharides*. *ChemSusChem*, 2012. **5**(8): p. 1449-1454.
40. Vedantham, G., et al., *A holistic approach for protein secondary structure estimation from infrared spectra in H<sub>2</sub>O solutions*. *Analytical biochemistry*, 2000. **285**(1): p. 33-49.
41. Frishman, D. and P. Argos, *Knowledge-based protein secondary structure assignment*. *Proteins: Structure, Function, and Bioinformatics*, 1995. **23**(4): p. 566-579.
42. Vigano, C., et al., *Hydrogen-deuterium exchange in membrane proteins monitored by IR spectroscopy: A new tool to resolve protein structure and dynamics*. *Biopolymers*, 2004. **74**(1-2): p. 19-26.
43. Güler, G., et al., *Proteolytically-induced changes of secondary structural protein conformation of bovine serum albumin monitored by Fourier transform infrared (FT-IR)*

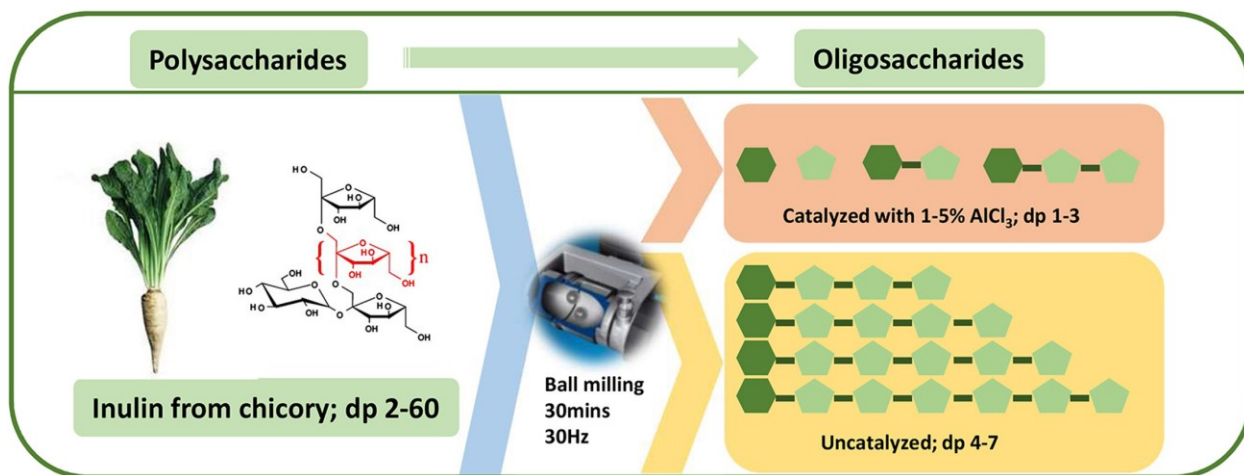
- and UV-circular dichroism spectroscopy*. *Spectrochimica Acta Part A: Molecular and Biomolecular Spectroscopy*, 2016. **161**: p. 8-18.
44. Pallarès, I., et al., *Amyloid Fibril Formation by a Partially Structured Intermediate State of  $\alpha$ -Chymotrypsin*. *Journal of Molecular Biology*, 2004. **342**(1): p. 321-331.
45. Mohammad, M.A., et al., *Effect of mechanical denaturation on surface free energy of protein powders*. *Colloids and Surfaces B: Biointerfaces*, 2016. **146**: p. 700-706.

## Connecting paragraph

Chapters 4 to 7 have demonstrated that ball milling is an excellent strategy to control the extent of the Maillard reaction between small molecules such as reducing sugars and amino acids. Furthermore, application of mechanochemistry was further extended to larger protein molecules such as lysozyme, and in this chapter to polysaccharides. To integrate this research in the context of food sustainability and to demonstrate the ability of ball milling to hydrolyze polysaccharides and generate reducing sugars needed for the Maillard reaction and fructo-oligosaccharides having prebiotic properties, we have chosen inulin as a viable carbohydrate biomass.

Chapter 8 was published in the *Carbohydrate Research*: Xing, H., & Yaylayan, V. A. (2018). Mechanochemical depolymerization of inulin. *Carbohydrate Research*, **460**, 14-18.

## Chapter 8 Mechanochemical depolymerization of inulin



## 8.1 Abstract

Although chemical reactions driven by mechanical force is emerging as a promising tool in the field of physical sciences, its applications in the area of food sciences are not reported. In this paper, we propose ball milling as an efficient tool for the controlled generation of fructooligosaccharide (FOS) mixtures from inulin with a degree of polymerization (dp) ranging between 4 and 7. The addition of catalytic amounts of  $\text{AlCl}_3$  together with ball milling (30 min, at 30Hz) generated mixtures rich in dehydrated disaccharides such as di-D-fructose dianhydrides. Based on anion exchange chromatography in conjunction with ESI/qTOF/MS/MS analysis, catalysis increased the overall content of mono-, di-, and tri- saccharides by around 30 fold compared to un-catalyzed milling. In addition, dialysis results of the untreated and treated samples have indicated that under catalysis the percent of depolymerisation (dp <12) reached 73.4% from the starting value of 27.6% in the untreated sample. Both processes resulted in mixtures of prebiotic value. The use of mechanical energy may be suitable for a fast, cost-efficient and green conversion of inulin to value-added food ingredients.

**Keywords:** Inulin, fructooligosaccharide, solvent-free hydrolysis, prebiotic oligosaccharides, ball milling

## 8.2 Introduction

Chemical transformations induced by ball milling has emerged as one of the most advantageous, environmentally-friendly alternatives to traditional routes for hydrolysis of biomass such as crystalline cellulose or lignocellulosic material [1-3]. The recovered monosaccharides are considered attractive renewable resources leading to valuable chemicals such as plastics, surfactants, gasoline, diesel fuels and medicines [4]. Featuring simplicity, high reproducibility, mild and short reaction times and solvent-free conditions, “mechanochemical pre-treatment” followed by thermal acid hydrolysis can offer near-complete recovery of sugar monomers from cellulosic biomass [2].

During depolymerization of biomasses, mechanical energy supplied in a reaction system via ball milling creates shear and stress on substances [5-8], breaking down solid particles to the smaller size and resulting in the greater surface area. Defects are introduced herein and finally leading to the amorphization state of the material [8-11]. Down to the molecular level, the arrangements of chemical structures of reactant are changed, mechanochemical activated chemical bonds leading to high reactivity intermediate and finally end products with altered properties [12, 13]. The efficiency and effectiveness of biomass depolymerization by mechanical force could be greatly enhanced by co-milling with various acid catalysts which termed as mechanocatalytical treatment [14, 15] because intimate mixing of reactants can enhance its contact between a catalyst and the substrate [1-3]. In mechanocatalytical treatments two main routes of introducing catalyst can be identified: the first is through impregnation, such as sulfuric acid [1, 2, 16], the second is directly mixing solid acids with samples followed by ball milling (also called co-milling or mix-milling) [3, 7] such as oxalic acid, maleic acid [1], and solid acid catalysts  $\text{SO}_4^{2-}/\text{SiO}_2\text{-Al}_2\text{O}_3/\text{La}^{3+}$  [17] etc. Despite the revival of mechanochemistry in physical sciences driven by the search for new and greener synthetic methodologies, its applications in food science are limited, of which starch is the most frequently studied material such as wheat starch [10, 18, 19], maize starch [11, 20], cornstarch [21] and amaranth flour [9] etc. It has been reported that ball milling starch granule results in particle size reduction [9, 11, 20, 22], loss in crystallinity and the gelatinization enthalpy [9, 10, 19], and increase in solubility[9, 11, 22]. Compared to native starch, the mechanically modified starch showed increased stability for food application such as in soup thickener [9] and bread ingredient[18].

The present study focuses on the controlled mechanochemical depolymerization process by ball-milling with the aim of generating prebiotic active oligosaccharide mixtures from inulin extracted from chicory that can be labeled as “green” and additive free. The process could be considered as a faster and cheaper alternative to the enzymatic methods. It is also the first reported attempt to mechanolysis of fructan-type polysaccharides. Aluminum chloride ( $\text{AlCl}_3$ ) was used as the solid acid catalyst and co-milled with inulin. The differences between mechanochemical and mechanocatalytical effects are also compared.

## **8.3 Materials and Methods**

### **8.3.1 Materials and reagents**

All reagents and chemicals were purchased from Sigma-Aldrich Chemical Co. (Oakville, ON, Canada) without further purification. Inulin from chicory (FOS;  $\text{C}_{6n}\text{H}_{10n+2}\text{O}_{5n+1}$ ) is composed of glucose-(fructose)<sub>n</sub> with  $\beta$ -2,1-linkage between the fructose monomer units. The length of the fructose chain varies from 2 to 60 sugar units with an average degree of polymerization (dp) of >10.

### **8.3.2 Ball-Milling**

Ball milling was conducted at an ambient temperature by placing 0.2 g of powdery sample in a stainless-steel grinding jar (10 ml) with 2 steel balls (3.2 mm in diameter; ball/sample ratio ~16:1) for creating inner friction. The jars were seated in the Retsch Mixer Mills MM 400 (Newtown, PA, US) and perform radial oscillations in a horizontal position without coolant (the external jar temperature was about 25 °C) at a frequency of 15 and 30Hz for 30 and 60 minutes.  $\text{AlCl}_3$  was added in some trials at 1%, 3%, and 5% by weight by simply mixing with FOS untreated sample. Samples collected after milling were refrigerated for further analysis.

### **8.3.3 Electrospray ionization/quadrupole time of flight/tandem mass spectrometry (ESI/qTOF/MS/MS) analysis**

The dry samples were dissolved in deionized water (Millipore, Billerica, MA) to a concentration of 1 mL/mg. The sample was then diluted 10-fold in 10% methanol prior to analysis by ESI-MS. A total of 1  $\mu\text{L}$  of the sample was injected directly into ESI-MS. The ESI-MS analysis included a Dionex Ultimate 3000 RS liquid chromatograph (Dionex, Germering, Germany) coupled to a Bruker Maxis Impact quadruple-time-of-flight mass spectrometer (Bruker Daltonics, Bremen, Germany) operating in positive mode with electrospray ionization as the source type. The

electrospray interphase settings were as follows: nebulizer pressure, 0.6 bar; drying gas, 4 L/min; temperature, 180 °C; and capillary voltage, 4500 V. The scan range was from  $m/z$  100 to 1500. The data were analyzed using Bruker Compass Data Analysis software, version 4.2. Tandem mass spectrometry (MS/MS) was carried out in MRM mode using 10.0 eV collision energy for the selected ions at  $[M+X]^+$  365, 527, 689, 851, 1004 and 1013 (dp range of 2-7).

#### 8.3.4 ESI-MS data processing

The raw spectra were processed by filtering the peaks with a signal-to-noise ratio (S/N) lower than 10 within the scan range from 100 to 1500  $m/z$ . Molecular formulae were assigned to all the observed peaks based on their exact  $m/z$  values by using the on-line software “ChemCalc” (Institute of Chemical Sciences and Engineering, Lausanne, Switzerland). The assigned molecular formulas were screened based on the FOS formula ( $C_{6n}H_{10n+2}O_{5n+1}$ ) of which some products were protonated, sodiated or potassiated (Table 8.1). For further processing, we calculated the percentage of each selected oligosaccharide with different chain lengths based on their contribution to the total intensity of all the identified peaks. The changing of oligosaccharides profile of each sample was reported and discussed. The identified fragments were classified into three groups based on their degree of polymerization (dp), namely dp1-3, dp 4-7, and dp 8-10. Each sample was labeled as follows M(X min)-(Y)%- (Z) Hz, where X indicates milling time, Y the percent of  $AlCl_3$  and Z the frequency of treatment. For example, M30-0%-15Hz indicates 30 minutes of milling at 30 Hz with 0%  $AlCl_3$ .

#### 8.3.5 Identification of mono- and oligosaccharides

Proposed structures and molecular formulas of oligosaccharides were based on high-resolution ESI/qTOF/MS analysis of their elemental composition and on their MS/MS spectra. Selected samples were also analyzed for their oligosaccharide composition by anion exchange chromatography with a pulsed amperometric detection (AEC-PAD) following the method of Böhm *et al.* [23], Briefly, a Metrohm MIC-8 modular IC system (Herisau, Switzerland) consisting of a pulsed amperometric detector Bioscan 817 operating at (E1) 0.15 V,  $t_1=400$  ms, (E2) 0.75 V,  $t_2=200$  ms; (E3) -0.15 V,  $t_3=400$  ms. A Metrohm pump 709, and a sample injection unit connected to Metrosep Carb1-150 anion exchange column thermostated at 32 °C was used for the analysis of mono-, di-, tri-, and tetra-saccharides. The injection volume was 20  $\mu$ L of samples containing 1000 ppm carbohydrate. Elution was performed using 100mM NaOH as mobile phase and the flow rate

at 1 mL/min. A 50 ppm sorbitol, glucose, fructose, sucrose, raffinose, and stachyose were used as standards for quantification, of which 50 ppm sorbitol was added in every sample as an internal standard for increased reproducibility.

### **8.3.6 Dialysis**

Slide-A-Lyzer™ G2 Dialysis Cassettes (1-3ml) with a molecular-weight cutoff (MWCO) of 2K (approximately equivalent to dp 12) were obtained from Thermo Scientific (Rockford, IL, USA). Briefly, 40 mg of inulin sample was dissolved in 3 ml water and placed into the dialysis cassette and then dialysis against 1.8 L water at room temperature following the typical dialysis procedure as indicated in the manual. After dialysis, samples were collected and dried under ventilation and weighed. Untreated inulin and FOS M30-5%30 Hz were dialysed in duplicates.

## **8.4 Results and Discussion**

According to the manufacturer's specification, the length of the fructooligosaccharide chain in the commercial inulin sample varied between 2 to 60 fructose molecules. Four different measurements were performed to monitor the oligosaccharide profile of the untreated inulin as a function of storage time and temperature. Untreated inulin was first measured shortly after receiving the sample (July 2016), the measurement was repeated after one year at room temperature (~25°C) storage (July 6, 2017), and replicated after one week (July 13, 2017). The sample was also analyzed after two months of refrigerated (2-8°C) storage (September 2017). The oligosaccharide profile was found to be dependent on storage time and temperature. The analysis of the initial sample as received by the supplier indicated that within the MS scan range (100-1500 m/z) there was no significant presence of detectable oligosaccharides, only five very low-intensity peaks (below the quantification limit of the PAD detector) but were identified by MS to be mono- and disaccharides. Subsequent measurements performed after one-year of storage at room temperature, have indicated an increase in the total qTOF/ESI/MS detectable oligosaccharides of which the majority were found to have a dp range of 4-10. These detectable oligosaccharides represent a small portion of inulin. Dialysis (MWCO of 2K) results also showed a 72.4%±1.1% w/w retentate for untreated inulin after one year of storage. The 2K cut off point is approximately equivalent to molecular weight of an oligosaccharide with a dp value of 12. These observations indicate that inulin undergo peeling or deglycation reactions to a certain extent under storage conditions. In a previous study, Böhm *et al.* have indicated that inulin is susceptible to thermal degradation and

that dry heating at 195 °C for 30 min completely converts inulin into mainly a mixture of di-D-fructose dianhydrides [23].

#### 8.4.1 ESI/qTOF/MS analysis of inulin

To generate prebiotic active mixtures, inulin samples were subjected to ball milling at a frequency of 15 or 30 Hz for 30 and 60 minutes.  $\text{AlCl}_3$  was added at 1%, 3%, and 5% levels in some trials to estimate the role of the Lewis acid in the depolymerization process. Samples collected after millings were refrigerated for further ESI/qTOF/MS analysis to determine their oligosaccharide profile. All the identified ions from these experiments are listed in Table 8.1. Their percent relative contribution to the content of variously treated samples of FOS are reported in Figure 8.1. According to this figure, milled samples without catalysis were richer in oligosaccharides with a dp range of 4-7, while catalyzed milled samples were richer in oligosaccharides with a dp range of 1-3. These observations have led us to hypothesize that mechanical treatments result in the formation and accumulation of mechanically stable products satisfying a certain mass range requirement, in particular a dp range of 4-7 in case of un-catalysed reactions and a dp range of 1-3 in case of catalyzed reactions shown in Figure 8.1. The term limiting molecular weight ( $M_{\text{lim}}$ ) may be borrowed from sonochemistry to describe this observation [24]. The  $M_{\text{lim}}$  is defined as the minimum molecular weight below which chain scission reactions cease to exist due to the chain length of the substrate being too short to experience the forces required for bond cleavage [24]. The accumulation of oligosaccharides with a dp range of 4-7 may be the most stable molecular weight range under the given milling conditions. The term limiting molecular weight range ( $M_{\text{lim range}}$ ) may be defined to apply to mechanochemical processes as the minimum molecular weight range below which chain scission reactions cease to exist. Furthermore, the above observations may further indicate that milling induced depolymerization occurs simultaneously with its reverse process polymerization since in the literature both processes are reported to occur during milling. For example, Meine, Rinaldi R *et al.* verified a non-stereospecific recombination of glucose forming oligosaccharides when an excessive amount of mechanical energy supplied during mechanolysis of an acid-impregnated cellulose system [25].

**Table 8.1** Elemental compositional of all the ions observed

dp <sup>a</sup>	Elemental composition	[M+X] <sup>+</sup>	Error (ppm) <sup>b</sup>	dp <sup>a</sup>	Elemental composition	[M+X] <sup>+</sup>	Error (ppm) <sup>b</sup>
1	C <sub>6</sub> H <sub>11</sub> O <sub>5</sub>	163.0588	2.1	5	C <sub>30</sub> H <sub>50</sub> KO <sub>21</sub>	785.2362	10.6
1	C <sub>6</sub> H <sub>12</sub> NaO <sub>6</sub>	203.0515	1.6	5	C <sub>30</sub> H <sub>50</sub> NaO <sub>25</sub>	833.2581	2.5
1	C <sub>6</sub> H <sub>12</sub> KO <sub>6</sub>	219.0269	6.3	6	C <sub>36</sub> H <sub>48</sub> NaO <sub>21</sub>	839.2539	1.0
2	C <sub>12</sub> H <sub>17</sub> O <sub>8</sub>	289.0910	2.2	6	C <sub>36</sub> H <sub>49</sub> NaO <sub>21</sub>	840.2580	1.9
2	C <sub>12</sub> H <sub>16</sub> NaO <sub>8</sub>	311.0731	0.6	6	C <sub>36</sub> H <sub>51</sub> KO <sub>20</sub>	842.2648	2.1
2	C <sub>12</sub> H <sub>21</sub> O <sub>10</sub>	325.1124	0.3	5	C <sub>30</sub> H <sub>51</sub> NaO <sub>26</sub>	850.2678	2.6
2	C <sub>12</sub> H <sub>20</sub> NaO <sub>10</sub>	347.0944	0.5	5	C <sub>30</sub> H <sub>52</sub> NaO <sub>26</sub>	851.2676	1.9
2	C <sub>12</sub> H <sub>21</sub> NaO <sub>10</sub>	348.0983	12.4	6	C <sub>36</sub> H <sub>54</sub> KO <sub>23</sub>	893.2713	6.9
2	C <sub>12</sub> H <sub>20</sub> KO <sub>10</sub>	363.0689	0.1	5	C <sub>30</sub> H <sub>60</sub> KO <sub>29</sub>	923.2923	0.05
2	C <sub>12</sub> H <sub>21</sub> KO <sub>10</sub>	364.0715	12.0	7	C <sub>42</sub> H <sub>52</sub> O <sub>23</sub>	924.2853	1.4
2	C <sub>12</sub> H <sub>22</sub> NaO <sub>11</sub>	365.1050	2.1	6	C <sub>36</sub> H <sub>60</sub> NaO <sub>30</sub>	995.3136	2.8
2	C <sub>12</sub> H <sub>22</sub> KO <sub>11</sub>	381.0841	1.8	7	C <sub>42</sub> H <sub>58</sub> NaO <sub>26</sub>	1001.3051	0.1
2	C <sub>12</sub> H <sub>24</sub> NaO <sub>12</sub>	383.1153	0.9	7	C <sub>42</sub> H <sub>59</sub> NaO <sub>26</sub>	1002.3089	3.9
3	C <sub>18</sub> H <sub>31</sub> O <sub>15</sub>	487.1657	0.8	7	C <sub>42</sub> H <sub>61</sub> KO <sub>25</sub>	1004.3203	1.4
3	C <sub>18</sub> H <sub>30</sub> NaO <sub>15</sub>	509.1495	1.3	6	C <sub>36</sub> H <sub>61</sub> O <sub>32</sub>	1005.3117	1.6
3	C <sub>18</sub> H <sub>31</sub> NaO <sub>15</sub>	510.1512	6.9	6	C <sub>36</sub> H <sub>62</sub> NaO <sub>31</sub>	1013.3239	0.1
3	C <sub>18</sub> H <sub>30</sub> O <sub>17</sub>	518.1528	11.0	7	C <sub>42</sub> H <sub>64</sub> KO <sub>28</sub>	1055.3231	6.6
3	C <sub>18</sub> H <sub>30</sub> KO <sub>15</sub>	525.1221	2.1	7	C <sub>42</sub> H <sub>67</sub> O <sub>32</sub>	1083.3612	1.0
3	C <sub>18</sub> H <sub>32</sub> NaO <sub>16</sub>	527.1588	1.3	6	C <sub>36</sub> H <sub>70</sub> KO <sub>34</sub>	1085.3477	0.6
3	C <sub>18</sub> H <sub>32</sub> KO <sub>16</sub>	543.1321	0.2	8	C <sub>48</sub> H <sub>62</sub> O <sub>28</sub>	1086.3377	0.1
4	C <sub>24</sub> H <sub>40</sub> NaO <sub>20</sub>	671.2038	0.9	8	C <sub>48</sub> H <sub>72</sub> KO <sub>30</sub>	1167.3640	4.3
4	C <sub>24</sub> H <sub>41</sub> NaO <sub>20</sub>	672.2046	5.7	9	C <sub>54</sub> H <sub>71</sub> O <sub>33</sub>	1247.4035	4.6
5	C <sub>30</sub> H <sub>41</sub> KO <sub>15</sub>	680.2121	2.2	9	C <sub>54</sub> H <sub>72</sub> O <sub>33</sub>	1248.3908	0.2
4	C <sub>24</sub> H <sub>42</sub> NaO <sub>21</sub>	689.2131	1.9	8	C <sub>48</sub> H <sub>80</sub> O <sub>42</sub>	1328.4140	7.2
5	C <sub>30</sub> H <sub>44</sub> KO <sub>18</sub>	731.2186	7.8	10	C <sub>60</sub> H <sub>91</sub> KO <sub>40</sub>	1490.4866	6.1

<sup>a</sup>dp = degree of polymerization; <sup>b</sup> Error in calculating elemental composition.

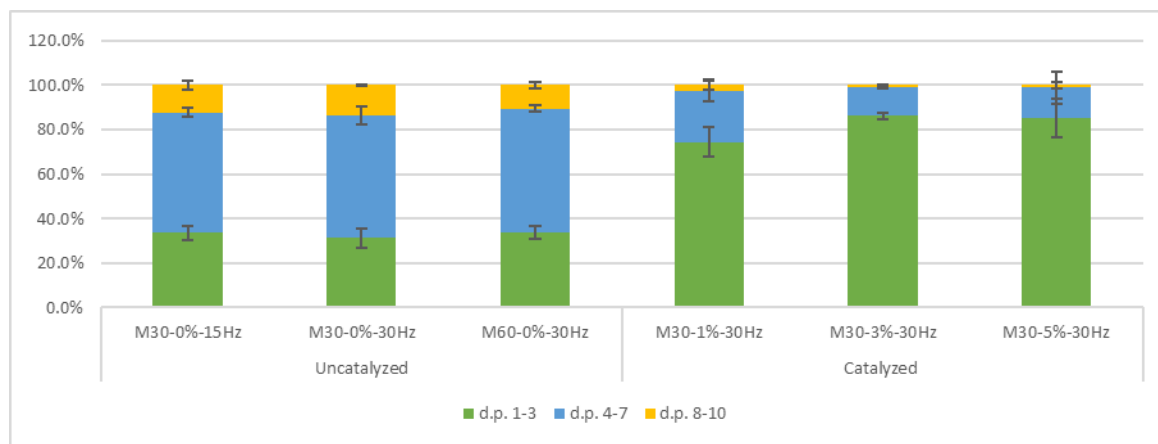


**Figure 8.1** Oligosaccharide profile after milling treatments. Expressed as percentage of total intensity of all identified peaks. Results are average of triplicate analysis, with error bars indicating standard deviation.

#### 8.4.2 The effect of milling time, frequency, and catalyst on the observed oligosaccharide profile

Process variables such as milling time, frequency, and catalysts affecting the observed oligosaccharide profile were investigated (Figure 8.1). The results showed that milling time (30 and 60 minutes) and frequency (15 and 30 Hz) do not have a significant effect on the oligosaccharides profile for samples processed without catalysis. Similarly, for catalyzed samples, the level of catalysis (1%, 3%, 5%; w/w) at the same milling time and frequency (30 minutes, 30 Hz) does not have a significant effect as well on the oligosaccharides profile. The difference was found only between catalyzed and samples processed without catalysis (see Figure 8.1). We further examined the detailed composition of the oligosaccharides in the dp range of 1-3. As shown in Table 8.2, the major components of the group dp 1-3 were disaccharides. According to the detailed mono-, and di-saccharide composition which was obtained from ESI-TOF-MS results (Table 8.2), mechano-catalytically produced mono-, di-, and tri-saccharides were mainly in their dehydrated forms. In the literature, acid catalyzed degradation of inulin have been shown to form mainly di-D-fructose dianhydrides (DFDAs) [26-28] as potential prebiotic mixture [29, 30]. According to Christian, Manley-Harris *et al.* [27], there are 14 isomeric forms of di-D-fructose dianhydrides that have been identified during thermolysis of citric acid impregnated inulin at 160-180 °C range. In

this study, based on the calculated molecular formulae there is relatively large percentage of peaks matching the elemental formula of di-D-fructose dianhydride generated in catalyzed milled samples (Table 8.1&8.2). Tandem mass spectrometry (MS/MS) was carried out for the ions identified as intact oligosaccharides based on their elemental composition and observed at  $[M+X]^+$  values of 365, 527, 689, 851, 1004 and 1013 (dp 2-7). The MS/MS fragment ions of the oligosaccharides mainly resulted from glycosidic cleavages generating intact sugar residues (see Table 8.3) as reported in the literature [31, 32]. In summary, the MS/MS results confirmed the presence of oligosaccharides in the milled systems.

**Table 8.2** Details of group dp 1-3 (see Figure 8.1), the relative content is expressed as percent of the all identified ions

		Uncatalyzed			Catalyzed		
		M30-0%- 15Hz	M30-0%- 30Hz	M60-0%- 30Hz	M30-1%- 30Hz	M30-3%- 30Hz	M30-5%- 30Hz
Mono- saccharides <sup>a</sup>	Total	5.06% ± 1.57%	3.84% ± 1.26%	4.17% ± 1.21%	18.48% ± 2.48%	23.55% ± 0.49%	22.93% ± 7.23%
	Dehydrated	1.58% ± 1.07%	1.27% ± 0.38%	2.35% ± 1.61%	3.58% ± 0.6%	6.96% ± 3.03%	4.46% ± 3.57%
Di- saccharides <sup>a</sup>	Total	21.87% ± 1.88%	21.32% ± 3.97%	23.79% ± 2.67%	41.18% ± 4.72%	50.01% ± 0.42%	50.16% ± 5.03%
	Dehydrated	1.2% ± 0.59%	2.7% ± 1.01%	1.65% ± 0.55%	27.53% ± 3.05%	30.63% ± 8.34%	41.56% ± 7.28%
Tri- saccharides <sup>a</sup>	Total	6.75% ± 0.85%	6.03% ± 1.19%	5.66% ± 0.92%	14.85% ± 0.03%	12.61% ± 0.53%	12.02% ± 3.63%
	Dehydrated	1.09% ± 0.58%	1.15% ± 0.43%	0% ± 0%	6.02% ± 2.01%	5.65% ± 2.21%	5.69% ± 0.87%

<sup>a</sup>: mono-, di-, tri-saccharides identified based on their elemental formulae as indicated in Table 8.1 with dp number 1, 2, and 3

**Table 8.3** MS/MS data for ions at [M+X]<sup>+</sup> 365, 527, 689, 851, 1004 and 1013 (dp 2-7).

dp	Parent ion	Daughter ions				
2	365.1050 (C <sub>12</sub> H <sub>22</sub> NaO <sub>11</sub> )	185.0424 (C <sub>6</sub> H <sub>10</sub> NaO <sub>5</sub> )	203.0524 (C <sub>6</sub> H <sub>12</sub> NaO <sub>6</sub> )			
3	527.1588 (C <sub>18</sub> H <sub>32</sub> NaO <sub>16</sub> )	185.0413 (C <sub>6</sub> H <sub>10</sub> NaO <sub>5</sub> )	347.0944 (C <sub>12</sub> H <sub>20</sub> NaO <sub>10</sub> )	365.106 (C <sub>12</sub> H <sub>22</sub> NaO <sub>11</sub> )		
4	689.2131 (C <sub>24</sub> H <sub>42</sub> NaO <sub>21</sub> )	347.0944 (C <sub>12</sub> H <sub>20</sub> NaO <sub>10</sub> )	365.1060 (C <sub>12</sub> H <sub>22</sub> NaO <sub>11</sub> )	509.1398 (C <sub>18</sub> H <sub>30</sub> NaO <sub>15</sub> )	511.129 (C <sub>19</sub> H <sub>27</sub> O <sub>16</sub> )	527.1571 (C <sub>18</sub> H <sub>32</sub> NaO <sub>16</sub> )
5	851.2676 (C <sub>30</sub> H <sub>52</sub> NaO <sub>26</sub> )	163.0586 (C <sub>6</sub> H <sub>11</sub> O <sub>5</sub> )	325.1125 (C <sub>12</sub> H <sub>21</sub> O <sub>10</sub> )	365.9907 (C <sub>12</sub> H <sub>22</sub> NaO <sub>11</sub> )	527.1571 (C <sub>18</sub> H <sub>32</sub> NaO <sub>16</sub> )	
6	1,004.3202 (C <sub>42</sub> H <sub>61</sub> KO <sub>25</sub> )	163.0597 (C <sub>6</sub> H <sub>11</sub> O <sub>5</sub> )	325.1125 (C <sub>12</sub> H <sub>21</sub> O <sub>10</sub> )	365.1001 (C <sub>12</sub> H <sub>22</sub> NaO <sub>11</sub> )	527.1571 (C <sub>18</sub> H <sub>32</sub> NaO <sub>16</sub> )	689.2135 (C <sub>24</sub> H <sub>42</sub> NaO <sub>21</sub> )
7	1,013.3239 (C <sub>36</sub> H <sub>62</sub> NaO <sub>31</sub> )	325.1125 (C <sub>12</sub> H <sub>21</sub> O <sub>10</sub> )	365.1114 (C <sub>12</sub> H <sub>22</sub> NaO <sub>11</sub> )			

dp = degree of polymerization; X = H<sup>+</sup> or Na<sup>+</sup>

#### 8.4.3 Milling efficiency

To obtain an estimate of the milling efficiency in converting inulin into mono-, di-, and tri-saccharides their total sum was quantified in various samples (see Table 8.4) and in untreated inulin sample using anion exchange chromatography and dialysis experiments as described in the Experimental Section. The concentrations of mono-, di-, and tri-saccharides in untreated inulin samples were very low and below the quantification limit of the detector. On the other hand, in a 20 µg of catalysed sample (M30-5%-30 Hz) the total amount of mono, di-, and tri-saccharides was found to be 4.3586±0.0665 µg, which represents a 21.79% yield by weight, compared to uncatalysed sample (M30-0%-30 Hz) the amount of which was 0.1524±0.0113 µg out of 20 µg representing a 0.76% yield, this amounts to a ~ 30-fold increase in concentration of small molecular weight oligosaccharides due to catalysis. The above results were further corroborated when untreated and treated samples (M30-5%-30 Hz) were dialyzed and the percent of retentates having molecular weights above 2K (dp of 12) were compared indicating 72.4% ± 1.1% w/w retention for the untreated sample and only 26.6% ± 2.1% w/w for the treated sample (M30-5%-30Hz) consistent with AEC-PAD results. In this study, the milling efficiency was not optimized.

**Table 8.4** Total amount of mono-, di-, and tri- saccharides detected in 20µg inulin using AEC-PAD.

	<b>Sample name</b>	<b>Total amount (µg)</b>	<b>Percentage <sup>a</sup></b>
Untreated	Inulin	N/D	N/D
Catalysed	M30-5%-30Hz	4.3586±0.0665	21.79%
	M30-5%-15Hz	3.4766±0.6503	17.38%
	M15-5%-30Hz	1.8338±0.2177	9.17%
	M15-5%-15Hz	0.8704±0.0934	4.35%
Uncatalyzed	M30-0%-30Hz	0.1524±0.0113	0.76%
	M30-0%-15Hz	0.1219±0.0126	0.61%
	M15-0%-30Hz	0.159±0.0274	0.80%
	M15-0%-15Hz	0.1188±0.0268	0.59%

<sup>a</sup>: Weight percentage

## 8.5 Conclusion

Different polymers absorb mechanical energy differently and result in different behavior in bond cleavage efficiency. Lignin apparently absorbs mechanical energy more effectively than cellulose due to its rigid structure [33]. Additionally, it has been reported that prolonged milling time on wheat starch granule results in an increase in low-molecular-weight amylopectin content but amylose content maintain the same, which indicate that branched amylopectin polymer could have a higher capacity of absorbing mechanical energy compared to linear amylose polymer.[20] This study demonstrates the ability of inulin to absorb mechanical energy especially under acid catalysis conditions and generate oligosaccharide mixtures of prebiotic value.

## 8.6 References

1. Schneider, L., et al., *Solid acid-catalyzed depolymerization of barley straw driven by ball milling*. Bioresource Technology, 2016. **206**: p. 204-210.
2. Yu, Y., Y. Long, and H. Wu, *Near-Complete Recovery of Sugar Monomers from Cellulose and Lignocellulosic Biomass via a Two-Step Process Combining Mechanochemical Hydrolysis and Dilute Acid Hydrolysis*. Energy & Fuels, 2016. **30**(3): p. 1571-1578.
3. Yabushita, M., et al., *Quantitative evaluation of ball-milling effects on the hydrolysis of cellulose catalysed by activated carbon*. Catalysis Science & Technology, 2014. **4**(8): p. 2312-2317.
4. Corma, A., S. Iborra, and A. Velty, *Chemical Routes for the Transformation of Biomass into Chemicals*. Chemical Reviews, 2007. **107**(6): p. 2411-2502.
5. Hon, D.N.S., *Formation and behavior of mechanoradicals in pulp cellulose*. Journal of Applied Polymer Science, 1979. **23**(5): p. 1487-1499.
6. Kuzuya, M., Y. Yamauchi, and S.-i. Kondo, *Mechanolysis of Glucose-Based Polysaccharides As Studied by Electron Spin Resonance*. The Journal of Physical Chemistry B, 1999. **103**(38): p. 8051-8059.
7. Silva, G.G.D., et al., *Effects of grinding processes on enzymatic degradation of wheat straw*. Bioresource Technology, 2012. **103**(1): p. 192-200.
8. James, S.L., et al., *Mechanochemistry: opportunities for new and cleaner synthesis*. Chemical Society Reviews, 2012. **41**(1): p. 413-447.
9. Roa, D.F., R.I. Baeza, and M.P. Tolaba, *Effect of ball milling energy on rheological and thermal properties of amaranth flour*. Journal of food science and technology, 2015. **52**(12): p. 8389-8394.
10. Thanatuksorn, P., et al., *Effects of ball-milling on the glass transition of wheat flour constituents*. Journal of the Science of Food and Agriculture, 2009. **89**(3): p. 430-435.
11. He, S., et al., *Effect of ball-milling on the physicochemical properties of maize starch*. Biotechnology Reports, 2014. **3**: p. 54-59.
12. Stolle, A., *Ball milling towards green synthesis: applications, projects, challenges*. 2014: Royal Society of Chemistry.

13. Margetic, D. and V. Štrukil, *Mechanochemical Organic Synthesis*. 2016: Elsevier.
14. Blair, R.G., S.M. Hick, and J.H. Truitt, *Solid acid catalyzed hydrolysis of cellulosic materials*. 2011, Google Patents.
15. Hick, S.M., et al., *Mechanocatalysis for biomass-derived chemicals and fuels*. *Green Chemistry*, 2010. **12**(3): p. 468-474.
16. Hilgert, J., et al., *Mechanocatalytic depolymerization of cellulose combined with hydrogenolysis as a highly efficient pathway to sugar alcohols*. *Energy & Environmental Science*, 2013. **6**(1): p. 92-96.
17. Li, H., et al., *An efficient pretreatment for the selectively hydrothermal conversion of corncob into furfural: The combined mixed ball milling and ultrasonic pretreatments*. *Industrial Crops and Products*, 2016. **94**: p. 721-728.
18. Schlesinger, J., *Results of ball-milling Buhler experimentally milled hard winter wheat flour*. *Cereal Chem*, 1964. **41**: p. 465-474.
19. Morrison, W., R. Tester, and M. Gidley, *Properties of damaged starch granules. II. Crystallinity, molecular order and gelatinisation of ball-milled starches*. *Journal of Cereal Science*, 1994. **19**(3): p. 209-217.
20. Tamaki, S., et al., *Structural Change of Maize Starch Granules by Ball-mill Treatment*. *Starch-Stärke*, 1998. **50**(8): p. 342-348.
21. Niemann, C. and R.L. Whistler, *Effect of acid hydrolysis and ball milling on porous corn starch*. *Starch-Stärke*, 1992. **44**(11): p. 409-414.
22. Lai, H.-M. and Y.-P. Huang, *Effects of ball milling on the properties of colored rice bran, in Gums and Stabilisers for the Food Industry 17*. 2014. p. 155-163.
23. Böhm, A., et al., *Heat-induced degradation of inulin*. *European Food Research and Technology*, 2005. **220**(5-6): p. 466-471.
24. Caruso, M.M., et al., *Mechanically-induced chemical changes in polymeric materials*. *Chemical Reviews*, 2009. **109**(11): p. 5755-5798.
25. Meine, N., R. Rinaldi, and F. Schüth, *Solvent-Free Catalytic Depolymerization of Cellulose to Water-Soluble Oligosaccharides*. *ChemSusChem*, 2012. **5**(8): p. 1449-1454.
26. Blize, A.E., M. Manley-Harris, and G.N. Richards, *Di-D-fructose dianhydrides from the pyrolysis of inulin*. *Carbohydrate research*, 1994. **265**(1): p. 31-39.

27. Christian, T.J., et al., *Kinetics of formation of di-D-fructose dianhydrides during thermal treatment of inulin*. Journal of agricultural and food chemistry, 2000. **48**(5): p. 1823-1837.
28. Manley-Harris, M. and G.N. Richards, *Dihexulose dianhydrides*. Advances in Carbohydrate Chemistry and Biochemistry, 1997. **52**: p. 207-267.
29. Wang, X., et al., *From fructans to difructose dianhydrides*. Applied Microbiology and Biotechnology, 2015. **99**(1): p. 175-188.
30. Minamida, K., et al., *Effects of ingestion of difructose anhydride III (DFA III) and the DFA III-assimilating bacterium Ruminococcus productus on rat intestine*. Bioscience, biotechnology, and biochemistry, 2006. **70**(2): p. 332-339.
31. Li, J., et al., *Determination of inulin-type fructooligosaccharides in edible plants by high-performance liquid chromatography with charged aerosol detector*. Journal of agricultural and food chemistry, 2014. **62**(31): p. 7707-7713.
32. Yang, Z., et al., *Isolation of inulin-type oligosaccharides from Chinese traditional medicine: Morinda officinalis How and their characterization using ESI-MS/MS*. Journal of separation science, 2010. **33**(1): p. 120-125.
33. Hon, D.N.-S., *Mechanochemistry of lignocellulosic materials*, in *Developments in Polymer Degradation—7*. 1987, Springer. p. 165-191.

## **Chapter 9 General conclusions, contributions to knowledge, and suggestions for future research**

## 9.1 General conclusions

Despite the emergence of mechanochemistry as a fast and efficient technology, its applications in the field of food science remain largely unexplored. The studies outlined in this thesis explored three promising applications of mechanochemistry in food science, i.e. generation of Maillard reaction flavor precursors, protein glycation, and depolymerization of polysaccharides. All applications performed better than conventional thermochemical methods in terms of selectivity and efficiency.

Furthermore, these studies showed the potential of using high-resolution mass spectrometry for understanding the molecular complexity of the Maillard reaction, as well as using the subsequent tandem mass spectrometry for unequivocal structural elucidations. Moreover, as a high throughput analytical platform with exceptional resolution, the HRMS allows the simultaneous detection of thousands of the Maillard reaction intermediates with accurate elemental composition, which can be used as a second strategy for resolving the isomeric intermediates based on their unique downstream degradation products if their lineage can be traced through isotope labeling technique. With this exceptional analytical platform, we provided an in-depth understanding of the mechanochemical induced Maillard reaction.

Additionally, the presented studies in this thesis were designed with the consideration of food sustainability and environmental impact. With mechanochemistry being a “green” methodology, we further proposed to obtain reaction precursors from abundant biomasses through the application of mechanochemistry. Finally, the presented studies not only positively contributed to our understanding of the Maillard reaction in general, but also specifically addressing the challenges facing the manufacturers of plant-based food products in terms of flavor intensification through Maillard reaction precursors, modification of protein functionality through glycation, and valorization through depolymerization of polysaccharides.

## 9.2 Contributions to the knowledge

The work presented in this thesis provided evidence for the first time of the following:

1. Development of diagnostic MS/MS fragmentation patterns in positive and negative ionization modes for the discrimination of isomeric intermediates in the Maillard reaction including Schiff bases, Amadori and Heyn's compounds.
2. Selective generation of Schiff bases and Amadori compounds through ball milling of glucose and amino acids.
3. The discovery that the acidity of the amino acid side chains determines the relative ratio of Schiff bases to the Amadori compounds generated mechanochemically.
4. Elucidation of the thermochemical reactivity of the mechanochemically generated Maillard reaction mixtures.
5. Mechanistic insight into the mechanochemistry of the Maillard reaction where the reaction proceeds via Schiff base intermediates rather than the Amadori product, and with subsequent formation of 5-oxazolidinone.
6. Identification of the conditions for the selective mono-glycation of lysozyme using mechanochemistry.
7. Mono-glycated lysozyme has stabilizing influence on its tertiary structure during ball milling.
8. Mechanochemical depolymerization of fructans and generation of prebiotic mixtures of short chain oligosaccharides.
9. Identification of the Lewis acid  $\text{AlCl}_3$  as a catalyst for the mechanochemical depolymerisation of oligosaccharides.

### 9.3 Suggestions for future research

Based on the findings of this thesis, future research can be pursued in the following topics:

1. Absolute quantification of the isomeric intermediate in the Maillard reaction mixtures through LC-MS/MS using the diagnostic ions reported in this thesis through multiple-reaction monitoring experiments.
2. Explore mechanochemical glycation of other food industry relevant proteins and identification of glycation sites through proteomics.
3. Polymerization of monosaccharides to generate oligosaccharides with prebiotic value and the investigation of the stereochemistry of the glycosidic bonds formed mechanochemically.
4. Taking advantage of the solvent-free condition of mechanochemistry to generate flavor precursors with improved stability. For example, the formation of 3-oxazoline, a stable precursor leading to aroma-active Strecker aldehydes, is favored under solid-state.
5. Taking advantage of the solvent-free conditions of mechanochemistry for non-soluble reactants, e.g. cellulose and plant proteins, and their valorization for food applications.
6. Design novel materials with applications in food based on widely available literature studies, e.g. nanocomposite and metal-organic frameworks (MOFs).
7. Investigation of mechano-enzymatic reactions for food applications.
8. Having an “omics” mindset for analysis of the Maillard reaction and explore other omics-analytic platforms in addition to HRMS for Maillard reaction analysis, e.g. high-resolution NMR.
9. Scaling up the mechanochemical reaction through rethinking of extrusion technology from the mechanochemical perspective.